Aus dem Rudolf-Zenker-Institut für Experimentelle Chirurgie

Direktorin: Univ.-Prof. Dr. med. Brigitte Vollmar

Analyse der Belastung von Versuchstieren und Evaluation einer experimentellen Therapie im murinen Modell des Pankreaskarzinoms

Kumulative Dissertation

zur

Erlangung des akademischen Grades

Doktor der Medizinwissenschaften (Dr. rer. hum.)

der

Universitätsmedizin Rostock

Vorgelegt von

Benjamin Schulz | geb. am 13.07.1989 in Schwerin

aus Rostock

Rostock | Juni 2024

https://doi.org/10.18453/rosdok_id00005107

Dissertation

Universitätsmedizin Rostock

Universität Rostock Traditio et Innovatio

Universitätsmedizin Rostock

Erstgutachter:
Apl. Prof. Dietmar Zechner, Ph.D.
Einrichtung:
Rudolf-Zenker-Institut für Experimentelle Chirurgie
Universitätsmedizin Rostock

Zweitgutachterin:
PD Dr. Claudia Maletzki
Einrichtung:
Zentrum für Innere Medizin
Medizinische Klinik III – Klinik für Hämatologie, Onkologie, Palliativmedizin
Universitätsmedizin Rostock

Drittgutachter:
Prof. André Bleich, Ph.D.
Einrichtung:
Institut für Versuchstierkunde und Zentrales Tierlaboratorium
Medizinische Hochschule Hannover

Einreichung:
Juni 2024

Verteidigung:
Februar 2025

Dissertation
Universitätsmedizin Rostock

Inhaltsverzeichnis

I. Studien der kumulativen Dissertation 1

II. Zusammenfassung 2

III. Einleitung 3

3.1 Belastungseinschätzung in Tierversuchen 3

3.2 Das Pankreaskarzinom 4

3.3 Zielstellung der Arbeit 8

IV. Methoden 9

4.1 Studie I 9

4.1.1 Tiermodelle 9

4.1.2 Belastungsanalyse 10

4.1.3 Statistik 11

4.2 Studie II 12

4.2.1 Inhibitoren 12

4.2.2 Zelllinien und Zellkultur 12

4.2.3 Assays 12

4.2.3.1 Proliferation 12

4.2.3.2 Quantifizierung der Biomasse 12

4.2.3.3 Apoptose und Nekrose 13

4.2.3.4 Evaluation der Inhibitor-Kombinationen 13

4.2.4 Statistik 13

4.3 Studie III 14

4.3.1 Inhibitoren 14

4.3.2 Zelllinie und Zellkultur 14

4.3.3 Assays 14

4.3.3.1 Proliferation 14

4.3.3.2 Apoptose und Nekrose 14

4.3.3.3 Evaluation der Inhibitor-Kombinationen 15

4.3.4 PDAC-Tiermodell und Therapie 15
4.3.5 Belastungsanalyse 15
4.3.6 Statistik 15
V. Ergebnisse 16
5.1 Studie I 16
5.2 Studie II 18
5.3 Studie III 20
VI. Diskussion 25
6.1 Belastung im Modell des Pankreaskarzinoms und durch therapeutische Intervention 25
6.2 Effektivität der kombinierten Inhibition von SOS1, MEK1/2 und PI3K *in vitro* und *in vivo* 29
VII. Literaturverzeichnis 33
VIII. Abbildungsverzeichnis 43
IX. Tabellenverzeichnis 44
X. Abkürzungsverzeichnis 45
XI. Lebenslauf 47
XII. Danksagung 49
XIII. Eidesstattliche Versicherung 50
XIV. Anhang 51
14.1 Studie I 52
14.2 Studie II 69
14.3 Studie III 91

I. Studien der kumulativen Dissertation

Studie I: Zechner D, **Schulz B**, Tang G, et al. Generalizability, Robustness and Replicability When Evaluating Wellbeing of Laboratory Mice with Various Methods. *Animals (Basel)*. 2022;12(21):2927. doi:10.3390/ani12212927
(IF 3,0)

Studie II: Ma Y, **Schulz B**, Trakooljul N, et al. Inhibition of KRAS, MEK and PI3K Demonstrate Synergistic Anti-Tumor Effects in Pancreatic Ductal Adenocarcinoma Cell Lines. *Cancers (Basel)*. 2022;14(18):4467. doi:10.3390/cancers14184467
(IF 5,2)

Studie III: **Schulz B**, Leitner E, Schreiber T, et al. Sex Matters-Insights from Testing Drug Efficacy in an Animal Model of Pancreatic Cancer. *Cancers (Basel)*. 2024;16(10):1901. doi:10.3390/cancers16101901
(IF 5,2)

Die Studien sind im Anhang ab Seite 51 zu finden.

II. Zusammenfassung

Tierexperimente leisten einen unverzichtbaren Beitrag zur Aufklärung und Therapie humaner Erkrankungen. Wissenschaftler sind durch Ethik und Gesetze verpflichtet, das Leiden der eingesetzten Versuchstiere auf ein Minimum zu reduzieren. Dazu ist eine objektive und robuste Einschätzung der Belastung von Versuchstieren nötig. Bisher ist jedoch nur wenig darüber bekannt, wie robust die Belastung von Versuchstieren anhand etablierter Methoden eingeschätzt werden kann. Da das Pankreaskarzinom durch das Fehlen effektiver Therapien weiterhin eine große Belastung für Patienten und das Gesundheitssystem darstellt, wurden die Untersuchungen in dieser Arbeit an einem syngenen, orthotopen Mausmodell des Pankreaskarzinoms vorgenommen. Studie I befasste sich mit der Eignung verschiedener Methoden der Belastungsanalyse zur Unterscheidung von Tieren in diesem Modell vor und nach der Induktion durch orthotope Injektion von Pankreaskarzinomzellen. Studie III untersuchte, ob männliche und weibliche Tiere im Modell unterschiedliche Belastung erfahren. Darüber hinaus wurde in den Studien I und III evaluiert, ob Methoden der Belastungsanalyse geeignet sind, Tiere vor und nach der Induktion des Modells mit und ohne Therapie zu unterscheiden und ob es Unterschiede in der Belastung zwischen Tieren mit und ohne Therapie gibt. Eine Schlussfolgerung von Studie I war, dass die Unterscheidung von Tieren vor und nach Induktion eines Pankreaskarzinommodells nur mit wenigen Methoden zuverlässig möglich ist. Im späteren Verlauf des Modells eignete sich insbesondere die Körpergewichtsveränderung als aussagekräftiger Parameter. Studie III zeigte, dass männliche und weibliche Tiere in der späten Phase des Modells unterschiedliche Belastung erfahren, was auf geschlechtsspezifische Unterschiede im Tumormodell zurückzuführen sein könnte. In den Studien I und III wurde keine zusätzliche Belastung durch die verwendeten Therapien festgestellt. Dies kann bedeuten, dass es keine zusätzliche Belastung durch die Therapien gab, oder dass die verwendeten Methoden nicht sensitiv genug sind, um eine zusätzliche Belastung zu erfassen. In den Studien II und III wurde eine neue Kombinationstherapie aus BI-3406, Trametinib und BKM120 in verschiedenen humanen und einer murinen PDAC-Zelllinie sowie im syngenen, orthotopen Mausmodell auf ihre Wirksamkeit untersucht. Dabei wurde auch der Einfluss des Geschlechts der verwendeten C57BL/6J-Mäuse auf die Effektivität der Therapie analysiert. Die untersuchte Therapie wirkte sowohl in den humanen als auch in der verwendeten murinen Zelllinie synergistisch hinsichtlich der Inhibition der Proliferation und der Induktion des Zelltods. Im Tierversuch konnte die Wirksamkeit der Therapie jedoch lediglich in männlichen Tieren nachgewiesen werden. In weiblichen Tieren wurde die therapeutische Effektivität sehr wahrscheinlich durch geschlechtsspezifische, immunsuppressive Effekte beeinflusst. Dennoch stellt diese Therapieoption einen vielversprechenden Ansatz dar und sollte im Hinblick auf die dringend benötigten effektiven Therapien des Pankreaskarzinoms weiter erforscht werden.

III. Einleitung

3.1 Belastungseinschätzung in Tierversuchen

Das Prinzip der 3R gilt seit seiner Veröffentlichung 1959 durch Russell und Burch[1] als Grundlage für die Implementation aktueller Tierschutzrichtlinien in der Wissenschaft. Das Ersetzen (Replacement) durch Alternativmethoden, die Reduktion (Reduction) der Tierzahlen und die Verbesserung von Tierversuchen (Refinement) zur Reduktion des Leidens auf ein unvermeidliches Minimum, gelten dabei als die Maßgabe tierexperimenteller Forschung. Dieser Anspruch hat 2010 mit der Richtlinie 2010/63/EU und 2013 mit der Novellierung des deutschen Tierschutzgesetzes Einzug in europäische und nationale Gesetzgebung gefunden[2,3]. Damit sind Wissenschaftler rechtlich unter anderem dazu verpflichtet, Maßnahmen zur Verbesserung der Versuchsdurchführung und damit zur Reduktion des Tierleides auf ein Minimum zu implementieren. Dies setzt voraus, dass der Zustand und das Leiden von Versuchstieren objektiv mittels evidenzbasierter Methoden quantifiziert werden kann[4]. Diese Methoden sollten idealerweise sensitiv genug sein, um Belastung auch in Beutetieren wie Mäusen oder Ratten zu erfassen. Diese Tiere unterdrücken instinktiv Zeichen von Schmerz und Leid[5,6] und stellen die Mehrheit der in der EU und Deutschland verwendeten Versuchstiere dar[7].

Methoden zur Einschätzung der Belastung von Versuchstieren messen in der Regel physiologische Parameter wie Körpergewicht[8-10] oder Konzentrationen von Stresshormonen im Kot[11,12], klinische Anzeichen von Belastung anhand klinischer Scoring-Systeme[13,14] sowie Änderungen in natürlichen Verhaltensweisen wie Nestbau- und Buddelverhalten oder der Aktivität im Laufrad[15-19]. All diese Methoden haben sich bisher als nützlich darin erwiesen, die Belastung von Versuchstieren zu evaluieren und Abbruchkriterien in Form von humanen Endpunkten zu etablieren[20-23]. Jedoch ist bisher wenig darüber bekannt, wie robust diese Methoden kranke von gesunden Tieren unterscheiden können. Robustheit wird hier im engeren Sinne als Stabilität der aus Experimenten gezogenen Schlussfolgerungen gegenüber Veränderungen wie verschiedenen Tiermodellen, therapeutischen Interventionen oder der Variation der zugrunde liegenden Daten verstanden[24]. Zur Überprüfung der Verlässlichkeit verschiedener Methoden zur Belastungsevaluation eignen sich Grenzwertoptimierungskurven, welche im Englischen als receiver operating characteristic (ROC) curves bezeichnet werden. ROC-Kurven finden in der Klinik regelmäßig Anwendung, um die Leistungsfähigkeit diagnostischer Tests zu evaluieren[25,26]. Als Parameter der Leistungsfähigkeit gilt die Fläche unter der Kurve einer ROC, auch als area under the curve (AUC) bezeichnet. Die AUC entsteht durch die Darstellung der richtig-positiv Rate (Sensitivität) und der falsch-positiv Rate (1 - Spezifität) mit Hilfe verschiedener Schwellenwerte. Eine diagonale Linie führt zu einer AUC von 0,5 und ist gleichbedeutend mit einem diagnostischen Test, der Testsubjekte, wie zum Beispiel Erkrankte und Gesunde, nicht besser als der Zufall voneinander unterscheiden kann[27]. Die AUC ist damit

ein Leistungsparameter der Unterscheidungsfähigkeit von Vorhersagemodellen[28]. Da ROC-Kurven als solches wenig intuitiv zu interpretieren sind, kann die AUC als einfach verständlicher Parameter dienen, um verschiedene Methoden der Belastungseinschätzung in Tierexperimenten zu vergleichen. Solch einfach zu vergleichende Parameter sind eine Grundvoraussetzung, um den gesetzlichen Anforderungen an Wissenschaftler und Tierversuche gerecht zu werden[4].

Da viele Tiermodelle, allen voran in der onkologischen Forschung, dazu dienen, neue Therapien zu evaluieren, können Methoden der Belastungsanalyse gleichermaßen dazu geeignet sein, um potentielle Nebenwirkungen dieser Therapien unabhängig von gesetzlich vorgeschriebenen toxikologischen Analysen[29] bereits frühzeitig im Tierversuch zu erkennen[30,31].

3.2 Das Pankreaskarzinom

Maligne Veränderungen des exokrinen Pankreas machen 95% der Tumorerkrankungen des Pankreas aus. Der Großteil davon sind duktale Adenokarzinome (PDAC). Das Pankreaskarzinom hat mit einer 5-Jahres Überlebensrate von ca. 10% unverändert eine der schlechtesten Prognosen aller soliden Tumorerkrankungen[32]. Die Grundlage der kurativen Behandlung ist die Resektion des Karzinoms, welche zum Zeitpunkt der Diagnose nur noch für 15 – 20% der Patienten infrage kommt[33]. Über 50% der Patienten sind bei Diagnose bereits von Metastasen betroffen und ein Großteil der Patienten nach Resektion entwickeln ebenfalls Metastasen, was auf das Vorhandensein kaum diagnostizierbarer Mikrometastasen zurückgeführt wird[32,34]. Neoadjuvante, adjuvante und palliative Chemotherapie sind daher die Grundpfeiler der Therapie des Pankreaskarzinoms. Als Erstlinientherapie hat sich die Behandlung mit FOLFIRINOX (Folinsäure, 5-Fluorouracil, Irinotecan und Oxaliplatin) und als Zweitlinientherapie die Behandlung mit nab-Paclitaxel und Gemcitabin etabliert[35,36]. Allerdings sind Resistenzen gegen die etablierten Therapieoptionen häufig, was die Forschung an neuen, zielgerichteten Therapien unabdingbar macht[37].

Eine Reihe von Mutationen in Tumorsuppressor – und Protoonkogenen sind assoziiert mit der Initiation und Progression des Pankreaskarzinoms von der pankreatischen intraepithelialen Neoplasie (PanIN) zum PDAC[38]. Tumorsuppressoren wie *TP53*, *CDKN2A* und *SMAD4* verlieren durch Mutationen häufig ihre schützende Funktion (loss-of-function), während das Protoonkogen *KRAS* durch Mutationen in der Regel konstitutiv aktiviert ist. Über 90% der Patienten sind von Mutationen in mindestens einem dieser Schlüsselgene betroffen[39].

Eine Sonderrolle in den genetischen Veränderungen, welche zum PDAC führen, nimmt *KRAS* (Kirsten rat sarcoma viral oncogene homolog) ein, da Mutationen in diesem Gen in der Regel

am Anfang der Progression stehen und in annähernd jedem PDAC zu finden sind[40]. KRAS ist eine GTPase und fungiert als Signaltransduktionsprotein, indem es nach Bindung von GTP nachfolgende Signalwege, allen voran den MAPK-Signalweg, aktiviert und damit unter anderem die Steuerung der Zellproliferation entscheidend beeinflusst[41]. KRAS benötigt für seine Funktion Guanin-Austauschfaktoren (GEFs), welche GDP von der Bindungsstelle verdrängen und zur Aktivierung durch Bindung von GTP führen sowie GTPase-aktivierende Proteine (GAPs), welche die Hydrolyse von GTP zu GDP und damit die Inaktivierung katalysieren, da die intrinsische GTPase-Aktivität von KRAS nur gering ist[42]. KRAS funktioniert dementsprechend als binärer, molekularer Schalter.

Die häufigste Mutation im humanen *KRAS*-Gen betrifft das Codon 12 in Exon 2, welches in über 90% der PDAC verändert ist[43]. Unter den dadurch verursachten Aminosäureaustauschen (G12D, G12V, G12R, G12C) ist G12D (Glycin zu Aspartat) mit ca. 40% mit Abstand am häufigsten vertreten[44]. Die verschiedenen Mutationen haben unterschiedliche biochemische Konsequenzen, welche vor allem die intrinsische und GAP-katalysierte GTP-Hydrolyse betreffen. So ist zum Beispiel die intrinsische GTP-Hydrolyserate durch G12C-Mutationen gegenüber dem Wildtyp kaum verringert, wohingegen G12D-Mutanten nur noch knapp ein Drittel der GTP-Hydrolyserate des Wildtyps aufweisen[45]. Gemeinsam ist den meisten KRAS-Mutanten, dass ihre durch GAPs katalysierte GTP-Hydrolyserate 50 – 1000fach gegenüber dem Wildtyp verringert ist[45]. Dies führt in der Endkonsequenz zu einer annähernd konstitutiven Aktivierung von KRAS, da GTP nicht mehr effektiv zu GDP hydrolysiert wird, wodurch nachfolgende Signalwege, wie Raf/MAPK und PI3K/Akt, ebenfalls überaktiviert werden[46].

KRAS galt aufgrund seiner ungewöhnlich „glatten“ Proteinstruktur ohne bekannte allosterische Bindungsstellen[47] sowie der im picomolaren Bereich liegenden Bindungsaffinität zu GTP[48] die längste Zeit als „undruggable“. Dieses Mantra hat sich in den letzten Jahren stark gewandelt[47] und es wurden mit den G12C-spezifischen Inhibitoren Adagrasib[49] und Sotorasib[50] die ersten mutationsspezifischen KRAS-Inhibitoren vorgestellt. In klinischen Studien mit diesen Inhibitoren wurden gute Ergebnisse erzielt und 2021 mit Sotorasib der erste mutationsspezifische KRAS-Inhibitor von der FDA für den Einsatz zur Behandlung von Lungenkrebs zugelassen. Allerdings betrifft die G12C-Mutation nur ca. 2% der PDAC-Patienten, weshalb diese klinischen Durchbrüche für die Therapie des PDAC bisher kaum von Bedeutung sind[51]. Der kürzlich vorgestellte G12D-spezifische Inhibitor MRTX1133 birgt großes Potential für die Behandlung des PDAC und wird derzeit klinisch evaluiert[52,53]. Eine Alternative zu mutationsspezifischen Inhibitoren stellen sogenannte pan-KRAS-Inhibitoren dar[54]. Da einige der mutierten Allele je nach Krebsart nur in sehr wenigen Patienten vorkommen, bilden pan-KRAS-Inhibitoren eine kosteneffiziente Ausgangsbasis für die Therapie dieser Patienten, wo die Entwicklung

eines mutationsspezifischen Inhibitors ökonomisch nicht sinnvoll erscheint. Weiterhin können pan-KRAS-Inhibitoren das Fundament einer Zweitlinientherapie stellen, für den Fall das Resistenzen gegen mutationsspezifische Inhibitoren im Therapieverlauf auftreten, was während Therapie mit G12C-spezifischen Inhibitoren bereits beobachtet werden konnte[55,56]. Einer dieser pan-KRAS-Inhibitoren ist BI-3406, entwickelt von Boehringer Ingelheim[57]. BI-3406 bindet die katalytische Domäne des GEF Son of Sevenless Homolog 1 (SOS1) und verhindert so die Interaktion mit KRAS-GDP, was dazu führt, dass KRAS im inaktiven GDP-beladenen Zustand verbleibt[57]. In Kombination mit Trametinib (MEK1/2-Inhibitor) hat BI-3406 erfolgreich der adaptiven Resistenz gegen MEK1/2-Inhibition entgegengewirkt, welche durch Feedback-Mechanismen im MAPK-Signalweg und daraus resultierender Reaktivierung der Signaltransduktion zustande kommt[57-59]. Inhibitionen im MAPK-Signalweg können außerdem zur kompensatorischen Überaktivierung des PI3K/Akt-Signalweges führen, einem der Haupteffektoren im KRAS-Signalweg[60,61]. Da KRAS essentielle Abläufe in der Zelle reguliert, ist die Funktion der Signaltransduktion durch diverse Feedback-Mechanismen redundant gesichert, was zur Folge hat, dass ein Inhibitor vermutlich niemals zu einer anhaltenden Inaktivierung der onkogenen KRAS-Signaltransduktion führen wird[62]. Die Interdependenz innerhalb der Signaltransduktion lässt daher verschiedene Strategien der kombinierten Inhibition zu. Buparlisib (BKM120) ist ein zugelassener pan-Klasse 1 PI3K-Inhibitor, mit dem als einzelnes Therapeutikum bisher kaum klinisch relevante Ergebnisse erzielt werden konnten[63]. In Kombination mit Trametinib wurden in einigen Krebsarten gute Ergebnisse erzielt, wobei das PDAC nicht dazu gehört[64]. Dies lässt darauf schließen, dass die Signaltransduktion an weiteren Stellen im Signalweg unterbrochen werden muss. Eine Kombination aus BI-3406 (pan-KRAS-Inhibitor), Trametinib

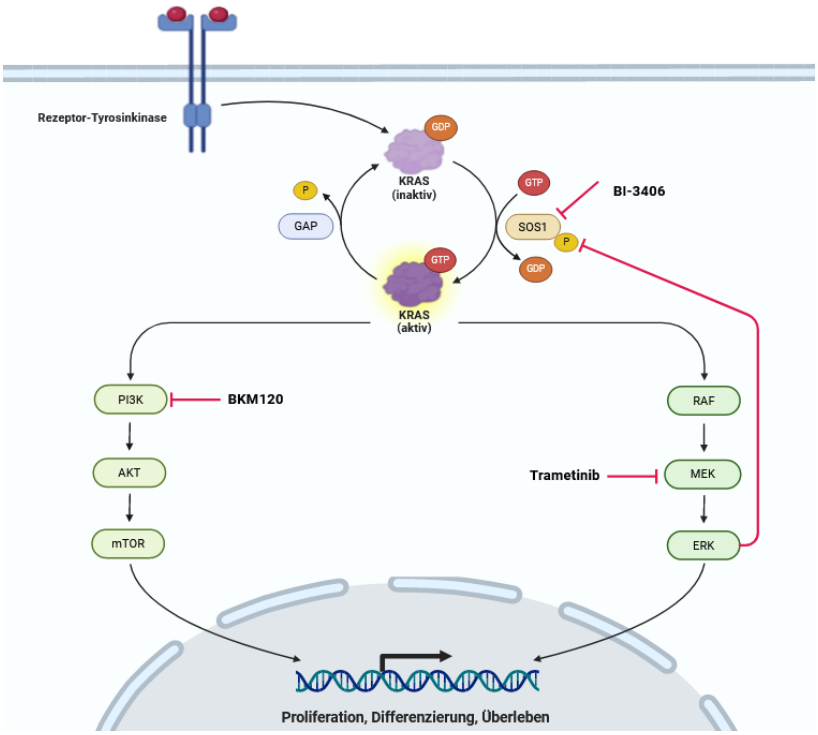

Abbildung 1: Strategie einer kombinierten Inhibition von KRAS:SOS1, MEK1/2 und PI3K
Die kombinierte Inhibition von KRAS:SOS1, MEK1/2 und PI3K könnte eine geeignete Strategie sein, um Feedback-Mechanismen zu unterdrücken und eine dauerhafte Unterbrechung der Signaltransduktion zu gewährleisten, welche Proliferation und Überleben der Karzinomzelle vermittelt.

(MEK1/2-Inhibitor) und BKM120 (pan-Klasse 1 PI3K-Inhibitor) könnte sich als geeignet erweisen, die Lücke einer effektiven PDAC-Therapie zu füllen (Abbildung 1).

Verschiedenste Tiermodelle sind etabliert, um präklinisch neue PDAC-Therapien zu evaluieren. Am häufigsten genutzt werden genetisch veränderte (GEMMs), syngen implantierte und vom Patienten abgeleitete (Xenograft) Modelle[65]. Jedes Modell hat Vor – und Nachteile und wird für spezifische Fragestellungen genutzt. GEMMs eignen sich vor allem, um die Karzinogenese vom PanIN bis zum Karzinom sowie die beteiligten Gene und Signalwege nachzuvollziehen. Es existiert eine lange Liste von genetischen Modellen, in denen *KRAS* mit seinen verschiedenen mutierten Allelen exprimiert wird und gleichzeitig Tumorsuppressoren, wie *TP53*, gezielt ausgeknockt sind[65]. Für gezieltes Suchen nach antitumorigenen Substanzen sind GEMMs aufgrund ihrer langen Latenz und hohen Kosten weniger geeignet. In der Präklinik werden zu diesem Zweck vor allem Xenograft-Modelle genutzt, in denen humane Tumorzellen, oftmals von Patienten abgeleitet, implantiert werden[66]. Der große Vorteil dieser Modelle besteht in der Translation, da humane Zellen eingesetzt werden und so die Nähe zum Zielorganismus gegeben ist. Das ist allerdings nur in Mausstämmen wie NOD.Cg-*Prkdc*^{scid}*Il2rg*^{tm1Wjl}/SzJ (NSG) möglich, welche immundefizient sind und damit Zellen anderer Spezies nicht abstoßen[66]. Darin liegt gleichermaßen der große Nachteil von Xenograft-Modellen, denn die Implikation des Immunsystems in Progression und Therapie des Tumors kann nicht analysiert werden. Einen Kompromiss bieten syngene Modelle. Da Mausstämme wie C57BL/6J ingezüchtet[67] sind, werden die Tiere dieses Stammes als syngen angesehen. Das Implantieren von Tumorzellen aus einem Tumor mit demselben genetischen Hintergrund ist eine zeit – und kosteneffiziente Methode, um beispielsweise orthotope Tumore zu induzieren und antitumorigene Substanzen zu testen. Ebenso ist die Analyse der Immunantwort möglich, da der Stamm immunkompetent ist.

Als immer wichtiger wird auch die Einbeziehung des Geschlechts als biologische Variable angesehen[68-70]. Jahrzehntelang vernachlässigt, zeigt sich inzwischen, dass das Geschlecht ein maßgeblicher Faktor für die Überlebenswahrscheinlichkeit und das Ansprechen auf bestimmte Krebstherapien ist[71-74]. In Bezug auf Tiermodelle verschiedener Karzinomentitäten hat sich herausgestellt, dass Geschlechtshormone ein entscheidender Modulator der adaptiven Immunantwort sind[75-78]. Diese Interaktionen lassen sich in immundefizienten Mausstämmen nicht nachvollziehen, weshalb syngene Modelle hier von großem Vorteil sind. Daher verwendeten wir ein syngenes, orthotopes Modell, um den Einfluss des Geschlechts auf die Wirkung der Kombinationstherapie aus BI-3406, Trametinib und BKM120 zu evaluieren.

3.3 Zielstellung der Arbeit

Studie I hatte die Analyse zum Ziel, wie robust verschiedene Methoden der Belastungsanalyse zwischen gesunden und kranken Tieren in verschiedenen Tiermodellen, nach verschiedenen Interventionen und in verschiedenen Kohorten unterscheiden können. Innerhalb dieser Arbeit wurde dabei besonderer Fokus auf das Modell des Pankreaskarzinoms gelegt. In Studie II sollte überprüft werden, ob Kombinationstherapien aus Trametinib, BKM120 und entweder Sotorasib oder BI-3406 geeignet sind, in humanen Pankreaskarzinomzelllinien mit verschiedenen mutierten *KRAS*-Allelen die Proliferation zu inhibieren und den Zelltod zu induzieren. Innerhalb der vorliegenden Arbeit wurde ein besonderer Schwerpunkt auf die Kombination BI-3406, Trametinib und BKM120 sowie auf Zelllinien mit G12D oder G12C-KRAS-Mutation gelegt. Studie III sollte Aspekte der beiden vorangegangen Studien kombinieren und einerseits evaluieren, ob sich innerhalb des Modells des Pankreaskarzinoms Unterschiede in der Belastung von männlichen und weiblichen Mäusen ergeben und andererseits, ob die in Studie II in humanen Zellen getestete Therapie in einem syngenen, orthotopen Mausmodell des Pankreaskarzinoms Wirksamkeit zeigt, zusätzliche Belastung durch Nebenwirkungen auslöst und ob sich Unterschiede in der Wirksamkeit zwischen den Geschlechtern ergeben.

IV. Methoden

Die in den jeweiligen Studien verwendeten Materialien und Methoden sind in den entsprechenden Publikationen im Anhang ab Seite 51 detailliert aufgelistet und beschrieben. Folgend sind nur die Methoden beschrieben, die für das Verständnis der in dieser Arbeit vorgestellten Ergebnisse von Bedeutung sind.

4.1 Studie I

In dieser Studie wurden keine neuen tierexperimentellen Daten generiert, sondern anhand bereits publizierter Daten verschiedene Methoden der Belastungsanalyse in unterschiedlichen Tiermodellen auf ihre Generalisierbarkeit, Robustheit und Reproduzierbarkeit untersucht.

4.1.1 Tiermodelle

Die in dieser Studie verwendeten Tiermodelle werden hier nur in Kürze beschrieben. Ausführlichere Angaben sind in der Publikation im Anhang sowie in den zugrundeliegenden Publikationen zu finden. Für die Transmitterimplantation[79] wurden männliche C57BL/6J Mäuse (Medianalter: 17,3 Wochen) in Narkose mit Isofluran laparotomiert und ein ETA-F-10 Transmitter (Data Sciences International, St. Paul, USA) in die Bauchhöhle eingesetzt. Die Elektroden wurden am großen Brustmuskel und den schrägen Bauchmuskeln mit Nähten fixiert und das Peritoneum sowie die Oberhaut mit Nähten (Johnson & Johnson Medical GmbH, Norderstedt, Deutschland) verschlossen. Die Prozedur dauerte 45 – 50 Minuten. Für das Modell des Pankreaskarzinoms[80] wurden männliche C57BL/6J Mäuse (Medianalter: 18,6 Wochen) mit Isofluran narkotisiert und anschließend laparotomiert. Es wurden 5 µL einer 6606PDA-Zellsuspension (2,5 x 10^5 Zellen) mit Hilfe einer 25 µL Spritze (Hamilton, Reno, USA) in das Pankreas injiziert. Das Abdomen wurde wie zuvor beschrieben mit Nähten verschlossen. Die Prozedur dauerte 15 – 20 Minuten. Ab Tag 4 nach Zellinjektion wurde den Tieren täglich intraperitoneal Metformin (125 mg/kg in PBS, Merck, Darmstadt, Deutschland) und α-Cyano-4-hydroxyzimtsäure (15 mg/kg in 50% DMSO, Tocris Bioscience, Bristol, UK) oder die entsprechende Vehikellösung injiziert. Für das Modell der Gallengangsligatur[81] wurden männliche BALB/cANCrl Mäuse (Medianalter: 10,9 Wochen) mit Isofluran narkotisiert und anschließend laparotomiert. Der Hauptgallengang wurde mit drei chirurgischen Knoten ligiert und zwischen den beiden distalen Ligationen durchtrennt. Das Abdomen wurde wie zuvor beschrieben mit Nähten verschlossen. Die Prozedur dauerte 25 – 40 Minuten. Den Tieren wurde einen Tag vor Gallengangsligatur bis zum Ende des Experimentes täglich der NLRP3-Inflammasom-Inhibitor MCC950 (20 mg/kg, Sigma-Aldrich, St. Louise, USA) oder die Vehikellösung (Wasser) intraperitoneal injiziert. Zur chemischen Induktion eines Leberschadens wurde männlichen BALB/cANCrl Mäusen (Medianalter: 10 Wochen) zweimal in der Woche intraperitoneal

0,25 mL/kg Tetrachlorkohlenstoff (CCl_4, Merck Millipore, Eschborn, Deutschland) injiziert. Chronische Pankreatitis[82] in männlichen C57BL/6J Mäusen (Medianalter: 15,3 Wochen) wurde durch kontinuierliche intraperitoneale Injektion (drei Injektionen im Abstand einer Stunde an drei Tagen der Woche) von Cerulein (50 µg/kg in 0,9% NaCl, Bachem, Bubendorf, Deutschland) ausgelöst und bis zum Ende des Experimentes aufrechterhalten. Der microRNA-21-Inhibitor (miRCURY LNA™ microRNA-21a-5p inhibitor; # 339203 YCO0070656, Sequenz: TCAGTCTGATAAGCT) und die entsprechende Kontrolle (miRCURY LNA™ microRNA-21a-5p control; # 339203 YCO0070657, Sequenz: TCAGTATTAGCAGCT) wurden von Qiagen (Hilden, Deutschland) gekauft, in PBS gelöst und in einer Konzentration von 10 mg/kg an Tag 0 (Beginn der Cerulein-Injektionen) und Tag 14 des Experimentes subkutan injiziert.

4.1.2 Belastungsanalyse

Die Belastung wurde anhand des Körpergewichts, des Buddelverhaltens, des Nestbauverhaltens, eines klinischen Belastungsscores und der Konzentration fäkaler Kortikosteronmetabolite evaluiert. Jeder Parameter wurde an zwei Zeitpunkten (pre 1 und pre 2) vor und direkt nach der jeweiligen Intervention (siehe Tiermodelle) evaluiert. Die jeweiligen Phasen des Experimentes (early, middle, late) richteten sich nach der Gesamtlänge des Experimentes (z.B. BDL 14 Tage versus PDAC 37 Tage). Für Details siehe Publikation im Anhang. Das Buddelverhalten wurde mithilfe einer Röhre (Länge 15 cm, Durchmesser 6,5 cm) gefüllt mit 200 g Nahrungspellets evaluiert[16,83]. Die Röhre wurde 2 – 3 h vor der Dunkelphase im Käfig platziert und die in der Röhre verbliebenen Pellets nach jeweils 2 h und 17 ± 2 h gewogen. Das Nestbauverhalten wurde mittels eines Baumwollnestlets (5 cm Quadrat aus gepresster Baumwolle, Zoonlab GmbH, Castrop-Rauxel, Deutschland) evaluiert, welches 30 – 60 Minuten vor der Dunkelphase im Käfig platziert und am nächsten Morgen (9:30 ± 2 h) ausgewertet wurde. Die Auswertung entspricht dem System von Deacon[16], erweitert um einen sechsten Auswertungspunkt: Das Nest sieht aus wie ein Krater und 90% des Umfangs des Nestes sind höher als die Körperhöhe der eingerollten Maus. Der Belastungsscore basiert auf bereits publizierten Scores[9,84] und wurde in der hier verwendeten Form bereits publiziert[80]. Innerhalb des Scores sind verschiedene Kriterien (Spontanverhalten, Fluchtverhalten, Zustand des Körpers etc.) zusammengefasst. Um die Konzentration von Kortikosteronmetaboliten im Kot zu bestimmen, wurde der Kot über 24 h im Käfig gesammelt, für 4 h bei 65 °C getrocknet und bei -20 °C gelagert. Anschließend wurden 50 mg getrockneter Kot mit 1 ml 80% Methanol extrahiert und die Konzentration mittels eines 5-pregnane-3,11,21-triol-20-one ELISA[11,85-87] bestimmt.

4.1.3 Statistik

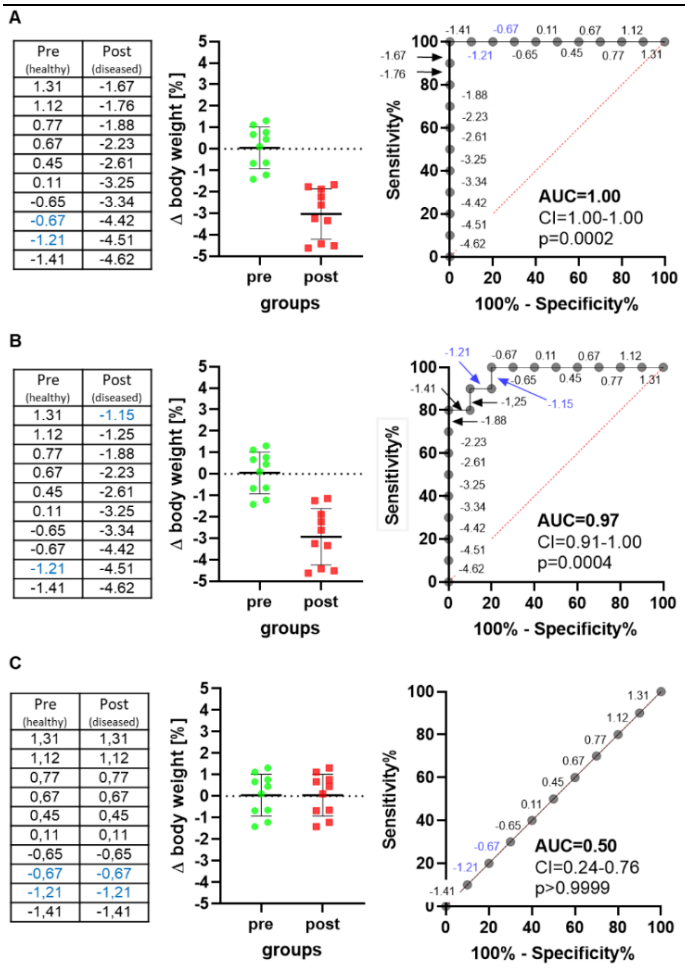

Abbildung 2: Beispiele für ROC-Kurven

Zwei fiktionale Datensätze der Veränderung des Körpergewichts von Mäusen (pre = gesund, post = krank) sollen beispielhaft der Erklärung von ROC-Analysen dienen. Das Auftragen der verschiedenen Cut-Offs (Körpergewichtsänderungen der jeweiligen Tiere) dient der Konstruktion einer ROC und der Berechnung der AUC. A: Die Veränderung des Körpergewichts lässt theoretisch eine perfekte Unterscheidung von gesunden und kranken Tieren zu (AUC = 1), da es Cut-Off Werte gibt, an denen sich die Datensätze nicht überschneiden (-1,41% bis -1,67%). B: Ein Cut-Off zwischen -1,21% und -1,15% Körpergewichtsänderung erlaubt eine Diagnose von kranken Tieren mit 90% Sensitivität (9 von 10 kranken Tieren werden erkannt) und einer Spezifität von 80% (8 von 10 Tieren werden als gesund klassifiziert). C: Da sich beide Datensätze komplett überschneiden, führt eine mit allen Cut-Offs konstruierte ROC zu einer AUC von 0,5.

Alle Graphen und die statistische Analyse wurden mit GraphPad Prism 8 (GraphPad Software Inc., San Diego, USA) erstellt bzw. durchgeführt. Um zu evaluieren, wie gut die jeweiligen Belastungsparameter zwischen gesunden und kranken Tieren unterscheiden können, wurden ROC-Kurven genutzt. ROC-Kurven setzen sich aus der Sensitivität (richtig-positive Rate) aufgetragen gegen 1 - Spezifität (falsch-positive Rate) über eine Reihe verschiedener Schwellenwerte zusammen. Die Fläche unter dieser Kurve wird als Area Under the Curve (AUC) bezeichnet. Hier wurde die AUC mit dem entsprechenden 95% Konfidenzintervall als Leistungsparameter verwendet (Abbildung 2). Eine AUC von 1 entspricht einer perfekten Unterscheidungsfähigkeit zwischen gesunden und kranken Tieren (Abbildung 2A). Der Wert der AUC kann zwischen 0,5 und 1 liegen (Abbildung 2B). 0,5 entspricht dabei keiner Unterscheidungsfähigkeit des Belastungsparameters zwischen den Datensätzen (Abbildung 2C). Zusätzlich zum Leistungsparameter der AUC enthält die Analyse einen p-Wert, welcher anzeigt, ob die jeweilige AUC sich signifikant von einer AUC von 0,5 unterscheidet. Dieser p-Wert dient als Vergleichsbasis zwischen den Parametern (siehe Ergebnisse der Studie 1).

4.2 Studie II

4.2.1 Inhibitoren

BI-3406 (KRAS:SOS1-Inhibitor, Chemietek, Indianapolis, USA), BKM120 (pan-PI3K-Inhibitor) und Trametinib (MEK1/2-Inhibitor) (beide gekauft von Absource Diagnostics GmbH, München, Deutschland) wurden in DMSO in einer Konzentration von 10 mM gelöst und bei -80 °C gelagert.

4.2.2 Zelllinien und Zellkultur

Die Zelllinie AsPC-1 wurde von der Universitätsmedizin Greifswald und die Zelllinie MIA PaCa-2 wurde von Prof. Robert Jaster (Universitätsmedizin Rostock) zur Verfügung gestellt. Die AsPC-1-Zellen wurden in RPMI1640 Medium (PAN Biotech GmbH, Aidenbach, Deutschland) mit 10% FCS und 1% Penicillin-Streptomycin-Lösung (P/S, 10000 U/mL, 10 mg/mL; PAN Biotech GmbH) kultiviert. MIA PaCa-2-Zellen wurden in DMEM (PAN Biotech GmbH) mit 10% FCS und 1% P/S kultiviert.

4.2.3 Assays

Die Zellen wurden nach Zugabe der Inhibitoren für 72 h bei 37 °C und 5% CO_2 inkubiert.

Tabelle 1: Verwendete Konzentrationen für kombinierte Inhibitor-Applikation

Zelllinie	BI-3406 [µM]	Trametinib [µM]	BKM120 [µM]
AsPC-1	4	0,001	0,3
MIA PaCa-2	4	0,0025	0,6

4.2.3.1 Proliferation

Die Analyse der Zellproliferation wurde mithilfe einer Trypanblau (Sigma-Aldrich Chemie GmbH, Steinheim, Deutschland) Färbung durchgeführt. Die Zellen wurden in einer Konzentration von 3,3 x 10^4 Zellen/mL in 24-Well Platten ausgesät (1,5 mL pro Well). Die Inhibitoren wurden in den Konzentrationen aus Tabelle 1 hinzugegeben und die Zellen 72 h nach Inkubation mittels Zählkammer gezählt. Die mit DMSO behandelte Kontrollgruppe entspricht 100%.

4.2.3.2 Quantifizierung der Biomasse

Die Analyse der Biomasse der Zellen wurde mittels Kristallviolett (KV) Färbung durchgeführt. Die Zellen wurden in einer Konzentration von 3,3 x 10^4 Zellen/mL in 96-Well Platten ausgesät (150 µL pro Well). Die Zugabe der Inhibitoren und die Inkubation erfolgten analog zur Analyse der Proliferation. Nach Inkubation mit den Inhibitoren wurden die Zellen mit PBS gewaschen

und mit 0,2% KV-Lösung für 10 Minuten auf einem Schüttler bei Raumtemperatur (RT) inkubiert. Die Zellen wurden zweimal mit PBS gewaschen, es wurde 1% SDS-Lösung hinzugegeben und 10 Minuten bei RT inkubiert. Die Absorption bei 570 nm wurde auf einem Promega GloMax®-Multi Microplate Multimode Reader gemessen. Die mit DMSO behandelte Kontrollgruppe entspricht 100%.

4.2.3.3 Apoptose und Nekrose

Die Apoptose und Nekrose der Zellen wurden mittels Durchflusszytometrie mit Annexin-V-FITC (BD GmbH, Heidelberg, Deutschland) und Propidiumiodid (PI, Sigma-Aldrich Chemie GmbH) analysiert. Die Zellen wurden nach der Behandlung mit den Inhibitoren und dem DMSO-Vehikel geerntet und gewaschen. Anschließend wurden die Zellen mit Annexin-V-FITC (5 µL für 15 Minuten bei RT) und PI (20 µg/mL direkt vor der Messung) inkubiert und mit einem FACSVerse™ (BD GmbH) Durchflusszytometer gemessen. Annexin-V-/PI- Zellen wurden als vital, Annexin-V+/PI- Zellen als frühe apoptotische Zellen und Annexin-V+/PI+ Zellen als späte apoptotische/nekrotische Zellen betrachtet. Die Daten wurden mit der BD FlowJo™ Software (BD GmbH) analysiert.

4.2.3.4 Evaluation der Inhibitor-Kombinationen

Die Wechselwirkung zwischen den Inhibitoren wurde anhand des Bliss-independent-Modells bewertet. Die Wechselwirkung der Hemmstoffkombination wurde anhand der Differenz zwischen der beobachteten (E_O) und vorhergesagten (E_P) Hemmung der Kombinationstherapie bestimmt. Bei der Anwendung von zwei Inhibitoren wurde E_P mit der folgenden Gleichung berechnet: $E_P = E_A + E_B - E_A \times E_B$, wobei E_A und E_B die relative Hemmung der Einzelinhibitoren A und B sind. Bei der Anwendung von drei Inhibitoren wurde E_P mit der folgenden Gleichung berechnet: $E_P = E_A + E_B + E_C - E_A \times E_B - E_A \times E_C - E_B \times E_C - E_A \times E_B \times E_C$, wobei E_A, E_B und E_C die relative Hemmung der Einzelinhibitoren A, B und C sind. $E_O > E_P$ deutet auf eine synergistische Wirkung hin, $E_O = E_P$ auf eine additive Wirkung und $E_O < E_P$ deutet auf eine antagonistische Wirkung hin. Die Bliss-Werte für die Inhibitor-Kombinationen wurden auf der Grundlage der Ergebnisse der Proliferation und Quantifizierung der Biomasse berechnet.

4.2.4 Statistik

Jedes Experiment wurde in mindestens 3 biologisch unabhängigen Wiederholungen durchgeführt. Die Ergebnisse der Proliferationsanalyse, der Quantifizierung der Biomasse und der Analyse der Apoptose/Nekrose wurden als Mittelwert ± Standardabweichung (SD) angegeben.

Die statistische Signifikanz wurde mittels einfaktorieller ANOVA oder Kruskal-Wallis-Test (jeweils nach einem Test auf Normalverteilung) analysiert und wie folgt dargestellt: *: $p < 0,033$, **: $p < 0,002$, ***: $p < 0,001$.

4.3 Studie III

4.3.1 Inhibitoren

BI-3406 wurde von Boehringer Ingelheim (Ingelheim am Rhein, Deutschland) über das opnMe Innovationsportal zur Verfügung gestellt. Trametinib und BKM120 wurden von Chemietek gekauft. Für *in vitro* Untersuchungen wurden alle Inhibitoren in DMSO gelöst und in den angegeben Konzentrationen verwendet. Für *in vivo* Untersuchungen wurden die Inhibitoren in einer Mischung aus 60% Phosal50PG (Lipoid GmbH, Ludwigshafen, Deutschland), 30% PEG400 (Merck KGaA) und 10% Ethanol (99,6%, unvergällt) gelöst.

4.3.2 Zelllinie und Zellkultur

Die 6606PDA-Zelllinie war ein freundliches Geschenk von Prof. Tuveson (Cold Spring Harbor Laboratory, USA)[88]. Die Zellen wurden in DMEM (4,5 g/L Glucose, PAN Biotech GmbH) mit 10 % fetalem Kälberserum (FCS, PAN Biotech GmbH) und Penicillin/Streptomycin (100 U/ml, PAN Biotech GmbH) kultiviert.

4.3.3 Assays

Die Zellen wurden nach Zugabe der Inhibitoren für 48 h bei 37 °C und 5% CO_2 inkubiert.

4.3.3.1 Proliferation

Zur Evaluation der Zellproliferation wurden 6606PDA-Zellen in einer Dichte von 2 x 10^3 Zellen in 96-Well Platten (Greiner Bio-One GmbH, Frickenhausen, Deutschland) ausgesät und 5-Brom-2'-Deoxyuridin (BrdU, Merck KGaA, Darmstadt, Deutschland) hinzugegeben. Die Quantifizierung erfolgte mit einem kolorimetrischen Zellproliferations-ELISA-Kit (Roche Diagnostics, Mannheim, Deutschland) gemäß den Empfehlungen des Herstellers. Die Absorption wurde bei 450 nm mit einem Perkin Elmer Victor X3 Modell 2030 Multilabel Plate Reader (PerkinElmer, Waltham, USA) gemessen.

4.3.3.2 Apoptose und Nekrose

6606PDA-Zellen wurden in einer Dichte von 3 x 10^4 Zellen in 12-Well Platten (Greiner Bio-One GmbH) ausgesät und Apoptose und Nekrose wurden analog zu Studie II analysiert.

4.3.3.3 Evaluation der Inhibitor-Kombinationen

Die Wechselwirkung zwischen den Inhibitoren wurde wie in Studie II evaluiert.

4.3.4 PDAC-Tiermodell und Therapie

Die orthotope Zellinjektion wurde wie in Studie I beschrieben vorgenommen. Anders als in Studie I wurden hier sowohl männliche als auch weibliche C57BL/6J Mäuse verwendet (zwischen 16 und 23 Wochen alt) und es wurden jedem Tier zusätzlich 50 µL einer 6606PDA-Zellsuspension (in HBSS, PAN Biotech GmbH) mit einer Konzentration von 7 x 10^6 Zellen/mL intravenös mittels eines Katheters ((0.28 mm ID, 0.61 mm OD), Smiths Medical International Ltd., Hythe, UK) in die laterale Schwanzvene injiziert. An Tag 4 nach Operation wurden die Tiere in Behandlungsgruppen randomisiert (Vehikel oder eine Kombination aus BI-3406, Trametinib und BKM120). Die Testsubstanzen und das Vehikel wurden vom 4. Tag bis zur Euthanasie am 36. Tag über eine orale Schlundsonde an 5 Tagen der Woche verabreicht. Die pro Schlündelung verabreichten Wirkstoffkonzentrationen waren: BI-3406 in einer Konzentration von 50 mg/kg (2 x pro Tag), Trametinib in einer Konzentration von 0,1 mg/kg (2 x pro Tag) und BKM120 in einer Konzentration von 30 mg/kg (1 x pro Tag). An Tag 36 nach der Injektion der Tumorzellen wurden die Mäuse ein letztes Mal geschlündelt und BrdU (2,5 µL/g Körpergewicht, 20 mg/mL) 1,5 – 2 Stunden vor der Euthanasie durch zervikale Dislokation in tiefer Narkose (4 – 5 Vol.-% Isofluran) intraperitoneal injiziert. Tumore, Lungen und Lebern wurden entnommen und entweder in 4 % PBS-gepuffertem Paraformaldehyd (PFA, Formafix GmbH, Düsseldorf, Deutschland) oder in flüssigem Stickstoff konserviert.

4.3.5 Belastungsanalyse

Die Analyse der Belastung erfolgte wie bereits für Studie I beschrieben.

4.3.6 Statistik

Alle Daten wurden mit GraphPad Prism 8 (GraphPad Software Inc.) analysiert und als Box-Plot (einzelne Datenpunkte, Whisker zeigen Minimum und Maximum) oder als Balkendiagramm dargestellt. Die Überlebenswahrscheinlichkeit wurde mittels Kaplan-Meier-Schätzer evaluiert. Die statistische Signifikanz wurde je nach Anzahl der unabhängigen Variablen und den Datenmerkmalen mit unterschiedlichen Methoden ermittelt. Einzelheiten sind in den Abbildungslegenden der Abbildungen 5 – 7 im Ergebnisteil der Studie III und der entsprechenden Publikation zu finden. Unterschiede mit $p < 0,05$ wurden als signifikant angesehen.

V. Ergebnisse

5.1 Studie I

Ziel dieser Studie war es, mittels ROC-Kurven zu evaluieren, wie gut verschiedene Methoden der Belastungsanalyse zwischen gesunden und kranken Tieren (nach einer chirurgischen Intervention oder Induktion einer gastrointestinalen Erkrankung) unterscheiden können. Gleichzeitig wurde die Generalisierbarkeit, Robustheit und Reproduzierbarkeit der Methoden und der daraus resultierenden Interpretationen betrachtet. Besonderer Fokus soll hier auf dem Modell des Pankreaskarzinoms liegen.

Die Veränderung des Körpergewichts nach Implantation eines Transmitters soll als Beispiel für die Unterscheidungsfähigkeit zwischen gesunden und kranken Tieren dienen (Abbildung 3A – C). Der Vergleich des Körpergewichts zwischen einem Zeitpunkt vor der Transmitterimplantation (pre 1) mit dem Tag direkt danach (post) zeigt, dass die Tiere Gewicht verlieren (Abbildung 3A) und die mit diesen Daten generierte ROC-Kurve (AUC 0,90, 0,75 – 1,00 95% KI) eine signifikant bessere Unterscheidung ermöglicht, als es eine Methode mit einer AUC von 0,50 würde ($p = 0,0028$). Bei Veränderung der Ausgangsdaten (pre 2) bleibt diese Schlussfolgerung bestehen (Abbildung 3B). Eine Darstellung der Körpergewichtsveränderung als prozentuale Veränderung nach dem Eingriff (post) verglichen mit der Veränderung zwischen den beiden Basistagen ((pre 1 – pre 2) x 100/pre 2) ermöglicht eine noch bessere Unterscheidung beider Datensätze und damit eine AUC von 1,00 (perfekte Unterscheidungsfähigkeit) mit einem p-Wert von 0,0002 (Abbildung 3C).
Um die verschiedenen Methoden der Belastungsanalyse (Körpergewicht (BW), Buddeln (B), Nestbauverhalten (N), Belastungsscore (DSC) und FCM) miteinander vergleichen zu können, wurden die p-Werte in einer Heatmap dargestellt (Abbildung 3D – F). Nur zwei Methoden (Körpergewicht und FCM) waren in der Lage, Tiere vor und nach orthotoper Injektion von 6606PDA-Zellen in das Pankreas zu unterscheiden (Abbildung 3D, roter Rahmen). Zur Überprüfung, wie replizierbar diese Erkenntnis ist, wurden die Methoden zur Belastungsanalyse in zwei Kohorten von Tieren untersucht, die zu einem späteren Zeitpunkt verschiedene Therapien erhalten haben (Abbildung 3E). Die Ergebnisse in beiden Gruppen waren annähernd identisch und die Methoden innerhalb dieses Modells damit als replizierbar anzusehen. Um zu evaluieren, ob kranke und gesunde Tiere über die Progression des Pankreaskarzinommodells hinweg unterschieden werden können, wurden die verschiedenen Methoden in der frühen, mittleren und späten Phase mit dem jeweiligen Wert vor Zellinjektion verglichen (Abbildung 3F). Anhand der prozentualen Veränderung des Körpergewichts konnte zwischen Tieren vor Zellinjektion und in der mittleren und späten Phase des Krankheitsverlaufs unterschieden werden, in der frühen Phase nur anhand des Buddelverhaltens (Abbildung 3F, roter Rahmen).

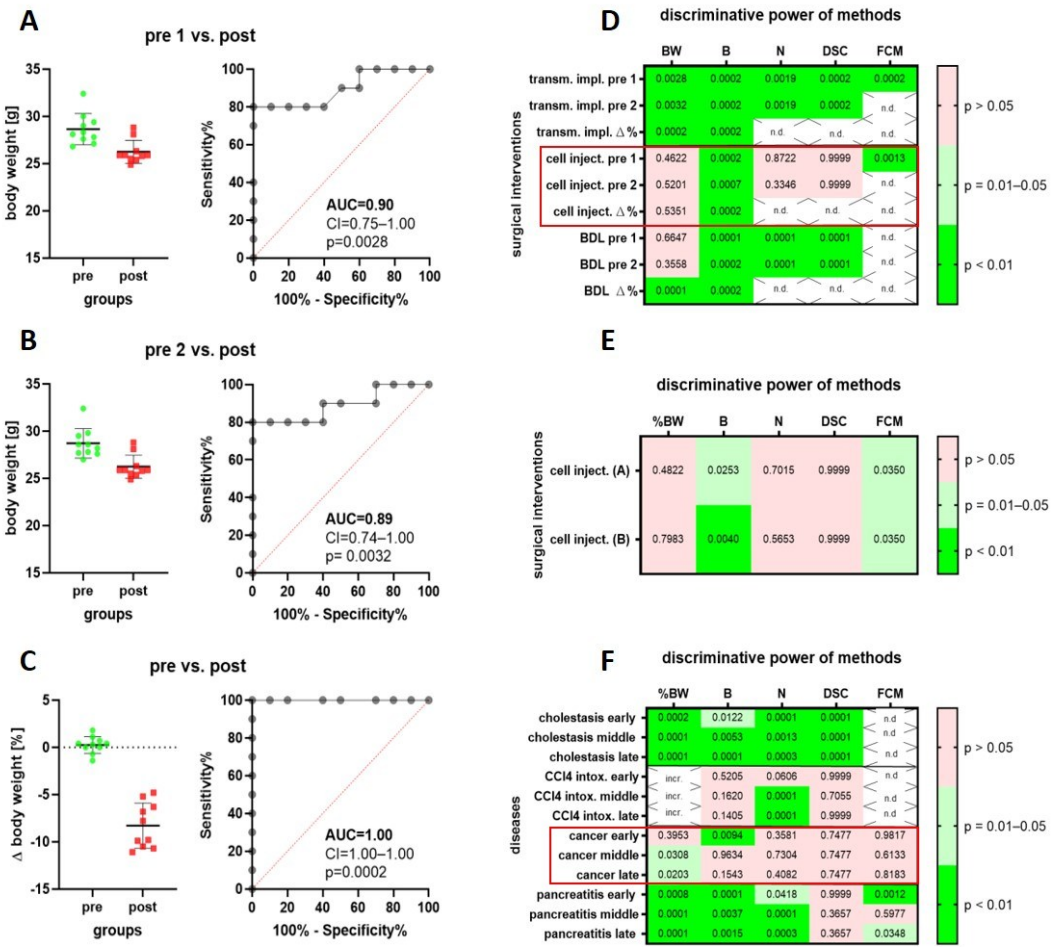

Abbildung 3: ROC-Kurven als Instrument zur Einschätzung der Diskriminierungsfähigkeit von Methoden der Belastungsanalyse

Streudiagramme und ROC-Kurven beschreiben die Veränderungen des Körpergewichts von Mäusen nach der Implantation eines Transmitters (A – C). Die ROC-Kurven wurden durch Auftragen der Sensitivität (richtig-positive Rate) gegen 1 - Spezifität (falsch-positive Rate) generiert. Das Körpergewicht einen Tag nach der Implantation (post) wird verglichen mit dem Körpergewicht 5 Tage vor der Implantation, dargestellt als Zeitpunkt pre 1 (A), oder mit dem Körpergewicht 2 Tage vor der Implantation, dargestellt als Zeitpunkt pre 2 (B). Die prozentuale Körpergewichtsänderung zwischen den beiden Tagen vor der Implantation wird mit der prozentualen Körpergewichtsänderung zwischen dem postoperativen Tag und dem Zeitpunkt pre 1 verglichen (C). Evaluation der Unterscheidungsfähigkeit der Methode zwischen Tieren vor und nach der Implantation eines Transmitters anhand der Fläche unter der Kurve (AUC), des Konfidenzintervalls (CI) und des p-Wertes, der angibt, wie signifikant der Unterschied zur Referenzlinie (rote gestrichelte Linie, keine Unterscheidungskraft) ist. N = 10 Mäuse. D: p-Werte zeigen an, wie signifikant unterschiedlich zu einer AUC von 0,5 (keine Unterscheidungskraft) die jeweiligen Belastungsparameter (BW = Körpergewicht, B = Buddelverhalten, N = Nestbauverhalten, DSC = Belastungsscore, FCM = fäkale Kortikosteronmetabolite) zwischen Tieren vor und nach Injektion von Pankreaskarzinomzellen unterscheiden können (roter Rahmen = C57Bl/6J Mäuse vor und nach Injektion von Pankreaskarzinomzellen, N = 14). E: Reproduzierbarkeit und Robustheit der Unterscheidungsfähigkeit der einzelnen Methoden der Belastungseinschätzung. Beiden Gruppen (A und B) wurden 6606PDA-Zellen orthotop injiziert und zu einem späteren Zeitpunkt erfolgte eine Behandlung entweder mit Vehikel (N = 7) oder CHC + Met (N = 7). F: p-Werte zeigen an, wie signifikant unterschiedlich zu einer AUC von 0,5 (keine Unterscheidungskraft) die jeweiligen Belastungsparameter zwischen Tieren vor Injektion von Pankreaskarzinomzellen und während der einzelnen Phasen des Experimentes (früh, mittel, spät) unterscheiden können (roter Rahmen, N = 14 Mäuse).

5.2 Studie II

In dieser Studie wurden der SOS1:KRAS-Inhibitor BI-3406 und der KRAS-G12C-Inhibitor Sotorasib in verschiedenen Konzentrationen sowie in Kombination mit Buparlisib (BKM120) und Trametinib in humanen Pankreaskarzinomzelllinien mit verschiedenen Mutationen getestet. Hier wird im Detail nur auf Kombinationen mit BI-3406 und Zelllinien mit KRAS-G12D bzw. G12C-Mutation (AsPC-1 und MIA PaCa-2) eingegangen.

BI-3406 allein erzielte selbst in der höchsten getesteten Konzentration von 10 µM nur einen maximalen inhibitorischen Effekt von 50% bezogen auf Proliferation und Biomasse der verschiedenen Zelllinien (Abbildung 4A). Die Kombination von BI-3406 mit BKM120 oder Trametinib führte zu signifikant verringerter Proliferation und Biomasse in AsPC-1-Zellen verglichen mit der DMSO-Kontrolle (Abbildung 4B). Die Dreifachkombination aus BI-3406, BKM120 und Trametinib wirkte dabei signifkant besser als jegliche Zweifachkombination (Abbildung 4B). Für alle getesteten Kombinationen konnte ein synergistischer Effekt festgestellt werden. Die Dreifachkombination wirkte ebenso besser als jegliche Zweifachkombination in der Induktion von Apoptose und Nekrose in AsPC-1-Zellen (Abbildung 4C). In MIA PaCa-2-Zellen zeigte sich ein vergleichbares Bild. Die Zweifachkombinationen aus BI-3406 und BKM120 oder Trametinib verringerten Proliferation und Biomasse der Zellen signifikant gegenüber der Kontrolle (Abbildung 4D). Die Dreifachkombination erzielte auch hier signifikant verringerte Proliferation und Biomasse verglichen mit den Zweifachkombinationen (Abbildung 4D). Ebenso konnte ein synergistischer Effekt aller getesteten Kombinationen festgestellt werden. In der Induktion des Zelltodes war die Dreifachkombination auch in dieser Zelllinie signifikant besser als jegliche Zweifachkombination (Abbildung 4E).

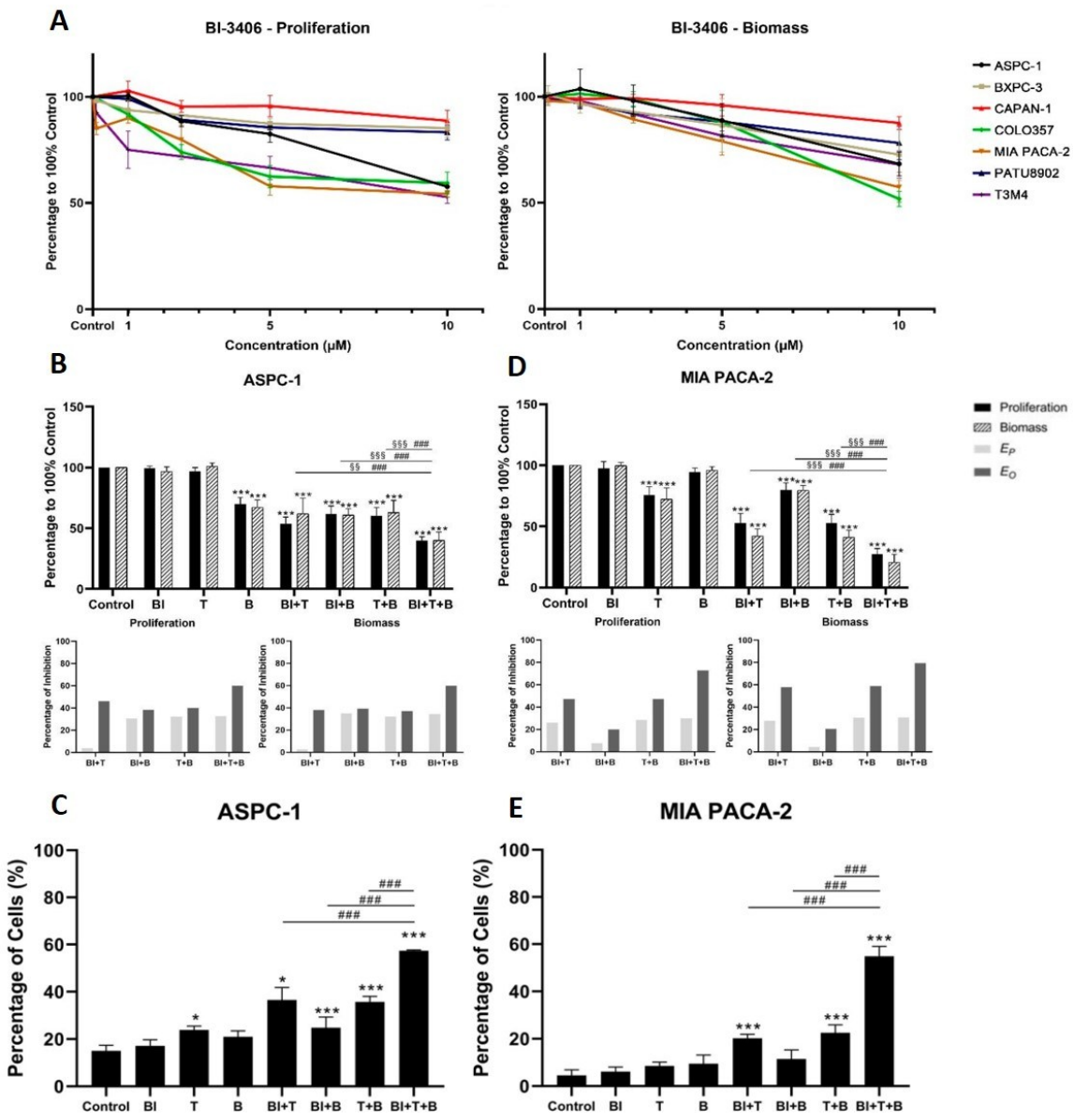

Abbildung 4: Inhibition von Proliferation und Induktion von Zelltod durch BI-3406 allein und in Kombination
A: Änderung der Proliferationsrate und Biomasse in verschiedenen humanen PDAC-Zelllinien durch Exposition mit verschiedenen Konzentrationen von BI-3406. B: Proliferation und Biomasse von AsPC-1-Zellen 72 h nach Zugabe von 4 µM BI-3406, 0,001 µM Trametinib und 0,3 µM BKM120 allein oder in Kombination und Analyse des Synergismus mittels Bliss-independent-Modell. C: Analyse des Zelltodes (Apoptose + Nekrose) in AsPC-1-Zellen 72 h nach Zugabe von 4 µM BI-3406, 0,001 µM Trametinib und 0,3 µM BKM120 allein oder in Kombination. D: Proliferation und Biomasse von MIA PaCa-2-Zellen 72 h nach Zugabe von 4 µM BI-3406, 0,0025 µM Trametinib und 0,6 µM BKM120 allein oder in Kombination und Analyse des Synergismus mittels Bliss-independent-Modell. E: Analyse des Zelltodes (Apoptose + Nekrose) in MIA PaCa-2-Zellen 72 h nach Zugabe von 4 µM BI-3406, 0,0025 µM Trametinib und 0,6 µM BKM120 allein oder in Kombination. N = mind. 3 unabhängige biologische Replikate. Die Daten sind als Mittelwert ± Standardabweichung (SD) angegeben. Die Signifikanz eines Behandlungseffekts im Vergleich zur DMSO-Kontrolle wurde mittels einfaktorieller ANOVA bestimmt und als *: $p < 0,033$, **: $p < 0,002$, ***: $p < 0,001$ dargestellt. Die Signifikanz des Behandlungseffektes für zwei Inhibitoren im Vergleich zu drei Inhibitoren wurde durch einfaktorielle ANOVA bestimmt und als # (Proliferation), § (Biomasse): $p < 0,033$; ##, §§: $p < 0,002$, ###; §§§: $p < 0,001$ dargestellt. BI: BI-3406; T: Trametinib; B: BKM120; E_P: vorhergesagter Effekt durch das Bliss-independent-Modell; E_O: beobachteter Effekt.

5.3 Studie III

Die in Studie II *in vitro* getestete Kombination aus BI-3406, Trametinib und BKM120 wurde in dieser Studie in einem syngenen, orthotopen und metastasierten Modell des Pankreaskarzinoms in weiblichen und männlichen Mäusen C57BL/6J getestet.

Zunächst wurden die Unterschiede zwischen Männchen und Weibchen ohne therapeutische Intervention (Vehikelgruppe) evaluiert. Männliche Mäuse hatten eine signifikant geringere Überlebenswahrscheinlichkeit als weibliche (Abbildung 5A). Das Tumorgewicht 36 Tage nach Tumorzellinjektion war in Weibchen signifikant geringer als in Männchen (Abbildung 5B), obwohl es keinen Unterschied in der Proliferation der Tumorzellen zwischen den Geschlechtern gab (Abbildung 5C). Die Anzahl CD8-positiver Zellen im Tumor war in Weibchen signifikant höher als in Männchen (Abbildung 5D).

In den Belastungsparametern Körpergewicht, Buddeln und dem Belastungsscore ergaben sich signifikante Unterschiede zwischen Männchen und Weibchen in der späten Phase des Experimentes (Abbildung 5E – G). Das Körpergewicht der männlichen Tiere war am Ende des Experimentes signifikant gegenüber dem der Weibchen verringert (Abbildung 5E). Ebenso war das Buddelverhalten der männlichen Tiere signifikant gegenüber dem der weiblichen Tiere verringert (Abbildung 5F). Der Belastungsscore in männlichen Mäusen war signifikant erhöht im Vergleich zu weiblichen Mäusen in der späten Phase (Abbildung 5G). Das Nestbauverhalten und die Konzentration fäkaler Kortikosteronmetabolite unterschieden sich hingegen nicht signifikant zwischen den Geschlechtern (Abbildung 5H – I).

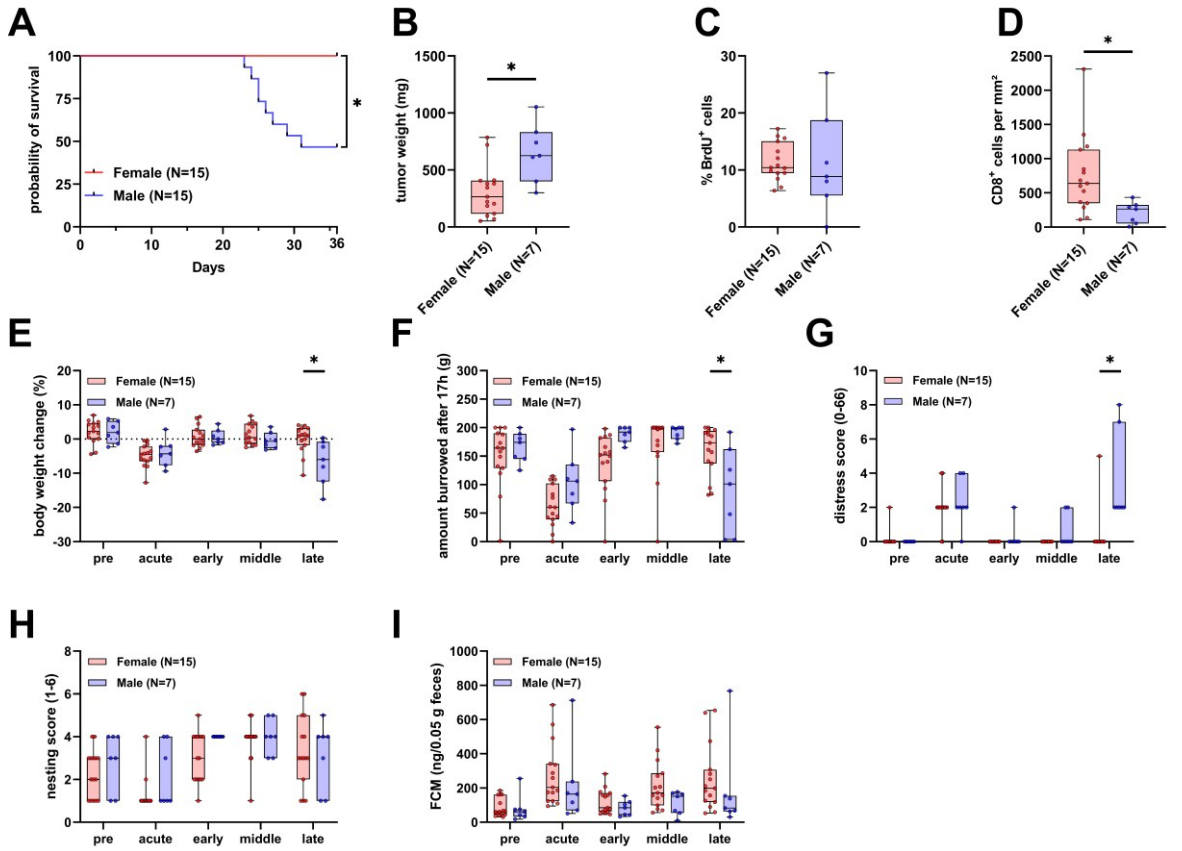

Abbildung 5: Unterschiede in Überlebenswahrscheinlichkeit, Tumorgewicht, -proliferation und -infiltration sowie Belastung zwischen Männchen und Weibchen im PDAC-Modell

A: Überlebenswahrscheinlichkeit von Weibchen und Männchen (Kaplan-Meier-Schätzer und Log-Rang Mantel-Cox-Test, * $p < 0,05$). B: Tumorgewicht überlebender weiblicher und männlicher Tiere 36 Tage nach 6606PDA-Zellinjektion (t-Test für unabhängige Stichproben mit Welch-Korrektur, * $p < 0,05$). C: Vergleich der Tumorzellproliferation in überlebenden weiblichen und männlichen Tieren 36 Tage nach 6606PDA-Zellinjektion (t-Test für unabhängige Stichproben mit Welch-Korrektur, NS). D: Vergleich CD8α-positiver Zellen in überlebenden weiblichen und männlichen Tieren 36 Tage nach 6606PDA-Zellinjektion (Mann-Whitney-Test, * $p < 0,05$). E – I: Körpergewichtsänderung (E), Buddelverhalten (F), Belastungsscore (G), Nestbauverhalten (H) und fäkale Kortikosteronmetabolite (I)verglichen zwischen überlebenden weiblichen und männlichen Tieren (zweifaktorielle ANOVA mit Messwiederholung und Sidak-Post-hoc-Test, * $p < 0,05$). Prä, akute, frühe, mittlere und späte Phase entsprechen den Phasen des Experimentes. Details der Methodik sind der Publikation zu entnehmen.

Die Wirkung der in Studie II erfolgreich an humanen Zelllinien getesteten Dreifachtherapie sollte in dieser Studie anhand der für die Tumorinduktion verwendeten, murinen Zelllinie 6606PDA (KRAS-G12D-Mutation) verifiziert werden. Die verwendeten Konzentrationen (BI-3406: 10 µM, Trametinib: 0,064 µM, BKM120: 1 µM) entsprachen gerundet der halben IC_{50} für die Inhibition der Proliferation der einzelnen Verbindungen (Fig. S4, Studie III[89]). Im Vergleich zur DMSO-Kontrolle, den einzelnen Therapeutika und den Zweifachkombinationen verringerte die Dreifachtherapie die Proliferation der Zellen signifikant mehr (Abbildung 6A). Für alle getesteten Kombinationen konnten synergistische Effekte in der Inhibition der Proliferation festgestellt werden (Abbildung 6B). Die Dreifachkombination induzierte signifikant mehr Zelltod als die DMSO-Kontrolle, die einzelnen Therapeutika und die Kombination aus BI-3406 und BKM120 (Abbildung 6C). Auch für die Induktion des Zelltodes konnten für alle Kombinationen synergistische Effekte festgestellt werden (Abbildung 6D).

Nach erfolgreicher *in vitro* Evaluation wurde die Dreifachtherapie *in vivo* in weiblichen und männlichen C57BL/6J-Mäusen getestet, welchen orthotop und intravenös murine 6606PDA-Pankreaskarzinomzellen injiziert wurden. Den Tieren wurde täglich, außer am Wochenende, zweimal BI-3406 und Trametinib sowie einmal BKM120 oder ausschließlich die Vehikellösung per Schlundsonde verabreicht.
Weder in weiblichen noch in männlichen Tieren konnte bis zum Ende des Experimentes eine signifikante Verbesserung der Überlebenswahrscheinlichkeit durch die Therapie erreicht werden (Abbildung 7A – B). In weiblichen Tieren erreichte die Therapie keine signifikante Veränderung des Tumorgewichtes verglichen mit der Vehikelgruppe (Abbildung 7C), während das Tumorgewicht in männlichen mit der Therapie behandelten Tieren signifikant verringert war (Abbildung 7D). Die auf das durchschnittliche Tumorgewicht mit Vehikel behandelter Tiere des jeweiligen Geschlechts normalisierte Therapieeffektivität war signifikant höher in Männchen als in Weibchen (Abbildung 7E). Auf die Proliferation der Tumorzellen hatte die Therapie weder in Weibchen noch in Männchen einen signifikanten Einfluss (Abbildung 7F – G). Die Anzahl der CD8-positiven Zellen im Tumor wurde in Weibchen durch die Therapie signifikant negativ beeinflusst (Abbildung 7H), während in Männchen keine signifikante Änderung beobachtet wurde (Abbildung 7I).

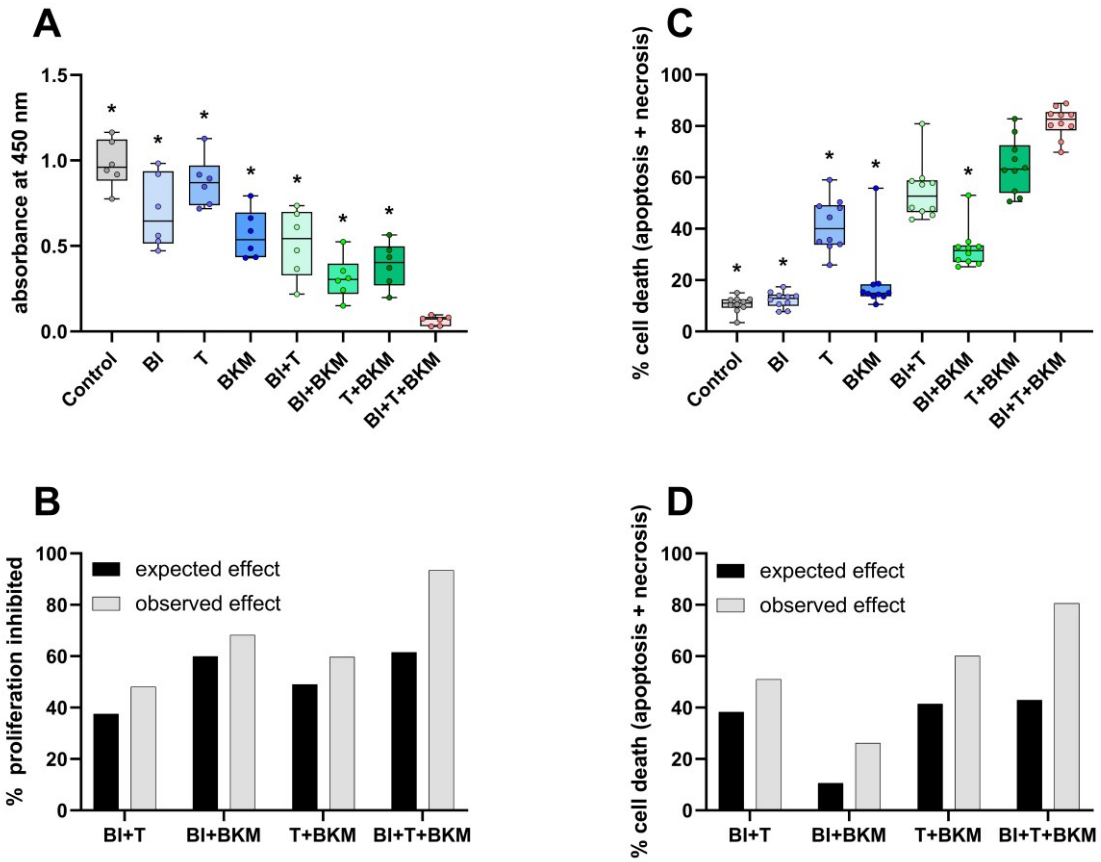

Abbildung 6: Inhibition von Proliferation und Induktion von Zelltod durch BI-3406 allein und in Kombination in 6606PDA-Zellen

A: Änderung der Proliferationsrate von 6606PDA-Zellen nach 48 h Inkubation mit 10 µM BI-3406 (BI), 0,064 µM Trametinib (T) und 1 µM BKM120 (BKM) einzeln oder in Kombination (N = 6, Vergleich mit Dreifachkombination, einfaktorielle ANOVA mit Dunnet-Post-hoc-Test, * $p < 0,05$). B: Analyse der Synergie der drei Therapeutika in der Inhibition der Proliferation mit dem Bliss-independent-Modell. C: Induktion des Zelltodes von 6606PDA-Zellen nach 48 h Inkubation mit 10 µM BI-3406 (BI), 0,064 µM Trametinib (T) und 1 µM BKM120 (BKM) einzeln oder in Kombination (N = 10, Vergleich mit Dreifachkombination, Kruskal-Wallis-Test mit Dunn-Post-hoc-Test, * $p < 0,05$). D: Analyse der Synergie der drei Therapeutika in der Induktion des Zelltodes mit dem Bliss-independent-Modell.

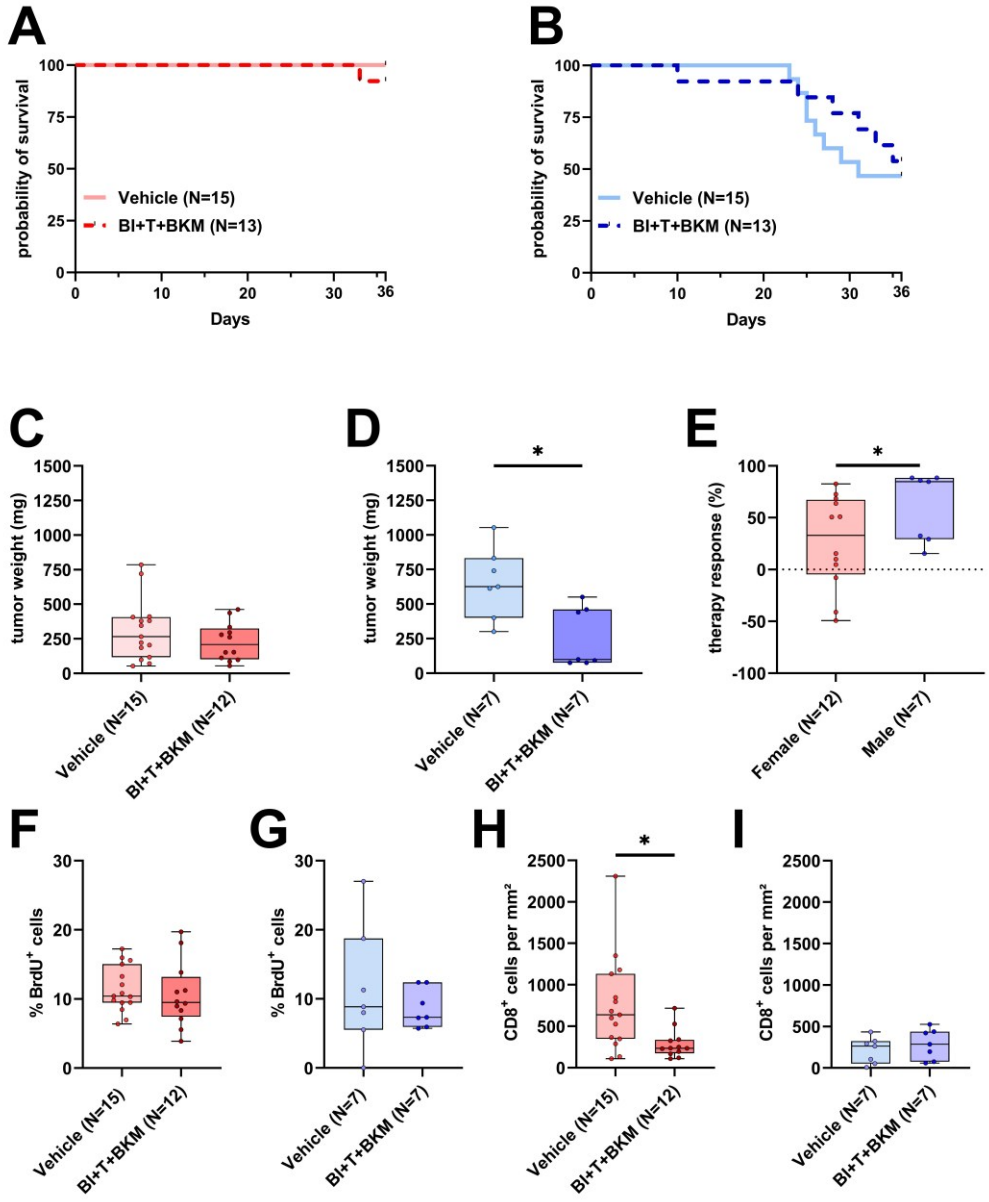

Abbildung 7: *in vivo* Effekte der Dreifachtherapie (BI-3406, Trametinib, BKM120) im Vergleich zum Vehikel in männlichen und weiblichen Mäusen

A, B: Überlebenswahrscheinlichkeit von weiblichen (A) und männlichen (B) Tieren, die entweder eine Dreifachtherapie aus BI-3406, Trametinib und BKM120 oder Vehikellösung erhalten haben (Kaplan-Meier-Schätzer und Log-Rang Mantel-Cox-Test, NS). C, D: Tumorgewicht in weiblichen (C) und männlichen (D) Tieren, die entweder eine Dreifachtherapie aus BI-3406, Trametinib und BKM120 oder Vehikellösung erhalten haben (C: t-Test für unabhängige Stichproben, NS; D: Mann-Whitney-Test, * $p < 0,05$). E: Ansprechen der Therapie als auf das durchschnittliche Tumorgewicht der mit Vehikel behandelten Tiere des gleichen Geschlechts normalisierter Quotient in Prozent, verglichen zwischen Weibchen und Männchen (Mann-Whitney-Test, * $p < 0,05$). F, G: Tumorzellproliferation in weiblichen (F) und männlichen (G) Tieren, die entweder eine Dreifachtherapie aus BI-3406, Trametinib und BKM120 oder Vehikellösung erhalten haben (t-Test für unabhängige Stichproben, NS). H, I: CD8α-positive Zellen in weiblichen (H) und männlichen (I) Tieren, die entweder eine Dreifachtherapie aus BI-3406, Trametinib und BKM120 oder Vehikellösung erhalten haben (H: Mann-Whitney-Test, * $p < 0,05$, I: t-Test für unabhängige Stichproben, NS).

VI. Diskussion

6.1 Belastung im Modell des Pankreaskarzinoms und durch therapeutische Intervention

Experimentelle Prozeduren sind belastend für Labortiere[90]. Diese Belastung kann sich negativ auf das Ergebnis und die Validität wissenschaftlicher Studien auswirken[91,92]. Refinement, das Verbessern experimenteller Prozeduren in tierexperimentellen Studien, steht als eine der drei grundlegenden Säulen des 3R-Prinzips dafür, die Belastung von Tieren während dieser experimentellen Studien zu minimieren. Das setzt voraus, dass die Belastung von Tieren in Versuchen verlässlich evaluiert werden kann.

Im Rahmen dieser Arbeit wurde in Studie I untersucht, inwieweit verschiedene Methoden der Belastungsanalyse geeignet sind, um in einem syngenen, orthotopen Modell des Pankreaskarzinoms Tiere vor und nach Induktion des Tiermodells zu unterscheiden. Desweiteren wurde in Studie III die Frage beantwortet, ob männliche und weibliche Tiere innerhalb des Modells unterschiedliche Belastung erfahren. In den Studien I und III wurde ebenfalls evaluiert, ob Methoden der Belastungsanalyse geeignet sind, Tiere vor und nach Induktion des Modells mit und ohne Therapie zu unterscheiden und ob es Unterschiede in der Belastung zwischen Tieren mit und ohne Therapie gibt.

Bezogen auf das Modell des Pankreaskarzinoms zeigte sich in Studie I, dass nur wenige Methoden geeignet sind, um Tiere vor und nach Injektion von Karzinomzellen zu unterscheiden. Die Analyse des Buddelverhaltens sowie die Analyse der FCM waren geeignet, um Tiere vor und direkt nach Induktion des Modells zu unterscheiden. Eine Erklärung dafür, warum andere Methoden in der Unterscheidung scheiterten, kann sein, dass die Injektion von Karzinomzellen rein als Intervention keine Belastung auslöst, die mit Methoden wie der Analyse des Körpergewichts, dem Nestbauverhalten oder dem klinischen Belastungsscore gemessen werden kann. Ebenso kann ein Einfluss der perioperativen Analgesie angenommen werden. Besonders für den Parameter des Buddelverhaltens hat sich gezeigt, dass perioperative Analgesie das Buddelverhalten nach Laparotomie verbessern kann[93]. Im Vergleich mit zum Beispiel der Implantation eines Transmitters zeigt sich, dass jegliche Methode geeignet ist, Tiere vor und direkt nach der Implantation anhand der akuten Belastung zu unterscheiden. Die Implantation eines Transmitters nimmt deutlich mehr Zeit in Anspruch und führt sehr wahrscheinlich auch nach dem Eingriff zu reduziertem Wohlergehen, da der Transmitter ein erhebliches Volumen im Bauchraum einnimmt. Dies wird umso deutlicher, wenn man die Belastung, welche durch eine Transmitterimplantation verursacht wird, direkt mit der Belastung durch Karzinomzellinjektion vergleicht. Kumstel et al. konnten zeigen, dass alle hier besprochenen Belastungsparameter auf signifikant höhere Belastung durch eine Transmitterimplantation verglichen mit der

Injektion von Karzinomzellen hindeuten[79]. Daher ist es denkbar, dass einige dieser Methoden nicht sensitiv genug sind, die durch die Injektion der Karzinomzellen ausgelöste Belastung zu erfassen. Die Unterscheidungsfähigkeit von Tieren direkt vor und nach Injektion von Karzinomzellen anhand der Buddelaktivität und FCM können als robust angesehen werden, da in zwei verschiedenen Kohorten die gleichen Ergebnisse erhalten und daher die gleichen Schlussfolgerungen gezogen wurden. Die Analyse im Zeitverlauf des Tiermodells zeigte, dass grundsätzlich nur die Körpergewichtsänderung geeignet ist, um Tiere vor Injektion der Karzinomzellen und in der mittleren bzw. späten Phase zu unterscheiden. Tumorerkrankungen sind generell progressiver Natur und Kachexie als Symptom einer Tumorerkrankung ist in vielen Karzinommodellen zu beobachten[94]. Daher wird die Inklusion des Körpergewichts als Parameter für die Bewertung einer Kachexie in präklinischen Krebsstudien empfohlen[95,96]. Ebenso gilt die Änderung des Körpergewichts als einer der zuverlässigsten Parameter, um humane Endpunkte für verschiedenste Tiermodelle zu definieren[8]. Allerdings gilt dies nicht uneingeschränkt für alle Tumormodelle, da vor allem schnell wachsende Tumore einen Verlust des Körpergewichts maskieren können[97] und daher zusätzliche Methoden, wie der Body-Condition Score (BCS)[84] oder das um das Tumorgewicht bereinigte Körpergewicht[98] nötig sein können. Weiterhin zeigte sich, dass speziell für orthotope Modelle des Pankreaskarzinoms reduziertes Wohlergehen und Gewichtsverlust mit dem Ort der orthotopen Zellinjektion assoziiert sein können. In einer Vergleichsstudie zwischen Tumorzellinjektionen in den Kopf und den Schwanz des Pankreas wurde festgestellt, dass Tiere durch Injektionen in den Pankreaskopf durch Invasion des Tumors in das Duodenum und durch Verschluss des Gallengangs früher eine Beeinträchtigung des Gesundheitszustandes entwickelten und früher verstarben[99]. In dieser Studie wurden ausschließlich männliche Tiere verwendet und auch im Rahmen der vorliegenden Arbeit konnte innerhalb von Studie III signifikant häufiger invasives Tumorwachstum in männlichen Tieren beobachtet werden (Fig. 1F, Studie III[89]). Dies könnte ebenso darauf hindeuten, dass je nach Krankheitsmodell einige Parameter der Belastungsanalyse nur eine geschlechtsspezifische Aussagekraft haben.
Allgemein war in Studie I die Generalisierbarkeit der Methoden über verschiedene Tiermodelle hinweg gering, was dafür spricht, dass je nach Tiermodell unterschiedliche Methoden verwendet werden sollten, um die Belastung von Tieren optimal zu erfassen. Diese Ergebnisse spiegeln sich auch in dem Bestreben wider, Belastung mit Hilfe von multiparametrischen „composite scores“ zu analysieren[100,101].

Innerhalb von Studie III wurde untersucht, ob sich männliche und weibliche Tiere in der Belastung während des Experimentes unterscheiden. Grundsätzlich unterschieden sich männliche und weibliche Tiere anhand ihrer Belastung nur in der späten Phase des Experimentes signifikant. Männchen verloren mehr Körpergewicht, zeigten weniger Buddelaktivität und hatten

einen höheren Belastungsscore. Das Nestbauverhalten und FCM unterschieden sich auch in der späten Phase nicht signifikant zwischen den Geschlechtern. Da männliche Tiere im Karzinommodell mit signifikant höherer Wahrscheinlichkeit vor Ende des Experimentes anhand definierter Endpunkte euthanasiert werden mussten und ebenso signifikant größere Tumore ausbildeten, war eine grundsätzlich höhere Belastung zu erwarten. Dabei muss jedoch beachtet werden, dass für die Auswertung der Belastung nur Tiere analysiert wurden, die bis zum Ende des Experimentes überlebt haben. Tiere, die bereits früher hohe Belastung erfahren haben und aufgrund dieser euthanasiert wurden, sind nicht in die Auswertung eingegangen. Ebenso muss beachtet werden, dass ein Verlust des Körpergewichtes von mehr als 10% auch immer in einem erhöhten Belastungsscore resultiert. Der signifikant höhere Verlust des Körpergewichtes und der signifikant erhöhte Belastungsscore in Männchen müssen also im Zusammenhang betrachtet werden. Geschlechtsunterschiede in Inzidenz, Mortalität und Ausprägung verschiedener Krebserkrankungen sind klinisch etabliert und in aller Regel sind Männer stärker betroffen als Frauen[73,102,103]. In verschiedenen immunkompetenten Tumormodellen konnten diese Geschlechtsunterschiede ebenfalls beobachtet werden und vor allem die Inhibition der adaptiven Immunantwort durch Androgene in männlichen Tieren als ursächlicher Faktor ausfindig gemacht werden[75,104,105]. Unterschiede in der adaptiven Immunantwort konnten auch in dem in dieser Arbeit besprochenen Modell beobachtet werden, da männliche Tiere signifikant weniger intratumorale CD8-positive Zellen aufwiesen als weibliche. Ebenso konnten Metastasen und invasives Tumorwachstum signifikant häufiger in Männchen beobachtet werden (Fig. 1E und F, Studie III[89]). Die höhere Belastung in Männchen hat also mit hoher Wahrscheinlichkeit einen physiologischen Ursprung in der deutlich stärkeren Ausprägung des Tumormodells.

Weiterhin wurde im Rahmen der Belastungseinschätzung in Studie I und III untersucht, ob sich die Therapie des Pankreaskarzinoms in einer veränderten Belastung niederschlägt. In Studie I wurde der Frage nachgegangen, ob Tiere vor Injektion der Karzinomzellen und danach anhand der Therapie (Vehikel oder Metformin + CHC) unterschieden werden können (Fig. 4, Studie I[106]). Keine der untersuchten Methoden war in der Lage, Tiere vor und nach Injektion der Karzinomzellen zu unterscheiden, unabhängig von der verabreichten Therapie. Das kann bedeuten, dass die Interventionstherapie (Metformin + CHC) nicht plötzlich dazu führt, dass Tiere vor und nach Injektion der Karzinomzellen + Therapie unterschieden werden können und die Therapie daher nicht zu einer erhöhten Belastung führt. Allerdings sind die meisten der untersuchten Methoden, je nach Fragestellung, ohnehin kaum in der Lage zwischen Tieren vor und nach Zellinjektion zu unterscheiden, möglicherweise weil das Modell kaum Belastung verursacht oder die Methoden nicht sensitiv genug sind, um diese zu erfassen. Ebenso wurden hier die Daten aus den verschiedenen Phasen (früh, mittel, spät) des Experimentes gepoolt

und mit der Präphase verglichen und desweiteren die Vehikelgruppe nicht mit der Interventionsgruppe sondern nur die jeweiligen Gruppen vor und nach Injektion der Zellen + Therapie verglichen. Die Aussagekraft der Daten im Hinblick auf eine potentielle Belastung durch die Therapie ist daher mit Einschränkungen zu betrachten.

In Studie III wurde eine mögliche Belastung durch die Therapie anhand der bisher besprochenen Belastungsparameter (Fig. S8, Studie III[89]) sowie laborchemischer Parameter (AST, ALT, Kreatinin, LDH, C-Peptid; Fig. 5, Studie III[89]) im Vergleich der Vehikelgruppe mit der Therapiegruppe (BI-3406 + Trametinib + BKM120) pro Geschlecht analysiert. Im Vergleich der Belastungsparameter gab es lediglich einen signifikanten Unterschied im Belastungsscore zwischen mit Vehikel und mit der Therapie behandelten weiblichen Tieren. Alle anderen Parameter unterschieden sich weder in Männchen noch in Weibchen signifikant. Der signifikant erhöhte Belastungsscore in weiblichen mit Therapie behandelten Tieren war nicht durch einen signifikanten Körpergewichtsverlust im Vergleich mit der Vehikelgruppe bedingt, sondern maßgeblich durch die Beobachtung eines gesträubten Fells, welches mit 2 bewertet wird. Diese Beobachtung ist generell sehr subjektiv und abhängig vom Beobachter. Die Interpretation, dass die Therapie weibliche Tiere übermäßig dazu veranlasst ihre Fellpflege zu vernachlässigen, ist möglich aber wenig wahrscheinlich, da keine anderen Parameter auf eine erhöhte Belastung hinweisen. Weiterhin ergab die Analyse der laborchemischen Parameter in beiden Geschlechtern eine signifikant erhöhte C-Peptid Plasmakonzentration. Diese Erhöhung kann auf den Wirkmechanismus von BKM120 zurückgeführt werden, welches über die Inhibition der PI3K ein Insulin-Feedback auslöst und so ebenfalls die C-Peptid Plasmakonzentration erhöht[107-109]. Da es in Männchen keine signifikanten Unterschiede in der Belastung zwischen mit Vehikel und Therapie behandelten Tieren gab und in Weibchen der Unterschied in der Belastung lediglich auf der subjektiven Beobachtung des gesträubten Fells in therapierten Tieren beruhte, spiegelte sich die signifikante Erhöhung der C-Peptid Plasmakonzentration scheinbar nicht in der Belastung der Tiere wider. Grundsätzlich sind die hier verwendeten Methoden der Belastungsanalyse zumindest teilweise geeignet, um unterschiedliche Belastung während Therapie des orthotopen Pankreaskarzinommodells zu evaluieren[30]. Daher kann geschlussfolgert werden, dass die hier verwendete Therapie keine zusätzliche Belastung in den Tieren auslöst oder die verwendeten Methoden der Belastungsanalyse nicht sensitiv genug sind, eine zusätzliche Belastung durch die Therapie zu erfassen.

Zusammenfassend ist zu sagen, dass nur wenige Methoden geeignet sind, um Tiere vor und nach Induktion des Pankreaskarzinommodells zu unterscheiden. Im späteren Verlauf des Modells bietet sich vor allem die Körpergewichtsänderung als Parameter zur Unterscheidung an. Weiterhin zeigte sich, dass männliche und weibliche Tiere in der späten Phase des Modells

unterschiedlich stark belastet sind, was durch die geschlechtsspezifische Ausprägung des Tumormodells erklärt werden kann. Weiterhin ist die Analyse der zusätzlichen Belastung durch eine therapeutische Intervention grundsätzlich möglich, jedoch konnte weder für die in Studie I noch die in Studie III verwendete Therapie eine zusätzliche Belastung festgestellt werden, wobei diese Interpretation vor allem mit Blick auf die Analyse in Studie I mit Bedacht betrachtet werden sollte.

6.2 Effektivität der kombinierten Inhibition von SOS1, MEK1/2 und PI3K *in vitro* und *in vivo*

KRAS-Mutationen zählen zu den häufigsten Treibermutationen in diversen Krebsarten[110]. Die Auswahl an wirksamen und zielgerichteten Therapien hat sich in den letzten Jahren zwar erweitert, doch für die häufigste PDAC-Mutation, G12D, existieren bislang keine spezifischen, zugelassenen Therapien. Da bereits kurz nach der Markteinführung Resistenzen gegen G12C-Inhibitoren wie Sotorasib beobachtet wurden[55], spielt die Suche nach effektiven Kombinationstherapien weiterhin eine wichtige Rolle.

Im Rahmen dieser Arbeit wurde in Studie II und Studie III eine bis dahin ungetestete Kombinationstherapie aus BI-3406, Trametinib und BKM120 in verschiedenen PDAC-Zelllinien (human und murin) sowie in einem syngenen, orthotopen Mausmodell auf ihre Wirksamkeit untersucht. Zusätzlich wurde der Einfluss des Geschlechts der verwendeten C57BL/6J Mäuse auf die Wirksamkeit der Therapie analysiert.

Die alleinige Applikation von BI-3406 erwies sich in Konzentrationen von bis zu 10 µM als unzureichend, um die Proliferation und Biomasse verschiedener humaner PDAC-Zelllinien um mehr als 50% zu verringern. In Kombination mit Trametinib und BKM120 zeigten sich starke synergistische Effekte und sowohl in AsPC-1 (G12D) als auch in MIA PaCa-2-(G12C) Zellen konnten Proliferation und Biomasse effektiv verringert und Zelltod induziert werden. Interessanterweise wirkten im Vergleich Kombinationen mit Sotorasib statt BI-3406 in AsPC-1-Zellen nur additiv (Fig. 4a, Studie II[111]) und ein synergistischer Effekt konnte nur in MIA PaCa-2-Zellen bestätigt werden (Fig. 4d, Studie II[111]). Dies unterstreicht, dass während Kombinationen mit Sotorasib effektiv in G12C-mutierten Zellen eingesetzt werden können, Kombinationen mit BI-3406 ein breiteres Wirkspektrum bieten und so die Grundlage einer Therapie verschiedenster *KRAS*-mutierter Tumore bilden können.
Die Ergebnisse der Experimente mit Kombinationen aus BI-3406, Trametinib und BKM120 konnten größtenteils in der murinen Zelllinie 6606PDA reproduziert werden. Die Dreifachkombination verringerte die Proliferation und induzierte den Zelltod in synergistischer Weise.

Trametinib als einzelne Verbindung war in der angewandten Konzentration bereits sehr effektiv darin, Zelltod in 6606PDA-Zellen zu induzieren. In Kombination mit BI-3406 und BKM120 ergaben sich so zwar synergistische Effekte, allerdings keine signifikant besseren Ergebnisse verglichen mit Zweifachkombinationen aus Trametinib und BKM120 oder BI-3406. Bereits in Studie II konnte Trametinib in AsPC-1-Zellen signifikant mehr Zelltod induzieren als die DMSO-Kontrolle, obwohl um den Faktor 6 geringere Konzentrationen verwendet wurden als für die Inkubation der 6606PDA-Zellen in Studie III. Andere humane G12D-Zelllinien, wie PANC-1 oder SW1990, sind eher mit erhöhter Resistenz gegenüber MEK-Inhibition assoziiert[112,113] und die Sensitivität der AsPC-1 Zelllinie gegenüber MEK-Inhibition könnte unter anderem durch die zusätzlichen Mutationen in *SMAD4* und *CDKN2A* begründet sein[112]. Da die murine 6606PDA-Zelllinie ähnlich sensitiv auf alleinige MEK-Inhibition reagiert, sollten für zukünftige Studien mit dieser Zelllinie mögliche Mutationen in weiteren Schlüsselgenen mittels Whole Exome Sequencing (WES) aufgeklärt werden.

Im Tierversuch zeigte sich, dass die Therapie lediglich in Männchen eine effektive Wirkung entfaltete. Die Therapie verringerte nur in männlichen Tieren verglichen mit der Vehikelgruppe das Tumorgewicht signifikant, erhöhte die Überlebenswahrscheinlichkeit geringfügig und führte zu etwas weniger invasivem Tumorwachstum (Fig. 4G, Studie III[89]). Die Therapie verringerte in keinem der beiden Geschlechter die Proliferation der Tumorzellen im Vergleich zur Vehikelgruppe signifikant. Diese Ergebnisse deuten auf einen erheblichen Einfluss des Geschlechts auf die Wirksamkeit der Therapie hin. Die Expression von Rezeptoren für Geschlechtshormone auf PDAC-Zellen wurde bereits nachgewiesen[114-116] und insbesondere ß-Estradiol soll in der Lage sein, PDAC-Zellen für Chemotherapie zu sensitivieren[115]. Im Rahmen der Studie III kamen wir in Zellkulturexperimenten, die evaluieren sollten, welchen Einfluss sowohl männliche als auch weibliche Sexualhormone auf die Effektivität der getesteten Dreifachtherapie haben, zu gegensätzlichen Ergebnissen (Fig. S6, Studie III[89]). ß-Estradiol verringerte in physiologischen Konzentrationen[117] die Effektivität der Therapie signifikant, sowohl im Vergleich zur Kontrolle ohne Sexualhormone als auch im Vergleich zur Therapie + Testosteron. Daher ist ein direkter, inhibitorischer Effekt auf die Therapie durch weibliche Sexualhormone durchaus denkbar. Desweiteren sind Geschlechtsunterschiede in Pharmakodynamik und –kinetik weithin publiziert[118,119]. Als zugrundeliegende Mechanismen sind unter anderem die geschlechtsspezifische Expression von Effluxpumpen und metabolisierenden Enzymen sowie der direkte Einfluss von Sexualhormonen beschrieben[120-123]. Dies kann direkten Einfluss auf die systemische Verfügbarkeit und Eliminierung verabreichter Substanzen haben. Für die in Studie II und III verwendete Substanzklasse der niedermolekularen Verbindungen (small molecules) scheint der systemische Substanzspiegel nur ein suboptimales Korrelat für den Substanzspiegel am Wirkort, wie zum Beispiel im Tumor, zu sein[124]. Daher wurde in Studie III in einem Teil der Tiere sowohl im Plasma als auch im Tumor der Wirkstoffgehalt mittels LC/MS-

MS bestimmt (Tabellen 1 und S8, Studie III[89]). Dabei wurde festgestellt, dass zum Zeitpunkt der Euthanasie weder im Tumor noch im Plasma bedeutsame Unterschiede in den Mediankonzentrationen zwischen Männchen und Weibchen vorherrschten. Obwohl die Interpretation dieser Daten weitgehend durch eine geringe Stichprobengröße limitiert ist, bleibt die wichtige Aussage, dass die Therapie in beiden Geschlechtern ihren Zielort, den Tumor, erreicht. Unter anderem die Verringerung der Anzahl der CD8-positiven Zellen durch die Therapie in Weibchen deutete auf einen geschlechtsspezifischen inhibitorischen Effekt auf die adaptive Immunantwort hin. Sowohl Trametinib als auch BKM120 sind als potente Inhibitoren der Immunzellproliferation, -aktivierung und -funktion in der Literatur beschrieben[125-129]. In therapierten weiblichen Tieren wurden verglichen mit der Vehikelgruppe sowohl die Anzahl CD8-positiver Zellen als auch die PD-L1-positive Fläche (Fig. S13A, Studie III[89]) im Tumor signifikant verringert, was in männlichen Tieren (Fig. S13B, Studie III[89]) nicht beobachtet wurde. Die PD-L1-positive Fläche in mit Vehikellösung behandelten Weibchen war stark assoziiert mit immunologischen Läsionen, geprägt durch verschiedene, in den Tumor infiltrierende Immunzellen. In einigen klinischen Studien verschiedener Krebserkrankungen hat sich die PD-L1-Expression auf Immunzellen als positiver prognostischer Faktor herausgestellt[130-133], weshalb die Verringerung der Anzahl der CD8-positiven Zellen und der PD-L1-positiven Fläche in therapierten Weibchen zusammengenommen als Hinweis auf die immunsuppressive Wirkung der Therapie interpretiert werden kann. Auch das Auftreten von Lungenmetastasen in weiblichen Tieren wurde nur unter Therapie beobachtet (Fig. 4H, Studie III[89]). Zusammengenommen lassen diese Daten den Schluss zu, dass die Therapie vor allem in Weibchen immunsuppressive Effekte hat, welche eine effektivere Therapiewirkung, wie sie in männlichen Tieren beobachtet wurde, verhindern. Limitiert wird die Aussagekraft dieser Daten vor allem durch die Verwendung von nur einem Tiermodell. Syngene, orthotope Karzinommodelle sind effizient, da sie mit wenig Aufwand und Kosten relevante Ergebnisse liefern können[134]. Jedoch ist die translationale Nähe von (Patienten-abgeleiteten) Xenograft-Modellen in Allograft-Modellen nicht gegeben[66]. Allerdings wären die geschlechtsspezifischen immunologischen Effekte, wie sie im hier verwendeten syngenen Modell beobachtet wurden, in einem immuninkompetenten Tierstamm unentdeckt geblieben. Dies unterstreicht sowohl die Wichtigkeit der Implikation des Immunsystems als auch der Inklusion beider Geschlechter in präklinische Therapiestudien, da Geschlechtsunterschiede im klinischen Alltag durchaus ernsthafte Konsequenzen wie Unterdosierung oder schwere Nebenwirkungen haben können[119,135,136].

Zusammenfassend wirkt die Therapie sowohl in humanen als auch in der verwendeten murinen Zelllinie synergistisch in der Inhibition der Proliferation und der Induktion des Zelltods. Im Tiermodell konnte eine Wirkung nur in männlichen Tieren gezeigt werden und die Wirksamkeit

der Therapie wird durch geschlechtsspezifische, immunsuppressive Effekte in Weibchen beeinflusst. Nichtsdestotrotz bietet die Therapie das Potential für weitere Studien, da effektive Therapien des Pankreaskarzinoms weiterhin dringend benötigt werden.

VII. Literaturverzeichnis

1. Russell WMS, Burch RL. *The Principles of Humane Experimental Technique.* Methuen; 1959.
2. European Parliament. *Directive 2010/63/EU of the European Parliament and of the Council of 22 September 2010 on the Protection of Animals Used for Scientific Purposes.* Text with EEA Relevance (2010).
3. TierSchG - Tierschutzgesetz. Accessed April 3, 2024. https://www.gesetze-im-internet.de/tierschg/BJNR012770972.html
4. Bleich A, Tolba RH. How can we assess their suffering? German research consortium aims at defining a severity assessment framework for laboratory animals. *Lab Anim.* 2017;51(6):667.
5. Stasiak KL, Maul D, French E, Hellyer PW, VandeWoude S. Species-specific assessment of pain in laboratory animals. *Contemp Top Lab Anim Sci*. 2003;42(4):13-20.
6. Carbone L. Do “Prey Species” Hide Their Pain? Implications for Ethical Care and Use of Laboratory Animals. *J Appl Anim Ethics Res*. 2020;2(2):216-236.
7. Understanding Animal Research. EU-wide animal research statistics, 2020. Accessed April 4, 2024. https://www.understandinganimalresearch.org.uk/news/eu-wide-animal-research-statistics-2020
8. Talbot SR, Biernot S, Bleich A, et al. Defining body-weight reduction as a humane endpoint: a critical appraisal. *Lab Anim.* 2020;54(1):99-110.
9. Morton DB, Griffiths PH. Guidelines on the recognition of pain, distress and discomfort in experimental animals and an hypothesis for assessment. *Vet Rec*. 1985;116(16):431-436.
10. Morton DB. A Systematic Approach for Establishing Humane Endpoints. *ILAR Journal*. 2000;41(2):80-86.
11. Touma C, Palme R, Sachser N. Analyzing corticosterone metabolites in fecal samples of mice: a noninvasive technique to monitor stress hormones. *Horm Behav*. 2004;45(1):10-22.
12. Auer KE, Kußmaul M, Möstl E, Hohlbaum K, Rülicke T, Palme R. Measurement of Fecal Testosterone Metabolites in Mice: Replacement of Invasive Techniques. *Animals*. 2020;10(1):165.
13. Fentener van Vlissingen JM, Borrens M, Girod A, Lelovas P, Morrison F, Torres YS. The reporting of clinical signs in laboratory animals: FELASA Working Group Report. *Lab Anim*. 2015;49(4):267-283.
14. Xie W, Palme R, Schafmayer C, Zechner D, Vollmar B, Grambow E. Distress Analysis of Mice with Cervical Arteriovenous Fistulas. *Animals*. 2021;11(11):3051.
15. Deacon RMJ. Assessing nest building in mice. *Nat Protoc*. 2006;1(3):1117-1119.

16. Deacon RMJ. Burrowing in rodents: a sensitive method for detecting behavioral dysfunction. *Nat Protoc*. 2006;1(1):118-121.
17. Schwabe K, Boldt L, Bleich A, et al. Nest-building performance in rats: impact of vendor, experience, and sex. *Lab Anim.* 2020;54(1):17-25.
18. Weegh N, Zentrich E, Zechner D, et al. Voluntary wheel running behaviour as a tool to assess the severity in a mouse pancreatic cancer model. *PLOS ONE*. 2021;16(12):e0261662.
19. Weegh N, Füner J, Janke O, et al. Wheel running behaviour in group-housed female mice indicates disturbed wellbeing due to DSS colitis. *Lab Anim.* 2020;54(1):63-72.
20. How to determine humane endpoints for research animals. *Lab Animal*. 2015;45(1):19.
21. Helgers SOA, Talbot SR, Riedesel AK, et al. Body weight algorithm predicts humane endpoint in an intracranial rat glioma model. *Sci Rep.* 2020;10(1):9020.
22. Herrmann K, Flecknell P. The application of humane endpoints and humane killing methods in animal research proposals: A retrospective review. *Altern Lab Anim.* 2018;46(6):317-333.
23. Zhang X, Kumstel S, Tang G, et al. A rational approach of early humane endpoint determination in a murine model for cholestasis. *ALTEX*. 2020;37(2):197-207.
24. Goodman SN, Fanelli D, Ioannidis JP. What does research reproducibility mean?. *Sci Transl Med.* 2016;8(341):341ps12.
25. Mandrekar JN. Receiver operating characteristic curve in diagnostic test assessment. *J Thorac Oncol.* 2010;5(9):1315-1316.
26. Sudre CH, Murray B, Varsavsky T, et al. Attributes and predictors of long COVID [published correction appears in Nat Med. 2021 Jun;27(6):1116]. *Nat Med.* 2021;27(4):626-631.
27. Hanley JA, McNeil BJ. The meaning and use of the area under a receiver operating characteristic (ROC) curve. *Radiology*. 1982;143(1):29-36.
28. Janssens ACJW, Martens FK. Reflection on modern methods: Revisiting the area under the ROC Curve. *Int J Epidemiol.* 2020;49(4):1397-1403.
29. Non-clinical: toxicology | European Medicines Agency. Accessed May 16, 2024. https://www.ema.europa.eu/en/human-regulatory-overview/re-search-and-development/scientific-guidelines/non-clinical-guidelines/non-clinical-toxicology
30. Kumstel S, Wendt EHU, Eichberg J, et al. Grading animal distress and side effects of therapies. *Ann N Y Acad Sci.* 2020;1473(1):20-34.
31. Rix A, Drude N, Mrugalla A, Mottaghy FM, Tolba RH, Kiessling F. Performance of severity parameters to detect chemotherapy-induced pain and distress in mice. *Lab Anim.* 2020;54(5):452-460.

32. Grossberg AJ, Chu LC, Deig CR, et al. Multidisciplinary standards of care and recent progress in pancreatic ductal adenocarcinoma. *CA Cancer J Clin*. 2020;70(5):375-403.
33. Li D, Xie K, Wolff R, Abbruzzese JL. Pancreatic cancer. *Lancet*. 2004;363(9414):1049-1057.
34. Neoptolemos JP, Stocken DD, Friess H, et al. A randomized trial of chemoradiotherapy and chemotherapy after resection of pancreatic cancer. *N Engl J Med*. 2004;350(12):1200-1210.
35. Conroy T, Desseigne F, Ychou M, et al. FOLFIRINOX versus gemcitabine for metastatic pancreatic cancer. *N Engl J Med*. 2011;364(19):1817-1825.
36. Portal A, Pernot S, Tougeron D, et al. Nab-paclitaxel plus gemcitabine for metastatic pancreatic adenocarcinoma after Folfirinox failure: an AGEO prospective multicentre cohort. *Br J Cancer*. 2015;113(7):989-995.
37. Quiñonero F, Mesas C, Doello K, et al. The challenge of drug resistance in pancreatic ductal adenocarcinoma: a current overview. *Cancer Biol Med*. 2019;16(4):688-699.
38. Hu HF, Ye Z, Qin Y, et al. Mutations in key driver genes of pancreatic cancer: molecularly targeted therapies and other clinical implications. *Acta Pharmacol Sin*. 2021;42(11):1725-1741.
39. Poruk KE, Moran A, Doctor V, et al. Mutational landscape of pancreatic adenocarcinoma identified by prospective clinical sequencing in a nationwide cancer network. *J Clin Oncol*. 2022;40(16_suppl):4137.
40. Bailey P, Chang DK, Nones K, et al. Genomic analyses identify molecular subtypes of pancreatic cancer. *Nature*. 2016;531(7592):47-52.
41. Bahar ME, Kim HJ, Kim DR. Targeting the RAS/RAF/MAPK pathway for cancer therapy: from mechanism to clinical studies. *Sig Transduct Target Ther*. 2023;8(1):1-38.
42. Pantsar T. The current understanding of KRAS protein structure and dynamics. *Comput Struct Biotechnol J*. 2020;18:189-198.
43. Haigis KM. KRAS Alleles: The Devil Is in the Detail. *Trends Cancer.* 2017;3(10):686-697.
44. Shen H, Lundy J, Strickland AH, et al. KRAS G12D Mutation Subtype in Pancreatic Ductal Adenocarcinoma: Does It Influence Prognosis or Stage of Disease at Presentation?. *Cells*. 2022;11(19):3175.
45. Hunter JC, Manandhar A, Carrasco MA, Gurbani D, Gondi S, Westover KD. Biochemical and Structural Analysis of Common Cancer-Associated KRAS Mutations. *Mol Cancer Res*. 2015;13(9):1325-1335.
46. Hou P, Wang YA. Conquering oncogenic KRAS and its bypass mechanisms. *Theranostics*. 2022;12(13):5691-5709.

47. The Lancet Oncology. Undruggable KRAS-time to rebrand?. *Lancet Oncol.* 2021;22(3):289.
48. John J, Sohmen R, Feuerstein J, Linke R, Wittinghofer A, Goody RS. Kinetics of interaction of nucleotides with nucleotide-free H-ras p21. *Biochemistry*. 1990;29(25):6058-6065.
49. Bekaii-Saab TS, Yaeger R, Spira AI, et al. Adagrasib in Advanced Solid Tumors Harboring a KRASG12C Mutation. *J Clin Oncol*. 2023;41(25):4097-4106.
50. Strickler JH, Satake H, Hollebecque A, et al. First data for sotorasib in patients with pancreatic cancer with KRAS p.G12C mutation: A phase I/II study evaluating efficacy and safety. *J Clin Oncol*. 2022;40(36_suppl):360490.
51. Shoucair S, Habib JR, Pu N, et al. Comprehensive Analysis of Somatic Mutations in Driver Genes of Resected Pancreatic Ductal Adenocarcinoma Reveals KRAS G12D and Mutant TP53 Combination as an Independent Predictor of Clinical Outcome. *Ann Surg Oncol*. 2022;29(4):2720-2731.
52. Wei D, Wang L, Zuo X, Maitra A, Bresalier RS. A Small Molecule with Big Impact: MRTX1133 Targets the KRASG12D Mutation in Pancreatic Cancer. *Clin Cancer Res.* 2024;30(4):655-662.
53. ClinicalTrials.gov (2024.000Z). Study of MRTX1133 in Patients With Advanced Solid Tumors Harboring a KRAS G12D Mutation. Updated on 5/21/2024.000Z, accessed on 5/31/2024.272Z.Available online at https://clinicaltrials.gov/study/NCT05737706.
54. Corcoran RB. A single inhibitor for all KRAS mutations. *Nat Cancer*. 2023;4(8):1060-1062.
55. Tanaka N, Lin JJ, Li C, et al. Clinical Acquired Resistance to KRASG12C Inhibition through a Novel KRAS Switch-II Pocket Mutation and Polyclonal Alterations Converging on RAS-MAPK Reactivation. *Cancer Discov.* 2021;11(8):1913-1922.
56. Awad MM, Liu S, Rybkin II, et al. Acquired Resistance to KRASG12C Inhibition in Cancer. *N Engl J Med*. 2021;384(25):2382-2393.
57. Hofmann MH, Gmachl M, Ramharter J, et al. BI-3406, a Potent and Selective SOS1–KRAS Interaction Inhibitor, Is Effective in KRAS-Driven Cancers through Combined MEK Inhibition. *Cancer Discov*. 2021;11(1):142-157.
58. Corbalan-Garcia S, Yang SS, Degenhardt KR, Bar-Sagi D. Identification of the mitogen-activated protein kinase phosphorylation sites on human Sos1 that regulate interaction with Grb2. *Mol Cell Biol.* 1996 Oct;16(10):5674-82.
59. Lake D, Corrêa SAL, Müller J. Negative feedback regulation of the ERK1/2 MAPK pathway. *Cell Mol Life Sci*. 2016;73(23):4397-4413.

60. Turke AB, Song Y, Costa C, et al. MEK Inhibition Leads to PI3K/AKT Activation by Relieving a Negative Feedback on ERBB Receptors. *Cancer Res*. 2012;72(13):3228-3237.
61. Vitiello PP, Cardone C, Martini G, et al. Receptor tyrosine kinase-dependent PI3K activation is an escape mechanism to vertical suppression of the EGFR/RAS/MAPK pathway in KRAS-mutated human colorectal cancer cell lines. *J Exp Clin Cancer Res*. 2019;38(1):1-12.
62. Lietman CD, Johnson ML, McCormick F, Lindsay CR. More to the RAS Story: KRASG12C Inhibition, Resistance Mechanisms, and Moving Beyond KRASG12C. *Am Soc Clin Oncol Educ Book*. 2022;42:1-13.
63. Garrido-Castro AC, Saura C, Barroso-Sousa R, et al. Phase 2 study of buparlisib (BKM120), a pan-class I PI3K inhibitor, in patients with metastatic triple-negative breast cancer. *Breast Cancer Res*. 2020;22(1):1-13.
64. Bedard PL, Tabernero J, Janku F, et al. A phase Ib dose-escalation study of the oral pan-PI3K inhibitor buparlisib (BKM120) in combination with the oral MEK1/2 inhibitor trametinib (GSK1120212) in patients with selected advanced solid tumors. *Clin Cancer Res*. 2015;21(4):730-738.
65. Mota-Reyes C, Gärtner P, Rosenkranz L, Grippo PJ., Demir IE. (2021). In vivo Mouse Models of Pancreatic Ductal Adenocarcinoma. *Pancreapedia: Exocrine Pancreas Knowledge Base.* Accessed April 16, 2024. https://www.pancreapedia.org/node/9843
66. Garcia PL, Miller AL, Yoon KJ. Patient-Derived Xenograft Models of Pancreatic Cancer: Overview and Comparison with Other Types of Models. *Cancers (Basel)*. 2020 May 22;12(5):1327.
67. The Jackson Laboratory. 000664 - B6 Strain Details. Accessed April 16, 2024. https://www.jax.org/strain/000664
68. Heidari S, Babor TF, Castro P de, Tort S, Curno M. Sex and Gender Equity in Research: rationale for the SAGER guidelines and recommended use. *Res Integr Peer Rev*. 2016;1(1):1-9.
69. Arnegard ME, Whitten LA, Hunter C, Clayton JA. Sex as a Biological Variable: A 5-Year Progress Report and Call to Action. *J Womens Health (Larchmt)*. 2020;29(6):858-864.
70. Zucker I, Prendergast BJ, Beery AK. Pervasive Neglect of Sex Differences in Biomedical Research. *Cold Spring Harb Perspect Biol.* 2022;14(4):a039156.
71. Kim J, Ji E, Jung K, Jung IH, Park J, Lee JC, Kim JW, Hwang JH, Kim J. Gender Differences in Patients with Metastatic Pancreatic Cancer Who Received FOLFIRINOX. *J Pers Med*. 2021 Jan 30;11(2):83.

72. Ma J, Yao Y, Tian Y, Chen K, Liu B. Advances in sex disparities for cancer immunotherapy: unveiling the dilemma of Yin and Yang. *Biol Sex Differ*. 2022;13(1):1-12.
73. Vera R, Juan-Vidal O, Safont-Aguilera MJ, La Peña FA de, Del Alba AG. Sex differences in the diagnosis, treatment and prognosis of cancer: the rationale for an individualised approach. *Clin Transl Oncol*. 2023;25(7):2069-2076.
74. Conforti F, Pala L, Bagnardi V, et al. Sex-Based Heterogeneity in Response to Lung Cancer Immunotherapy: A Systematic Review and Meta-Analysis. *J Natl Cancer Inst*. 2019;111(8):772-781.
75. Kwon H, Schafer JM, Song NJ, et al. Androgen conspires with the CD8+ T cell exhaustion program and contributes to sex bias in cancer. *Sci Immunol.* 2022;7(73):eabq2630.
76. White-Gilbertson S, Davis M, Voelkel-Johnson C, Kasman LM. Sex differences in the MB49 syngeneic, murine model of bladder cancer. *Bladder (San Franc).* 2016;3(1):e22.
77. Yang C, Jin J, Yang Y, et al. Androgen receptor-mediated CD8+ T cell stemness programs drive sex differences in antitumor immunity. *Immunity*. 2022;55(7):1268-1283.e9.
78. Zhang X, Cheng L, Gao C, et al. Androgen Signaling Contributes to Sex Differences in Cancer by Inhibiting NF-κB Activation in T Cells and Suppressing Antitumor Immunity. *Cancer Res*. 2023;83(6):906-921.
79. Kumstel S, Vasudevan P, Palme R, et al. Benefits of non-invasive methods compared to telemetry for distress analysis in a murine model of pancreatic cancer. *J Adv Res*. 2020;21:35-47.
80. Kumstel S, Tang G, Zhang X, Kerndl H, Vollmar B, Zechner D. Grading Distress of Different Animal Models for Gastrointestinal Diseases Based on Plasma Corticosterone Kinetics. *Animals (Basel)*. 2019;9(4):145.
81. Tang G, Seume N, Häger C, et al. Comparing distress of mouse models for liver damage. *Sci Rep.* 2020;10(1):19814.
82. Abdelrahman A, Kumstel S, Zhang X, et al. A novel multi-parametric analysis of non-invasive methods to assess animal distress during chronic pancreatitis. *Sci Rep*. 2019;9(1):14084.
83. Deacon R. Assessing burrowing, nest construction, and hoarding in mice. *J Vis Exp*. 2012;(59):e2607.
84. Paster EV, Villines KA, Hickman DL. Endpoints for Mouse Abdominal Tumor Models: Refinement of Current Criteria. *Comp Med*. 20;59(3):234-241.

85. Touma C, Sachser N, Möstl E, Palme R. Effects of sex and time of day on metabolism and excretion of corticosterone in urine and feces of mice. *Gen Comp Endocrinol*. 2003;130(3):267-278.
86. Mallien AS, Becker L, Pfeiffer N, et al. Dopamine Transporter Knockout Rats Show Impaired Wellbeing in a Multimodal Severity Assessment Approach. *Front Behav Neurosci*. 2022;16:924603.
87. Kroll T, Kornadt-Beck N, Oskamp A, et al. Additional Assessment of Fecal Corticosterone Metabolites Improves Visual Rating in the Evaluation of Stress Responses of Laboratory Rats. *Animals (Basel).* 2021;11(3):710.
88. Hingorani SR, Petricoin EF, Maitra A, et al. Preinvasive and invasive ductal pancreatic cancer and its early detection in the mouse. *Cancer Cell*. 2003;4(6):437-450.
89. Schulz B, Leitner E, Schreiber T, et al. Sex Matters–Insights from Testing Drug Efficacy in an Animal Model of Pancreatic Cancer. *Cancers (Basel)*. 2024;16(10):1901.
90. Balcombe JP, Barnard ND, Sandusky C. Laboratory routines cause animal stress. *Contemp Top Lab Anim Sci*. 2004;43(6):42-51.
91. Drude S, Geissler A, Olfe J, et al. Side effects of control treatment can conceal experimental data when studying stress responses to injection and psychological stress in mice. *Lab Animal*. 2011;40(4):119-128.
92. Poole T. Happy animals make good science. *Lab Anim.* 1997;31(2):116-124.
93. Jirkof P, Cesarovic N, Rettich A, Nicholls F, Seifert B, Arras M. Burrowing behavior as an indicator of post-laparotomy pain in mice. *Front Behav Neurosci*. 2010;4:165.
94. Li L, Wazir J, Huang Z, Wang Y, Wang H. A Comprehensive Review of Animal Models for Cancer Cachexia: Implications for Translational Research. *Genes & Diseases*. 2023:101080.
95. Workman P, Aboagye EO, Balkwill F, et al. Guidelines for the welfare and use of animals in cancer research. *Br J Cancer*. 2010;102(11):1555-1577.
96. Orellana-Muriana JM. (2012). Animal Models in Cancer Research: Assessment of Severity and the Application of Humane Endpoints. In: Martínez Murillo, R., Martínez, A. (eds) Animal Models of Brain Tumors. *Neuromethods*, vol 77. Humana Press, Totowa, NJ.
97. Han YH, Mun JG, Jeon HD, et al. The Extract of Arctium lappa L. Fruit (Arctii Fructus) Improves Cancer-Induced Cachexia by Inhibiting Weight Loss of Skeletal Muscle and Adipose Tissue. *Nutrients.* 2020;12(10):3195.
98. Xie W, Kordt M, Palme R, Grambow E, Vollmar B, Zechner D. Diagnostic Ability of Methods Depicting Distress of Tumor-Bearing Mice. *Animals (Basel).* 2021;11(8):2155.

99. Nikfarjam M, Yeo D, He H, et al. Comparison of two syngeneic orthotopic murine models of pancreatic adenocarcinoma. *J Invest Surg.* 2013;26(6):352-359.
100. Reiber M, von Schumann L, Buchecker V, et al. Evidence-based comparative severity assessment in young and adult mice. *PLoS One.* 2023;18(10):e0285429.
101. Talbot SR, Kumstel S, Schulz B, et al. Robustness of a multivariate composite score when evaluating distress of animal models for gastrointestinal diseases. *Sci Rep*. 2023;13(1):1-14.
102. Haupt S, Caramia F, Klein SL, Rubin JB, Haupt Y. Sex disparities matter in cancer development and therapy. *Nat Rev Cancer*. 2021;21(6):393-407.
103. Siegel RL, Miller KD, Wagle NS, Jemal A. Cancer statistics, 2023. *CA Cancer J Clin*. 2023;73(1):17-48.
104. Dakup PP, Porter KI, Little AA, Zhang H, Gaddameedhi S. Sex differences in the association between tumor growth and T cell response in a melanoma mouse model. *Cancer Immunol Immunother*. 2020;69(10):2157-2162.
105. Ray AL, Nofchissey RA, Khan MA, et al. The role of sex in the innate and adaptive immune environment of metastatic colorectal cancer. *Br J Cancer*. 2020;123(4):624-632.
106. Zechner D, Schulz B, Tang G, et al. Generalizability, Robustness and Replicability When Evaluating Wellbeing of Laboratory Mice with Various Methods. *Animals (Basel)*. 2022;12(21):2927.
107. Mishra R, Patel H, Alanazi S, Kilroy MK, Garrett JT. PI3K Inhibitors in Cancer: Clinical Implications and Adverse Effects. *Int J Mol Sci*. 2021;22(7):3464.
108. Noch EK, Palma LN, Yim I, et al. Insulin feedback is a targetable resistance mechanism of PI3K inhibition in glioblastoma. *Neuro Oncol.* 2023;25(12):2165-2176.
109. Hopkins BD, Pauli C, Du X, et al. Suppression of insulin feedback enhances the efficacy of PI3K inhibitors. *Nature*. 2018;560(7719):499-503.
110. Bailey MH, Tokheim C, Porta-Pardo E, et al. Comprehensive Characterization of Cancer Driver Genes and Mutations. *Cell*. 2018;173(2):371-385.e18.
111. Ma Y, Schulz B, Trakooljul N, et al. Inhibition of KRAS, MEK and PI3K Demonstrate Synergistic Anti-Tumor Effects in Pancreatic Ductal Adenocarcinoma Cell Lines. *Cancers (Basel).* 2022;14(18):4467.
112. Zhang X, Mao T, Xu H, et al. Synergistic blocking of RAS downstream signaling and epigenetic pathway in *KRAS* mutant pancreatic cancer. *Aging (Albany NY)*. 2022;14(8):3597-3606.
113. Tan YQ, Sun B, Zhang X, et al. Concurrent inhibition of pBADS99 synergistically improves MEK inhibitor efficacy in KRASG12D-mutant pancreatic ductal adenocarcinoma. *Cell Death Dis*. 2024;15(2):173.

114. Andrén-Sandberg Å, Johansson J. Influence of sex hormones on pancreatic Cancer. *Int J Pancreatol*. 1990;7(1):167-176.
115. Akula SM, Candido S, Abrams SL, et al. Abilities of β-Estradiol to interact with chemotherapeutic drugs, signal transduction inhibitors and nutraceuticals and alter the proliferation of pancreatic cancer cells. *Adv Biol Regul.* 2020;75:100672.
116. Liao YN, Gai YZ, Qian LH, et al. Progesterone receptor potentiates macropinocyto-sis through CDC42 in pancreatic ductal adenocarcinoma. *Oncogenesis*. 2024;13(1):1-15.
117. Nilsson ME, Vandenput L, Tivesten Å, et al. Measurement of a Comprehensive Sex Steroid Profile in Rodent Serum by High-Sensitive Gas Chromatography-Tandem Mass Spectrometry. *Endocrinology*. 2015;156(7):2492-2502.
118. Wheatley-Price P, Le Maître A, Ding K, et al. The influence of sex on efficacy, adverse events, quality of life, and delivery of treatment in National Cancer Institute of Canada Clinical Trials Group non-small cell lung cancer chemotherapy trials. *J Thorac Oncol.* 2010;5(5):640-648.
119. Davidson M, Wagner AD, Kouvelakis K, et al. Influence of sex on chemotherapy efficacy and toxicity in oesophagogastric cancer: A pooled analysis of four randomised trials. *Eur J Cancer.* 2019;121:40-47.
120. Mitchell SC, Smith RL, Waring RH. The menstrual cycle and drug metabolism. *Curr Drug Metab*. 2009;10(5):499-507.
121. Spoletini I, Vitale C, Malorni W, Rosano GM. Sex differences in drug effects: interaction with sex hormones in adult life. *Handb Exp Pharmacol*. 2012;(214):91-105.
122. Suzuki T, Zhao YL, Nadai M, et al. Gender-related differences in expression and function of hepatic P-glycoprotein and multidrug resistance-associated protein (Mrp2) in rats. *Life Sci*. 2006;79(5):455-461.
123. Valodara AM, Sr KJ. Sexual Dimorphism in Drug Metabolism and Pharmacokinetics. *Curr Drug Metab*. 2019;20(14):1154-1166.
124. Zhang D, Hop CECA, Patilea-Vrana G, et al. Drug Concentration Asymmetry in Tissues and Plasma for Small Molecule-Related Therapeutic Modalities. *Drug Metab Dispos*. 2019;47(10):1122-1135.
125. Yamaguchi T, Kakefuda R, Tanimoto A, Watanabe Y, Tajima N. Suppressive effect of an orally active MEK1/2 inhibitor in two different animal models for rheumatoid arthritis: a comparison with leflunomide. *Inflamm Res*. 2012;61(5):445-454.
126. Wieder E, Kolonias D, Benjamin C, et al. Trametinib Selectively Inhibits Alloreactivity While Sparing Virus-Specific T Cells. *Biol Blood Marrow Transplant*. 2014;20(2):S283.
127. Vella LJ, Pasam A, Dimopoulos N, et al. MEK inhibition, alone or in combination with BRAF inhibition, affects multiple functions of isolated normal human lymphocytes and dendritic cells. *Cancer Immunol Res*. 2014;2(4):351-360.

128. Vella LJ, Andrews MC, Pasam A, Woods K, Behren A, Cebon JS. The kinase inhibitors dabrafenib and trametinib affect isolated immune cell populations. *Oncoimmunology*. 2014;3(7):e946367.
129. Allegrezza MJ, Rutkowski MR, Stephen TL, et al. IL15 Agonists Overcome the Immunosuppressive Effects of MEK Inhibitors. *Cancer Res.* 2016;76(9):2561-2572.
130. Mocan LP, Craciun R, Grapa C, et al. PD-L1 expression on immune cells, but not on tumor cells, is a favorable prognostic factor for patients with intrahepatic cholangiocarcinoma. *Cancer Immunol Immunother*. 2023;72(4):1003-1014.
131. Kim Y, Wen X, Cho NY, Kang GH. Intratumoral immune cells expressing PD-1/PD-L1 and their prognostic implications in cancer: a meta-analysis. *Int J Biol Markers*. 2018:1724600818770941.
132. Blažek T, Petráš M, Knybel L, Cvek J, Soumarová R. Programmed Cell Death Ligand 1 Expression on Immune Cells and Survival in Patients With Nonmetastatic Head and Neck Cancer: A Systematic Review and Meta-analysis. *JAMA Netw Open*. 2023;6(3):e236324.
133. Zhong Q, Shou J, Ying J, et al. High PD-L1 expression on immune cells, but not on tumor cells, is a favorable prognostic factor in urothelial carcinoma. *Future Oncol*. 2021;17(22):2893-2905.
134. Qiu W, Su GH. Development of orthotopic pancreatic tumor mouse models. Methods *Mol Biol.* 2013;980:215-223.
135. Zucker I, Prendergast BJ. Sex differences in pharmacokinetics predict adverse drug reactions in women. *Biol Sex Differ*. 2020;11(1):32.
136. Wagner AD, Oertelt-Prigione S, Adjei A, et al. Gender medicine and oncology: report and consensus of an ESMO workshop. *Ann Oncol*. 2019;30(12):1914-1924.

VIII. Abbildungsverzeichnis

Abbildung 1: Strategie einer kombinierten Inhibition von KRAS:SOS1, MEK1/2 und PI3K .. 6
Abbildung 2: Beispiele für ROC-Kurven 11
Abbildung 3: ROC-Kurven als Instrument zur Einschätzung der Diskriminierungsfähigkeit von Methoden der Belastungsanalyse 17
Abbildung 4: Inhibition von Proliferation und Induktion von Zelltod durch BI-3406 allein und in Kombination 19
Abbildung 5: Unterschiede in Überlebenswahrscheinlichkeit, Tumorgewicht, -proliferation und -infiltration sowie Belastung zwischen Männchen und Weibchen im PDAC-Modell..... 21
Abbildung 6: Inhibition von Proliferation und Induktion von Zelltod durch BI-3406 allein und in Kombination in 6606PDA-Zellen 23
Abbildung 7: *in vivo* Effekte der Dreifachtherapie (BI-3406, Trametinib, BKM120) im Vergleich zum Vehikel in männlichen und weiblichen Mäusen 24

IX. Tabellenverzeichnis

Tabelle 1: Verwendete Konzentrationen für kombinierte Inhibitor-Applikation 12

X. Abkürzungsverzeichnis

Akt	Proteinkinase B
ALT	Alanin-Aminotransferase
ANOVA	Analysis of variance (Varianzanalyse)
AST	Aspartat-Aminotransferase
AUC	Area under the curve (Fläche unter der Kurve)
B	Burrowing (Buddelaktivität)
BDL	Bile duct ligation (Gallengangsligatur)
BrdU	5-Brom-2'-Deoxyuridin
BW	Body weight (Körpergewicht)
CD8	Cluster of differentiation 8 (CD8-Rezeptor)
CDKN2A	Cyclin dependent kinase inhibitor 2A
CHC	α-Cyano-4-hydroxyzimtsäure
DMEM	Dulbeccos Modified Eagle Medium
DMSO	Dimethylsulfoxid
DSC	Distress score (klinischer Belastungsscore)
ELISA	Enzyme-linked Immunosorbent Assay
EO	Observed effect (beobachteter Effekt)
EP	Predicted effect (vorausgesagter Effekt)
FCM	Fecal corticosterone metabolites (Fäkale Kortikosteronmetabolite)
FCS	Fetal calf serum (Fetales Kälberserum)
FITC	Fluoresceinisothiocyanat
FOLFIRINOX	Folinsäure, 5-Fluorouracil, Irinotecan und Oxaliplatin
GAP	GTPase-aktivierende Proteine
GDP	Guanosindiphosphat
GEF	Guanine nucleotide exchange factor (Guaninnukleotid-Austauschfaktor)
GEMM	Genetically engineered mouse models (Genetisch veränderte Mausmodelle)
GTP	Guanosintriphosphat
HBSS	Hanks' Balanced Salt Solution
ID	Inner diameter (Innendurchmesser)
KRAS	Kirsten rat sarcoma viral oncogene homolog
KV	Kristallviolett
LDH	Lactatdehydrogenase

MAPK	Mitogen-activated protein kinases
MEK1/2	Dual specificity mitogen-activated protein kinase kinase 1/2
N	Nesting (Nestbauverhalten)
Nab-Paclitaxel	Nanopartikel-Albumin gebundenes Paclitaxel
NS	Nicht signifikant
NSG	NOD-Scid-Gamma Mausstamm (NOD.Cg-*Prkdc*^{scid}*Il2rg*^{tm1Wjl}/SzJ)
OD	Outer diameter (Außendurchmesser)
PanIN	Pankreatische intraepitheliale Neoplasie
PBS	Phosphate-buffered saline (Phosphatgepufferte Salzlösung)
PDAC	Pancreatic ductal adenocarcinoma (Pankreaskarzinom)
PD-L1	Programmed cell death ligand 1
PEG	Polyethylenglycol
PFA	4% Paraformaldehyd in PBS
PI	Propidiumiodid
PI3K	Phosphoinositid-3-Kinasen
Raf	Rapidly accelerated fibrosarcoma protein
ROC	Receiver operating characteristic
RPMI	Roswell Park Memorial Institute
RT	Raumtemperatur
SD	Standardabweichung
SDS	Sodium-Dodecyl-Sulfate (Natrium-Dodecylsulfat)
SMAD4	SMAD family member 4
SOS1	Son of Sevenless Homolog 1
TP53	Tumor protein p53

XI. Lebenslauf

Angaben zur Person

Name:	Benjamin Schulz
Anschrift:	Friesenstraße 5, 18057 Rostock
Geburtsdatum und –ort:	13.07.1989, Schwerin
E-Mail Adresse:	benjamin8989@web.de
Telefonnummer:	0173 9120271

Praktische Erfahrung

01/2021 – heute	Wissenschaftlicher Mitarbeiter am Institut für Experimentelle Chirurgie
12/2017 – 12/2020	Studentische Hilfskraft am Oscar Langendorff Institut für Physiologie
08/2017 – 09/2017	Praktikum Fraunhofer IMTE Lübeck

Ausbildung

01/2021 – heute	Promotion an der Universitätsmedizin Rostock
10/2018 – 09/2020	Master of Science in Medizinische Biotechnologie („Sehr gut“) Masterarbeit: „Optogenetische Kontrolle und photodynamische Manipulation der kontraktilen Aktivität des isolierten Magens der Maus“
10/2015 – 07/2018	Bachelor of Science in Medizinische Biotechnologie („Gut“) Bachelorarbeit: „Entwicklung und Charakterisierung eines murinen ex vivo Modells der Gastroparese“
08/2012 – 10/2015	Ausbildung Kaufmann im Groß – und Außenhandel, ThyssenKrupp Plastics GmbH Rostock

Publikationen

Schulz B, Leitner E, Schreiber T, et al. Sex Matters-Insights from Testing Drug Efficacy in an Animal Model of Pancreatic Cancer. *Cancers (Basel)*. 2024;16(10):1901. doi:10.3390/cancers16101901

Ma Y, **Schulz B**, Trakooljul N, et al. Inhibition of KRAS, MEK and PI3K Demonstrate Synergistic Anti-Tumor Effects in Pancreatic Ductal Adenocarcinoma Cell Lines. *Cancers (Basel)*. 2022;14(18):4467. doi:10.3390/cancers14184467

Zechner D, **Schulz B**, Tang G, et al. Generalizability, Robustness and Replicability When Evaluating Wellbeing of Laboratory Mice with Various Methods. *Animals (Basel)*. 2022;12(21):2927. doi:10.3390/ani12212927

Talbot SR, Kumstel S, **Schulz B**, et al. Robustness of a multivariate composite score when evaluating distress of animal models for gastrointestinal diseases. *Sci Rep*. 2023;13(1):2605. doi:10.1038/s41598-023-29623-8

Vogt M, **Schulz B**, Wagdi A, et al. Direct optogenetic stimulation of smooth muscle cells to control gastric contractility. *Theranostics*. 2021;11(11):5569-5584. doi:10.7150/thno.53883

Konferenzbeiträge

Schulz B, Schwarz R, Aboutara N, Lindner T, Hinz B, Vollmar B, Zechner D. Sex matters: Insights from a syngeneic orthotopic model of metastasized pancreatic cancer. (Posterpräsentation 12th World Congress on Alternatives and Animal Use in the Life Sciences 2023, Niagara Falls, Kanada)

Schulz B, Patejdl R. Erstellung und Charakterisierung eines photodynamisch induzierbaren murinen ex vivo Modells der Gastroparese. (Vortrag und Gewinn des Titelwettbewerbs für den Programmflyer, Jahrestagung der Deutschen Gesellschaft für Neurogastroenterologie und Motilität e.V. 2019, Berlin)

Weitere Kenntnisse und Fähigkeiten

Zertifikate und Weiterbildungen:

- Versuchstierkunde der GV-SOLAS (FELASA B Äquivalent)
- Good Clinical Practice (GCP) Grundlagen – und Aufbaukurs nach AMG (Koordinierungszentrum für Klinische Studien, Universitätsmedizin Rostock)

Fremdsprachen:

- Englisch: sehr gut in Wort und Schrift (C1 Level)

XII. Danksagung

An dieser Stelle möchte ich mich bei allen bedanken, die auf dieser Reise dabei waren und die Promotion unterstützt haben.

Zunächst ein großes Dankeschön an die „Chefin“, Prof. Dr. Brigitte Vollmar, die meine Promotion und diese Dissertation erst ermöglichte, indem ich an Ihrem Institut arbeiten und forschen durfte. Es gab viel zu lernen und auch viel zu lachen. Dafür bin ich dankbar.

Ebenso gilt mein ausdrücklicher Dank apl. Prof. Dr. Dietmar Zechner, der als themenvergebender Betreuer für die Durchführung der Promotion nicht weniger essentiell war. Wir haben viel (manchmal sehr viel) diskutiert, er hatte immer ein offenes Ohr und am Ende hat mich diese Erfahrung für die Zukunft geprägt. Meine kritische und sture Art war sicherlich eine Herausforderung. Außerdem möchte ich mich bei all meinen aktuellen und ehemaligen Arbeitskollegen der AG Zechner bedanken. Danke Wiebke, Emily und Annika. Spezieller Dank gilt natürlich auch den Kollegen der AG Kumstel, allen voran Tim, Simone und Jakob.

Weiterhin gilt mein Dank allen aktuellen und ehemaligen Mitarbeitern des Rudolf-Zenker-Instituts für Experimentelle Chirurgie, die an dieser Arbeit beteiligt waren. Besonders bei unseren lieben TAs; Berit, Doro, Eva, Maren, Anne, Joanna und Janett möchte ich mich bedanken. Eure technische Expertise und viele Arbeit haben diese Dissertation erst möglich gemacht. Ebenso dürfen natürlich Mareike, Ilona und Chantal nicht fehlen. Ihr habt auch spezielle Wünsche wahrgemacht, habt die Tiere an vielen Wochenenden versorgt und hattet auch sonst ein offenes Ohr. Anja sei an dieser Stelle ganz speziell und besonders gedankt. Du bist die Beste! Ansonsten bedanke ich mich auch bei allen anderen; Henni, Valeska, Tobi, Anna, Angie, Susanne, Praveen, Luisa, Nicole, Marcel und allen, die ich möglicherweise vergessen habe.

Zu guter Letzt danke ich meiner Familie und meinen Freunden, die mich während dieser Zeit unterstützt haben und immer für mich da waren. Ganz besonders bedanke ich mich bei Eva, die über die Jahre hinweg immer für mich da war, mein Rückzugsort war und nur zu gut verstanden hat, wenn die Arbeit mehr Zeit in Anspruch nehmen musste.

XIII. Eidesstattliche Versicherung

Ich versichere eidesstattlich durch eigenhändige Unterschrift, dass ich die Arbeit selbstständig und ohne Benutzung anderer als der angegebenen Hilfsmittel angefertigt habe. Alle Stellen, die wörtlich oder sinngemäß aus Veröffentlichungen entnommen sind, habe ich als solche kenntlich gemacht.

Die Arbeit ist noch nicht veröffentlicht und ist in gleicher oder ähnlicher Weise noch nicht als Studienleistung zur Anerkennung oder Bewertung vorgelegt worden. Ich weiß, dass bei Abgabe einer falschen Versicherung die Prüfung als nicht bestanden zu gelten hat.

Rostock _____ _____

(Abgabedatum) (Vollständige Unterschrift)

XIV. Anhang

Anhang 1: Studie I

Anhang 2: Studie II

Anhang 3: Studie III

14.1 Studie I

Studie I: Zechner D, **Schulz B**, Tang G, et al. Generalizability, Robustness and Replicability When Evaluating Wellbeing of Laboratory Mice with Various Methods. *Animals (Basel)*. 2022;12(21):2927. doi:10.3390/ani12212927
(IF 3,0)

animals

MDPI

Article

Generalizability, Robustness and Replicability When Evaluating Wellbeing of Laboratory Mice with Various Methods

Dietmar Zechner [1,*], Benjamin Schulz [1], Guanglin Tang [1], Ahmed Abdelrahman [1], Simone Kumstel [1], Nico Seume [1], Rupert Palme [2] and Brigitte Vollmar [1]

[1] Rudolf-Zenker-Institute of Experimental Surgery, Rostock University Medical Center, 18057 Rostock, Germany
[2] Unit of Physiology, Pathophysiology and Experimental Endocrinology, Department of Biomedical Sciences, University of Veterinary Medicine Vienna, 1210 Vienna, Austria
* Correspondence: dietmar.zechner@uni-rostock.de; Tel.: +49-381-494-2512; Fax: +49-381-494-2502

Simple Summary: It is in the interest of the general public as well as the scientific community to optimize the wellbeing of animals during scientific research. To reach this goal, methods need to be defined which can reliably evaluate the wellbeing of animals. In this study, we assessed whether various methods, such as measuring body weight, burrowing activity, nesting behavior, a distress score and fecal corticosterone metabolites can differentiate between healthy mice and mice after surgical intervention or during the progression of a gastrointestinal disease. The ability of each method to differentiate between these two states of wellbeing was different between distinct surgical interventions and gastrointestinal diseases. These data suggest that scientists cannot rely on a single method, but have to combine many methods when assessing the wellbeing of animals.

Abstract: An essential basis for objectively improving the status of animals during in vivo research is the ability to measure the wellbeing of animals in a reliable and scientific manner. Several non-invasive methods such as assessing body weight, burrowing activity, nesting behavior, a distress score and fecal corticosterone metabolites were evaluated in healthy mice and after three surgical interventions or during the progression of four gastrointestinal diseases. The performance of each method in differentiating between healthy and diseased animals was assessed using receiver operating characteristic curves. The ability to differentiate between these two states differed between distinct surgical interventions and distinct gastrointestinal diseases. Thus, the generalizability of these methods for assessing animal wellbeing was low. However, the robustness of these methods when assessing wellbeing in one gastrointestinal disease was high since the same methods were often capable of differentiating between healthy and diseased animals independent of applied drugs. Moreover, the replicability when assessing two distinct cohorts with an identical surgical intervention was also high. These data suggest that scientists can reach valid conclusions about animal wellbeing when using these methods within one specific animal model. This might be important when optimizing methodological aspects for improving animal wellbeing. The lack of generalizability, however, suggests that comparing animal models by using single methods might lead to incorrect conclusions. Thus, these data support the concept of using a combination of several methods when assessing animal welfare.

Keywords: distress of animals; suffering; severity assessment; 3Rs; animal welfare science

check for updates

Citation: Zechner, D.; Schulz, B.; Tang, G.; Abdelrahman, A.; Kumstel, S.; Seume, N.; Palme, R.; Vollmar, B. Generalizability, Robustness and Replicability When Evaluating Wellbeing of Laboratory Mice with Various Methods. *Animals* **2022**, *12*, 2927. https://doi.org/10.3390/ani12212927

Academic Editor: Leslie Irvine

Received: 15 September 2022
Accepted: 21 October 2022
Published: 25 October 2022

Publisher's Note: MDPI stays neutral with regard to jurisdictional claims in published maps and institutional affiliations.

Copyright: © 2022 by the authors. Licensee MDPI, Basel, Switzerland. This article is an open access article distributed under the terms and conditions of the Creative Commons Attribution (CC BY) license (https://creativecommons.org/licenses/by/4.0/).

1. Introduction

Since Russell and Burch proposed the 3Rs (replacement, reduction and refinement of animal experiments) as principles for humane experimental procedures in 1959 [1], scientists and governments have adopted and expanded these principles. The passing of Directive 2010/63/EU in 2010 made the assessment of animal wellbeing in scientific

procedures mandatory in the European Union [2]. In a similar fashion, animal welfare regulations are implemented and enforced by Animal Care and Use Committees in the United States [3]. While the legal framework in all member states of the EU explicitly demands prospective and retrospective assessment and classification of the severity of procedures, scientists struggle to implement objective, evidence-based and validated methods to assess animal wellbeing in the face of ever-expanding quantities of animal models for diseases.

In general, the assessment of animal wellbeing is often based on physiological parameters such as body weight [4–6] or fecal corticosterone metabolites (FCMs) [7–11]. In addition, clinical signs of distress [12,13]) or behavior such as nesting [14–18] burrowing [18–21] or wheel-running [22,23] are also often assessed as indicators for wellbeing of rodents. Although it is believed that a combination of different methods yields a more precise conclusion than relying on single parameters [24–26], these single parameters should ideally be sensitive enough on their own to discriminate between distressed and non-distressed animals. Thus, it is of interest to check each method if it reliably detects distress when study design (different disease models or therapeutic interventions) or input data (different datasets, baseline data) are varied. In clinical settings, receiver operating characteristic (ROC) curves are often used to measure the performance of a diagnostic test [27–30]. These curves are generated by plotting sensitivity (true positive rate) versus 1-specificity (false positive rate) using a range of thresholds. A diagonal line indicates no discriminatory power (diseased versus non-diseased) of the diagnostic test. This diagonal line equals an area under the curve (AUC) of 0.5. An AUC of 1 indicates that a diagnostic test has 100% sensitivity and 100% specificity and, therefore, has perfect discriminatory power. The AUC was originally also described as corresponding to the probability of classifying a randomly chosen diseased subject as diseased with a higher suspicion than a random non-diseased subject [31]. Thus, the AUC is a measure of the discriminative ability of prediction models [32]. The AUC can serve as an easy-to-use metric to define and compare the diagnostic ability of different methods to differentiate between two states (e.g., healthy versus diseased). As scientists and governmental agencies would like to base their decisions on robust methods, which can define animal wellbeing with a high replicability, it is an important step in the area of animal welfare science to compare these methods for their diagnostic capabilities.

In accordance with Goodman et al. [33] and the Subcommittee on Replicability in Science [34], we define the term replicability as follows: "Replicability refers to the ability of a researcher to duplicate the results of a prior study if the same procedures are followed but new data are collected. That is, a failure to replicate a scientific finding is commonly thought to occur when one study documents relations between two or more variables and a subsequent attempt to implement the same operations fails to yield the same relations with the new data" [34]. For example, replicability is given when a second experiment applies the same procedures and confirms the conclusion of a first experiment. Robustness refers to the stability of experimental conclusions to variations in either baseline assumptions or experimental procedures [33]. For example, a method for assessing animal wellbeing would be robust when the same conclusion can be reached and when minor methodological changes are implemented. Robustness is related to the concept of generalizability, which refers to the persistence of an effect in settings different from and outside of an experimental framework [33]. For example, a method for assessment of animal wellbeing would have very high generalizability when it can measure animal wellbeing in diverse animal models.

In this study, we applied ROC curves to assess if burrowing activity, nesting activity, changes in body weight, a distress score and FCMs can distinguish between healthy and distressed animals after diverse surgical interventions or during the progression of four different gastrointestinal diseases. In extension of this goal, we evaluated the replicability of conclusions when using distinct cohorts of animals. Furthermore, we assessed how robust conclusions are when using different baseline data, different methods of presenting data or using different therapeutic interventions (vehicle or therapy). This compilation of data should also give a first impression on the generalizability of these methods, when assessing various surgical interventions and gastrointestinal diseases. Please note that

this project was not started with a clearly defined hypothesis. Thus, the following data interpretation is exploratory rather than confirmatory research.

2. Materials and Methods

2.1. Animals

2.1.1. Study Concept and Animal Husbandry

This study did not use new animals, but re-evaluated data generated for previous projects with the novel focus on summarizing and comparing the performance of distinct methods when differentiating between healthy mice and mice after surgical intervention or during a disease. Mice, which had to be euthanized during the experiment, were excluded from the analysis. During the experiments, all mice were kept single-housed in type III cages (Zoonlab GmbH, Castrop-Rauxel, Germany) at a 12 h light–dark cycle (dark: 7 pm–7 am), a temperature of 21 ± 2 °C and relative humidity of 60 ± 20% with food (pellets, 10 mm, ssniff-Spezialdiäten GmbH, Soest, Germany) and tap water available ad libitum. Enrichment was provided by nesting material (shredded tissue paper, Verbandmittel GmbH, Frankenberg, Germany), a paper roll (75 × 38 mm, H 0528–151, ssniff-Spezialdiäten GmbH) and a wooden stick (40 × 16 × 10 mm, Abedd, Vienna, Austria). The health of the animal stock was routinely checked (Helicobacter sp., *Rodentibacter pneumotropicus*, and murine Norovirus were detected in few mice; these animals were not used for any experiments). All animal experiments were approved by the German local authority: Landesamt für Landwirtschaft, Lebensmittelsicherheit und Fischerei Mecklenburg-Vorpommern (-1-062/16, -1-019/15, and -1-002/17).

2.1.2. Surgical Interventions and Induction of Diseases

For the transmitter implantation, methodological details and some data were published previously [35]. In brief, male C57BL/6J mice (age: 17.3/17.0–17.45, median/interquartile range in weeks) were anaesthetized on day 0 with isoflurane, a midline laparotomy was performed and an ETA-F-10 transmitter (Data Sciences International, St. Paul, MN, USA; weight: 1.6–1.7 g) was placed in the abdominal cavity. The negative electrode was lead subcutaneously to the right pectoralis major muscle, where it was fixed by sutures. The positive electrode was guided subcutaneously to the left side and was sutured onto the external oblique muscle. The peritoneum and the skin lesion was closed with sutures as described previously [35]. The surgical procedure took 45–50 min.

For the pancreatic cancer model, male C57BL/6J mice (age: 18.6/18.6–19.7, median/interquartile range in weeks) were anaesthetized on day 0 with isoflurane, the abdominal cavity was opened by laparotomy and 5 µL of a cell suspension containing 2.5×10^5 6606PDA cells was injected slowly into the pancreas using a 25-µL syringe (Hamilton Syringe, Reno, NV, USA). The abdominal cavity was closed with sutures as described previously [36]. The surgery lasted 15–20 min. Starting on day 4, and after cell injection, mice were intraperitoneally injected on a daily basis with either metformin (Met; 125 mg/kg in phosphate buffered saline) and α-cyano-4-hydroxycinnamate (CHC; 15 mg/kg in 50% dimethylsulfoxide) or the corresponding vehicle solutions until euthanasia on day 37. More methodological details and some data were published previously [36].

For the ligation of the bile duct, methodological details and some data were published previously [26]. In brief, male BALB/cANCrl mice (age: 10.9/9.6–13.7, median/interquartile range in weeks) were anaesthetized on day 0 with isoflurane and the abdominal cavity was opened by laparotomy. The common bile duct was ligated by three surgical knots and was then transected between the two distal ligations. The abdominal cavity was closed by absorbable sutures and the skin lesions were sewed using a prolene suture. The surgical procedure took 25–40 min. In order to evaluate the possible therapeutic efficacy of NLRP3, inflammasome inhibitor MCC950 (Sigma Aldrich, St. Louise, MO, USA), 20 mg/kg MCC950 or aqua (vehicle) was intraperitoneally injected (volume: 10 µL/g body weight) daily from day 1 before BDL to day 13 after BDL. The mice were euthanized on day 14 after bile duct ligation.

When inducing intoxification with carbon tetrachloride, male BALB/cANCrl mice (age: 10.0/7.9–10.4 median/interquartile range in weeks) were intraperitoneally injected on days 0, 4, 7, 11, 14, 18, 21, 25, 28, 32, 35 and 39 with 0.25 mL/kg body weight CCl_4 (Merck Millipore, Eschborn, Germany, code 1.02209.1000, volume: 1 µL/g body weight after 4x dilution with corn oil). The experiment ended on day 42. Methodological details and some data were published previously [26].

Chronic pancreatitis was induced with cerulein (Bachem, H-3220.0005, Bubendorf, Switzerland), which was dissolved in 0.9% sodium chloride and was administered by consecutive intraperitoneal injections (dosage: 50 µg/kg, volume: 5 µL/g body weight, three hourly injections/day; three days/week (on days 0, 2, 4, 7, 9, 11, 14, 16, 18, 21, 23, 25, 28 and 30) into male C57Bl/6J mice (age: 15.3/14.7–15.3 median/interquartile range in weeks). The microRNA-21 inhibitor (miRCURY LNA™ microRNA-21a-5p inhibitor; cat. # 339203 YCO0070656, sequence: TCAGTCTGATAAGCT) and its corresponding control (miRCURY LNA™ microRNA-21a-5p control; cat. # 339203 YCO0070657, sequence: TCAGTATTAGCAGCT) were purchased from Qiagen (Hilden, Germany), resuspended in PBS and injected subcutaneously at a dosage of 10 mg/kg (volume: 5 µL/g body weight) on day 0 and day 14. The experiment ended on day 33 after the first cerulein injection. Methodological details and some data were published previously [37].

The following refinement measures were implemented. Before surgical intervention, a single subcutaneous injection of 5 mg/kg carprofen (Rimadyl®, Pfizer, GmbH, Berlin, Germany) was applied (volume: 2µL/g body weight) and the eyes of the mouse were kept wet by using eye ointment (Jenapharm, Jena, Germany). During as well as after surgical intervention, the mice were warmed by a warming plate or a warming lamp. In all experiments, 1250 mg/L metamizol (Ratiopharm, Ulm, Germany) was provided daily in the drinking water until euthanasia was performed on the animals.

2.2. Assessment of Animal Wellbeing

In order to evaluate animal wellbeing, the body weight, burrowing activity, nesting behavior, the distress score and FCMs were assessed for each mouse at distinct time points. All these parameters were evaluated at two time points before (pre 1, pre 2) and directly after surgical intervention (post). For example, the distress score was evaluated on day 0 (30 min after finishing surgery), burrowing and nesting activity was assessed from the evening of day 0 to the morning of day 1 and on day 1 after surgery, body weight was determined and feces were collected (see Suppl. Figure S1). In order to get an overview of the wellbeing of animals during the progression of a disease, all parameters were assessed during the early (cholestasis: day 1–2; CCl_4 intoxication: day 4–5; pancreatic cancer: day 4–8; chronic pancreatitis: day 2–3), middle (cholestasis: day 4–5; CCl_4 intoxication: day 18–19; pancreatic cancer: day 18–19; chronic pancreatitis: day 16–17) and late phase (cholestasis: day 13–14; CCl_4 intoxication: day 39–40; pancreatic cancer: day 34–35; chronic pancreatitis: day 30–31) of each disease.

The burrowing activity was analyzed using a tube (length: 15 cm, diameter: 6.5 cm) filled with 200 g of food pellets [18,19]. The tube was placed into the mouse cage 2–3 h before the dark phase and the remaining pellets were weighed after 2 h (for C57Bl/6J mice) or 17 ± 2 h (for BALB/cANCrl mice).

To analyze nest-building behavior, a cotton nestlet (5 cm square of pressed cotton batting, Zoonlab GmbH, Castrop-Rauxel, Germany) was placed into the cage 30 to 60 min before the dark phase. The nests were scored in the morning of the following day at 9:30 ± 2 h, by using a scoring system developed by Deacon [18]. However, a 6th score point was added to this scoring system. This score defined a perfect nest: The nest looked like a crater and more than 90% of the circumference of the nest wall was higher than the body height of the coiled-up mouse.

In addition, the wellbeing of mice was evaluated by assessing multiple parameters with the help of a distress score sheet. This score sheet was based on other score sheets [5,38]

and previously published by our group [39]. The score summarizes various defined criteria (e.g., spontaneous behavior, flight behavior, or general body conditions).

In order to assess the concentration of fecal corticosterone metabolites [7], feces dropped within 24 h in the home cage were collected, dried for 4 h at 65 °C and stored at −20 °C. Afterwards, 50 mg of dry feces were extracted with 1 mL 80% methanol for subsequent analysis using a 5α-pregnane-3β,11β,21-triol-20-one enzyme immunoassay [7,10,40,41]

2.3. Data Presentation and Statistical Analysis

Graphs and all biostatistical analysis were done using GraphPad Prism8 (GraphPad Software Inc., San Diego, CA, USA). To determine how well a parameter distinguishes between healthy and diseased animals, we used the ROC curve analysis and determined the area under the curve (AUC) with corresponding 95% confidence intervals (CI) as a measurement for the performance of the methods. In addition, this software gives the asymptotic *p*-value that determines if the AUC is significantly different from an AUC of 0.5 (an AUC of 0.5 suggests no discriminative ability of a diagnostic test). For examples of ROC curve analysis and explanatory notes, see Suppl. Figure S2. GraphPad Prism computes a *p*-value (two tailed) using the z ratio, which was calculated using the equation $z = (A - 0.5)/SE$. Since the *p*-value considers both the AUC and data variability, we used the *p*- value for giving a representative overview in the form of heat maps. Differences with $p = 0.01–0.05$ were considered to be significant, and differences with $p < 0.01$ were considered to be highly significant.

3. Results

We first assessed animal wellbeing before and after a common surgical intervention using the intraperitoneal implantation of a telemetric transmitter. When comparing the body weight on the day after transmitter implantation (post) to a day before transmitter implantation (pre 1), a reduction in body weight was observed (Figure 1A). The ROC curves, measuring the performance of this method in differentiating between these two states of animal wellbeing (healthy animals versus animals after surgical intervention), yielded an AUC of 0.90 with a 95% confidence interval of 0.75–1.00 (Figure 1A). The discriminatory power of this method was, therefore, significantly higher ($p = 0.0028$) than methods without any discriminative power, yielding an AUC of 0.5. When choosing another day as baseline (pre 2), the same conclusion with a similar AUC was reached (Figure 1B).

Another way of presenting data is comparing the percentage in body weight change between the two time points, (pre 1−pre 2) × 100/pre 2, before surgical intervention, and the percentage in body weight change between the day after surgical intervention and the first time point, (post−pre 2) × 100/pre 2. Transmitter implantation caused a reduction in body weight (Figure 1C), and the performance of this method reached a very high AUC of 1.00 with a 95% confidence interval of 1.00–1.00 (Figure 1C). The discriminatory power was, therefore, also significantly higher ($p = 0.0002$) than methods without any discriminative power. All three ways of calculating changes in body weight led to the same conclusion that measuring body weight could differentiate quite well between animals before and after implantation of a transmitter. However, the third method had the highest discriminative power.

In a similar manner, we evaluated burrowing activity, nesting behavior, a distress score and FCMs for their discriminative power to differentiate between animals before and after transmitter implantation. Burrowing activity, nesting behavior, the distress score and FCMs could very well discriminate between animals before versus after telemeter implantation (see Suppl. Figure S3).

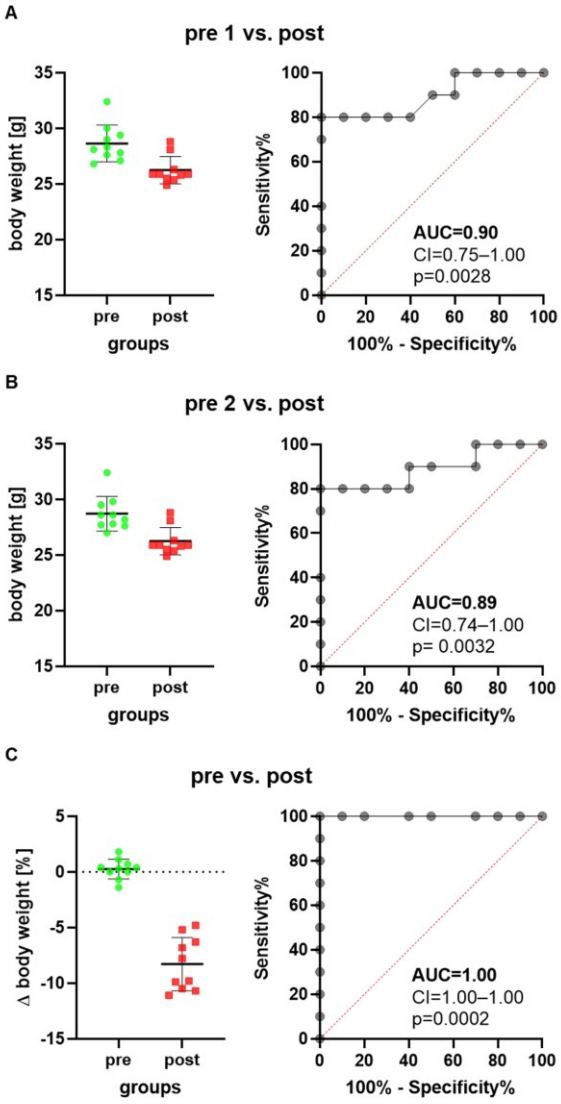

Figure 1. Scatter plots and ROC curves describe changes in body weight of mice when implanting a telemetric transmitter. The ROC curves are generated by plotting sensitivity (true positive rate) versus 1-specificity (false positive rate). The body weight one day after transmitter implantation (post) is compared to the body weight 5 days before transmitter implantation, presented as timepoint pre 1 (**A**), or to the body weight 2 days before transmitter implantation, presented as time point pre 2 (**B**). The percentage in body weight change between the two days before transmitter implantation is compared to the percentage in body weight change between the postoperative day and pre 1 (**C**). The classifier performance of this method in differentiating between animals before and after implanting a transmitter was characterized by the area under the curve (AUC), the confidence interval (CI) and the *p* value indicating how significant the difference was to the reference line (red dotted line indicating no discriminative power). $n = 10$ mice.

The same evaluations were done with two other surgical interventions, laparotomy followed by injection of cancer cells into the pancreas or laparotomy followed by bile duct ligation. In order to give an overview on the discriminative power of body weight, burrowing activity, nesting activity, the distress score and FCMs on all three surgical interventions, we plotted the *p*-values in a heat map (Figure 2) and presented AUC, 95% confidence interval and the number of data points analyzed in Suppl. Table S1. All methods (body weight change, burrowing, nesting distress score and FCMs) had a very high discriminative power ($p < 0.01$), when differentiating between animals before and after transmitter implantation (Figure 2). However only two methods, the evaluation of burrowing activity and assessing FCMs, had a very high discriminative power ($p < 0.01$) when differentiating between animals before and after cell injection into the pancreas (Figure 2). Three methods (the evaluation of burrowing activity, nesting behavior and assessing a distress score) had a very high discriminative power ($p < 0.01$) that differentiated between animals before and after bile duct ligation (Figure 2). A fourth method, assessing the body weight of the animals, had only a very high discriminative power, when comparing the percentage in body weight change. Comparing the body weight of mice as raw data (measured in grams) before and after bile duct ligation had, however, very low discriminative power ($p > 0.05$).

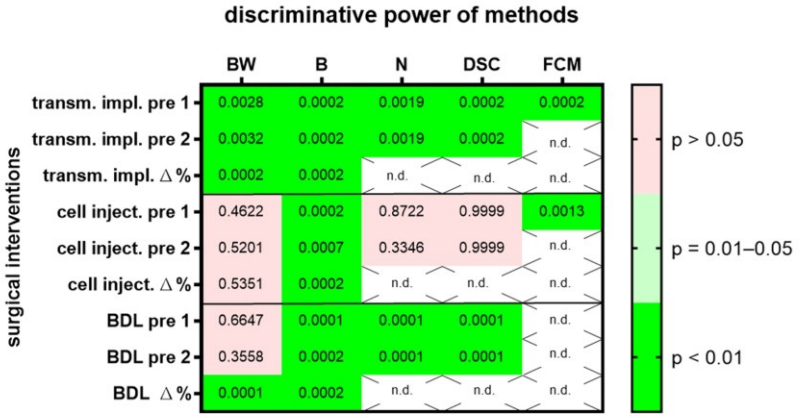

Figure 2. The heat map presents the *p*-value, which indicates how significant the discriminative power of each method was when differentiating between animals before and after surgical intervention. A laparotomy with transmitter implantation (transm. impl.), cancer cell injection into the pancreas (cell inject.) or bile duct ligation (BDL) was performed. The change in body weight (BW), burrowing activity (B), nesting behavior (N), a distress score (DSC) and fecal corticosterone metabolites (FCMs) was assessed. Animal wellbeing after transmitter implantation was compared to a timepoint, pre 1, or to another time point, pre 2, before implantation with most methods. In addition, the percentage of body weight change and burrowing activity between the two days before transmitter implantation is compared to the percentage in body weight change between the postoperative day and pre 1. The heat map differentiates between no ($p > 0.05$), a high ($p = 0.01$–0.05) and a very high ($p < 0.01$) discriminative power. Data analysis was not done (n.d.) for percent calculations of non-metric data (N, DSC) or for FCMs after BDL, since corticosterone metabolites need a functional bile duct so that it can be assayed in the feces. Transmitter implantation: $n = 10$ mice. Cell injection: $n = 14$. BDL: $n = 14$ for N ($n = 7$ vehicle-treated and $n = 7$ MCC950-treated) and $n = 16$ for BW, B and DSC ($n = 9$ vehicle-treated and $n = 7$ MCC950-treated).

These results indicate that some of these methods lack generalizability, because their suitability to differentiate between healthy and distressed animals was dependent on the specific surgical intervention. Alternatively, it might also be possible that the predictive power of the methods cannot be replicated, even when the same surgical intervention is performed.

To assess this hypothesis, we analyzed two groups of mice before and one day after a laparotomy with cell injection into the pancreas. Since treatment with a drug started four days after cell injection, these groups were treated as identical during data collection. For this surgical intervention, a high (p = 0.01–0.05) or very high (p < 0.01) discriminative power was observed in both groups, group A and group B, for the evaluation of burrowing activity and FCMs (Figure 3A; for AUC and confidence interval see Suppl. Table S2). Thus, the conclusion, based on which methods can differentiate between healthy animals and animals after this surgical intervention, can be replicated. However, a high variability in the p value was sometimes observed in these experiments, possibly because we only analyzed a few (n = 7) mice. As a next step, we assessed if methods can differentiate between healthy and distressed animals in a robust manner when an identical surgical intervention has been performed but different therapies were applied. Both cohorts had the identical surgical intervention, a bile duct ligation, but were intraperitoneally injected either with MCC950 or a vehicle solution (Figure 3B; for AUC and confidence interval see Suppl. Table S2). A high (p = 0.01–0.05) or very high (p < 0.01) discriminative power was observed for the evaluation of body weight change, burrowing activity, nesting behavior and assessment of the distress score when differentiating between animals before and after bile duct ligation, independent of which cohort was analyzed (Figure 3B).

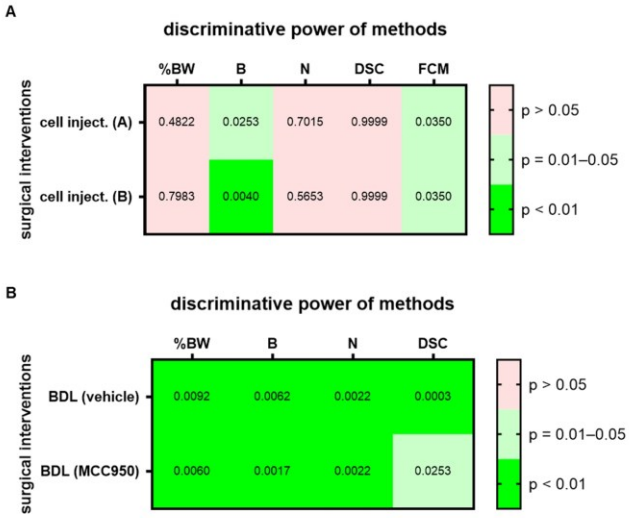

Figure 3. Replicability and robustness of the discriminative power of each method when assessing animal welfare. The heat map indicates the discriminative power when differentiating between animals before and after cell injection (cell inject.) into the pancreas (**A**). Both groups of animals (group A and B) received identical treatment. The discriminative power when differentiating between animals before and after bile duct ligation (BDL) is also presented in form of a heat map (**B**). Mice were treated with either a drug (MCC950) or vehicle solution (vehicle). The percentage in body weight change (%BW), burrowing activity (B), nesting behavior (N), a distress score (DSC) and fecal corticosterone metabolites (FCMs) was assessed. The heat maps present the p-values differentiating between no (p > 0.05), high (p = 0.01–0.05) and very high (p < 0.01) discriminative power between animals before and after surgical intervention. Since corticosterone is metabolized in the liver, no FCMs were analyzed after BDL (n.d.). For cell injection of cohort A (treated at a later time point with vehicle): n = 7. For cell injection of cohort B (treated at a later time point with CHC and Met): n = 7. For BDL and vehicle treatment: n = 7 mice (for N) or n = 9 (for %BW, B and DSC). For BDL and MCC950 treatment: n = 7 (for %BW, B, N and DSC).

We then assessed animal wellbeing before and during various gastrointestinal diseases. For each gastrointestinal disease, we compared two different cohorts, one treated with a specific drug and the other cohort with the respective vehicle solution. Change in body weight, burrowing activity, nesting behavior and the distress score had high (p = 0.01–0.05) or very high (p < 0.01) discriminative power when discriminating between healthy animals and animals during bile duct ligation-induced cholestasis (Figure 4; for AUC and confidence interval see Suppl. Table S3). This was observed in the animal cohort treated with MCC950 and in the animal cohort treated with the respective vehicle solution. However, only one method, evaluation of nesting behavior, had very high (p < 0.01) discriminative power when discriminating between healthy animals and animals with CCl_4-induced liver fibrosis (Figure 4). Again, this was observed in the animal cohort treated with MCC950 and in the cohort treated with the vehicle solution. None of the tested methods could differentiate well between healthy animals and animals with pancreatic cancer (Figure 4). This was observed in both cohorts of animals, independent of the animals that were treated with α-cyano-4-hydroxycinnamate and metformin or the vehicle solution. When analyzing an animal model for chronic pancreatitis, the change in body weight, burrowing activity and nesting behavior had high (p = 0.01–0.05) or very high (p < 0.01) discriminative power when differentiating between healthy animals and mice suffering from chronic pancreatitis (Figure 4). FCMs had only significant discriminative power when mice with chronic pancreatitis were treated with the vehicle solution, but not when they were treated with the microRNA-21 inhibitor (Figure 4).

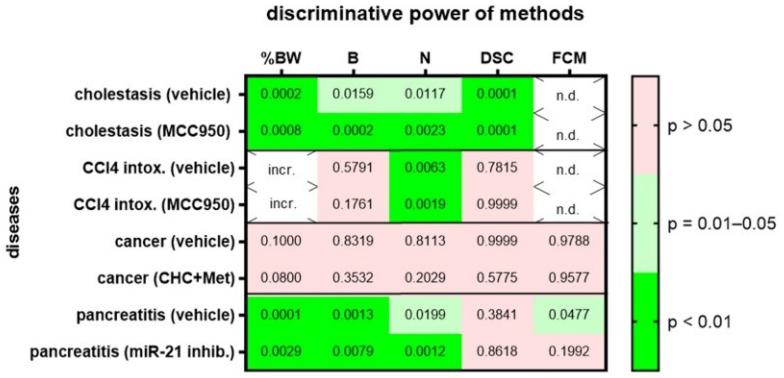

Figure 4. Heat map presenting the p-value, which indicates how significant the discriminative power of each method was when differentiating between animals before and after induction of a disease (pooling the data from early, middle and late disease phase). Two groups of mice with cholestasis, intoxification by CCl_4, pancreatic cancer or chronic pancreatitis were either treated by the indicated drugs or by a solution lacking the drug (vehicle). The percentage in body weight change (%BW), burrowing activity (B), nesting behavior (N), the distress score (DSC) and fecal corticosterone metabolites (FCMs) was assessed. The heat map differentiates between no (p > 0.05), high (p = 0.01–0.05) and very high (p < 0.01) discriminative power. Since corticosterone is metabolized in the liver, no FCMs were analyzed during diseases with liver damage (n.d.). Since mice showed an increase rather than a decrease in body weight after treatment with CCl_4, we did not consider this to be an indication of reduced animal welfare (incr.) and did not show the data. Mice used for cholestasis: n = 7 (vehicle-treated for N), n = 9 (vehicle-treated for %BW, B and DSC), n = 7 (MCC950-treated for %BW, B, N and DSC). Mice used for CCl4 intoxification: n = 6 (vehicle-treated for N), n = 3 (vehicle-treated for %BW, B and DSC), n = 6 (MCC950-treated for N) and n = 7 (MCC950-treated for %BW, B and DSC). Mice used for pancreatic cancer: n = 7 (vehicle-treated for %BW, B, N, DSC and FCM), n = 7 (CHC and Met treated for %BW, B, N, DSC and FCM). Mice used for chronic pancreatitis: n = 8 (vehicle-treated for %BW, B, N and DSC), n = 8 (miRNA21 inhibitor treated for %BW, B, N, DSC and FCM).

We then assessed animal wellbeing separately during three different time points, the early, middle and late phases of each gastrointestinal disease. Change in body weight, burrowing activity, nesting behavior and the distress score had high (p = 0.01–0.05) or very high (p < 0.01) discriminative power when discriminating between healthy animals and cholestatic animals at all phases of cholestasis (Figure 5). However, only nesting behavior had high (p = 0.01–0.05) or very high (p < 0.01) discriminative power when differentiating between healthy animals and animals with CCl_4-induced liver fibrosis (Figure 5; for AUC and confidence interval see Suppl. Table S4). In the animal model for pancreatic cancer, body weight had high (p = 0.01–0.05) discriminative power only during the middle and late phase of cancer progression, whereas burrowing activity had very high (p < 0.01) discriminative power only during the early phase of cancer progression (Figure 5). In the animal model for chronic pancreatitis, changes in body weight, burrowing activity and nesting behavior had very high (p < 0.01) discriminative power when differentiating between healthy and diseased animals. However, FCMs only had high (p = 0.01–0.05) or very high (p < 0.01) discriminative power in the early and late phases of chronic pancreatitis.

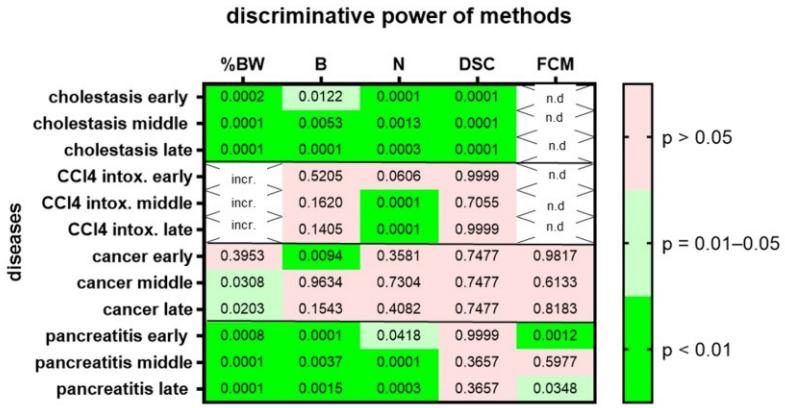

Figure 5. Heat map presenting the p-value, which indicates how significant the discriminative power of each method was when differentiating between animals before and at the early middle or late phase of a disease (pooling the data from mice treated with drugs and mice treated with vehicle). The percentage in body weight change (%BW), burrowing activity (B), nesting behavior (N), distress score (DSC) and fecal corticosterone metabolites (FCMs) was assessed. The heat map differentiates between no (p > 0.05), high (p = 0.01–0.05) and very high (p < 0.01) discriminative power. Since corticosterone is metabolized in the liver, no FCMs were analyzed during diseases with liver damage (n.d.). Since mice showed an increase rather than a decrease in % body weight after treatment with CCl_4, we did not consider this to be an indication of reduced animal welfare (incr.) and decided not to present the p-value. Mice used for cholestasis: n = 14 for N (n = 7 vehicle-treated and n = 7 MCC950-treated), n = 16 for %BW, B and DSC (n = 9 vehicle-treated and n = 7 MCC950-treated). Mice used for CCl4 intoxification: n = 12 for N (n = 6 vehicle-treated and n = 6 MCC950-treated), n = 10 for %BW, B and DSC. (n = 3 vehicle-treated and n = 7 MCC950-treated). Mice used for pancreatic cancer: n = 14 for %BW, B, N, DSC and FCM (n = 7 vehicle-treated and n = 7 CHC and Met treated). Mice used for chronic pancreatitis: n = 16 for %BW, B, N, DSC and FCM (n = 8 vehicle-treated and n = 8 miRNA21 inhibitor treated).

4. Discussion

The presented data suggest that the replicability of conclusions about the wellbeing of animals when analyzing body weight, burrowing, nesting, the distress score or FCMs can be high. Moreover, the robustness of these methods when varying calculation methods

or drug treatment can also be quite high. However, the generalizability of these methods, when used for different animal models, seems to be low.

Several limitations in the interpretation of these data exist. First of all, ROC curves do have advantages but also some limitations. An advantage is that ROC curves can analyze ordinal, non-continuous data [42]. This was essential for the analysis of non-continuous data, such as the distress score or the score for nesting activity. However, ROC analysis with few and unevenly distributed ordinal data may cause unreliable estimations [42]. We observed few and unevenly distributed data points especially when evaluating the distress score. Thus, future work should critically evaluate, how reliable ROC analysis is when describing the diagnostic ability of the distress score. In addition, we want to emphasize that we analyzed three to five methods simultaneously to differentiate between healthy and diseased animals without correcting for the accumulation of the alpha error. This might also contribute to an overestimation of the benefit of these methods when differentiating between healthy and diseased animals. Another limitation is that ROC curves derived from small-sample data sets may not always reliably reflect a classifier's true performance [43]. The sample size for reliably determining if the method is better than random guessing depends on the AUC and the allocation ratio [44]. For example, for an AUC = 0.95 (a Type I error = 0.05, a power of 0.8, and an allocation ratio of 3) $n = 3$ and $n = 9$ data points, whereas for an AUC = 0.65 (a Type I error = 0.05, a power of 0.8, and an allocation ration of 3) $n = 29$ and $n = 87$ data points are suggested [44,45]. Thus, methods described by ROC curves with low AUC will especially benefit from a higher number of data points.

Another major limitation of this study, but also of many studies in the area of animal welfare, is that one measures differences between healthy animals and animals after a surgical intervention or induction of a disease. Any difference observed is often interpreted as proof of reduced wellbeing. One should be aware that this is only one possible interpretation. This limitation is especially evident when only one method supports the interpretation of reduced wellbeing. For example, when repetitively injecting CCl_4 into mice, only nesting behavior was reduced (Figure 5). No reduction of body weight, burrowing activity and no increase in the distress score was noticed. This suggests that nesting activity is either the most sensitive method to detect distress or CCl_4 causes a specific change in nesting behavior independent of inducing distress. Consistent with the second hypothesis is the observation that CCl_4 can change protein expression, reduce the number of neurons in the brain [46] and can also lead to brain damage [47]. Such changes in the central nervous system could influence complex behavior such as nesting activity.

Another limitation is that only one data set described replicability (Figure 3A). It demonstrates that two out of five methods (burrowing and FCMs) can differentiate between the state of the animals before and after an surgical intervention and that this conclusion can be replicated with a second set of data (Figure 3A). One could attempt to quantify replicability by describing that the conclusion concerning all five methods was replicated to 100%. Thus, between the two sets of experiments, the identical methods had or did not have discriminative ability between healthy mice and mice after this surgical intervention. However, please note that this conclusion is based on $p < 0.05$, which determines if the AUC is significantly different from an AUC of 0.5. Such a p-value is a completely arbitrary threshold [48] and there is the danger of over-interpreting conclusions based on such an arbitrary p-value [49–51]. However, this approach helps to simplify observations and to present a simplified overview in the form of a heat map in order to notice patterns in complex data and suggest hypotheses, which can be verified or falsified in future experiments. This experiment suggests that an intra-laboratory replicability can be given for a certain experimental set up (Figure 3A). It does not demonstrate that replicability is given for all other surgical interventions.

Several data sets support the concept that a high robustness is given, when different ways of defining the baseline during an experiment are evaluated (Figure 1, Figure 2 and Figure S1). Using data measured on different days before a surgical intervention did not have a major influence on the conclusion, or whether a method can differentiate between

the distress level before and after a surgical intervention. However, when analyzing a laparotomy with bile duct ligation, there was a difference when using raw data or the percentage in body weight change between two time points (Δ% compared to pre 1 or pre 2 in Figure 2). Using the percentage in body weight change was very well suited to differentiate between distress levels before and after surgical intervention, whereas using raw data (body weight in g) did not differentiate well between these two levels of distress. Please note that in this experiment, animals with a high variability in age were used (age: 10.9/9.6–13.7, median/interquartile range in weeks). Thus, we suggest that the percentage in body weight change rather than raw data should be used, especially when evaluating the distress of animals of different ages and therefore different body weights.

Several data sets support the conclusion that these methods can differentiate well between two levels of distress in a robust manner when treating animals, for example, with a drug or control vehicle (Figures 3B and 4). Only one exception was noticed when analyzing FCMs during chronic pancreatitis (Figure 4). Analyzing FCMs could differentiate with a high ($p = 0.0477$) discriminative power between healthy mice and mice with chronic pancreatitis when these mice were treated with a vehicle solution. However, FCMs failed to differentiate between these two states of distress ($p = 0.1992$) when the mice were treated with an miR-21 inhibitor. As mentioned above, such a conclusion is based on $p < 0.05$, an arbitrary threshold. Because $p = 0.0477$ is very close to this arbitrary threshold, one should avoid over-interpreting this result. This overall robustness to small changes in the experimental protocol suggests that these methods are well suited to assess measures of refinement during animal experiments.

When evaluating, if a method can discriminate between healthy and diseased animals at different disease phases, the robustness for some methods was high, but for other methods it was lower (Figure 5). For example, nesting activity had a high or low discriminative power in all four animal models independent of the phase analyzed (100% robustness). Burrowing, however, was or was not a good method to discriminate in all phases only in three of four animal models (75% robustness). These data demonstrate that the capability of methods to measure differences between healthy and diseased animals can vary during the course of a disease.

The generalizability of some methods was surprisingly low. This was observed when analyzing three different surgical interventions, but also when assessing four gastrointestinal diseases (Figures 2 and 4). For example, nesting behavior could differentiate well between healthy mice and mice after a laparotomy with transmitter implantation and after a laparotomy with bile duct ligation (Figure 2). However, nesting behavior could not differentiate well between healthy mice and mice after a laparotomy with cancer cell injection. The same was observed when using the distress score (Figure 2). To explain these results, one could assume that a laparotomy with cancer cell injection causes less distress than the other two surgical interventions and that nesting behavior and the distress score are not sensitive enough to measure these low levels of distress. Sometimes, the length of a surgical intervention can be a good indication for the complexity of the intervention and for the complications after the intervention [52]. Indeed, a laparotomy with cancer cell injection was done within 15–20 min, whereas a laparotomy and transmitter implantation or a laparotomy with bile duct ligation took 45–50 min or 25 to 40 min, respectively. This supports the hypothesis that a laparotomy with cancer cell injection might cause less distress than the other two surgical interventions. However, the concept that nesting behavior has very low sensitivity when detecting the distress of animals seems to be in contrast to data presented in Figure 4. Thus, it supports the hypothesis described above, whereby CCl_4 might reduce nesting activity directly without reducing animal welfare.

When analyzing gastrointestinal diseases, nesting behavior had the highest generalizability of all methods tested, since it could actually discriminate between healthy and diseased animals in three out of four animal models (75%), whereas burrowing activity could only discriminate in two out of four animal models (50%).

A low generalizability of methods could also be explained by the assumption that certain methods only work well in specific mouse strains. However, strain specificity of certain methods cannot explain the observed lack of generalizability in this study. For example, analyzing change in body weight, burrowing activity and the distress score discriminated well between healthy and diseased animals when analyzing cholestasis in BALB/c mice. These methods failed, however, during CCl_4 intoxication using the same mouse strain. Similarly, nesting could discriminate well between healthy mice and mice suffering from chronic pancreatitis, but failed in mice with pancreatic cancer. Both experiments were done with C57Bl/6 mice.

The presented data demonstrate that different animal models can have diverse effects on various read out parameters for distress. We suggest that mainly two aspects influence whether these methods can differentiate between healthy and diseased mice in an animal model. One major aspect is the level of distress experienced by an animal during the experiment. A second aspect might be that some experiments might influence certain read out parameters and that this is independent from the distress experienced by an animal. Both aspects might reveal a biologically valid mechanism. This emphasizes the need to evaluate distress with several methods and not rely on one or few methods for describing animal wellbeing. However, we do not know yet what the methods with the highest generalizability to assess distress are and how many methods suffice for a correct evaluation of animal wellbeing. A few concepts have been tested to combine multiple methods to reach a conclusion about animal welfare. For example, one can perform such an analysis using z-scores [53], k-means clustering [54], principal component analysis [55,56] binary logistic regression [36,37] or support vector machine classification [26]. Another recently developed tool for a multivariate analysis of animal wellbeing is the Relative Severity Score (RELSA), which was developed by Talbot et al. [25], and is currently tested by various research groups [57]. In this study, we gave an overview on the ability of several methods to differentiate between healthy and diseased animals. We hope that the evaluation of additional animal models and methods will clarify within the following years, which methods are most suitable to assess and compare animal welfare. When distress is assessed, one key issue will be the question as to when the distress was actually measured. Please note that it was our intention to always measure the maximal level of distress. For example, we assessed the distress score always 30 min after an intervention, at a time point when a high impact on the distress score was observed (see Suppl. Figure S1). The body weight, however, was measured 24 h after the intervention because a reduction in body weight can best be observed in the morning of the following day. We do not dare to predict yet if such first steps towards a data-based evaluation of animal welfare will ever allow us to define maximally allowed thresholds of distress an animal should be allowed to experience in a scientific, non-arbitrary manner.

5. Conclusions

We conclude that ROC curves can evaluate the performance of certain methods when differentiating between healthy and diseased mice. We suggest that this approach should also be conducted when evaluating other methods (e.g., running activity or mouse grimace scale). ROC curves or similar strategies might also be useful for assessing welfare of other species, such as pigs or sheep. However, for each species, different methods might be especially valuable for assessing the welfare of animals. Assessing the replicability, robustness and generalizability of the performance of certain methods in many different laboratories could provide a basis for deciding which methods are most suitable for multivariate analyses of animal wellbeing. Defining methods, which are highly replicable and robust might support scientists when assessing measures of refinement or when comparing the severity of animal models. However, so far, we have only analyzed a limited number of animal models. There is still the need to explore the robustness of methods in additional to animal models. Moreover, we also know little about the influence of sex and genetic background of

animals on distinct methods or inter-personal as well as inter-laboratory differences when assessing animal wellbeing.

Supplementary Materials: The following supporting information can be downloaded at: https://www.mdpi.com/article/10.3390/ani12212927/s1, Figure S1: Timeframe of measuring animal distress. Figure S2: Examples of Roc curve analysis. Figure S3: Presentation of classifier performance of various methods. Tables S1–S4: Supplemental information to Figures 2–5.

Author Contributions: Individual author contributions were as follows: D.Z. and B.V. acquired the funding. D.Z. and B.V. developed the study concept. D.Z., G.T., A.A., S.K. and N.S. developed the concept for experiments and data evaluation. D.Z., G.T., A.A., S.K. and N.S. carried out the experiments. R.P. was responsible for analysing FCMs. D.Z. analysed the data. B.S. and D.Z. wrote the manuscript. All authors have read and agreed to the published version of the manuscript.

Funding: This study was supported by the Deutsche Forschungsgemeinschaft (DFG research group FOR 2591, ZE 712/1-1, ZE 712/1-2, VO 450/15-1 and VO 450/15-2).

Institutional Review Board Statement: All animal experiments were approved by the German local authority: Landesamt für Landwirtschaft, Lebensmittelsicherheit und Fischerei Mecklenburg-Vorpommern (-1-062/16, -1-019/15, and -1-002/17).

Informed Consent Statement: Not applicable.

Data Availability Statement: The data presented in this study are available at https://doi.org/10.6084/m9.figshare.21388989.

Acknowledgments: The authors kindly thank Edith Klobetz-Rassam (Department of Biomedical Sciences, University of Veterinary Medicine Vienna) for her excellent technical assistance.

Conflicts of Interest: The authors declare no conflict of interest.

References

1. The Principles of Humane Experimental Technique. *Med. J. Aust.* **1960**, *1*, 500. [CrossRef]
2. Office, P. Directive 2010/63/EU of the European Parliament and of the Council of 22 September 2010 on the Protection of Animals Used for Scientific Purposes. Text with EEA relevance. *Off. J. Eur. Union* **2010**, *L 276*, 33–79.
3. National Research Council. *Guide for the Care and Use of Laboratory Animals*, 8th ed.; National Academies Press: Washington, DC, USA, 2011; ISBN 9780309154000.
4. Talbot, S.R.; Biernot, S.; Bleich, A.; van Dijk, R.M.; Ernst, L.; Häger, C.; Helgers, S.O.A.; Koegel, B.; Koska, I.; Kuhla, A.; et al. Defining body-weight reduction as a humane endpoint: A critical appraisal. *Lab. Anim.* **2020**, *54*, 99–110. [CrossRef]
5. Morton, D.B.; Griffiths, P.H. Guidelines on the recognition of pain, distress and discomfort in experimental animals and an hypothesis for assessment. *Vet. Rec.* **1985**, *116*, 431–436. [CrossRef]
6. Morton, D.B. A systematic approach for establishing humane endpoints. *ILAR J.* **2000**, *41*, 80–86. [CrossRef]
7. Touma, C.; Palme, R.; Sachser, N. Analyzing corticosterone metabolites in fecal samples of mice: A noninvasive technique to monitor stress hormones. *Horm. Behav.* **2004**, *45*, 10–22. [CrossRef]
8. Auer, K.E.; Kußmaul, M.; Möstl, E.; Hohlbaum, K.; Rülicke, T.; Palme, R. Measurement of Fecal Testosterone Metabolites in Mice: Replacement of Invasive Techniques. *Animals* **2020**, *10*, 165. [CrossRef]
9. Kolbe, T.; Palme, R.; Tichy, A.; Rülicke, T. Lifetime Dependent Variation of Stress Hormone Metabolites in Feces of Two Laboratory Mouse Strains. *PLoS ONE* **2015**, *10*, e0136112. [CrossRef]
10. Mallien, A.S.; Becker, L.; Pfeiffer, N.; Terraneo, F.; Hahn, M.; Middelman, A.; Palme, R.; Creutzberg, K.C.; Begni, V.; Riva, M.A.; et al. Dopamine Transporter Knockout Rats Show Impaired Wellbeing in a Multimodal Severity Assessment Approach. *Front. Behav. Neurosci.* **2022**, *16*, 924603. [CrossRef]
11. Palme, R. Non-invasive measurement of glucocorticoids: Advances and problems. *Physiol. Behav.* **2019**, *199*, 229–243. [CrossRef]
12. van Fentener Vlissingen, J.M.; Borrens, M.; Girod, A.; Lelovas, P.; Morrison, F.; Torres, Y.S. The reporting of clinical signs in laboratory animals: FELASA Working Group Report. *Lab. Anim.* **2015**, *49*, 267–283. [CrossRef] [PubMed]
13. Xie, W.; Palme, R.; Schafmayer, C.; Zechner, D.; Vollmar, B.; Grambow, E. Distress Analysis of Mice with Cervical Arteriovenous Fistulas. *Animals* **2021**, *11*, 3051. [CrossRef] [PubMed]
14. Schwabe, K.; Boldt, L.; Bleich, A.; van Dijk, R.M.; Helgers, S.O.A.; Häger, C.; Nowakowska, M.; Riedesel, A.-K.; Schönhoff, K.; Struve, B.; et al. Nest-building performance in rats: Impact of vendor, experience, and sex. *Lab. Anim.* **2020**, *54*, 17–25. [CrossRef] [PubMed]
15. Deacon, R.M.J. Assessing nest building in mice. *Nat. Protoc.* **2006**, *1*, 1117–1119. [CrossRef]
16. Gaskill, B.N.; Karas, A.Z.; Garner, J.P.; Pritchett-Corning, K.R. Nest building as an indicator of health and welfare in laboratory mice. *J. Vis. Exp.* **2013**, *82*, e51012. [CrossRef]

17. Jirkof, P.; Fleischmann, T.; Cesarovic, N.; Rettich, A.; Vogel, J.; Arras, M. Assessment of postsurgical distress and pain in laboratory mice by nest complexity scoring. *Lab. Anim.* **2013**, *47*, 153–161. [CrossRef]
18. Deacon, R. Assessing burrowing, nest construction, and hoarding in mice. *J. Vis. Exp.* **2012**, *59*, e2607. [CrossRef]
19. Deacon, R.M.J. Burrowing in rodents: A sensitive method for detecting behavioral dysfunction. *Nat. Protoc.* **2006**, *1*, 118–121. [CrossRef]
20. Jirkof, P. Burrowing and nest building behavior as indicators of well-being in mice. *J. Neurosci. Methods* **2014**, *234*, 139–146. [CrossRef]
21. Gjendal, K.; Ottesen, J.L.; Olsson, I.A.S.; Sørensen, D.B. Burrowing and nest building activity in mice after exposure to grid floor, isoflurane or ip injections. *Physiol. Behav.* **2019**, *206*, 59–66. [CrossRef]
22. Weegh, N.; Füner, J.; Janke, O.; Winter, Y.; Jung, C.; Struve, B.; Wassermann, L.; Lewejohann, L.; Bleich, A.; Häger, C. Wheel running behaviour in group-housed female mice indicates disturbed wellbeing due to DSS colitis. *Lab. Anim.* **2020**, *54*, 63–72. [CrossRef]
23. Weegh, N.; Zentrich, E.; Zechner, D.; Struve, B.; Wassermann, L.; Talbot, S.R.; Kumstel, S.; Heider, M.; Vollmar, B.; Bleich, A.; et al. Voluntary wheel running behaviour as a tool to assess the severity in a mouse pancreatic cancer model. *PLoS ONE* **2021**, *16*, e0261662. [CrossRef] [PubMed]
24. Keubler, L.M.; Hoppe, N.; Potschka, H.; Talbot, S.R.; Vollmar, B.; Zechner, D.; Häger, C.; Bleich, A. Where are we heading? Challenges in evidence-based severity assessment. *Lab. Anim.* **2020**, *54*, 50–62. [CrossRef] [PubMed]
25. Talbot, S.R.; Struve, B.; Wassermann, L.; Heider, M.; Weegh, N.; Knape, T.; Hofmann, M.C.J.; von Knethen, A.; Jirkof, P.; Keubler, L.; et al. One Score to Rule Them All: Severity Assessment in Laboratory Mice. *bioRxiv* **2020**. [CrossRef]
26. Tang, G.; Seume, N.; Häger, C.; Kumstel, S.; Abshagen, K.; Bleich, A.; Vollmar, B.; Talbot, S.R.; Zhang, X.; Zechner, D. Comparing distress of mouse models for liver damage. *Sci. Rep.* **2020**, *10*, 19814. [CrossRef]
27. Mandrekar, J.N. Receiver operating characteristic curve in diagnostic test assessment. *J. Thorac. Oncol.* **2010**, *5*, 1315–1316. [CrossRef]
28. Wacker, C.; Prkno, A.; Brunkhorst, F.M.; Schlattmann, P. Procalcitonin as a diagnostic marker for sepsis: A systematic review and meta-analysis. *Lancet Infect. Dis.* **2013**, *13*, 426–435. [CrossRef]
29. Ovadia, C.; Seed, P.T.; Sklavounos, A.; Geenes, V.; Di Ilio, C.; Chambers, J.; Kohari, K.; Bacq, Y.; Bozkurt, N.; Brun-Furrer, R.; et al. Association of adverse perinatal outcomes of intrahepatic cholestasis of pregnancy with biochemical markers: Results of aggregate and individual patient data meta-analyses. *Lancet* **2019**, *393*, 899–909. [CrossRef]
30. Sudre, C.H.; Murray, B.; Varsavsky, T.; Graham, M.S.; Penfold, R.S.; Bowyer, R.C.; Pujol, J.C.; Klaser, K.; Antonelli, M.; Canas, L.S.; et al. Attributes and predictors of long COVID. *Nat. Med.* **2021**, *27*, 626–631. [CrossRef]
31. Hanley, J.A.; McNeil, B.J. The meaning and use of the area under a receiver operating characteristic (ROC) curve. *Radiology* **1982**, *143*, 29–36. [CrossRef]
32. Janssens, A.C.J.W.; Martens, F.K. Reflection on modern methods: Revisiting the area under the ROC Curve. *Int. J. Epidemiol.* **2020**, *49*, 1397–1403. [CrossRef] [PubMed]
33. Goodman, S.N.; Fanelli, D.; Ioannidis, J.P.A. What does research reproducibility mean? *Sci. Transl. Med.* **2016**, *8*, 341ps12. [CrossRef] [PubMed]
34. Bollen, K.; Cacioppo, J.T.; Kaplan, R.M.; Krosnick, J.A.; Olds, J.L.; Dean, H. Social, behavioral, and economic sciences perspectives on robust and reliable science. Report of the Subcommittee on Replicability in Science Advisory Committee to the National Science Foundation Directorate for Social, Behavioral, and Economic Sciences. 2015. Available online: https://nsf.gov/sbe/AC_Materials/SBE_Robust_and_Reliable_Research_Report.pdf (accessed on 12 October 2022).
35. Kumstel, S.; Vasudevan, P.; Palme, R.; Zhang, X.; Wendt, E.H.U.; David, R.; Vollmar, B.; Zechner, D. Benefits of non-invasive methods compared to telemetry for distress analysis in a murine model of pancreatic cancer. *J. Adv. Res.* **2020**, *21*, 35–47. [CrossRef] [PubMed]
36. Kumstel, S.; Wendt, E.H.U.; Eichberg, J.; Talbot, S.R.; Häger, C.; Zhang, X.; Abdelrahman, A.; Schönrogge, M.; Palme, R.; Bleich, A.; et al. Grading animal distress and side effects of therapies. *Ann. N. Y. Acad. Sci.* **2020**, *1473*, 20–34. [CrossRef]
37. Abdelrahman, A.; Kumstel, S.; Zhang, X.; Liebig, M.; Wendt, E.H.U.; Eichberg, J.; Palme, R.; Thum, T.; Vollmar, B.; Zechner, D. A novel multi-parametric analysis of non-invasive methods to assess animal distress during chronic pancreatitis. *Sci. Rep.* **2019**, *9*, 14084. [CrossRef]
38. Paster, E.V.; Villines, K.A.; Hickman, D.L. Endpoints for mouse abdominal tumor models: Refinement of current criteria. *Comp. Med.* **2009**, *59*, 234–241.
39. Kumstel, S.; Tang, G.; Zhang, X.; Kerndl, H.; Vollmar, B.; Zechner, D. Grading Distress of Different Animal Models for Gastrointestinal Diseases Based on Plasma Corticosterone Kinetics. *Animals* **2019**, *9*, 145. [CrossRef]
40. Kroll, T.; Kornadt-Beck, N.; Oskamp, A.; Elmenhorst, D.; Touma, C.; Palme, R.; Bauer, A. Additional Assessment of Fecal Corticosterone Metabolites Improves Visual Rating in the Evaluation of Stress Responses of Laboratory Rats. *Animals* **2021**, *11*, 710. [CrossRef]
41. Touma, C.; Sachser, N.; Möstl, E.; Palme, R. Effects of sex and time of day on metabolism and excretion of corticosterone in urine and feces of mice. *Gen. Comp. Endocrinol.* **2003**, *130*, 267–278. [CrossRef]
42. Hadjiiski, L.; Chan, H.P.; Sahiner, B.; Helvie, M.A.; Roubidoux, M.A. Quasi-continuous and discrete confidence rating scales for observer performance studies: Effects on ROC analysis. *Acad. Radiol.* **2007**, *14*, 38–48. [CrossRef]

43. Hanczar, B.; Hua, J.; Sima, C.; Weinstein, J.; Bittner, M.; Dougherty, E.R. Small-sample precision of ROC-related estimates. *Bioinformatics* **2010**, *26*, 822–830. [CrossRef] [PubMed]
44. Goksuluk, D.; Korkmaz, S.; Zararsiz, G.; Karaagaoglu, A.E. easyROC: An Interactive Web-tool for ROC Curve Analysis Using R Language Environment. *R J.* **2016**, *8*, 213–230. [CrossRef]
45. easyROC: A Web-Tool for ROC Curve Analysis (Ver. 1.3.1). Available online: http://www.biosoft.hacettepe.edu.tr/easyROC/ (accessed on 12 October 2022).
46. Jiménez-Torres, C.; El-Kehdy, H.; Hernández-Kelly, L.C.; Sokal, E.; Ortega, A.; Najimi, M. Acute Liver Toxicity Modifies Protein Expression of Glutamate Transporters in Liver and Cerebellar Tissue. *Front. Neurosci.* **2020**, *14*, 613225. [CrossRef]
47. Altinoz, E.; Erdemli, M.E.; Gul, M.; Aksungur, Z.; Gul, S.; Bag, H.G.; Kaya, G.B.; Turkoz, Y. Neuroprotection against CCl4 induced brain damage with crocin in Wistar rats. *Biotech. Histochem.* **2018**, *93*, 623–631. [CrossRef]
48. National Academies Press (US). *Reproducibility and Replicability in Science*; National Academies Press: Washington, DC, USA, 2019, ISBN 9780309486163.
49. Dirnagl, U. The *p* value wars (again). *Eur. J. Nucl. Med. Mol. Imaging* **2019**, *46*, 2421–2423. [CrossRef] [PubMed]
50. Amrhein, V.; Greenland, S.; McShane, B. Scientists rise up against statistical significance. *Nature* **2019**, *567*, 305–307. [CrossRef] [PubMed]
51. Wasserstein, R.L.; Schirm, A.L.; Lazar, N.A. Moving to a World Beyond "$p < 0.05$". *Am. Stat.* **2019**, *73*, 1–19. [CrossRef]
52. Cheng, H.; Clymer, J.W.; Po-Han Chen, B.; Sadeghirad, B.; Ferko, N.C.; Cameron, C.G.; Hinoul, P. Prolonged operative duration is associated with complications: A systematic review and meta-analysis. *J. Surg. Res.* **2018**, *229*, 134–144. [CrossRef]
53. Peng, M.; Zhang, C.; Dong, Y.; Zhang, Y.; Nakazawa, H.; Kaneki, M.; Zheng, H.; Shen, Y.; Marcantonio, E.R.; Xie, Z. Battery of behavioral tests in mice to study postoperative delirium. *Sci. Rep.* **2016**, *6*, 29874. [CrossRef]
54. Häger, C.; Keubler, L.M.; Talbot, S.R.; Biernot, S.; Weegh, N.; Buchheister, S.; Buettner, M.; Glage, S.; Bleich, A. Running in the wheel: Defining individual severity levels in mice. *PLoS Biol.* **2018**, *16*, e2006159. [CrossRef]
55. Buchecker, V.; Koska, I.; Pace, C.; Talbot, S.R.; Palme, R.; Bleich, A.; Potschka, H. Toward evidence-based severity assessment in mouse models with repeated seizures: (II.) Impact of surgery and intrahippocampal kainate. *Eur. Surg. Res.* **2022**, *in press*. [CrossRef] [PubMed]
56. Möller, C.; Wolf, F.; van Dijk, R.M.; Di Liberto, V.; Russmann, V.; Keck, M.; Palme, R.; Hellweg, R.; Gass, P.; Otzdorff, C.; et al. Toward evidence-based severity assessment in rat models with repeated seizures: I. Electrical kindling. *Epilepsia* **2018**, *59*, 765–777. [CrossRef] [PubMed]
57. Mallien, A.S.; Pfeiffer, N.; Brandwein, C.; Inta, D.; Sprengel, R.; Palme, R.; Talbot, S.R.; Gass, P. Comparative Severity Assessment of Genetic, Stress-Based, and Pharmacological Mouse Models of Depression. *Front. Behav. Neurosci.* **2022**, *16*. [CrossRef] [PubMed]

14.2 Studie II

Studie II: Ma Y, **Schulz B**, Trakooljul N, et al. Inhibition of KRAS, MEK and PI3K Demonstrate Synergistic Anti-Tumor Effects in Pancreatic Ductal Adenocarcinoma Cell Lines. *Cancers (Basel)*. 2022;14(18):4467. doi:10.3390/cancers14184467 (IF 5,2)

cancers

MDPI

Article

Inhibition of KRAS, MEK and PI3K Demonstrate Synergistic Anti-Tumor Effects in Pancreatic Ductal Adenocarcinoma Cell Lines

Yixuan Ma [1], Benjamin Schulz [2], Nares Trakooljul [3], Moosheer Al Ammar [1], Anett Sekora [1], Sina Sender [1], Frieder Hadlich [3], Dietmar Zechner [2], Frank Ulrich Weiss [4], Markus M. Lerch [4,5], Robert Jaster [6], Christian Junghanss [1] and Hugo Murua Escobar [1,*]

[1] Department of Medicine Clinic III, Hematology, Oncology and Palliative Medicine, Rostock University Medical Center, 18057 Rostock, Germany
[2] Institute for Experimental Surgery, Rostock University Medical Center, 18057 Rostock, Germany
[3] Institute of Genome Biology, Research Institute for Farm Animal Biology (FBN), 18196 Dummerstorf, Germany
[4] Department of Medicine A, University Medicine Greifswald, 17475 Greifswald, Germany
[5] Ludwig Maximilian University Hospital, Ludwig Maximilian University of Munich, 81377 Munich, Germany
[6] Department of Medicine II, Division of Gastroenterology, Rostock University Medical Center, 18057 Rostock, Germany
* Correspondence: hugo.murua.escobar@med.uni-rostock.de; Tel.: +49-381494-7519 or +49-381494-7639; Fax: +49-381494-45803

Simple Summary: Small molecule inhibitors and targeted therapy are considered to have significant potential for pancreatic ductal adenocarcinoma therapies. Preclinical studies of novel inhibitors and inhibitor combinations can elucidate their acting mechanisms and provide valuable data for in vivo research and clinical trials. We explored the antitumor efficacy of KRAS inhibitors BI-3406 and sotorasib alone or in combination with the downstream inhibitors trametinib and buparlisib in PDAC cell lines, characterized by different *KRAS* mutational statuses. The two KRAS inhibitors demonstrated different anti-tumor efficacy and displayed synergistic or additive effects, when combined with downstream pathway inhibitors. These data emphasized the importance of KRAS as a therapeutic target for PDAC and indicate two distinct mechanisms of KRAS inhibition and their interactions with downstream pathway inhibitors.

Abstract: Kirsten rat sarcoma virus (*KRAS*) mutations are widespread in pancreatic ductal adenocarcinoma (PDAC) and contribute significantly to tumor initiation, progression, tumor relapse/resistance, and prognosis of patients. Although inhibitors against *KRAS* mutations have been developed, this therapeutic approach is not routinely used in PDAC patients. We investigated the anti-tumor efficacy of two KRAS inhibitors BI-3406 (KRAS::SOS1 inhibitor) and sotorasib (KRAS G12C inhibitor) alone or in combination with MEK1/2 inhibitor trametinib and/or PI3K inhibitor buparlisib in seven PDAC cell lines. Whole transcriptomic analysis of combined inhibition and control groups were comparatively analyzed to explore the corresponding mechanisms of inhibitor combination. Both KRAS inhibitors and corresponding combinations exhibited cytotoxicity against specific PDAC cell lines. BI-3406 enhance the efficacy of trametinib and buparlisib in BXPC-3, ASPC-1 and MIA PACA-2, but not in CAPAN-1, while sotorasib enhances the efficacy of trametinib and buparlisib only in MIA PACA-2. The whole transcriptomic analysis demonstrates that the two triple-inhibitor combinations exert antitumor effects by affecting related cell functions, such as affecting the immune system, cell adhesion, cell migration, and cytokine binding. As well as directly involved in RAF/MEK/ERK pathway and PI3K/AKT pathway affect cell survival. Our current study confirmed inhibition of KRAS and its downstream pathways as a potential novel therapy for PDAC and provides fundamental data for in vivo evaluations.

Keywords: pancreatic ductal adenocarcinoma; KRAS; kinase inhibitors; gene expression

check for updates

Citation: Ma, Y.; Schulz, B.; Trakooljul, N.; Al Ammar, M.; Sekora, A.; Sender, S.; Hadlich, F.; Zechner, D.; Weiss, F.U.; Lerch, M.M.; et al. Inhibition of KRAS, MEK and PI3K Demonstrate Synergistic Anti-Tumor Effects in Pancreatic Ductal Adenocarcinoma Cell Lines. *Cancers* **2022**, *14*, 4467. https://doi.org/10.3390/cancers14184467

Academic Editors: Paola Ghiorzo, William Bruno and Lorenza Pastorino

Received: 26 August 2022
Accepted: 12 September 2022
Published: 14 September 2022

Publisher's Note: MDPI stays neutral with regard to jurisdictional claims in published maps and institutional affiliations.

Copyright: © 2022 by the authors. Licensee MDPI, Basel, Switzerland. This article is an open access article distributed under the terms and conditions of the Creative Commons Attribution (CC BY) license (https://creativecommons.org/licenses/by/4.0/).

1. Introduction

Kirsten rat sarcoma viral oncogene homolog (*KRAS*) is one of the most frequently mutated oncogenes in human pancreatic ductal adenocarcinoma (PDAC); oncogenic *KRAS* mutations can be detected in approximately 92% of the PDAC genomes [1–6]. The *KRAS* gene encodes the protein KRAS, which is a guanosine triphosphatase (GTPase), and regulates signal transduction by cycling between active guanosine triphosphate (GTP) bound and inactive guanosine diphosphate (GDP) bound statuses [7]. *KRAS* point mutations downregulate the GTPase activity of RAS and prevent the GTPase from promoting the conversion of GTP to GDP. The status of permanent GTP-binding activates downstream signaling pathways, such as the PI3K/AKT pathway or RAF/MEK/ERK pathway, which in turn leads to the initiation and development of PDAC [8]. Moreover, *KRAS* cooperates with other common oncogenes, such as *TP53*, *CDKN2A*, *BRCA3*, *SMAD4*, etc., to cause the initiation and development of PDAC [9–13].

KRAS mutations not only cause the initiation and development of PDAC, but they also affect the efficacy of treatment routines and the long-term survival of patients. A considerable number of studies have revealed that *KRAS* mutations lead to a poor prognosis for patients, regardless of whether they undergo surgery [14]. At the same time, a study pointed out that *KRAS* activation plays an important role in the resistance to gemcitabine treatment and relapse after treatment [15]. Another study reported that specific *KRAS* mutation subtypes (G12V, G12D, and G12A) shortened the median overall survival of PDAC patients [16].

Due to the important role of *KRAS* in PDAC, a growing number of studies consider *KRAS* as a target for the treatment of PDAC. Sotorasib is the first small molecule inhibitor against KRAS G12C mutations and was approved by the FDA for the treatment of non-small cell lung cancer (NSCLC) in 2021. Studies have reported that it can effectively inhibit various cell lines that carry *KRAS* G12C mutations, including PDAC cell lines [17]. According to the recently disclosed CodeBreaK 100 clinical trial results, sotorasib displayed good efficacy in the treatment of advanced KRAS G12C-mutated PDAC, with 8 of the 38 patients having a partial response and 32 of 38 patients displaying disease control. The side effects of sotorasib are described as mild, as only a few patients were affected by grade 3 diarrhea, fatigue, and abdominal pain; no grade 4 side effects were observed in the patients [18]. Currently (2022), there are 18 clinical trials targeting KRAS by sotorasib in progress [19]. However, almost all the clinical trials target NSCLC and colorectal cancer and only a very small number of PDAC patients are enrolled. In addition, other reported KRAS G12C inhibitors (adagrasib, JNJ-74699157, and LY3499446) have also achieved distinct effects in cell experiments, and corresponding clinical trials are also ongoing [20,21]. At the same time, inhibitors that directly target other KRAS mutations (e.g., KS-58 targeting KRAS G12D) are under development.

Although the KRAS G12C inhibitors achieved satisfactory effects on its corresponding mutation, *KRAS* G12C mutations accounted for only 1.42% of all *KRAS* mutated PDAC patients. The specific inhibitors for *KRAS* G12D and G12V mutations, which currently represent the majority (40.45% and 32.14%, respectively), are still under development and have not yet entered any clinical trials [22]. Therefore, how to target other types of *KRAS* mutations is also an urgent problem to be solved. It is well known that there are dynamic positive feedback and negative feedback regulation loops in the RAS signaling pathway. A key role in this feedback regulation is the guanine exchange factor son of sevenless 1 (SOS1) [23]. In unstimulated cells, SOS1 hyperphosphorylation caused by mitogen-activated protein kinase (MAPK) activation catalyzes the activation of RAS. At the same time, SOS1 hyperphosphorylation in stimulated cells will cause it to separate from cytosolic glutathione reductase (GRC2) and cause RAS inactivation [23,24]. Moreover, down-regulation or loss of SOS1 lead to a decrease in the survival rate of tumor cells carrying *KRAS* mutations [25]. Based on these studies, Hoffman et al. developed an inhibitor BI-3406 that can block the interaction between SOS1 and KRAS. It can effectively inhibit a variety of *KRAS* mutant tumor cell lines in vivo and in vitro, including *KRAS*

G12C/V/S/A, and G13D, and also achieved excellent efficacy in the PDAC cell line MIA PACA-2. Moreover, the experimental animals displayed good tolerance to BI-3406 treatment [26]. Therefore, BI 1701963, another inhibitor closely related to BI-3406, has entered phase I clinical trials.

Although studies on the inhibition of *KRAS* have achieved encouraging results, there are still limitations that exist, especially for PDAC. At present, most studies still focus on NSCLS, while little attention has been paid to PDAC. There are also few studies that investigate the combined application of multiple inhibitors. In the existing studies on PDAC, only the MIA PACA-2 cell line was investigated. As a result, we were unable to evaluate the efficacy of these *KRAS* inhibitors on PDAC cells carrying other *KRAS* mutations. Therefore, we studied the efficacy of multiple *KRAS* mutation inhibitor BI-3406 and specific *KRAS* mutation inhibitor sotorasib in different *KRAS* mutations and wild-type *KRAS* PDAC cell lines. At the same time, we explored the efficacy of *KRAS* inhibitors and their downstream pathways (PI3K/AKT/mTOR pathway and RAF/MEK/ERK pathway) inhibitors in combination. RNA sequencing was performed after the combined application to explore the mechanism of the influence of the multi-inhibitor combination on the pathway.

2. Materials and Methods

2.1. Kinase Inhibitors

BI-3406 (KRAS::SOS1 inhibitor) was purchased from Chemietek (Chemietek, Indianapolis, IN, USA), sotorasib (KRAS G12C inhibitor), buparlisib (pan-PI3K inhibitor), and trametinib (MEK1/2 inhibitor) were purchased from Selleck Chemicals (Absource Diagnostics GmbH, Munich, Germany). According to the manufacturer's instructions, all inhibitors were separately dissolved in dimethyl sulfoxide (DMSO) (Sigma Aldrich Chemie GmbH, Steinheim, Germany) as a stock solution, at a final concentration of 10 mM. The stock solutions were stored at −80 °C and diluted into corresponding working concentrations before each experiment.

2.2. Cell Lines and Cell Culture

PDAC cell lines ASPC-1, BXPC-3, CAPAN-1, COLO357, PATU8902, and T3M4 were kindly provided by the University Medicine Greifswald and MIA PACA-2 was kindly provided by Prof. Robert Jaster from Rostock University Medical Center. ASPC-1, BXPC-3, COLO357, and T3M4 were cultured in RPMI1640 medium (PAN-Biotech, Aidenbach, Germany), supplemented with 10% heat-inactivated fetal calf serum (FCS) (PAN-Biotech) and 1% penicillin-streptomycin solution (P/S) (10,000 U/mL penicillin, 10 mg/mL streptomycin) (PAN-Biotech). CAPAN-1 was cultured in RPMI1640 medium, supplemented with 15% heat-inactivated FCS and 1% P/S solution. MIA PACA-2 was cultured in DMEM medium (PAN-Biotech), supplemented with 1% heated-inactivated FCS and 1% P/S solution. PATU8902 was cultured in DMEM/F12 medium (PAN-Biotech), supplemented with 10% heated-inactivated FCS and 1% P/S solution. After verifying that all cell lines were not contaminated by mycoplasma, these PDAC cell lines were maintained in a 5% CO_2 incubator with a humidified atmosphere at 37 °C.

2.3. Inhibitor Application Experiments

For the single inhibitor application experiments, the PDAC cell lines were seeded at a density of 3.3×10^4 cells per milliliter in a 24-well plate (in total, 1.5 mL per well, for cell proliferation assay) or a 96-well plate (in total, 150 µL per well, for biomass quantification assay). After 24 h, the supernatant was discarded and media containing increasing concentrations (range from 0.1 to 10 µM for BI-3406, 0.001 to 10 µM for sotorasib) of inhibitors or vehicle (DMSO, as control) were added to the corresponding PDAC cell lines.

The results of single inhibitor application and related experiments were comprehensively analyzed, and specific PDAC cell lines and inhibitor concentrations were selected for further combined application experiments and the concentrations are listed in Table 1 (the results of the buparlisib inhibition assay are detailed in a previously published paper, and the

results of the trametinib inhibition assay are detailed in the Supplementary Table S14) [27]. Inhibitor concentrations are displayed in Table 1. The PDAC cell lines were seeded in 6-well plates (for RNA isolation), 24-well plates (for proliferation assay, morphological examination, and apoptosis/necrosis analysis), or 96-well plates (for biomass quantification assay). After 24 h, the supernatant was discarded and media containing different combinations of inhibitors were added to the corresponding PDAC cell lines.

Table 1. Inhibitor concentrations used for combined application.

Cell Lines	BI-3406	Sotorasib	Trametinib	Buparlisib
ASPC-1	4 µM	4 µM	0.001 µM	0.3 µM
BXPC-3	4 µM	4 µM	0.001 µM	1 µM
CAPAN-1	4 µM	4 µM	0.005 µM	0.3 µM
MIA PACA-2	4 µM	0.005 µM	0.0025 µM	0.6 µM

The treated cells were incubated for 72 h at 37 °C with 5% CO_2. At the indicated time points, all cell experiments evaluated at least three biologically independent replicates.

2.4. Cell Viability Assays

2.4.1. Proliferation

Proliferation was evaluated by absolute counting, which was determined by trypan blue (Sigma-Aldrich Chemie GmbH, Steinheim, Germany) staining. After inhibitor exposure in 24-well plates, the cells were harvested and washed with 1× PBS (PAN-Biotech). Following the cells being stained with trypan blue, the number of viable cells was determined by counting with a hemocytometer. Proliferation was expressed as a percentage of viable cells treated with the inhibitor to the vehicle-treated control (control = 100%).

2.4.2. Biomass Quantification

Biomass quantification was carried out by crystal violet (CV) staining. After exposure to the corresponding inhibitors, cells in 96-well plates were washed once with PBS and stained with 50 µL 0.2% CV solution on a shaker at room temperature for 10 min. Thereafter, the plates were washed twice with PBS. To elute bound CV, 100 µL 1% sodium dodecyl sulfate (SDS) was added to each well and incubated on a shaker at room temperature for 10 min. Finally, absorbances at a measuring wavelength of 570 nm and at the reference wavelength of 620 nm were measured by a Promega GloMax®-Multi Microplate Multimode Reader. The absorbance value of the reference wavelength was subtracted from that of the corresponding measuring wavelength. The value of cells exposed to the vehicle was used as a control and the value of culture media was used as the background. The background value was subtracted from the control and experimental values. The amount of CV directly correlates to cell biomass. The result is expressed as a percentage of the inhibitor-treated group to vehicle-treated controls (control = 100%).

2.5. Apoptosis and Necrosis Analyses

Apoptosis and necrosis were evaluated by Annexin V FITC (Becton, Dickinson and Company, Heidelberg, Germany) and propidium iodide (PI) (Sigma-Aldrich Chemie GmbH) double staining by flow cytometry. After exposure to the vehicle control, and both single and combined inhibitors, cells were harvested and washed twice with cold PBS. After the washing step, the cell pellet was resuspended in 100 µL Annexin V binding buffer (1×) (Becton, Dickinson and Company), and incubated with 5 µL of Annexin V FITC for 15 min at room temperature in the dark. Then, cells were stained with PI (final concentration: 20 µg/mL) straightway before measurement. Unstained and single-stained cells were used to determine the negative and positive boundaries and measured in each experiment. Annexin V^-/PI^- cells were considered to be viable cells, Annexin V^+/PI^- cells were considered to be early apoptotic cells, and Annexin V^+/PI^+ cells were considered to be late apoptotic/necrotic cells. Flow cytometry measurement was performed on FACSVerse™

(Becton, Dickinson and Company) and all data were analyzed by BD FlowJo™ software (Becton, Dickinson and Company).

2.6. Evaluation of Combined Inhibitor Application

The interaction among the inhibitors was evaluated by the Bliss independent model. The interaction of the inhibitor combination was determined by the difference between the observed (E_O) and predicted (E_P) inhibition of the combination therapy.

In double inhibitor application, E_P was calculated with the following equation:

$$E_P = E_A + E_B - E_A \times E_B,$$

where E_A and E_B are the relative inhibition of single-inhibitors A and B.

In triple inhibitor application, E_P was calculated with the following equation:

$$E_P = E_A + E_B + E_C - E_A \times E_B - E_A \times E_C - E_B \times E_C - E_A \times E_B \times E_C,$$

where E_A, E_B, and E_C are the relative inhibition of single-inhibitors A, B, and C.

$E_O > E_P$ indicated a synergistic effect, $E_O = E_P$ indicated an additional effect; $E_O < E_P$ indicated an antagonistic effect. Bliss values for inhibitor combinations were calculated based on the results of proliferation and cell biomass of PDAC cell lines [28].

2.7. Examination of Cell Morphology Changes

Examination of PDAC cell line morphology changes was carried out by Pappenheim staining. After 72 h of exposure to the vehicle control, single inhibitor, or combined inhibitor, supernatants were collected and cells were harvested. After counting the cells, we resuspended the cell pellet and adjusted the cell density of the control group and each experimental group to 5×10^4 cells/200 µL. Then, 200 µL of the cell suspension was fixed on a glass slide using Shandon Cytospin 3 centrifuge (Shandon, Frankfurt/Main, Germany), and two cell slides were made for each group. After 24 h of air-drying, the slides were stained with May–Grünwald solution (Merck, Darmstadt, Germany) for 6 min, washed with phosphate buffer solution (pH = 7.2) (Merck) three times for 1 min, then stained with Giemsa solution (1:10) (Merck) for 20 min, and washed with phosphate buffer solution three times for 1 min again. After the slides were air-dried for 24 h, the morphology of cells was examined and visualized with Evos XL Core Imaging System (Life Technologies, Darmstadt, Germany), magnified 100 times. Each experiment was repeated 3 times to eliminate random errors.

2.8. RNA Extraction

Total RNAs were extracted using the miRNeasy Mini Kit (QIAGEN GmbH, Hilden, Germany) according to the manufacturer's instructions. For each cell line, only the RNA of the DMSO control group and the triple inhibitor application group were extracted. In brief, at least 5×10^6 cells were harvested and washed twice with cold sterile PBS. Cell pellets were resuspended in 700 µL QIAzol Lysis Reagent (QIAGEN GmbH), then the aqueous phase that contains the total RNA of the lysed cells was extracted and purified by a silica membrane of RNeasy Mini spin columns. At last, total RNA was eluted by 30 µL of RNAse-free water.

After extraction, RNA concentrations, as well as OD 260/280 and OD 260/230 ratios, were measured with the NanoDrop 1000 Spectrophotometer (Thermo Fisher Scientific Inc., Waltham, MA, USA).

2.9. RNA Sequencing Analysis

The RNA quality was assessed using the Agilent RNA 6000 Nano Kit (Agilent Technologies Inc., Waldbronn, Germany) on the 2100 Bioanalyzer system (Agilent Technologies Inc.). Only samples with an RNA integrity number (RIN) >8 were proceeded to DNA library preparation using the Illumina Stranded mRNA Sample Preparation Kit (Illumina Inc., San Diego, CA, USA). Briefly, 800 ng of total RNA was enriched for mRNA via poly-T oligo-coated magnetic beads, and chemically fragmented under elevated temperature. The RNA fragments were then reverse-transcribed into the first- and second-strand cDNA using random hexamers. Double-stranded cDNA fragments were ligated with anchor primers and PCR-amplified for 10 rounds, using 10bp unique dual index primers (UDIs). The quality of the libraries was evaluated for fragment length distribution on the Agilent DNA-1000 Chip (Agilent Technologies Inc.). The library concentration was quantified using a Qubit dsDNA HS Assay kit (Life Technologies), normalized to 2 nM and equally pooled. The multiplexing library pool was sequenced for 2 × 101 bp paired-end reads at a final loading concentration of 750 pM on the NextSeq 2000 system and P3 Flow Cell at the sequencing facility of Research Institute for Farm Animal Biology (FBN), Dummerstorf, Germany.

2.10. Data Pre-Processing and Differentially Expressed Genes (DEGs) Analysis

Sample de-multiplexing and FASTQ generation of raw sequencing reads were conducted using on-board DRAGEN BCL Convert analysis workflow (Illumina). The data were quality-checked pre- and post-processing using FastQC version 0.11.9 [29]. Data pre-processing was performed using Trim Galore v.0.6.7 with the following options: -q 20—paired—stringency 3—length 20—illumine [29]. The remaining high quality paired reads were then aligned to the reference genome, Homo_sapiens.GRCh38 from Ensembl release 106 using Hisat2 version 2.2.1 [30]. The number of reads uniquely mapped to each gene was extracted from the HISAT2 mapping results using HTSeq version 2.0.1, with the following options: -f bam -r name—stranded = reverse -t exon -i gene_id -m union [31]. The resulting gene count data were further analyzed for DEGs using DESeq2 package [32]. DEGs that passed a threshold of $|\mathrm{Log_2}(\text{Fold Change})| > 1$ and adjusted p value (padj) < 0.05 were considered analytically valuable and proceeded to Gene Ontology (GO) and Kyoto Encyclopedia of Genes and Genomes (KEGG) enrichment analysis.

The GO and KEGG enrichment analysis were applied for the functional annotation and pathway analysis using the gene set enrichment analysis (GSEA) [33,34]. The functional enrichment analyses of DEGs were explored by R package clusterProfiler4.0 and Pathview [35,36]. GO and KEGG enrichment analysis with a p-value < 0.05 and q-value < 0.25 were considered to have a significant impact and were selected for further analysis.

2.11. Statistical Analyses

Each experiment was performed in at least 3 biologically independent repetitions. Results of proliferation, biomass quantification, and apoptosis/necrosis analysis were expressed as mean ± standard deviation (SD). Statistical significance was determined by one-way ANOVA (after proving the data within each group conformed to the Gaussian distribution) or Kruskal–Wallis test (the data within each group conformed to the non-Gaussian distribution) and displayed as follows: *: $p < 0.033$, **: $p < 0.002$, ***: $p < 0.001$ versus the control group.

3. Results

3.1. KRAS Status of the PDAC Cell Lines

The analyzed seven PDAC cell lines were characterized by the following *KRAS* mutational statuses: one *KRAS* wild-type cell line (BXPC-3), one *KRAS* G12C (c.34G>T) cell line (MIA PACA-2), one *KRAS* Q61H (c.183A>C) cell line (T3M4), two *KRAS* G12D (c.35G>A) cell lines (ASPC-1and COLO357), and two *KRAS* G12V (c.35G>T) cell lines (CAPAN-1 and PATU8902). The information about each cell line includes the chromosomal location (#Chr), the zygosity (hom: homozygous, het: heterozygous), reference base (Ref), observed base

(Obs), allele frequency (VAF), base change, and amino acid substitution, which are listed in Table 2. Thereby, COLO357 and T3M4 represent the only two cell lines characterized by a heterozygotic *KRAS* genotype.

Table 2. *KRAS* status of PDAC cell lines.

Cell Line	#Chr	Start	End	Ref	Obs	Zygosities	VAF	Gene	Base Change	AA Change
BXPC-3	chr12	25398284	25398284	G	G	hom	100	*KRAS*	-	-
ASPC-1	chr12	25398284	25398284	G	A	hom	100	*KRAS*	NM_033360.2:c.35G>A	G12D
COLO357	chr12	25398284	25398284	G	A	het	23.8	*KRAS*	NM_033360.2:c.35G>A	G12D
CAPAN-1	chr12	25398284	25398284	G	T	hom	97.1	*KRAS*	NM_033360.2:c.35G>T	G12V
PATU8902	chr12	25398284	25398284	G	T	hom	100	*KRAS*	NM_033360.2:c.35G>T	G12V
MIA PACA-2	chr12	25398285	25398285	G	T	hom	99.6	*KRAS*	NM_004985.5:c.34G>T	G12C
T3M4	chr12	25380275	25380275	A	C	het	32.6	*KRAS*	NM_033360.2:c.183A>C	Q61H

3.2. Single Application of KRAS Inhibitors BI-3406 and Sotorasib to PDAC Cell Lines

The *KRAS* G12C inhibitor sotorasib had almost no inhibitory effect on the *KRAS* Q61H cell line T3M4 (Figure 1). At the highest tested concentration of 10 µM, cell proliferation and biomass were reduced by only 6% and 0%, respectively. In addition, sotorasib displayed similar inhibitory effects on *KRAS* wild-type and *KRAS* G12V cell lines, and the biomass of cell proliferation decreases ranged from 25% to 38% at the concentration of 10 µM. Notably, the inhibitory effects of sotorasib on ASPC-1 (VAF: 100) and COLO357 (VAF: 23.8), which both carry *KRAS* G12D, are quite different; cell proliferation decreased by 50% and 37%, and biomass decreased by 41% and 27%, respectively. Sotorasib appears to be more effective against *KRAS* G12D mutations with high VAF.

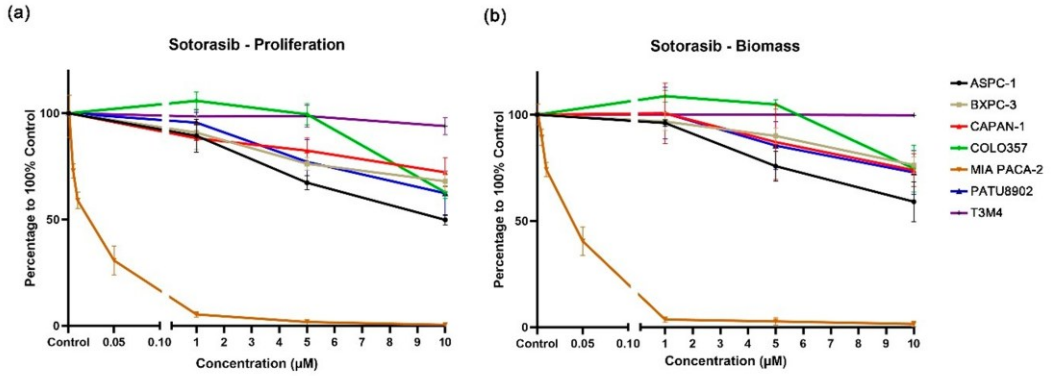

Figure 1. Proliferation (**a**) and biomass (**b**) changes in PDAC cell lines after exposure to different concentrations of sotorasib.

As expected, sotorasib showed a very strong inhibitory effect on MIA PACA-2, which carry a *KRAS* G12C mutation. A significant inhibitory effect can be observed at a concentration of 0.005 µM, while at 0.05 µM, cell proliferation and biomass were reduced by 69% and 60%, respectively (Figures 1 and S1, Supplementary Table S1).

Compared with the DMSO control group, the KRAS::SOS1 inhibitor BI-3406 demonstrated a weak inhibitory effect on PDAC cell lines carrying KRAS G12V (CAPAN-1 and PATU8902). At the highest test concentration of 10 µM, cell proliferation only decreased by 11% and 17%, and the biomass decreased by 12% and 21%, respectively (Supplementary Table S2). In addition, the inhibitory effect of BI-3406 on the cell proliferation and biomass of the KRAS wild-type cell line BXPC-3 is similar to the inhibition observed in the KRAS G12V cell lines. The cell proliferation and biomass of BXPC-3 were reduced by only 15% and

27% at the concentration of 10 µM. BI-3406 demonstrated an increased, but still limited, inhibitory effect on the cell lines carrying the other three KRAS mutations (ASPC-1 and COLO357, KRAS G12D; MIA PACA-2, *KRAS* G12C; T3M4, *KRAS* Q61H). At the highest tested concentration, cell proliferation and biomass were only reduced between 30 and 50% (Figures 2 and S2, Supplementary Table S2).

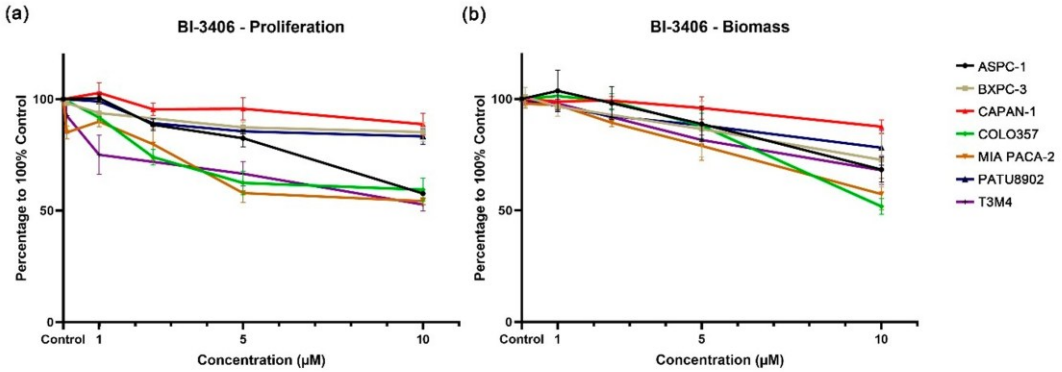

Figure 2. Proliferation (**a**) and biomass (**b**) changes in PDAC cell lines after exposure to different concentrations of BI-3406.

3.3. Combined Applications of KRAS, PI3K, and MEK1/2 Inhibitors Enhance Inhibition of PDAC Cell Lines

For BI-3406 in combination with trametinib and buparlisib, a significant increase in the inhibition of cell proliferation and biomass was observed when compared with the DMSO control group, regardless of whether double-inhibitor combinations or triple-inhibitor combinations were tested (Figure 3 and Supplementary Tables S3 and S4). When comparing the effect of the triple-inhibitor with the effects of the double-inhibitor, a significantly increased inhibition in cell proliferation can also be observed in ASPC-1, BXPC-3, and MIA PACA-2. In CAPAN-1, a significant increase was only observed when comparing the triple therapy with the combination of BI-3406 and buparlisib. As for the other two combinations (BI-3406 + trametinib, trametinib + buparlisib), no significant increase could be observed. Moreover, we also observed similar inhibitory effects in the biomass quantification assay.

For the combination of sotorasib with trametinib and buparlisib, significant inhibition of cell proliferation and biomass was observed in the triple combination compared to the DMSO control group (Figure 4 and Supplementary Tables S5 and S6). The addition of sotorasib significantly improved inhibition in ASPC-1 and MIA PACA-2 compared with a single application of trametinib or buparlisib. In addition, when focusing on the efficacy of the triple combination (sotorasib + trametinib + buparlisib) versus the double combination (trametinib + buparlisib), a significant increase in inhibitory effect was only observed in ASPC-1 and MIA PACA-2.

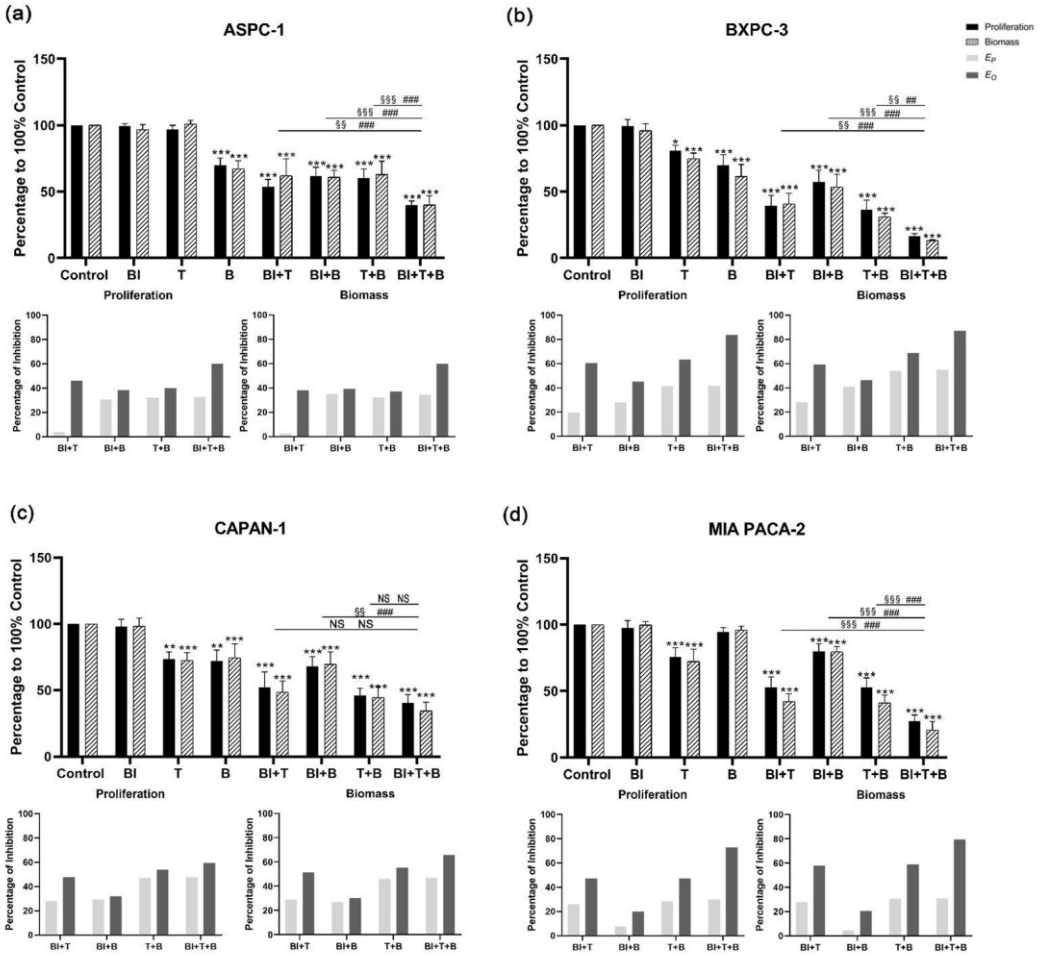

Figure 3. Cell proliferation and biomass of ASPC-1 (**a**), BXPC-3 (**b**), CAPAN-1 (**c**), and MIA PACA-2 (**d**) after 72 h BI-3406, trametinib, buparlisib or inhibitor combination exposure, as well as analysis of synergistic effect using Bliss independent model. Data are presented as mean ± SD. Significance of a treatment effect compared to the DMSO control was determined by one-way ANOVA and displayed as *: $p < 0.033$, **: $p < 0.002$, ***: $p < 0.001$ ($n \geq 3$). The significance of the treatment effect for double inhibition compared to triple inhibition was determined by one-way ANOVA and was shown as # (proliferation), § (biomass): $p < 0.033$; ##, §§: $p < 0.002$, ###; §§§: $p < 0.001$. BI: BI-3406; T: trametinib; B: buparlisib; NS: not significant; E_P: predicted inhibition by Bliss independent model; E_O: observed inhibition.

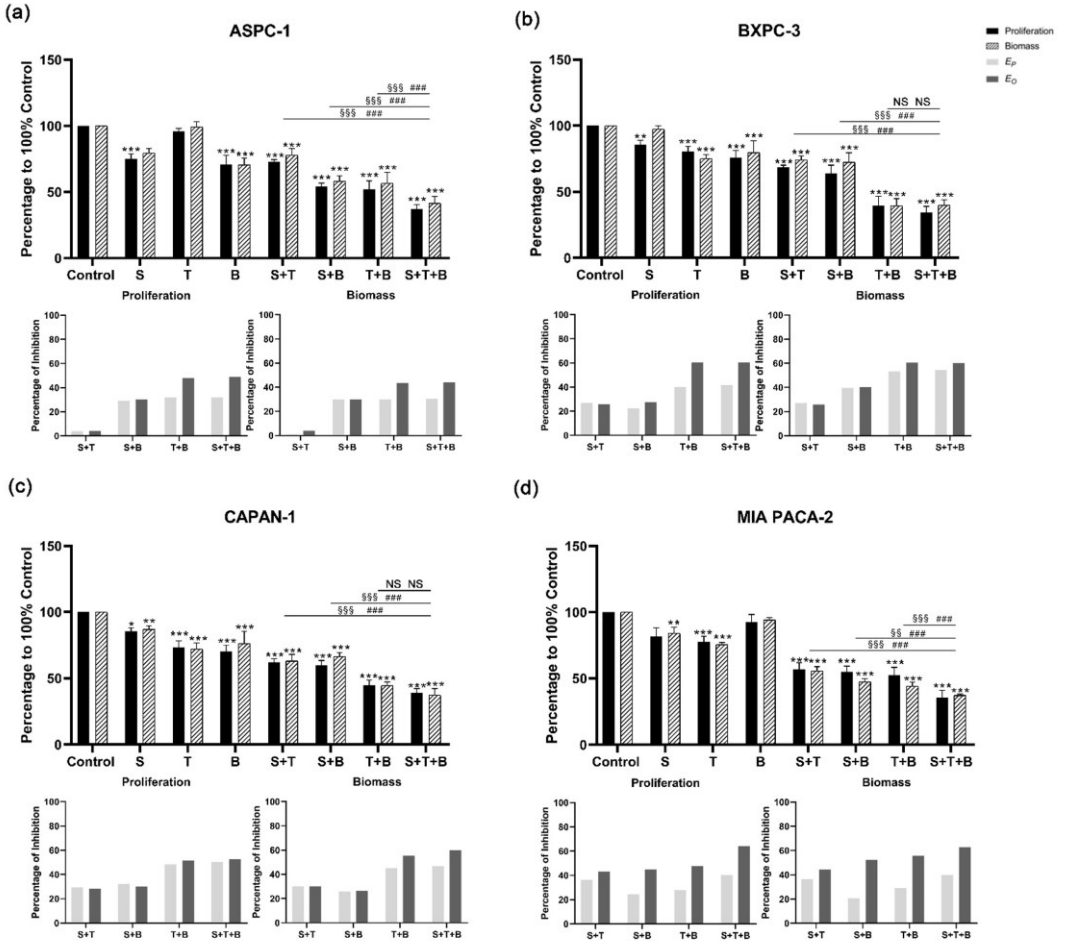

Figure 4. Cell proliferation and biomass of ASPC-1 (**a**), BXPC-3 (**b**), CAPAN-1 (**c**), and MIA PACA-2 (**d**) after 72 h sotorasib, trametinib, buparlisib or inhibitor combination exposure, as well as analysis of synergistic effect using Bliss independent model. Data are presented as mean ± SD. Significance of a treatment effect compared to the DMSO control was determined by one-way ANOVA and displayed as *: $p < 0.033$, **: $p < 0.002$, ***: $p < 0.001$ ($n \geq 3$). The significance of the treatment effect for double inhibition compared to triple inhibition was determined by one-way ANOVA and was shown as # (proliferation), § (biomass): $p < 0.033$; §§: $p < 0.002$, ###; §§§: $p < 0.001$. S: sotorasib; T: trametinib; B: buparlisib; NS: not significant; E_P: predicted inhibition by Bliss independent model; E_O: observed inhibition.

3.4. Bliss Analysis Revealed the Synergistic Effects of Double- and Triple-Application

The Bliss prediction effects were calculated based on the results of proliferation and biomass inhibition. For the BI-3406-based triple inhibitor combination, the Bliss predicted that inhibition (E_P) is lower than the observed inhibition results (E_O) in all cell lines (Figure 3). When focusing on comparing the double combination of trametinib + buparlisib and the triple combination of BI-3406 + trametinib + buparlisib, ASPC-1, BXPC-3, and MIA PACA-2 showed significantly higher inhibitory efficacy. However, this significant improvement did not appear in CAPAN-1, suggesting that BI-3406 was not able to enhance the inhibitory efficacy of trametinib + buparlisib in CAPAN-1. For the sotorasib-based triple inhibitor combination, E_P was observed to be lower than E_O in all cell lines. When focusing on comparing the double combination of trametinib + buparlisib and the triple combination of sotorasib + trametinib + buparlisib, only MIA PACA-2 demonstrated a significant improvement in inhibitory efficacy. Furthermore, in the other three cell lines, the inhibitory effects were not affected by the addition of sotorasib. These data indicated that the sotorasib-based triple inhibitor combination is synergistic in MIA PACA-2 cells that express the KRAS G12C mutant (using 0.005 μM sotorasib).

In the BI-3406-based double inhibitor combination, the combination of BI-3406 + trametinib demonstrated a significantly increased inhibitory effect in all four cell lines (Figure 3). The differences from E_O and E_P were between 20 and 43% (proliferation) and 23 and 36% (biomass) (Supplementary Table S4). The combination of BI-3406 + buparlisib also demonstrated a synergistic effect in all four cell lines; the differences between E_O and E_P were between 3 and 15% (proliferation) and 4 and 16% (biomass) (Supplementary Table S6). In addition, for sotorasib, either in combination with trametinib or in combination with buparlisib, synergistic effects were only observed in MIA PACA-2, with differences between E_O and E_P of 7%, 21% (proliferation) and 8%, 32% (biomass), respectively (Supplementary Figure S6). In the other cell lines that do not harbor the KRAS G12C variant, the difference between E_P and E_O was almost 0, suggesting that sotorasib does not act synergistically in these cell lines when combined with trametinib or buparlisib.

3.5. Combined Application of KRAS, PI3K, and MEK1/2 Inhibitors Induce Apoptosis and Necrosis of PDAC Cell Lines

Apoptosis/necrosis assays were performed on ASPC-1, BXPC-3, CAPAN-1, and MIA PACA-2 cells after exposure to BI-3406-based inhibitor combinations and MIA PACA-2 after exposure to sotorasib-based inhibitor combinations. Compared to the DMSO control group, Annexin V/propidium iodide (PI) double staining revealed a significant increase in induced apoptosis/necrosis, when using the triple-inhibitor combinations (Supplementary Figures S3 and S4, Supplementary Table S7). These triple-inhibitor combinations also significantly increased cell death when compared with all double-inhibitor combinations. In addition, most of the double-inhibitor combinations caused a significant increase in cell death when compared to the control group. Only in MIA PACA-2 cells, the combination of BI-3406 and buparlisib was not able to significantly increase cell death.

Furthermore, the microscopic evaluation at 100× magnification of Pappenheim stained samples indicated that the cells clearly demonstrated signs of cell death, including numerous vacuoles in the cytoplasm, splitting or breaking up of the nucleoli (karyorrhexis), protrusions of the plasma membrane, and apoptotic bodies, as well as morphological deformation (Figures 5 and S5). These morphological changes were also observed in the samples that have been exposed to the double inhibitor combinations. However, there was more evidence after the application of the triple inhibitor combination.

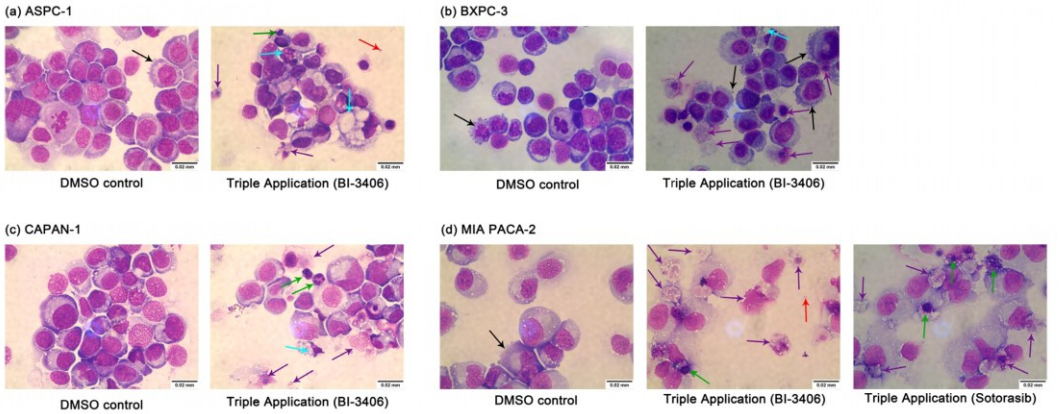

Figure 5. Morphology changes in ASPC-1 (**a**), BXPC-3 (**b**), CAPAN-1 (**c**), and MIA PACA-2 (**d**) after DMSO or triple inhibitor combination exposure. Magnification: 100×. ↑ membrane bubbles, membrane bound apoptotic body, ↑ vacuolization, ↑ apoptotic body, ↑ nuclear condensation/fragmentation; ↑ rupture of the plasma membrane.

3.6. Comparative Analysis of Differentially Expressed Genes (DEGs) between BI-3406 Combination-Treated and Non-Exposed PDAC Cell Lines

Differential expression analysis revealed several genes that were differentially regulated in triple combination-treated cells, when compared with the DMSO control exposed cells. For the combination of BI-3406 with trametinib and buparlisib, 587 DEGs were identified in ASPC-1 cells, 423 DEGs in BXPC-3 cells, 1191 DEGs in CAPAN-1 cells, and 1259 DEGs were identified in MIA PACA-2 cells (Supplementary Figures S6 and S7, Supplementary Table S8). Of these DEGs, only 12 DEGs were shared among all the tested PDAC cell lines (Figure 6a). In addition, in the top 25 up- and down-regulated genes identified in the 4 cell lines (Figure 6b), no gene was shared by all cell lines.

(a)

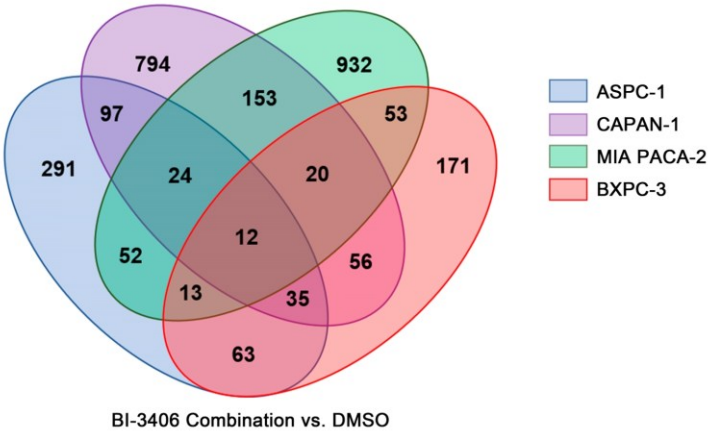

Figure 6. *Cont.*

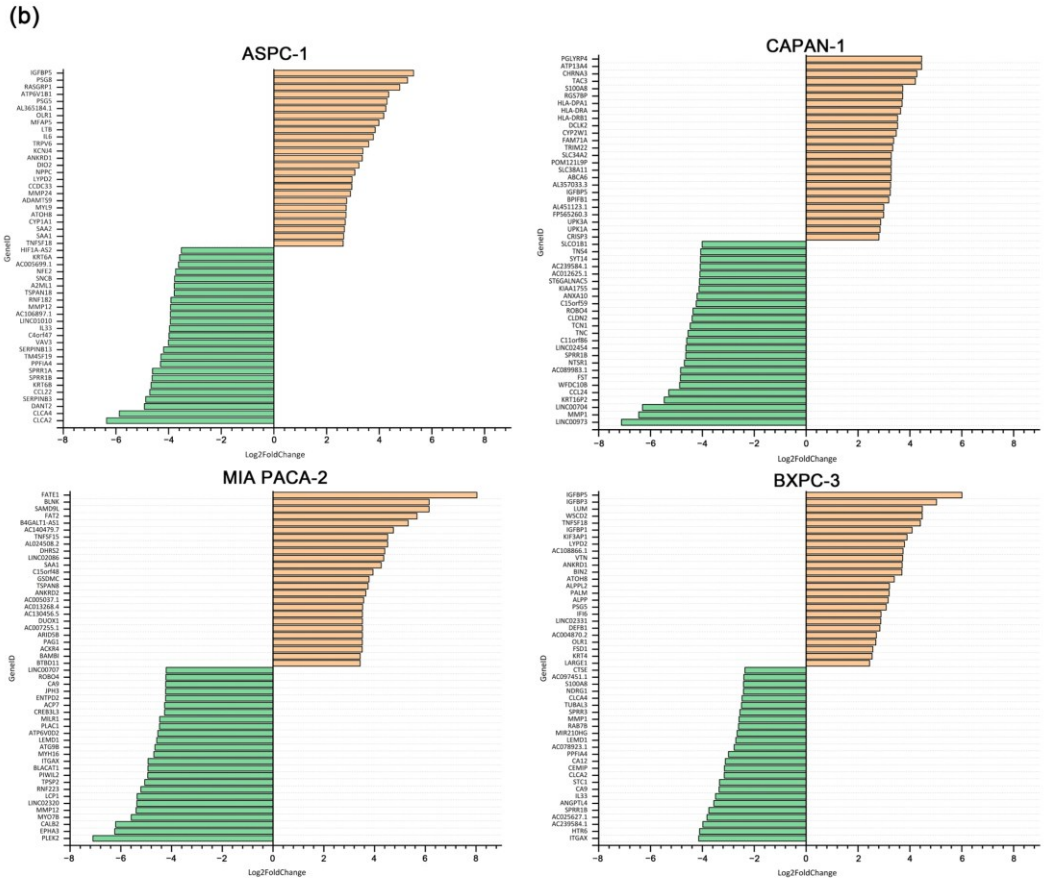

Figure 6. Number and overlap of DEGs in ASPC-1, BXPC-3, CAPAN-1 and MIA PACA-2 cell lines after exposure to BI-3406 combination (**a**) and the top 25 up- and down-regulated genes before and after BI-3406 combination exposure (**b**).

3.7. Comparative Analysis of DEG Changes Induced by BI-3406 Combination-Treated and Sotorasib Combination-Treated in MIA PACA-2 Cell Line

For the sotorasib triple combination, only MIA PACA-2 cells were analyzed. Compared to the DMSO control group, 928 DEGs were identified in MIA PACA-2 (Supplementary Figure S7, Supplementary Table S9). Comprehensive analysis of DEG changes in MIA PACA-2 using BI-3406 or sotorasib triple therapy revealed 778 DEGs that were up- or down-regulated by both inhibitor combinations (Figure 7a). In the top 25 up- and down-regulated genes, 17 overlapping up-regulated genes and 15 overlapping down-regulated genes were observed (Figure 7b).

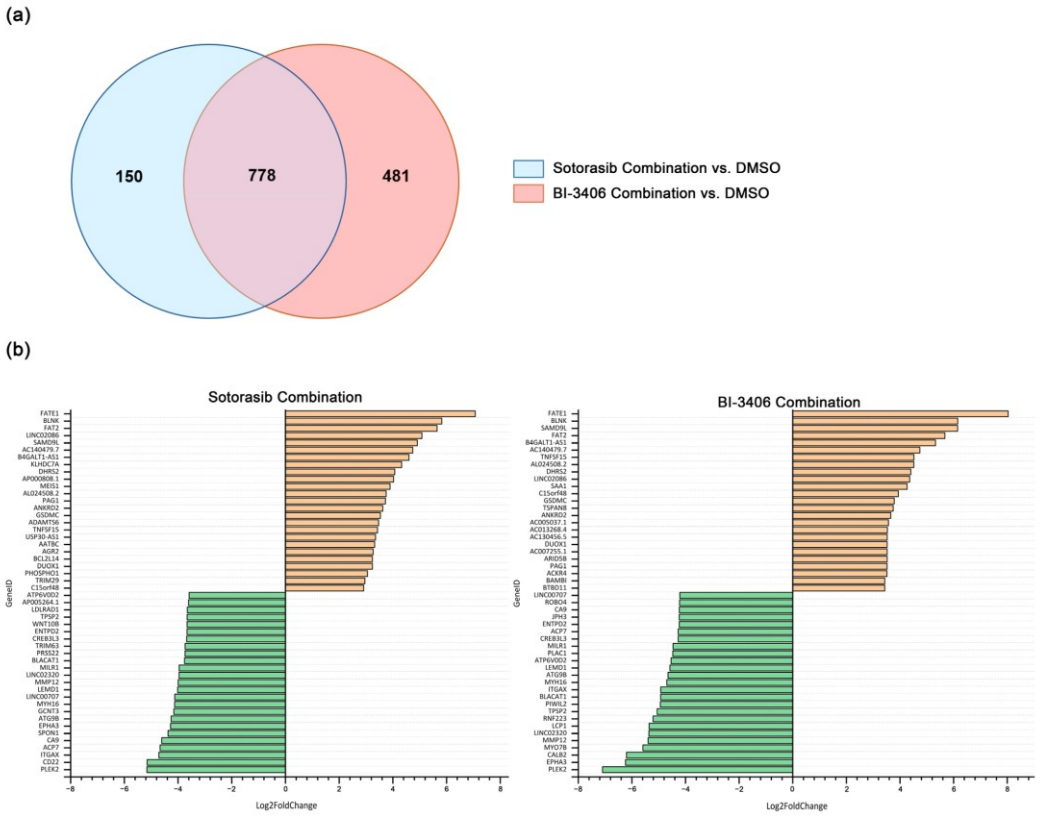

Figure 7. Number and overlap of DEGs in MIA PACA-2 cell lines after exposure to sotorasib combination or BI-3406 combination (**a**) and the top 25 up- and down-regulated genes before and after inhibitor combination exposure (**b**).

3.8. Functional and Pathway Enrichment Analysis of DEGs Induced by Combination-Treated PDAC Cell Lines

In order to assess the effect of inhibitor combinations on PDAC cell lines, GO and KEGG pathway analysis was performed on all of the DEGs selected in result 3.6 for each cell line.

For the BI-3406 triple inhibitor combination, GO and KEGG enrichment analysis demonstrated different results in different PDAC cell lines. The number of GO terms, including the biological process (BP), the cellular component (CC), and the molecular function (MF), as well as the number of KEGG pathways caused by BI-3406 triple inhibitor combination treatment, are displayed in Table 3. Detailed information is displayed in Supplementary Figures S7–S11 and Supplementary Tables S10 and S11.

Table 3. GO term and KEGG pathway enrichment analysis of DEGs induced by BI-3406 triple inhibitor combination treatment.

PDAC Cell Line	KRAS Mutation	GO Term			KEGG Pathway
		Biological Process	Cellular Components	Molecular Functions	
BXPC-3	Wild Type	847	49	96	24
ASPC-1	KRAS G12D	744	80	96	48
CAPAN-1	KRAS G12V	1447	116	168	59
MIA PACA-2	KRAS G12C	1053	76	120	66

Further analysis of the GO term function revealed that in the PDAC cell lines, DEGs were involved in regulating the immune system, cell adhesion, cell migration, localization, locomotion, and response to stimulus in biological process, cell membrane, and extracellular functions in cellular components, as well as cytokine binding in molecular functions. KEGG pathway enrichment analysis identified nine overlapping pathways, which were involved in cancer, cellular community, cardiovascular disease, and immune regulation and directly acting on PI3K/AKT and TNF pathways (Supplementary Table S11). Furthermore, the expected RAS signaling pathway was not observed to be affected in all of the tested cell lines. The KEGG pathway results revealed that the RAS pathway was affected in ASPC-1, BXPC-3, and MIA PACA-2, but not in CAPAN-1.

For the sotorasib combination, 928 DEGs in MIA PACA-2 were involved in 849 BP, 39 CC, and 63 MF; KEGG analysis revealed that DEGs were enriched in 58 pathways, which are mainly associated with cancer, signal transduction, and the immune system (Supplementary Figure S12 and Supplement Tables S12 and S13).

Comparing the GO terms and KEGG pathway enrichment analysis of MIA PACA-2 in the two inhibitor combinations did not reveal major differences. The GO term demonstrated that both inhibitor combinations were involved in similar cellular functions in MIA PACA-2. KEGG analysis revealed that both inhibitor combinations were involved in immune regulation, signal transduction (especially PI3K/AKT, TNF, and JAK-STAT signaling pathways), metabolic activity, and cancer pathways (especially proteoglycans in cancer). The BI-3406 triple combination additionally participated in the MAPK pathway; however, this effect was not observed in the sotorasib triple combination (Supplementary Tables S11 and S13).

4. Discussion

KRAS mutations are the most common mutations in PDAC patients and are characterized by poor prognosis and resistance to general treatment [6,14]. Although a series of targeted inhibitors have been developed for PDAC, so far, these inhibitors are still not routinely used in clinical treatment. In our study, sotorasib, which targets the *KRAS* G12C mutation, exhibited the expected inhibitory efficacy in MIA PACA-2, and significantly inhibited cell proliferation and biomass even at very low concentrations (0.005 μM). At the same time, sotorasib at 10 μM exhibited a partial inhibitory effect on other tested PDAC cell lines, except for T3M4 (KRAS Q61H). The cell proliferation and biomass decreased by 32–50% and 24–41%, respectively. However, in T3M4, minimal inhibition of cell proliferation and biomass was observed at all the concentrations tested. This may be due to the fact that the Q61H mutation has the lowest intrinsic GTPase activity and requires less upstream signaling to maintain a GTP-bound status [37]. In a previous report, the maximum plasma concentration of sotorasib was 7.5 μg/mL (13.4 μM) [38]. The results of this study demonstrated that sotorasib had inhibitory effects on KRAS G12D, G12V, and wild-type PDAC cell lines at a concentration of 10 μM, which can be achieved in clinical trials [38]. The incidence of serious adverse reactions at this concentration in clinical trials is low, suggesting that sotorasib can potentially become an interesting option for the development of novel approaches for the above-mentioned PDAC types [18,38]. Although sotorasib is currently only approved for the treatment of KRAS G12C-mutated NSCLC, the CodeBreaK100 study has confirmed its potential for the treatment of advanced KRAS G12C

mutated PDAC with low side effects. At the same time, the clinical trials demonstrated that the maximum plasma concentration is higher than 10 μM [18]. Combined with our findings, sotorasib may also have inhibitory effects on KRAS G12D and G12V mutated PDAC in vivo, suggesting that sotorasib may have further potential to treat KRAS wild type and other KRAS G12-mutated PDACs besides KRAS G12C.

Using the multi-KRAS mutation inhibitor BI-3406, our results were comparable to those previously reported in 2D cultures [26]. The biological response of cell lines carrying the KRAS G12V mutation (CAPAN-1 and PATU8902) was similar to that of the wild-type cell line BXPC-3, showing a decrease of only about 15% at 10 μM. In the cell lines carrying KRAS G12C and G12D mutations, the inhibition of cell proliferation and biomass at 10 μM concentration was higher than 30%, up to 48.18%. In the previously reported in vivo studies, the BI-3406 single-inhibitor demonstrated a good inhibitory effect on KRAS G12C-mutated MIA PACA-2 cells, and the tumor volume of the two different doses of the experimental group was significantly reduced compared with the control group. However, even at the highest dose, BI-3406 was only able to inhibit tumor growth, but could not reduce tumor volume below the baseline [26]. It is suggested that a single application of BI-3406 does not have a strong inhibitory effect on PDAC cell lines both in vivo and in vitro. Nonetheless, it demonstrated a distinct synergistic effect with downstream pathway inhibitors in combination inhibition, especially with the MEK1/2 inhibitor trametinib. The combination of BI-3406 and trametinib demonstrated a synergistic effect in both *KRAS*-mutated and wild-type PDAC cell lines, which is in agreement with previous reports, both confirming the synergistic effect of BI-3406 and trametinib [26]. This is probably because BI-3406 combined with trametinib can block the negative feedback regulatory mechanism by reducing phosphorylated (p)-MEK and p-ERK levels, resulting in a strong synergistic effect [26]. Since this regulatory mechanism exists both in *KRAS*-mutated and wild-type cell lines, this double-inhibitor combination was also effective in the BXPC-3 cells. For the combination of BI-3406 and buparlisib, a synergistic effect was only observed in MIA PACA-2. Since buparlisib does not reduce p-MEK and p-ERK levels, it is highly likely that it fails to activate the negative feedback loop, resulting in a small synergistic effect [26].

The double-inhibitor combination based on sotorasib also displayed a synergistic effect, but mainly in MIA PACA-2 cells. Since RAS directly forms a complex with PI3K to further activate the PI3K signaling pathway, inhibition of these two proteins greatly reduces the activation of this pathway and might explain the synergistic effect of these two inhibitors [39–42]. Additive effects were observed in ASPC-1, BXPC-3, and CAPAN-1 cells, indicating that sotorasib might target an unknown target protein at a high concentration and the inhibition of this target protein does not synergistically interact with inhibitors of MEK and PI3K.

The efficacy of the triple-inhibitor combination of BI-3406, trametinib, and buparlisib was significantly stronger than that of the double-inhibitor combination in ASPC-1, BXPC-3, and MIA PACA-2 cells. However, in CAPAN-1 cells, there was no significant improvement in the triple-inhibitor combination versus the double-inhibitor combination of buparlisib and trametinib. Moreover, the KEGG pathway enrichment analysis revealed that in CAPAN-1, the RAS pathway was not affected by the triple therapy, while the enrichment of DEGs in the RAS pathway was observed in the other three cell lines. In addition, a single application of BI-3406 did not significantly inhibit the proliferation and biomass of CAPAN-1. Although BI-3406 has previously been reported to achieve good inhibitory effects on KRAS G12V-mutated NSCLC cell lines, this antitumor effect appears to be poor for PDAC cell lines [26]. This suggests that in PDAC cell lines, BI-3406 is less able to block the interaction between KRAS G12V and SOS1, at least not causing changes at the gene expression level. This may account for the low response of the KRAS G12V cell lines to BI-3406 and the inability of the BI-3406 to enhance the efficacy of downstream inhibitors in CAPAN-1. Moreover, the triple inhibitor combination of sotorasib demonstrated only an additive effect in ASPC-1, BXPC-3 and CAPAN-1, further confirming that the inhibition

of non-KRAS G12C mutant cell lines by sotorasib is not affected by the changes in the RAS/RAF/MEK/ERK pathway or PI3K/AKT pathway.

The BI-3406 triple inhibitor combination modulated immunity, cell adhesion, migration, and targeted cancer pathways in all four cell lines. This indicates that this inhibitor combination can directly influence the pathophysiology of tumor cells, but might also indirectly inhibit the growth of PDAC cells by modulating the immune system, as well as cell-to-cell interactions. Furthermore, we observed that in all four cell lines, both triple inhibitor combinations regulated DEGs, which are involved in the response to hypoxia. These genes (*ALDOA*, *IL6*, *IL6R*, *EGF*, *VEFG*, *PDK-1*, *ENO1*, etc.) were all associated with the hypoxia inducible factor-1 (HIF-1) pathway, suggesting that both combinations can act on the HIF-1 pathway. Several studies have shown that HIF-1 is associated with tumor growth in a variety of cancers, including PDAC [43]. Inhibition of mTOR blocks the translation of HIF-1 mRNA, and inhibition of ERK can also lead to inhibition of HIF-1 [44,45]. The combination of the two inhibitors in this experiment affected both mTOR and ERK, leading to changes in the downstream HIF-1 pathway, which seems to be another mechanism of this inhibitor combination.

Altogether, our current study demonstrates the antiproliferative effects of KRAS inhibitors alone or in combination with downstream inhibitors in PDAC cell lines in vitro. Moreover, the dose of each inhibitor was greatly reduced when used in combination, thereby reducing the side effects of the inhibitor. The KRAS::SOS1 inhibitor BI-3406 was able to enhance the antiproliferative effect of downstream inhibitors in the KRAS wild-type, KRAS G12C, and KRAS G12D mutant cell lines, but not for the KRAS G12V mutant cell lines. The KRAS G12C inhibitor sotorasib mainly enhanced the anti-proliferative effect of downstream inhibitors in KRAS G12C mutant cell lines.

5. Conclusions

Our current study demonstrates the effects of two KRAS inhibitors, BI-3406 and sotorasib, as monotherapy for PDAC. This provides evidence for a potential extended application of sotorasib in non-KRAS G12C mutated PDAC and the application of BI-3406 as a multi-KRAS mutated inhibitor in PDAC. In addition, these two KRAS inhibitors act synergistically or additively with downstream pathway inhibitors, when reducing cell proliferation and biomass in PDAC cell lines with different *KRAS* statuses. The two triple combinations also demonstrated extraordinary effects in enhancing inhibitor efficacy and reducing inhibitor dose. These data emphasize the importance of KRAS as a therapeutic target for PDAC and validate two different mechanisms of KRAS inhibition and its interaction with downstream pathway inhibitors. The current study provides novel ideas for the drug treatment of PDAC; however, in vivo experiments and clinical trials are still needed to observe the real efficacy and adverse reactions of these inhibitors and inhibitor combinations for the treatment of PDAC.

Supplementary Materials: The following supporting information can be downloaded at: https://www.mdpi.com/article/10.3390/cancers14184467/s1, Figure S1: Cell Viability after 72 Hours Sotorasib Exposure in PDAC Cell Lines; Figure S2: Cell Viability after 72 Hours BI-3406 Exposure in PDAC Cell Lines; Figure S3: PDAC Cell Death Induction after 72 Hours BI-3406, Sotorasib, Trametinib, Buparlisib or Inhibitors Combination Exposure; Figure S4: Apoptosis/necrosis Dot Plot of PDAC Cell Lines after 72 Hours BI-3406, Trametinib, Buparlisib and Inhibitor Combination Exposure; Figure S5: Morphology Changes of PDAC Cell Lines after 72 Hours BI-3406, Sotorasib, Trametinib, Buparlisib and Inhibitor combination exposure; Figure S6: DEGs after PDAC Cell Lines Exposed to the Combination of BI-3401, Trametinib and Buparlisib; Figure S7: DEGs after MIA PACA-2 Exposed to the Combination of BI-3401, Trametinib and Buparlisib or Sotorasib, Trametinib and Buparlisib; Figure S8: GO and KEGG Enrichment Analysis of ASPC-1 after BI-3406+Trametinib+Buparlisib Exposure; Figure S9: GO and KEGG Enrichment Analysis of BXPC-3 after BI-3406+Trametinib+Buparlisib Exposure; Figure S10: GO and KEGG Enrichment Analysis of CAPAN-1 after BI-3406+Trametinib+Buparlisib Exposure; Figure S11: GO and KEGG Enrichment Analysis of MIA PACA-2 after BI-3406+Trametinib+Buparlisib Exposure; Figure S12: GO and KEGG

Enrichment Analysis of MIA PACA-2 after Sotorasib + Trametinib + Buparlisib Exposure. Table S1: Cell Viability Sotorasib; Table S2: Cell Viability BI-3406; Table S3: Combination Inhibition (BI-3406 + Trametinib + Buparlisib); Table S4: Bliss Independent Model (BI-3406 + Trametinib + Buparlisib); Table S5: Combination Inhibition (Sotorasib + Trametinib + Buparlisib); Table S6: Bliss Independent Model (Sotorasib + Trametinib + Buparlisib); Table S7: Combination Cell Death; Table S8: DEGs of PDAC Cell Lines after Exposure to the Combination of BI-3406, Trametinib and Buparlisib; Table S9: DEGs of MIA PACA-2 after Exposure to the Combination of Sotorasib, Trametinib and Buparlisib; Table S10: GO Enrichment Analysis after PDAC Cell Lines Exposure to the Combination of BI-3406, Trametinib and Buparlisib; Table S11: KEGG Pathway Enrichment Analysis after PDAC Cell Lines Exposure to the Combination of BI-3406, Trametinib and Buparlisib; Table S12: GO Enrichment Analysis after MIA PACA-2 Exposure to the Combination of Sotorasib, Trametinib and Buparlisib; Table S13: KEGG Pathway Enrichment Analysis after MIA PACA-2 Exposure to the Combination of Sotorasib, Trametinib and Buparlisib; Table S14: Cell Viability Trametinib.

Author Contributions: Conceptualization, B.S., C.J. and H.M.E.; Data curation, Y.M.; Formal analysis, Y.M., M.A.A. and S.S.; Funding acquisition, C.J. and H.M.E.; Investigation, Y.M., M.A.A. and A.S.; Methodology, Y.M., N.T., M.A.A. and A.S.; Project administration, H.M.E.; Resources, F.U.W., M.M.L. and R.J.; Software, Y.M., N.T. and F.H.; Supervision, C.J. and H.M.E.; Validation, Y.M., N.T. and H.M.E.; Writing—original draft, Y.M.; Writing—review and editing, S.S., D.Z., F.U.W., R.J. and H.M.E. All authors have read and agreed to the published version of the manuscript.

Funding: This research was funded by the PiCoP project (funded by European Community, Europäischer Fonds für regionale Entwicklung (EFRE), grant TBI-V-1-241-VBW-084/State Mecklenburg-Western-Pomerania, Germany).

Institutional Review Board Statement: Not applicable.

Informed Consent Statement: Not applicable.

Data Availability Statement: The data supporting the reported results can be found on the website in detail in the article.

Acknowledgments: The authors gratefully acknowledge the PiCoP project (funded by European Community, Europäischer Fonds für regionale Entwicklung (EFRE), grant TBI-V-1-241-VBW-084/state Mecklenburg. Western Pomerania, Germany) for supporting this research. We would like to appreciate Patrick Brennan (Department of Medicine Clinic III, Hematology, Oncology and Palliative Medicine, Rostock University Medical Center, Germany) for his contribution to the improvement of English language and style.

Conflicts of Interest: The authors declare no conflict of interest.

Abbreviations

A	Alanine
AKT	Protein kinase B
BP	Biological process
BRCA3	Breast cancer 3
C	Cysteine
CC	Cellular components
CDKN2A	Cyclin dependent kinase inhibitor 2A
CV	Crystal violet
D	Aspartic acid
DEG	Differentially expressed gene
DMSO	Dimethyl sulfoxide
E_O	Observed inhibition
E_P	Bliss predicted inhibition
ERK	Extracellular signal-regulated kinase
FCS	Fetal calf serum
G	Glycine

GDP	Guanosine diphosphate
GO	Gene Ontology
GRC2	Cytosolic glutathione reductase
GSEA	Gene set enrichment analysis
GTP	Guanosine triphosphate
H	Histidine
HIF-1	Hypoxia inducible factor-1
KEGG	Kyoto Encyclopedia of Genes and Genomes
KRAS	Kirsten rat sarcoma virus
MEK	Mitogen-activated protein kinase kinase
MF	Molecular function
mTOR	Mammalian target of rapamycin
NSCLC	Non-small cell lung cancer
P-	Phosphorylated-
P/S	Penicillin-streptomycin solution
PDAC	Pancreatic ductal adenocarcinoma
PI	Propidium iodide
PI3K	Phosphoinositide 3-kinase
Q	Glutamine
RAS	Rat sarcoma virus
RIN	RNA integrity number
SD	Standard deviation
SMAD4	Mothers against decapentaplegic homolog 4
SOS1	Son of sevenless 1
TP53	Tumor protein P53
V	Valine

References

1. Jones, S.; Zhang, X.; Parsons, D.W.; Lin, J.C.; Leary, R.J.; Angenendt, P.; Mankoo, P.; Carter, H.; Kamiyama, H.; Jimeno, A.; et al. Core signaling pathways in human pancreatic cancers revealed by global genomic analyses. *Science* **2008**, *321*, 1801–1806. [CrossRef]
2. Campbell, P.J.; Yachida, S.; Mudie, L.J.; Stephens, P.J.; Pleasance, E.D.; Stebbings, L.A.; Morsberger, L.A.; Latimer, C.; McLaren, S.; Lin, M.L.; et al. The patterns and dynamics of genomic instability in metastatic pancreatic cancer. *Nature* **2010**, *467*, 1109–1113. [CrossRef] [PubMed]
3. Biankin, A.V.; Waddell, N.; Kassahn, K.S.; Gingras, M.C.; Muthuswamy, L.B.; Johns, A.L.; Miller, D.K.; Wilson, P.J.; Patch, A.M.; Wu, J.; et al. Pancreatic cancer genomes reveal aberrations in axon guidance pathway genes. *Nature* **2012**, *491*, 399–405. [CrossRef] [PubMed]
4. Waddell, N.; Pajic, M.; Patch, A.M.; Chang, D.K.; Kassahn, K.S.; Bailey, P.; Johns, A.L.; Miller, D.; Nones, K.; Quek, K.; et al. Whole genomes redefine the mutational landscape of pancreatic cancer. *Nature* **2015**, *518*, 495–501. [CrossRef] [PubMed]
5. Witkiewicz, A.K.; McMillan, E.A.; Balaji, U.; Baek, G.; Lin, W.C.; Mansour, J.; Mollaee, M.; Wagner, K.U.; Koduru, P.; Yopp, A.; et al. Whole-exome sequencing of pancreatic cancer defines genetic diversity and therapeutic targets. *Nat. Commun.* **2015**, *6*, 6744. [CrossRef]
6. Bailey, P.; Chang, D.K.; Nones, K.; Johns, A.L.; Patch, A.M.; Gingras, M.C.; Miller, D.K.; Christ, A.N.; Bruxner, T.J.; Quinn, M.C.; et al. Genomic analyses identify molecular subtypes of pancreatic cancer. *Nature* **2016**, *531*, 47–52. [CrossRef]
7. Simanshu, D.K.; Nissley, D.V.; McCormick, F. RAS Proteins and Their Regulators in Human Disease. *Cell* **2017**, *170*, 17–33. [CrossRef]
8. Di Magliano, M.P.; Logsdon, C.D. Roles for KRAS in pancreatic tumor development and progression. *Gastroenterology* **2013**, *144*, 1220–1229. [CrossRef]
9. Hingorani, S.R.; Wang, L.; Multani, A.S.; Combs, C.; Deramaudt, T.B.; Hruban, R.H.; Rustgi, A.K.; Chang, S.; Tuveson, D.A. Trp53R172H and KrasG12D cooperate to promote chromosomal instability and widely metastatic pancreatic ductal adenocarcinoma in mice. *Cancer Cell* **2005**, *7*, 469–483. [CrossRef]
10. Bardeesy, N.; Cheng, K.H.; Berger, J.H.; Chu, G.C.; Pahler, J.; Olson, P.; Hezel, A.F.; Horner, J.; Lauwers, G.Y.; Hanahan, D.; et al. Smad4 is dispensable for normal pancreas development yet critical in progression and tumor biology of pancreas cancer. *Genes Dev.* **2006**, *20*, 3130–3146. [CrossRef]
11. Bardeesy, N.; Aguirre, A.J.; Chu, G.C.; Cheng, K.H.; Lopez, L.V.; Hezel, A.F.; Feng, B.; Brennan, C.; Weissleder, R.; Mahmood, U.; et al. Both p16(Ink4a) and the p19(Arf)-p53 pathway constrain progression of pancreatic adenocarcinoma in the mouse. *Proc. Natl. Acad. Sci. USA* **2006**, *103*, 5947–5952. [CrossRef] [PubMed]

12. Aguirre, A.J.; Bardeesy, N.; Sinha, M.; Lopez, L.; Tuveson, D.A.; Horner, J.; Redston, M.S.; DePinho, R.A. Activated Kras and Ink4a/Arf deficiency cooperate to produce metastatic pancreatic ductal adenocarcinoma. *Genes Dev.* **2003**, *17*, 3112–3126. [CrossRef] [PubMed]
13. Guerra, C.; Barbacid, M. Genetically engineered mouse models of pancreatic adenocarcinoma. *Mol. Oncol.* **2013**, *7*, 232–247. [CrossRef] [PubMed]
14. Bournet, B.; Buscail, C.; Muscari, F.; Cordelier, P.; Buscail, L. Targeting KRAS for diagnosis, prognosis, and treatment of pancreatic cancer: Hopes and realities. *Eur. J. Cancer* **2016**, *54*, 75–83. [CrossRef]
15. Zhao, H.; Wu, S.; Li, H.; Duan, Q.; Zhang, Z.; Shen, Q.; Wang, C.; Yin, T. ROS/KRAS/AMPK Signaling Contributes to Gemcitabine-Induced Stem-like Cell Properties in Pancreatic Cancer. *Mol. Oncolytics* **2019**, *14*, 299–312. [CrossRef]
16. Kawesha, A.; Ghaneh, P.; Andren-Sandberg, A.; Ograed, D.; Skar, R.; Dawiskiba, S.; Evans, J.D.; Campbell, F.; Lemoine, N.; Neoptolemos, J.P. K-ras oncogene subtype mutations are associated with survival but not expression of p53, p16(INK4A), p21(WAF-1), cyclin D1, erbB-2 and erbB-3 in resected pancreatic ductal adenocarcinoma. *Int. J. Cancer* **2000**, *89*, 469–474. [CrossRef]
17. Canon, J.; Rex, K.; Saiki, A.Y.; Mohr, C.; Cooke, K.; Bagal, D.; Gaida, K.; Holt, T.; Knutson, C.G.; Koppada, N.; et al. The clinical KRAS(G12C) inhibitor AMG 510 drives anti-tumour immunity. *Nature* **2019**, *575*, 217–223. [CrossRef]
18. Strickler, J.H.; Satake, H.; Hollebecque, A.; Sunakawa, Y.; Tomasini, P.; Bajor, D.L.; Schuler, M.H.; Yaeger, R.; George, T.J.; Garrido-Laguna, I.; et al. First data for sotorasib in patients with pancreatic cancer with KRAS p.G12C mutation: A phase I/II study evaluating efficacy and safety. *J. Clin. Oncol.* **2022**, *40*, 360490. [CrossRef]
19. ClinicalTrials.gov. Available online: https://www.clinicaltrials.gov/ (accessed on 25 August 2022).
20. Nagasaka, M.; Li, Y.; Sukari, A.; Ou, S.I.; Al-Hallak, M.N.; Azmi, A.S. KRAS G12C Game of Thrones, which direct KRAS inhibitor will claim the iron throne? *Cancer Treat Rev.* **2020**, *84*, 101974. [CrossRef]
21. Hallin, J.; Engstrom, L.D.; Hargis, L.; Calinisan, A.; Aranda, R.; Briere, D.M.; Sudhakar, N.; Bowcut, V.; Baer, B.R.; Ballard, J.A.; et al. The KRAS(G12C) Inhibitor MRTX849 Provides Insight toward Therapeutic Susceptibility of KRAS-Mutant Cancers in Mouse Models and Patients. *Cancer Discov.* **2020**, *10*, 54–71. [CrossRef]
22. Gao, J.; Aksoy, B.A.; Dogrusoz, U.; Dresdner, G.; Gross, B.; Sumer, S.O.; Sun, Y.; Jacobsen, A.; Sinha, R.; Larsson, E.; et al. Integrative analysis of complex cancer genomics and clinical profiles using the cBioPortal. *Sci. Signal.* **2013**, *6*, 1. [CrossRef] [PubMed]
23. Cherniack, A.D.; Klarlund, J.K.; Conway, B.R.; Czech, M.P. Disassembly of Son-of-sevenless proteins from Grb2 during p21ras desensitization by insulin. *J. Biol. Chem.* **1995**, *270*, 1485–1488. [CrossRef] [PubMed]
24. Waters, S.B.; Yamauchi, K.; Pessin, J.E. Insulin-stimulated disassociation of the SOS-Grb2 complex. *Mol. Cell. Biol.* **1995**, *15*, 2791–2799. [CrossRef] [PubMed]
25. Jeng, H.H.; Taylor, L.J.; Bar-Sagi, D. Sos-mediated cross-activation of wild-type Ras by oncogenic Ras is essential for tumorigenesis. *Nat. Commun.* **2012**, *3*, 1168. [CrossRef] [PubMed]
26. Hofmann, M.H.; Gmachl, M.; Ramharter, J.; Savarese, F.; Gerlach, D.; Marszalek, J.R.; Sanderson, M.P.; Kessler, D.; Trapani, F.; Arnhof, H.; et al. BI-3406, a Potent and Selective SOS1-KRAS Interaction Inhibitor, Is Effective in KRAS-Driven Cancers through Combined MEK Inhibition. *Cancer Discov.* **2021**, *11*, 142–157. [CrossRef]
27. Ma, Y.; Sender, S.; Sekora, A.; Kong, W.; Bauer, P.; Ameziane, N.; Al-Ali, R.; Krake, S.; Radefeldt, M.; Weiss, F.U.; et al. The Inhibitory Response to PI3K/AKT Pathway Inhibitors MK-2206 and Buparlisib Is Related to Genetic Differences in Pancreatic Ductal Adenocarcinoma Cell Lines. *Int. J. Mol. Sci.* **2022**, *23*, 4295. [CrossRef]
28. Goldoni, M.; Johansson, C. A mathematical approach to study combined effects of toxicants in vitro: Evaluation of the Bliss independence criterion and the Loewe additivity model. *Toxicol. Vitr.* **2007**, *21*, 759–769. [CrossRef]
29. Babraham Bioinformatics. Available online: http://www.bioinformatics.babraham.ac.uk/ (accessed on 1 May 2022).
30. Kim, D.; Paggi, J.M.; Park, C.; Bennett, C.; Salzberg, S.L. Graph-based genome alignment and genotyping with HISAT2 and HISAT-genotype. *Nat. Biotechnol.* **2019**, *37*, 907–915. [CrossRef]
31. Anders, S.; Pyl, P.T.; Huber, W. HTSeq—A Python framework to work with high-throughput sequencing data. *Bioinformatics* **2015**, *31*, 166–169. [CrossRef]
32. Love, M.I.; Huber, W.; Anders, S. Moderated estimation of fold change and dispersion for RNA-seq data with DESeq2. *Genome Biol.* **2014**, *15*, 550. [CrossRef]
33. Mootha, V.K.; Lindgren, C.M.; Eriksson, K.F.; Subramanian, A.; Sihag, S.; Lehar, J.; Puigserver, P.; Carlsson, E.; Ridderstrale, M.; Laurila, E.; et al. PGC-1alpha-responsive genes involved in oxidative phosphorylation are coordinately downregulated in human diabetes. *Nat. Genet.* **2003**, *34*, 267–273. [CrossRef] [PubMed]
34. Subramanian, A.; Tamayo, P.; Mootha, V.K.; Mukherjee, S.; Ebert, B.L.; Gillette, M.A.; Paulovich, A.; Pomeroy, S.L.; Golub, T.R.; Lander, E.S.; et al. Gene set enrichment analysis: A knowledge-based approach for interpreting genome-wide expression profiles. *Proc. Natl. Acad. Sci. USA* **2005**, *102*, 15545–15550. [CrossRef] [PubMed]
35. Luo, W.; Brouwer, C. Pathview: An R/Bioconductor package for pathway-based data integration and visualization. *Bioinformatics* **2013**, *29*, 1830–1831. [CrossRef] [PubMed]
36. Wu, T.; Hu, E.; Xu, S.; Chen, M.; Guo, P.; Dai, Z.; Feng, T.; Zhou, L.; Tang, W.; Zhan, L.; et al. clusterProfiler 4.0: A universal enrichment tool for interpreting omics data. *Innovation* **2021**, *2*, 100141. [CrossRef]

37. Hunter, J.C.; Manandhar, A.; Carrasco, M.A.; Gurbani, D.; Gondi, S.; Westover, K.D. Biochemical and Structural Analysis of Common Cancer-Associated KRAS Mutations. *Mol. Cancer Res.* **2015**, *13*, 1325–1335. [CrossRef]
38. Hong, D.S.; Fakih, M.G.; Strickler, J.H.; Desai, J.; Durm, G.A.; Shapiro, G.I.; Falchook, G.S.; Price, T.J.; Sacher, A.; Denlinger, C.S.; et al. KRAS(G12C) Inhibition with Sotorasib in Advanced Solid Tumors. *N. Engl. J. Med.* **2020**, *383*, 1207–1217. [CrossRef]
39. Rodriguez-Viciana, P.; Warne, P.H.; Dhand, R.; Vanhaesebroeck, B.; Gout, I.; Fry, M.J.; Waterfield, M.D.; Downward, J. Phosphatidylinositol-3-OH kinase as a direct target of Ras. *Nature* **1994**, *370*, 527–532. [CrossRef]
40. Rodriguez-Viciana, P.; Warne, P.H.; Vanhaesebroeck, B.; Waterfield, M.D.; Downward, J. Activation of phosphoinositide 3-kinase by interaction with Ras and by point mutation. *EMBO J.* **1996**, *15*, 2442–2451. [CrossRef]
41. Rubio, I.; Rodriguez-Viciana, P.; Downward, J.; Wetzker, R. Interaction of Ras with phosphoinositide 3-kinase gamma. *Biochem. J.* **1997**, *326 Pt 3*, 891–895. [CrossRef]
42. Vanhaesebroeck, B.; Welham, M.J.; Kotani, K.; Stein, R.; Warne, P.H.; Zvelebil, M.J.; Higashi, K.; Volinia, S.; Downward, J.; Waterfield, M.D. P110delta, a novel phosphoinositide 3-kinase in leukocytes. *Proc. Natl. Acad. Sci. USA* **1997**, *94*, 4330–4335. [CrossRef]
43. Semenza, G.L. Defining the role of hypoxia-inducible factor 1 in cancer biology and therapeutics. *Oncogene* **2010**, *29*, 625–634. [CrossRef] [PubMed]
44. Laughner, E.; Taghavi, P.; Chiles, K.; Mahon, P.C.; Semenza, G.L. HER2 (neu) signaling increases the rate of hypoxia-inducible factor 1alpha (HIF-1alpha) synthesis: Novel mechanism for HIF-1-mediated vascular endothelial growth factor expression. *Mol. Cell. Biol.* **2001**, *21*, 3995–4004. [CrossRef] [PubMed]
45. Pages, G.; Pouyssegur, J. Transcriptional regulation of the Vascular Endothelial Growth Factor gene—A concert of activating factors. *Cardiovasc. Res.* **2005**, *65*, 564–573. [CrossRef] [PubMed]

14.3 Studie III

Studie III: **Schulz B**, Leitner E, Schreiber T, et al. Sex Matters-Insights from Testing Drug Efficacy in an Animal Model of Pancreatic Cancer. *Cancers (Basel)*. 2024;16(10):1901. doi:10.3390/cancers16101901
(IF 5,2)

cancers

MDPI

Article

Sex Matters–Insights from Testing Drug Efficacy in an Animal Model of Pancreatic Cancer

Benjamin Schulz [1], Emily Leitner [1], Tim Schreiber [1], Tobias Lindner [2], Rico Schwarz [3], Nadine Aboutara [3], Yixuan Ma [4], Hugo Murua Escobar [4], Rupert Palme [5], Burkhard Hinz [3], Brigitte Vollmar [1] and Dietmar Zechner [1,*]

[1] Rudolf-Zenker-Institute of Experimental Surgery, Rostock University Medical Center, 18057 Rostock, Germany; benjamin.schulz@med.uni-rostock.de (B.S.)
[2] Core Facility Multimodal Small Animal Imaging, Rostock University Medical Center, 18057 Rostock, Germany; tobias.lindner@med.uni-rostock.de
[3] Institute of Pharmacology and Toxicology, Rostock University Medical Center, 18057 Rostock, Germany
[4] Department of Medicine Clinic III, Hematology, Oncology and Palliative Medicine, Rostock University Medical Center, 18057 Rostock, Germany
[5] Experimental Endocrinology, Department of Biological Sciences, University of Veterinary Medicine Vienna, 1210 Vienna, Austria
* Correspondence: dietmar.zechner@uni-rostock.de; Tel.: +49-381-494-2512

Simple Summary: Pancreatic ductal adenocarcinoma continues to be one of the deadliest cancers worldwide. Preclinical studies involving animals rarely include sex as a major biological variable in testing the efficacy of new drugs. In an animal model of pancreatic cancer, we analyzed the impact of sex on the pathological features of the disease and on an experimental small molecule-based therapy tested in vivo for the first time. While the therapy shows potential, the obtained results are confounded by sex-specific effects. This study, therefore, highlights the importance of sex-inclusive research while simultaneously providing a basis for further studies of the therapy tested.

Abstract: Preclinical studies rarely test the efficacy of therapies in both sexes. The field of oncology is no exception in this regard. In a model of syngeneic, orthotopic, metastasized pancreatic ductal adenocarcinoma we evaluated the impact of sex on pathological features of this disease as well as on the efficacy and possible adverse side effects of a novel, small molecule-based therapy inhibiting KRAS:SOS1, MEK1/2 and PI3K signaling in male and female C57BL/6J mice. Male mice had less tumor infiltration of CD8-positive cells, developed bigger tumors, had more lung metastasis and a lower probability of survival compared to female mice. These more severe pathological features in male animals were accompanied by higher distress at the end of the experiment. The evaluated inhibitors BI-3406, trametinib and BKM120 showed synergistic effects in vitro. This combinatorial therapy reduced tumor weight more efficiently in male animals, although the drug concentrations were similar in the tumors of both sexes. These results underline the importance of sex-specific preclinical research and at the same time provide a solid basis for future studies with the tested compounds.

Keywords: PDAC; KRAS; SOS1; PI3K; MEK1/2; sex; small molecule; BI-3406; trametinib; BKM120

check for updates

Citation: Schulz, B.; Leitner, E.; Schreiber, T.; Lindner, T.; Schwarz, R.; Aboutara, N.; Ma, Y.; Escobar, H.M.; Palme, R.; Hinz, B.; et al. Sex Matters–Insights from Testing Drug Efficacy in an Animal Model of Pancreatic Cancer. *Cancers* **2024**, *16*, 1901. https://doi.org/10.3390/cancers16101901

Academic Editor: Cosimo Sperti

Received: 27 April 2024
Accepted: 2 May 2024
Published: 16 May 2024

Copyright: © 2024 by the authors. Licensee MDPI, Basel, Switzerland. This article is an open access article distributed under the terms and conditions of the Creative Commons Attribution (CC BY) license (https://creativecommons.org/licenses/by/4.0/).

1. Introduction

For a long time, male animals and patients were predominantly used in both preclinical and clinical biomedical research [1,2]. Results were often applied to women without adequate justification, leading to potentially serious consequences for women [2,3]. The underrepresentation of women in drug trials became particularly apparent when the U.S. Food and Drug Administration (FDA) withdrew ten prescription drugs from the market between 1997 and 2000, four of which have led to more severe adverse events in women. This included the antihistamine Hismanal, which triggered torsade de pointes [3,4]. To

address this issue, the 21st Century Cures Act in 2016 called on the National Institutes of Health (NIH) to revise guidelines for the inclusion of women in clinical trials and outlined requirements for reporting analyses by gender, race, and ethnicity in phase III clinical trials [5]. Today, women represent 50% or more of participants in NIH-funded studies [6].

While progress has been made in incorporating female participants in clinical trials, the extension of this inclusion to animal experiments is still insufficient [6,7]. The omission of females from preclinical research was motivated by concerns among researchers about potential variations induced by the estrus cycle, along with apprehensions about increased costs [8,9]. However, since hormonal differences play an important role not only in the development of diseases such as anxiety and depression, asthma, and inflammatory bowel disease but also in pharmacokinetics, it was important to establish guidelines that define sex as a biological variable [10–14]. Therefore, in 2016, the Association of Science Editors published the SAGER guidelines (Sex and Gender Equity in Research), which regulate reporting on sex and gender in scientific publications [2,15].

The lack of sex-specific investigations in preclinical and clinical studies becomes particularly evident within the field of cancer and cancer therapeutics [16]. An evolving awareness emphasizes that sex not only shapes susceptibility to cancer but also influences disease progression and responses to therapeutic interventions [17,18]. In general, men exhibit elevated cancer incidence and mortality rates compared to women [17,18]. Sex hormones have been identified as influential factors affecting both tumor growth and the tumor microenvironment [19,20]. In addition, females exhibit heightened innate and adaptive immune responses, resulting in a lower cancer incidence compared to males and a different response to immunotherapies such as immune checkpoint inhibitors [19,21–23]. While men appear to respond better to immune checkpoint inhibitors, women tend to respond better to multimodal immunotherapies [23,24]. For example, a 2021 study by Kim et al. investigated the impact of sex when treating pancreatic cancer patients with FOLFIRINOX [25]. This study reported a markedly enhanced overall survival among females compared to males despite a more rapid dose reduction during each treatment cycle.

Pancreatic ductal adenocarcinoma (PDAC) represents an enormous challenge due to its heterogeneity, plasticity, and aggressive biological nature, making it the fourth leading cause of cancer-related mortality with a 5-year survival rate of approximately 10% [26]. The most frequently affected oncogene, at around 90%, is the Kirsten-rat sarcoma viral oncogene homolog *KRAS* [27]. The mutation affects the GTPase activity of KRAS by altering the homeostatic balance of GDP and GTP binding towards the active state [27]. This occurs either by reducing GTP hydrolysis or by increasing the GTP loading rate [27,28]. As a result, intracellular signaling pathways, such as phosphoinositide 3-kinase/protein kinase B (PI3K/AKT) or RAF/MEK/ERK, are activated and carcinogenesis is promoted [29].

An example of novel therapeutic agents successfully targeting specific KRAS mutations is sotorasib, the first FDA-approved drug for the treatment of KRAS G12C-mutated non-small cell lung cancer (NSCLC) [30]. Sotorasib's mechanism of action is to prevent the exchange of the inactive GDP-bound form to its active GTP-loaded state, thereby deactivating downstream signaling pathways [31]. However, G12C mutations occur only in about 1.5% of PDAC patients, with G12D mutations predominating at 39%, followed by G12V mutations [32]. Hence, pan-KRAS therapies offer a treatment option that simultaneously targets multiple KRAS mutations [33,34].

Hofmann et al. developed BI-3406, a son of sevenless homolog 1 (SOS1) inhibitor, which decreases the formation of GTP-loaded RAS and limits the proliferation in a broad spectrum of KRAS-driven cancers [35]. BI-3406 also blocks the feedback activation of RAS signaling observed after the inhibition of MEK by trametinib. A combination of BI-3406 with trametinib consequently led to a strong regression in KRAS-driven tumors [35]. However, tumor growth stasis was observed in colorectal and pancreatic PDX models following the combination of SOS1/MEK inhibitors, suggesting further feedback mechanisms and the need for triple combination therapies to effectively disrupt KRAS signaling [35]. In a previous study, we observed a considerable reduction in the growth of several human

pancreatic cancer cell lines when buparlisib (BKM120, a pan-PI3K inhibitor) was combined with BI-3406 and trametinib [36].

This study aimed to assess the efficacy and potential adverse side effects of a combinatorial therapy using BI-3406, trametinib, and BKM120 in a pancreatic ductal adenocarcinoma (PDAC) mouse model. In addition, the inclusion of male and female mice allowed us to evaluate if sex influences cancer progression and therapeutic response.

2. Materials and Methods

2.1. Animals

C57BL/6J mice used in this study were bred under specified pathogen-free conditions (SPF) in our animal facility. The health status of the animal stock was routinely checked (*Helicobacter* sp., *Rodentibacter heylii*, and murine norovirus were detected in a few mice; these animals were not used). For the duration of the experiment, all mice were single-housed in type III cages (Zoonlab GmbH, Castrop-Rauxel, Germany) with a 12 h light-dark cycle, a temperature of 21 ± 2 °C and relative humidity of 60 ± 20% with food (pellets, 10 mm, ssniff-Spezialdiäten GmbH, Soest, Germany) and tap water ad libitum. Enrichment was provided by nesting material (shredded tissue paper, Verbandmittel GmbH, Frankenberg, Germany), a paper roll (75 × 38 mm, H 0528–151, ssniff-Spezialdiäten GmbH), and a wooden stick (40 × 16 × 10 mm, Abedd, Vienna, Austria). All animal experiments were approved by the German local authority: Landesamt für Landwirtschaft, Lebensmittelsicherheit und Fischerei Mecklenburg-Vorpommern (AZ: 1-016/21).

2.2. Cell Culture and In Vitro Analysis

The 6606PDA cell line was a kind gift from Prof. Tuveson (Cold Spring Harbor Laboratory, Cold Spring Harbor, NY, USA) [37]. The *Kras* G12D mutation was verified by sequencing and the sex of the cell line was determined by Jarid1c/d PCR [38] to be male (Figure S1 and Tables S1–S3). Sanger sequencing of the *Kras* PCR products was carried out by LGC Genomics GmbH (Berlin, Germany) on an ABI 3730 XL DNA Analyzer (Applied Biosystems, Waltham, MA, USA). The cells were routinely cultured in DMEM (4.5 g/L Glucose, PAN Biotech GmbH, Aidenbach, Germany) supplemented with 10% fetal calf serum (FCS, PAN Biotech GmbH, Aidenbach, Germany) and penicillin/streptomycin (100 U/ml, PAN Biotech GmbH, Aidenbach, Germany). To analyze the effects of BI-3406 (a kind gift from Boehringer Ingelheim, supplied through their Open Innovation Portal opnMe), trametinib and BKM120 (both bought from Chemietek, Indianapolis, IN, USA) on proliferation and cell death alone and in combination, cells were seeded at a density of 2×10^3 (proliferation) in 96-well plates (Greiner Bio-One GmbH, Frickenhausen, Germany) or 3×10^4 (cell death) in 12-well plates (Greiner Bio-One GmbH, Frickenhausen, Germany). The substances were dissolved in DMSO and were added at the indicated concentrations either alone or in combination and the cells were incubated for 48 h. Cell proliferation was assessed by the addition of 5-bromo-2′-deoxyuridine (BrdU, Merck KGaA, Darmstadt, Germany) and quantified with a colorimetric cell proliferation ELISA kit (Roche Diagnostics, Mannheim, Germany) according to the manufacturer's recommendations. The absorbance was measured on a Perkin Elmer Victor X3 model 2030 Multilabel Plate Reader (PerkinElmer, Waltham, MA, USA). Cell death (apoptosis and necrosis) was assessed by the addition of Annexin-V-FITC (BD Biosciences, Heidelberg, Germany) and propidium iodide (Merck KGaA, Darmstadt, Germany) after incubation with test substances. Subsequently, the cells were analyzed by flow cytometry (FACSVerse™, BD Biosciences, Heidelberg, Germany). Inhibitor interaction for proliferation and cell death was evaluated by use of the Bliss independent model as described before [36]. The interaction of the inhibitors was determined by the difference between the observed (E_O) and predicted (E_P) effect of the combination and deemed synergistic when $E_O > E_P$, additive when $E_O = E_P$ and antagonistic when $E_O < E_P$. For the analysis of the effects of the physiological and supra-physiological concentrations of sex hormones (testosterone (86500), dihydrotestosterone (10300), progesterone (P8783) and 17β-estradiol (E8875), all bought from Merck KGaA,

Darmstadt, Germany), 6606PDA cells were seeded at a density of 5×10^3 and cultured as described before with either 2% or 10% FCS and the sex hormones added at the indicated concentrations for 48 h. Cytotoxicity and cell viability were assessed by CellTox™ Green cytotoxicity assay and CellTiter-Glo® luminescent cell viability assay (both from Promega GmbH, Walldorf, Germany). To evaluate the impact of sex hormones on the efficacy of the combinatorial therapy at physiological concentrations, 6606PDA cells were cultured as described before and BI-3406, trametinib, BKM120, and the respective sex hormones were added at the indicated concentrations and incubated for 48 h. Cytotoxicity was assessed as described before.

2.3. Pancreatic Cancer Model and Therapeutic Intervention

Female and male C57BL/6J mice, between 16 and 23 weeks old, were anesthetized with 1–3 vol.% isoflurane. Carprofen (5 mg/kg) was injected subcutaneously as perioperative analgesia and eye ointment was applied. During surgery, the mice were kept warm on a heating plate at 37 °C. Each animal received an orthotopic and an intravenous cell injection. For intravenous injections, 6606PDA cells were resuspended in Hank's Balanced Salt Solution (HBSS, PAN Biotech GmbH, Aidenbach, Germany); 50 µL of the cell suspension (7×10^6 cells/mL) were injected into the tail vein through a catheter (Fine Bore Polyethylene Tubing (0.28 mm ID, 0.61 mm OD), Smiths Medical International Ltd., Hythe, UK). The orthotopic injection of tumor cells was performed as previously described [39–41]. Briefly, the abdomen was shaved, opened and the 6606PDA cells (2.5×10^5 cells in 5 µL PBS/Matrigel (BD Basement Membrane Matrix (354248), Corning Inc., New York, NY, USA) were injected with a 25 µL syringe (Hamilton, Reno, NV, USA) into the head of the pancreas. Afterward, the abdomen was closed with two sutures (Johnson & Johnson Medical GmbH, Norderstedt, Germany) and mice were placed in front of a heating lamp for 20–30 min; 3000 mg/L Metamizol (Novaminsulfon-ratiopharm 500 mg/mL, Ratiopharm GmbH, Ulm, Germany) was added daily to the drinking water for continuous analgesia until the end of the experiment. On day 4 after surgery, the animals were randomized into treatment groups (either vehicle or a combination of BI-3406, trametinib, and BKM120). The compounds were dissolved in a mixture of 60% Phosal50PG (Lipoid GmbH, Ludwigshafen, Germany), 30% PEG400 (Merck KGaA, Darmstadt, Germany) and 10% Ethanol (99.6%, undenatured). Test substances and vehicle were administered by oral gavage from day 4 until euthanasia at day 36 in a 5-days on/2-days off dosing scheme. The drug concentrations administered per gavage were as follows: BI-3406 at 50 mg/kg (2 × per day), trametinib at 0.1 mg/kg (2 × per day), and BKM120 at 30 mg/kg (1 × per day). Sham treatment was performed with the vehicle solution. On day 36 after tumor cell injection mice were gavaged (vehicle or drugs) and injected with BrdU (2.5 µL/g body weight at a concentration of 20 mg/mL) 1.5–2 h before euthanasia by cervical dislocation in deep narcosis (4–5 vol.% isoflurane). Tumors, lungs, livers, and kidneys were harvested and preserved in either 4% PBS-buffered paraformaldehyde (PFA, Formafix GmbH, Düsseldorf, Germany), TissueTek™ (Sakura Finetek Germany GmbH, Umkirch, Germany) or snap frozen in liquid nitrogen for later analysis. Sixty-four mice were used in total for all experiments, of which eight mice had to be excluded due to perioperative complications.

2.4. Assessment of Animal Wellbeing

In order to evaluate animal wellbeing, the body weight, burrowing activity, nesting behavior, distress score, and fecal corticosterone metabolites (FCMs) were assessed for each mouse at distinct time points. For example, the distress score was evaluated on day 0 (30 min after finishing surgery), burrowing and nesting activity was assessed from the evening of day 0 to the morning of day 1, and on day 1 after surgery the body weight was determined and the feces were collected. In order to obtain an overview of animal well-being over the course of the experiment, all the parameters were assessed before the cell injection (day −4 to −3), during the acute (day 0 to 1), early (day 4 to 5), middle (day 18 to 19) and late phase (day 35 to 36) of the experiment. The burrowing activ-

ity was analyzed using a 3D-printed tube (length: 15 cm, diameter: 6.5 cm) filled with 200 g of food pellets. The tube was placed into the mouse cage 2–3 h before the dark phase and the remaining pellets were weighed after 17 h on the next day. To analyze the nest-building behavior, a cotton nestlet (5 cm square of pressed cotton batting, Zoonlab GmbH, Castrop-Rauxel, Germany) was placed into the cage 30 to 60 min before the dark phase. The nests were scored at 9:30 a.m. ± 2 h on the next day by using a scoring system developed by Deacon [42]. A sixth score point was added to this scoring system, which defines a perfect nest: The nest looked like a crater and more than 90% of the circumference of the nest wall was higher than the body height of the coiled-up mouse. In addition, the wellbeing of mice was evaluated by assessing multiple parameters with the help of a score sheet previously published [43]. The score summarizes various defined criteria (e.g., spontaneous behavior, flight behavior, or general body conditions). In order to assess the concentration of fecal corticosterone metabolites [44], feces dropped within 24 h in a new cage were collected in every phase of the experiment and stored at −80 °C. Before extraction, the fecal pellets were dried for 4 h at 65 °C and stored at −20 °C. Afterward, 50 mg of the dry feces were extracted with 1 mL 80% methanol for subsequent analysis using a 5α-pregnane-3β,11β,21-triol-20-one enzyme immunoassay [44–46].

2.5. Tumor Volume (MRI)

For the quantification of tumor volume in vivo, a subset of both female and male mice was scanned 2–7 days before euthanasia with a 7 T MRI (magnetic resonance imaging, BioSpec 70/30, 7.0 Tesla, gradient insert: BGA-12S HP, transmit volume resonator (86 mm inner diameter) and receive-only 2x2-array surface coil (all Bruker BioSpin GmbH, Ettlingen, Germany). For scanning, animals were anesthetized with 1.0–2.5 vol.% isoflurane and were placed in a supine position on the bed of the scanner. The scanning protocol comprised three orthogonal morphological T2-weighted TurboRARE (Rapid Acquisition with Relaxation Enhancement) sequences with the parameters specified in Table S4. Tumor volume was further quantified in the axial slice faction with the software program ITK-SNAP 3.8.0 [47]. During all imaging procedures, the breathing rate and body temperature were monitored and the temperature of the animals was kept constant by a heating pad. All sequences were triggered by respiration.

2.6. Concentration of Tested Compounds In Vivo (LC-MS/MS)

Prior to an analysis by LC-MS/MS, all samples were subjected to appropriate work-up in order to be able to analyze trametinib, BI-3406 and BKM120 in one single run. Therefore, 10 µL mouse plasma or shredded mouse tissue (tumor, liver, kidney) was mixed with 80 µL acetonitrile; 10 µL of a 0.5 µM acridine orange solution was added as an internal standard. After vortexing the samples for 5 min, they were centrifuged at 14,000 rpm (26,342 g) for 5 min; 2 µL supernatant was injected for LC-MS/MS analysis. In order to generate a standard curve for the determination of the concentrations of trametinib, BKM120 and BI-3406 in the mouse samples, the stock solutions of the substances in DMSO were serially diluted using human plasma; 10 µL of these plasma concentrations were processed like the mouse samples. A concentration range of 0.5–5 µM was chosen for BKM120, 0.03125–2.5 µM for trametinib, and 0.25–5 µM for BI-3406. Separation was achieved using a Shimadzu LC-20AD HPLC with a Multospher 120 C18 AQ column 125 × 2 mm, 5 µm particle size (CS-Chromatographie Service GmbH, Langerwehe, Germany) coupled with a guard column (20 mm × 3 mm, 5 µm particle size). Water was chosen as mobile phase A and acetonitrile as mobile phase B, both containing 0.2% formic acid. The flow rate was 0.3 mL/min. A linear gradient from 20% B to 100% B within 4.5 min was chosen for the separation. This step was held for 0.5 min, then immediately reduced to 20% B and the column re-equilibrated for a further 3 min. The total run time was 8 min per run. The oven temperature was set to 40 °C. Mass spectrometric analysis was carried out on a Shimadzu LCMS-8050 triple quadrupole mass spectrometer. The substances were measured in positive or negative mode. The respective transitions and associated mass

spectrometric settings as well as the general settings of the triple quadrupole are shown in Tables S5 and S6. Calculation of the concentration of the tested compounds was conducted using the volume quantified by MRI-scanning to arrive at the molar concentrations in the tumor.

2.7. Histology

After fixation for at least 24 h in 4% PBS-buffered PFA the left lung lobe was serially cut into 4 µm sections and stained with hematoxylin and eosin to assess metastasis. The metastatic area was evaluated with QuPath 0.4.3. Tumors were fixed similarly and immunohistochemistry was subsequently performed for CD8α (1:100, 4SM15-Biotin, eBioscience, San Diego, CA, USA) with secondary detection by Streptavidin-AP (1:100, Invitrogen, Waltham, MA, USA), anti-BrdU (1:50, BU20a, Dako, Hamburg, Germany) with secondary detection by a HRP-conjugated antibody (polyclonal goat anti-mouse, 1:100, Dako, Hamburg, Germany) or anti-PD-L1 (1:200, D5V3B, Cell Signalling Technology, Danvers, MA, USA) with secondary detection by an AP-conjugated antibody (goat anti-rabbit, 1:200, 97048, Abcam, Waltham, MA, USA). Detection of BrdU-positive ($BrdU^+$) and CD8-positive ($CD8^+$) cells as well as PD-L1-positive tissue was performed with QuPath 0.4.3.

2.8. Quantitative Real-Time Polymerase Chain Reaction (TaqMan RT-qPCR)

Parts of the tumors were snap-frozen in liquid nitrogen during tissue harvest. Total RNA was extracted using QIAzol lysis reagent and the RNeasy Mini Kit (both from Qiagen, Hilden, Germany). Synthesis of cDNA was carried out with 100 ng of extracted RNA using the High-Capacity cDNA Reverse Transcription Kit (Applied Biosystems, Waltham, MA, USA). The calibrator consisted of RNA extracted from the lungs of four healthy female wild-type C57BL/6J mice. TaqMan qPCR was performed on a Bio-Rad IQ5 real-time qPCR system (Bio-Rad Laboratories GmbH, Feldkirchen, Germany) with probes (Applied Biosystems, Waltham, MA, USA) for *Gapdh* (Mm99999915_g1), *Ipo8* (Mm01255158_m1), *Ifn-γ* (Mm99999071_m1), *Il10* (Mm00439614_m1), *Il2* (Mm00434256_m1), *Tnf-α* (Mm00443258_m1) and *Il6* (Mm99999064_m1) and the cycling parameters detailed in Table S7. *Gapdh* and *Ipo8* served as reference genes. Ct values were calculated using the QuantStudio software (Version 2.1, Applied Biosystems, Waltham, MA, USA). The data were calculated as ΔCt ($Ct^{Avg\cdot Ref\ (Gapdh+Ipo8)} - Ct^{GOI}$) and ΔΔCt ($\Delta Ct^{Calibrator} - \Delta Ct$). Statistics have been analyzed using the ΔΔCt values.

2.9. Blood Chemistry

Blood was drawn immediately before euthanasia by retroorbital bleeding. The blood was subsequently centrifuged and the resulting plasma was stored at −80 °C for later analysis. Parameters of blood chemistry (AST, ALT, creatinine, LDH) were quantified on a cobas c111 (Roche Diagnostics, Mannheim, Germany) and c-peptide was quantified with a mouse c-peptide ELISA kit (ALPCO, Salem, MA, USA) according to the manufacturer's recommendations. Five healthy animals of either sex have been used as controls.

2.10. Data Presentation and Statistical Analysis

All data were analyzed and graphed with GraphPad Prism (version 8.0.1, GraphPad Software Inc., San Diego, CA, USA) and are presented as box plots (single data points are depicted and whiskers indicate minimum and maximum) or as bar graphs. Statistical significance was determined by different methods (for details see figure legends) based on the number of independent variables and data characteristics. If the influence of two independent variables (e.g., time and therapy) on one dependent variable (when using combined data) was analyzed, a two-way repeated measure ANOVA with Sidak's post-hoc test was performed. If the influence of one independent variable on a dependent variable was evaluated, the normality of data was checked by the Shapiro–Wilk normality test. When two groups were compared and data were not paired, either the unpaired *t*-test (with Welch's correction if sample sizes were unequal) or the Mann–Whitney rank sum test

was performed. When analyzing more than two groups, either a one-way ANOVA with Dunnett's post-hoc test or a Kruskal–Wallis test with Dunn's post-hoc test was performed. Therapy response was calculated as a normalized quotient of the tumor weight of individual drug-treated animals and the mean tumor weight of vehicle-treated animals.

$$normalized\ therapy\ response = 100 - \left(\frac{individual\ tumor\ weight(treated)}{mean\ tumor\ weight(vehicle)}\right) \times 100$$

The correlation between $CD8^+$ cells and tumor weight was assessed with Spearman correlation and linear regression including confidence intervals. Survival was evaluated by the Kaplan–Meier estimator followed by a log-rank test. Differences with $p < 0.05$ were considered to be significant.

3. Results

3.1. Key Pathological Features of the PDAC Model Are Sex-Dependent

Out of 15 male mice, eight had to be euthanized early due to reaching humane endpoints. In contrast, none of the 15 female mice had to be euthanized early and thus their probability of survival was significantly higher than in male mice (Figure 1A). The weight of the tumor in the pancreas was significantly lower in female mice with a median weight of 266 mg compared to male mice with a 625 mg median tumor weight (Figure 1B). The intravenous injection of 6606PDA cells led to the formation of small tumors in the lungs of 33.3% of male animals, while no lesions were detected in female animals (Figures 1C–E and S2). Duodenal invasion of the primary tumor is observed in a subset of animals (Figure S3). In this model, 73.3% of male animals were affected by invasive tumor growth compared to 6.6% of female animals (Figure 1F).

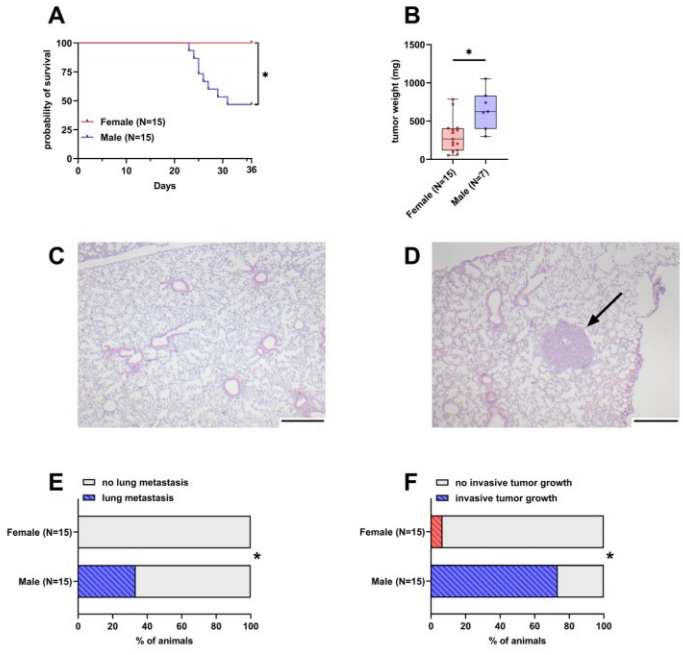

Figure 1. Differences in survival, tumor weight, lung metastasis, and invasive tumor growth between female and male mice. (**A**): Probability of survival in female and male mice (Kaplan–Meier estimator

and log-rank Mantel–Cox test, * $p < 0.05$). (**B**): Tumor weight in surviving female and male mice 36 days after orthotopic cell injection (unpaired *t*-test with Welch's correction, * $p < 0.05$). (**C**,**D**): Representative histological sections of lungs from female (**C**) and male (**D**) mice. The arrow in D highlights a lung metastasis (scale bar = 250 µm). (**E**): Percentage of mice with histologically detectable metastases (Fisher's exact test, * $p < 0.05$). (**F**): Percent of mice with invasive tumor growth (duodenal invasion, Fisher's exact test, * $p < 0.05$).

3.2. *Male Mice Experience More Distress in the Late Phase of the Experiment*

During the experiment, parameters of animal wellbeing, such as body weight, burrowing and nesting activity, a clinical distress score, and fecal corticosterone metabolites (FCMs) were assessed. Body weight, burrowing, and the clinical distress score were significantly different between the two sexes in the late phase of the experiment, where the burden of disease is expected to be highest (Figure 2A–C). Body weight and the burrowing activity of male mice were reduced compared to females and the clinical distress score was increased. There was no significant difference in nesting activity and FCMs between male and female mice over the course of the experiment (Figure 2D,E).

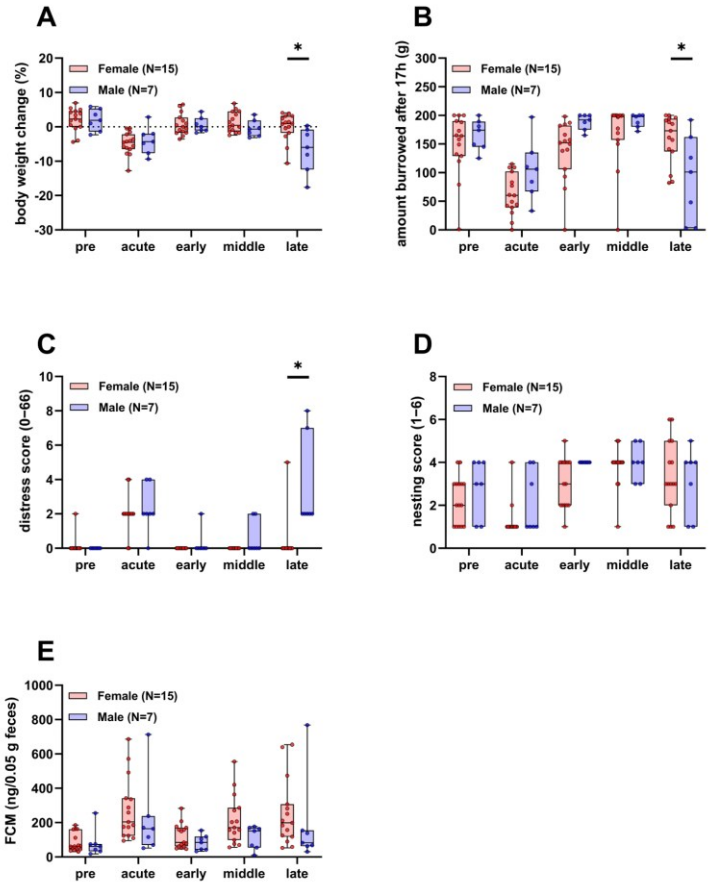

Figure 2. Parameters of animal wellbeing in female and male mice. Body weight (**A**), burrowing activity (**B**), distress score (**C**), nesting activity (**D**), and concentration of fecal corticosterone metabolites

(FCMs, (**E**)) compared between surviving female and male mice (Two-way repeated measures ANOVA with Sidak's post-hoc test, * $p < 0.05$). Pre, acute, early, middle, and late refer to the experimental phases as defined in the methods section.

3.3. An Experimental Small-Molecule-Based Therapy Shows Promising Results In Vitro

In order to evaluate the inhibitors of KRAS:SOS1, MEK1/2, and PI3K in 6606PDA cells, a combination of 10 µM BI-3406, 0.064 µM trametinib, and 1 µM BKM120 was tested in vitro. These concentrations correspond to approximately 50% of the IC_{50} value of each compound for inhibiting the proliferation of 6606PDA cells (Figure S4). The combinatorial treatment significantly reduced BrdU incorporation in 6606PDA cells when compared to the DMSO control group, single drugs, or a combination of only two drugs (Figure 3A). For all possible combinations of these drugs, the inhibition of proliferation was higher than what would be expected with an additive inhibitory effect (Figure 3B). This demonstrates a synergistic inhibition of proliferation. The combination of these three drugs also induced cell death in a synergistic manner (Figure 3C,D). Physiological [48] and supraphysiological concentrations of sex hormones (testosterone, progesterone, 17β-estradiol, and dihydrotestosterone) have no apparent concentration-dependent effect on the viability and cell death of 6606PDA cells cultured with either 10% or 2% FCS (Figure S5). To evaluate if these sex hormones impact the cytotoxic efficacy of the combinatorial therapy in vitro, 6606PDA cells were treated with the combination of BI-3406, trametinib and BKM120 plus each sex hormone separately (Figure S6). The combination of BI-3406, trametinib, and BKM120, with 17β-estradiol performed significantly worse than the control without sex hormones and the combination with testosterone. However, all the tested sex hormones had a quantifiable negative impact on the efficacy of the combinatorial therapy.

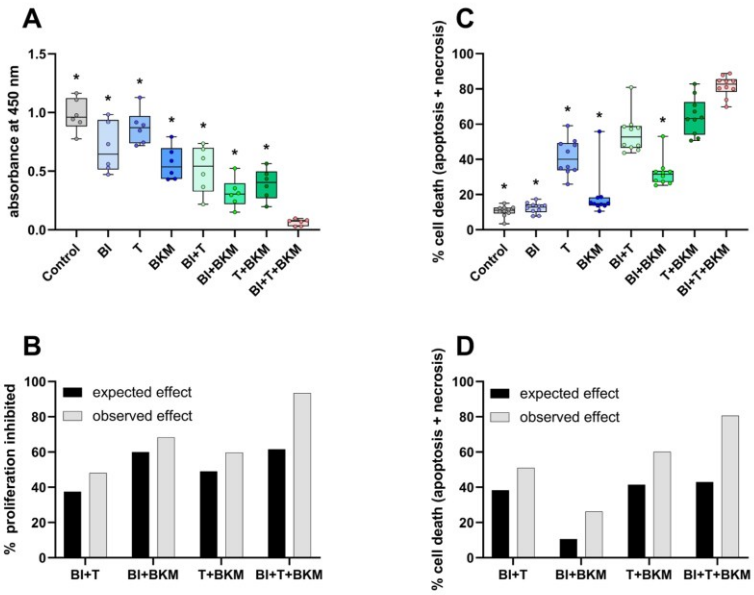

Figure 3. SOS1, MEK1/2 and PI3K inhibitors reduce proliferation and induce cell death. (**A**): Incorporation of BrdU in cells exposed to vehicle control (DMSO), 10 µM BI-3406 (BI), 0.064 µM trametinib (T), 1 µM BKM120 (BKM) or the indicated combinations of these drugs (ordinary one-way ANOVA with Dunnett's post-hoc test, * $p < 0.05$ compared with triple combination, N = 6). (**B**): The synergy of

drugs in inhibiting proliferation was determined using the Bliss independent model. (**C**): Induction of cell death (apoptosis and necrosis, Kruskal–Wallis test with Dunn's post-hoc test, * $p < 0.05$ compared with triple combination, N = 10). (**D**): Analysis of synergy by the Bliss independent model for induction of cell death for all combinations of the three compounds.

3.4. Sex Impacts the Response to Therapy In Vivo

After confirming the high efficacy of the drugs in vitro, the triple combination of inhibitors was tested in female and male C57BL/6J mice. Since BI-3406, trametinib, and BKM120 had been safely tested in mice before with concentrations of 50 mg/kg, 0.1 mg/kg, and 30 mg/kg, respectively [35,49], we utilized these concentrations in our study. One out of thirteen female mice in the treatment group had to be euthanized, while all vehicle-treated control animals survived until day 36 (Figure 4A). Of 13 drug-treated male mice, six had to be euthanized, while 8 out of 15 vehicle-treated male animals had to be euthanized (Figure 4B). The tumor weight of female animals was only slightly reduced by the compounds with a median weight of 208 mg compared to 266 mg in vehicle-treated animals (Figure 4C). In contrast, the tumor weight of male animals was significantly reduced to a median weight of 99 mg compared to 625 mg in vehicle-treated male mice (Figure 4D). The normalized therapy response was significantly higher in males compared to females (Figure 4E). While invasive tumor growth was detected in 6.6% of untreated female animals, this percentage increased to 15.3% when treated with drugs (Figure 4F). However, invasive tumor growth in male mice was reduced from 73.3% in untreated animals to 46.1% in drug-treated mice (Figure 4G). None of the female mice receiving vehicle solution were affected by lung metastasis, while unexpectedly 30.7% of drug-treated animals had detectable lesions in their left lung lobe (Figures 4H and S7A). In a similar manner, male mice showed an increase in metastasis from 33.3% in vehicle-receiving animals to 50% in drug-treated ones (Figures 4I and S7B).

To evaluate the concentration of each compound within the tumor, a subset of tumors was subjected to LC-MS/MS analysis. As shown in Table 1, the calculated median concentrations were not markedly different between female and male animals. A comparison with the concentrations used in vitro (Table 2) indicates that the median concentrations of trametinib and BKM120 were higher within the tumor than the concentration used in cell culture, while the median concentration for BI-3406 within the tumor was below the concentration used in vitro. Similarly, concentrations in the plasma, liver and kidney were evaluated in a subset of animals (Table S8). As before, no marked differences were observed and trametinib could not be detected in the plasma of either sex.

Table 1. Measured concentrations (LC-MS/MS) of drugs in the tumor (median with 5–95% confidence interval).

Male (N = 4)	**BI-3406 (µM)**	**Trametinib (µM)**	**BKM120 (µM)**
Median (5–95% CI)	2.4 (0.12–9.3)	0.21 (0.02–0.65)	2.1 (0.68–3.6)
Female (N = 6)	**BI-3406 (µM)**	**Trametinib (µM)**	**BKM120 (µM)**
Median (5–95% CI)	3.8 (0.16–38)	0.16 (0.01–1.4)	2.4 (0.41–24)

Table 2. Used concentrations of drugs in vitro.

Concentrations used in combination	BI-3406 (µM)	Trametinib (µM)	BKM120 (µM)
	10	0.064	1

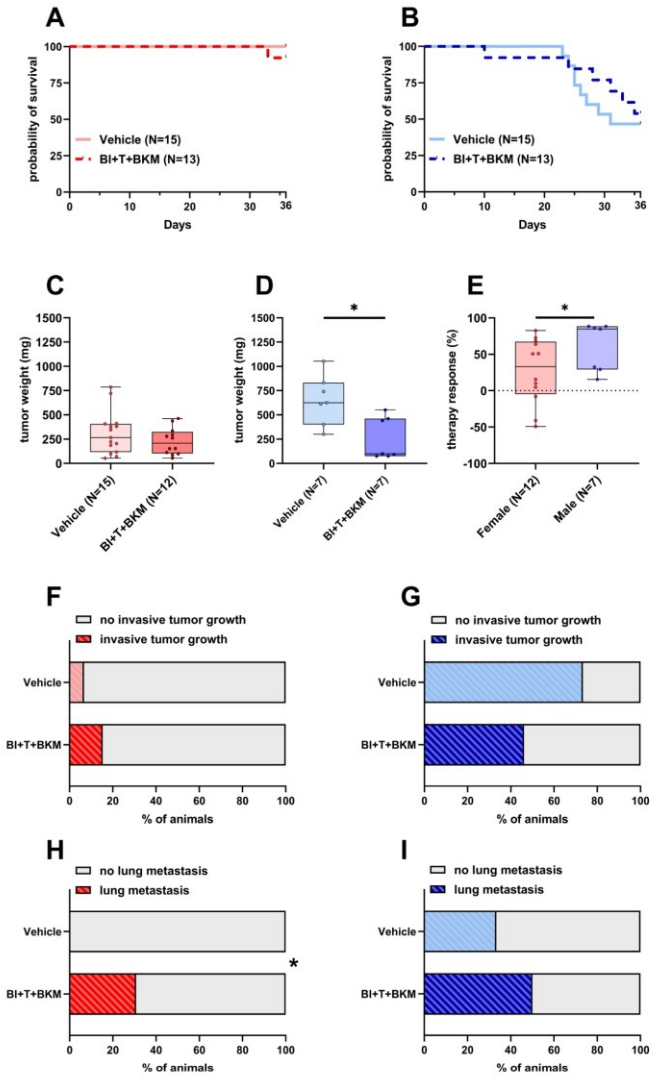

Figure 4. Effects of combinatorial therapy on survival, primary tumor weight, invasive tumor growth and metastasis. (**A**,**B**): Probability of survival in female (**A**) and male (**B**) mice receiving either vehicle or the drug combination consisting of BI-3406 (BI), trametinib (T), and BKM120 (BKM) (Kaplan–Meier estimator and log-rank Mantel–Cox test, ns). (**C**,**D**): Tumor weight of surviving female (**C**) and male (**D**) mice 36 days after tumor cell injection receiving either vehicle or combinatorial therapy ((**C**): unpaired *t*-test, ns; (**D**): Mann–Whitney test, * $p < 0.05$). (**E**): Therapy response of animals receiving therapy normalized to the mean tumor weight of vehicle-treated animals of the same sex (Mann–Whitney test, * $p < 0.05$). (**F**,**G**): Percentage of female (**F**) and male (**G**) animals with invasive tumor growth receiving either vehicle or combinatorial therapy (Fisher's exact test, ns). (**H**,**I**): Percentage of female (**H**) and male (**I**) animals with detectable lesions in serial histological slices of the left lung lobe receiving either vehicle or combinatorial therapy (Fisher's exact test, * $p < 0.05$).

3.5. Impact of Combinatorial Therapy on Parameters Associated with Adverse Side Effects

When assessing potential adverse side effects of the combinatorial therapy, no significant increases in transaminases (AST, ALT), creatinine and lactate-dehydrogenase (LDH) activity were observed in the blood plasma (Figure 5A–H). However, the combination of these drugs significantly increased the c-peptide concentration in both sexes (Figure 5I,J). In addition, the influence of these compounds on the wellbeing of animals was evaluated (Figure S8A–H). The therapy had no significant impact on body weight (Figure S8A,B) and burrowing activity (Figure S8C,D) of either sex. The distress score of drug-treated female mice was significantly increased during the late phase of drug administration (Figure S8E). No significant difference in distress scores was observed in male mice (Figure S8F). Neither nesting activity (Figure S8G,H) nor FCMs (Figure S8I,J) of both sexes were impacted by these drugs.

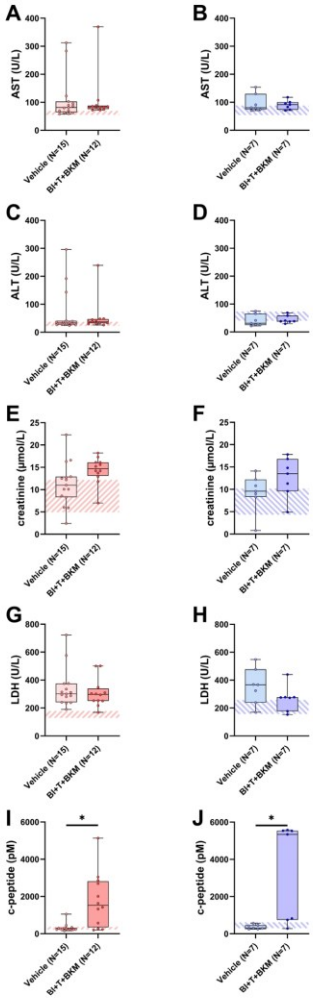

Figure 5. Effect of combinatorial therapy on blood chemistry. Analysis of AST (**A**,**B**), ALT (**C**,**D**), creatinine (**E**,**F**), LDH (**G**,**H**), and c-peptide (**I**,**J**) in blood plasma of surviving female and male mice

receiving either vehicle or a combination of drugs consisting of BI-3406 (BI), trametinib (T) and BKM120 (BKM). ((**A**,**C**,**G**,**I**,**J**): Mann–Whitney test, * $p < 0.05$; (**B**,**D**–**F**,**H**): unpaired *t*-test, ns). The striped area indicates the physiological range of each parameter, analyzed from the blood plasma of healthy female or male mice (N = 5 of each sex). For *p*-values of all tested differences see Table S9.

3.6. Quantification of Tumor Cell Proliferation, CD8⁺ cells and PD-L1 Expression in Males and Female

With the aim of determining the possible reasons for the marked differences in tumor weight between vehicle-treated female and male mice, we analyzed tumor cell proliferation and the amount of intratumoral CD8⁺ cells in the primary tumor. The median tumor cell proliferation did not differ significantly between the two sexes, with a median of 10% proliferating cells in females compared to 8.9% in males (Figure 6A–C). However, the amount of CD8⁺ cells per mm^2 was significantly different between female and male animals. Female mice had a median of 639 CD8⁺ cells/mm^2 tumor tissue compared to 263 CD8⁺ cells/mm^2 in male animals (Figure 6D–F). In both sexes, there was an inverse correlation between the amount of CD8⁺ cells and the tumor weight (Figure S9A,B). A comparison of relative gene expression of cytokines implicated in T cell activation (*Ifn-γ* and *Il2*) and inflammation (*Il10*, *Il6* and *Tnf-α*) between the sexes revealed a significantly higher relative *Ifn-γ* gene expression in tumors of female mice (Figure S10A), while there was no significant difference in the rest of the analyzed cytokines (Figure S10B–E). To assess if the difference in intratumoral CD8⁺ cells between the sexes was accompanied by a difference in PD-L1 expression in the tumor, the PD-L1-positive area in tumors of both sexes was analyzed. Surprisingly, the PD-L1-positive area in tumors was higher in females compared to males (Figure S11A). While differentiating between tumor cells and immune cells proved unfeasible in our non-multiplexed IHC setting, positive staining in females (Figure S11B) predominantly coincided with inflammatory lesions containing immune cells, which was rarely observed in males (Figure S11C).

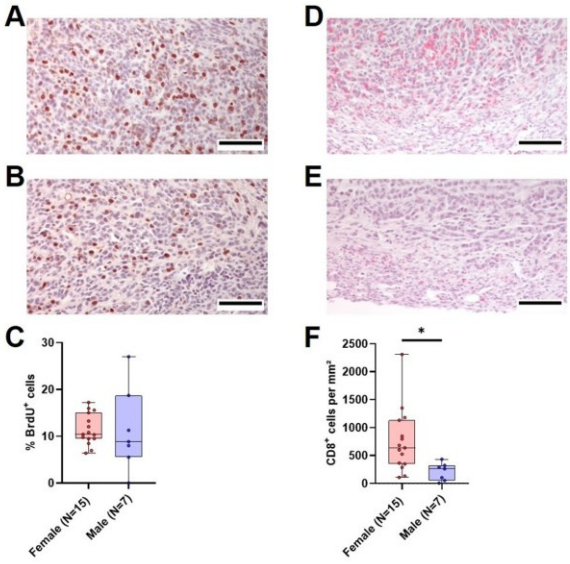

Figure 6. Tumor cell proliferation and intratumoral CD8⁺ cells in vehicle-treated animals. (**A**,**B**): Representative histological sections of anti-BrdU stained (brown nuclei) tumors of surviving female (**A**) and male (**B**) vehicle-treated mice (scale bar = 100 µm) and the quantitative analysis of the percentage of BrdU⁺ cells ((**C**), unpaired *t*-test with Welch's correction, ns). (**D**,**E**): Representative

histological sections of anti-CD8α stained (red) tumors of surviving female (**D**) and male (**E**) vehicle-treated mice (scale bar = 100 µm) and the quantitative analysis of CD8α-positive cells per mm^2 ((**F**), Mann–Whitney test, * $p < 0.05$).

3.7. The Combinatorial Therapy inhibits CD8⁺ Cell Tumor Infiltration and PD-L1 Expression in a Sex-Specific Manner

Similar to the evaluation of tumor cell proliferation and quantity of intratumoral $CD8^+$ cells in vehicle-treated animals, both parameters were analyzed in mice treated with combinatorial therapy. The drugs had no significant effect on tumor cell proliferation in both sexes compared to vehicle-treated animals (Figure 7A–D). However, $CD8^+$ cells were significantly reduced in females treated with the drugs compared to vehicle-treated ones, while the median amount of $CD8^+$ cells in males was barely affected (Figure 7E–H). Moreover, the negative correlation between the $CD8^+$ cell count and the tumor weight observed in vehicle-treated mice (Figure S9) disappeared in female drug-treated mice (Figure S12A), while it remained intact in male animals treated with these drugs (Figure S12B). Additionally, the expression of PD-L1 was analyzed in the tumors. Similarly to the observed effects on $CD8^+$ cells, PD-L1 expression was significantly reduced in the tumors of females treated with BI-3406, trametinib, and BKM120 compared to those who received the vehicle solution (Figure S13A). In male mice, the therapy had no significant effect on PD-L1 expression (Figure S13B).

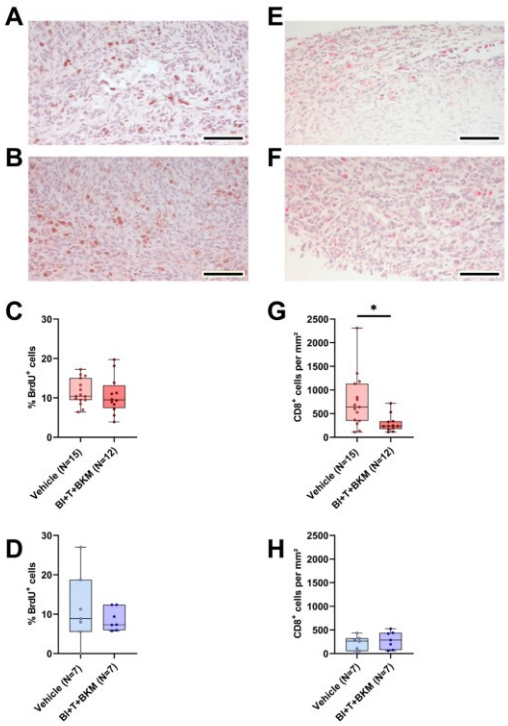

Figure 7. Effect of combinatorial therapy on tumor cell proliferation and amount of intratumoral $CD8^+$ cells. (**A**,**B**): Representative histological sections of anti-BrdU stained (brown nuclei) tumors of

surviving female (**A**) and male (**B**) mice receiving a combination of drugs consisting of BI-3406 (BI), trametinib (T) and BKM120 (BKM) (scale bar = 100 µm) and the quantitative analysis of the percentage of $BrdU^+$ cells in surviving female ((**C**), unpaired *t*-test, ns) and male ((**D**), unpaired *t*-test, ns) mice treated with these drugs or vehicle. (**E**,**F**): Representative histological sections of anti-CD8α stained (red) tumors of surviving female (**E**) and male (**F**) mice receiving these drugs (scale bar = 100 µm) and the quantitative analysis of CD8α-positive cells per mm^2 in female ((**G**), Mann–Whitney test, * $p < 0.05$) and male ((**H**), unpaired *t*-test, ns) mice treated with drugs or vehicle.

4. Discussion

We evaluated the influence of sex on the pathological features of a syngeneic, orthotopic and metastasized model of pancreatic cancer. Sex exerted a strong influence on survival, tumor weight, metastasis and tumor invasiveness. Male mice were more severely impacted (Figure 1) and experienced more distress (Figure 2A–C). In addition, a better therapy response was observed in males when using a combination of drugs consisting of BI-3406, trametinib and BKM120 (Figure 4E).

The larger tumor size observed in male mice could neither be attributed to a greater proliferation rate of tumor cells in male mice (Figure 6A–C) nor to a direct influence of sex hormones on cell viability or cell death of 6606PDA cells in vitro, since we have not observed a major reduction in cell viability or increased cytotoxicity when using more than 25 times the physiological concentrations of sex hormones typically found in C57BL/6J mice (Figure S5) [48]. An immunological response to male-specific antigens could also lead to reduced tumor sizes in female mice since the 6606PDA cell line was isolated from a male mouse (Figure S1A). In transplantation studies, it was demonstrated that female animals can develop a sex-specific immunological response to male antigens, which plays a prominent role in graft rejection [50–53]. However, several studies involving syngeneic tumor models show that male mice are more severely impacted, irrespective of the sex of the cell line used [54–58].

While a response to male-specific antigens might not be likely, a stronger adaptive immune response in female mice independent of sex-specific antigens is possible. Indeed, our data show more intratumoral $CD8^+$ cells in female tumors, indicating a distinct immune response in males and females (Figure 6D–F). This hypothesis is supported by several studies analyzing the role of $CD8^+$ cells in syngeneic tumor models and the impact of sex hormones on adaptive immunity [54–59]. For example, Kwon and colleagues demonstrated that injection of bladder cancer cells leads to smaller tumors in female mice compared to male mice, but that difference was reduced by depletion of $CD8^+$ cells [56]. In addition, several studies demonstrated that androgens increased tumor volume and at the same time decreased the number of $CD8^+$ cells within the tumor [57] or impaired their functionality [56–58]. Similar to more intratumoral $CD8^+$ cells, female mice also had a higher PD-L1 expression ($p = 0.0556$) in tumors, when compared to males (Figure S11A). Expression of PD-L1 was found on single cells and especially in inflammatory lesions within the tumors of female mice (Figure S11A). Interestingly, there is clinical evidence, showing that PD-L1 expression on immune cells correlates with improved outcomes in several different cancers [60–63]. This evidence is consistent with our observation that female mice have smaller tumors and a better survival rate than male mice. Thus, our data as well as the cited literature support the hypothesis that a reduced immune response in males leads to bigger tumors. This is also consistent with epidemiological studies proving the higher incidence and mortality of cancer in males [64].

In addition to analyzing the influence of sex on the pathological features of the cancer model, we also tested the efficacy of an experimental combination of drugs. BI-3406, trametinib, and BKM120 inhibited the proliferation of murine pancreatic cancer cells very efficiently in vitro in a synergistic manner (Figure 3A,B). The clinical relevance of this combinatorial treatment is also supported by a recent study of our group, demonstrating efficacy in several human PDAC cell lines expressing relevant KRAS mutations [36]. However, neither in vivo efficacy nor adverse side effects of this therapy were addressed in that study.

In the present study, the therapy reduced the tumor weight with higher efficacy in male mice, accompanied by a modest decrease in tumor invasiveness and increased probability of survival (Figure 4). These promising results suggest that this drug combination might be worth to be tested in additional studies since effective therapies for PDAC are still urgently needed [65].

Furthermore, we investigated whether the drugs caused adverse side effects. To this end, we assessed the parameters of organ damage and animal wellbeing. Compared to vehicle-treated animals, the combination of these drugs had no significant impact on the parameters of liver damage (Figure 5A–D), kidney function (Figure 5E,F), or tissue damage in general (Figure 5G,H). Distress-related parameters (Figure S8) also support the hypothesis that the therapy shows good tolerability in this model. Not unexpectedly, the triple drug combination increased c-peptide concentrations significantly in the blood plasma of both sexes (Figure 5I,J). This is a common phenomenon in clinical trials with BKM120 and pan-PI3K inhibitors, in general, and indicates a limitation of therapies inhibiting this signaling pathway [66]. However, preclinical evidence suggests that this side effect can be ameliorated by metformin or a ketogenic diet [67,68]. In summary, the tested therapy is efficacious in vivo and observed side effects can probably be managed.

However, as is evident from our in vivo data, drug efficacy in female animals is heavily confounded by sex-specific factors (Figure 4E). Indeed, PDAC cells have been found to express sex hormone receptors [69,70] and it has been shown that β-estradiol can sensitize PDAC cells to chemotherapy [71]. Interestingly, we observed the opposite effect in vitro. Especially female sex hormones inhibited the efficacy of the tested drug combination (Figure S6). Thus, it is possible that female sex hormones contribute to the observed reduction in therapy efficacy in vivo. Sex differences in pharmacokinetics and pharmacodynamics have also been reported previously [72–75]. The proposed mechanisms range from sex-dependent expression levels of efflux transporters and metabolizing enzymes to a direct impact of sex hormones [72,76–79]. This has a direct influence on the clearance and systemic availability of the administered drugs. However, the systemic drug level is often a poor substitute for the drug concentration at the target site (e.g. in the tumor), which seems to be particularly true for small molecule inhibitors such as those used here [80]. In an attempt to test the hypothesis that the drug efficacy in females is confounded by sex-specific differences in drug concentrations, we subjected tissue and plasma of a subset of animals to analysis by LC/MS-MS. The data show that there is no meaningful difference in the drug concentrations in tumors, as well as plasma, liver, or kidney between male and female animals (Tables 1 and S8). Although these data are limited by small sample sizes, the implications are important, as they prove that the compounds are bioavailable and reach their intended target site in males and females alike. Thus, we conclude that other mechanisms must cause higher drug efficacy in male mice. Interestingly, the pathways inhibited by these drugs are also vital for immune cells such as lymphocytes [81–83]. Both BKM120 and trametinib are known inhibitors of immune cell proliferation, activation, and effector function [84–88]. Indeed, our data demonstrate that this drug combination leads to immunosuppression primarily in female mice, demonstrated by the occurrence of metastasis in drug-treated females, which was not detected in vehicle-treated animals (Figures 4H and S7A). Furthermore, $CD8^+$ cells were significantly reduced in female mice receiving therapy compared to those who received vehicle solution (Figure 7G). This was not observed in male mice (Figure 7H). This reduction in $CD8^+$ cells was accompanied by a significant decrease in PD-L1 expression in tumors of female mice (Figure S13A). In female mice, PD-L1 expression was primarily found in inflammatory lesions within the tumors (Figure S11A) and clinical evidence suggests that PD-L1 expression on immune cells correlates with improved outcomes in several different cancers [60–63]. Based on these findings, we hypothesize that these drugs cause more immunosuppression in female than in male mice. This might prevent a strong reduction in tumor weight by the combinational therapy, an effect clearly observed in male mice (Figure S14).

The interpretation of the data presented in this study is subject to some limitations. One limitation is the unbalanced sample sizes due to the significantly lower probability of survival of male animals. However, unequal sample sizes are not inherently problematic, as the underlying problem of unequal sample sizes is often unequal variances. Non-parametric tests like Kruskal–Wallis or Mann–Whitney do not make assumptions about equal variances and unequal variances in *t*-tests can be corrected via Welch's correction, which has been conducted when comparing groups with different sample sizes (Figures 1B and 6C). Yet, ANOVA procedures strongly rely on the assumption of equal variances [89]. As there is no practical alternative for a two-way repeated measure ANOVA [90], we have opted for its use here to interpret animal wellbeing between the two sexes (Figure 2). Thus, these results have to be considered with care and further investigations should strive for equal sample sizes if statistical inference is to be interpreted robustly.

Another limitation of this study is the use of an orthotopic syngeneic mouse model as the only model. These models are easier to establish and more cost-efficient [91]. However, therapy responses in allograft implantation models can depend on location [92] and used cell lines [93], which leads to interpretations of results being specific to the features of the cell line [94]. There is a multitude of different models used in preclinical PDAC research, ranging from chemically induced models to genetically engineered or implantation models [95,96]. Patient-derived xenograft models are considered a standard in preclinical oncology because the use of human cell lines in treating human cancers is a clear translational advantage [97]. However, these models come with the important disadvantage of immunoincompetence of the host mouse strain, which is a prerequisite to ensure the engraftment of human cells in a different species. Sex differences based on immunological differences, as have been observed in this study, would have been missed in a similar study using immunocompromised strains. Genetically engineered models combine the advantages of immunocompetence and in situ carcinogenesis but significantly prolong experimental duration. Each of these models has advantages but also limitations. Therefore, it is crucial to recognize that the results of this study can be interpreted only within the context of the syngeneic orthotopic mouse model utilized. Replicating these findings across diverse models is essential to confirm their robustness. A retrospective analysis comparing clinical trial outcomes with preclinical data will be required in the future for assessing the translational significance of sex-specific variations observed in preclinical models. This issue holds significant importance, as disregarding sex-specific differences may lead to serious consequences such as inadequate dosing or adverse drug reactions [73,98,99].

5. Conclusions

In summary, the novel experimental therapy tested in this study leads to reduced tumor weight. Parameters associated with adverse side effects as well as animal wellbeing indicate that the drugs are well tolerated, with the exception of an observed increase in c-peptide plasma concentrations, which may be controlled by metformin or a ketogenic diet. As novel therapies to combat PDAC are urgently needed, this drug combination offers a promising basis for further studies. Sex-specific effects in female animals confound the obtained results, emphasizing the importance of sex-specific research. These results warrant further in vivo testing of these drugs in other models.

Supplementary Materials: The following supporting information can be downloaded at: https://www.mdpi.com/article/10.3390/cancers16101901/s1, Figure S1: Cell line sex determination and *Kras* G12D mutation verification; Figure S2: Influence of sex on lung metastasis, Figure S3: Duodenal invasion of the primary tumor, Figure S4: IC_{50} values for inhibition of proliferation (BrdU) for each compound, Figure S5: Effects of physiological and supraphysiological sex hormone concentrations on viability and cell death of 6606PDA cells, Figure S6. Impact of sex hormones on the efficacy of the combinatorial therapy, Figure S7: Effect of the combinatorial therapy on the metastatic area in the lung, Figure S8: Effect of combinatorial therapy on distress parameters, Figure S9. Correlation between the amount of $CD8^+$ cells and tumor weight in vehicle-treated animals, Figure S10. Comparison of relative gene expression of *Ifn-γ*, *Il10*, *Il2*, *Tnf-α* and *Il6* between both sexes, Figure S11. PD-L1 expression in

tumors of female and male mice treated with vehicle, Figure S12. Correlation between the amount of $CD8^+$ cells and tumor weight in animals treated with BI-3406, trametinib and BKM120, Figure S13. PD-L1 expression in tumors of female and male mice treated with vehicle or BI-3406, trametinib and BKM120, Figure S14. Visualization of hypothesized sex-specific effects, Table S1: Primers used for PCR and sequencing, Table S2: PCR conditions (Jarid 1c/d), Table S3: PCR conditions (*Kras* G12D and WT), Table S4: MRI sequences and parameters, Table S5: Parameters of the triple quadrupole interface, Table S6: Mass spectrometric parameters of BKM120, BI-3406, trametinib and the internal standard acridine orange, Table S7: TaqMan qPCR conditions, Table S8: Measured concentrations (LC-MS/MS) of therapeutics in the plasma, liver and kidney (median with 5–95% confidence interval), Table S9: *p*-values for Figure 5.

Author Contributions: Conceptualization, D.Z. and B.V.; methodology, D.Z. and B.S.; formal analysis, B.S.; investigation, B.S., D.Z., T.L., R.S., N.A., R.P. and Y.M.; data curation, B.S., D.Z. and T.S.; writing—original draft preparation, B.S., D.Z. and E.L.; writing—review and editing, all authors.; visualization, B.S.; supervision, D.Z., B.V., H.M.E. and B.H.; funding acquisition, D.Z. and B.V. All authors have read and agreed to the published version of the manuscript.

Funding: This study was supported by the Deutsche Forschungsgemeinschaft (DFG research group FOR 2591, ZE 712/1-2, and VO 450/15-2). The mass spectrometric analyses were performed with the triple quadrupole mass spectrometer LCMS-8050, co-funded by the Deutsche Forschungsgemeinschaft (DFG, INST 264/169-1 FUGG).

Institutional Review Board Statement: All animal experiments were approved by the German local authority: Landesamt für Landwirtschaft, Lebensmittelsicherheit und Fischerei Mecklenburg-Vorpommern (-1-016/21).

Informed Consent Statement: Not applicable.

Data Availability Statement: Data will be uploaded to figshare.com; https://doi.org/10.6084/m9.figshare.25144640.

Acknowledgments: The authors kindly thank Berit Blendow, Dorothea Frenz, Joanna Förster, Janett Jarchow, Edith Klobetz-Rassam (Department of Biological Sciences, University of Veterinary Medicine Vienna), Eva Lorbeer, Maren Nerowski, Anne Rupp and Anna Schildt for their technical assistance as well as Lorenzo Pilch and Hanna Krug for their help in data acquisition. We also thank Boehringer Ingelheim Pharma GmbH & Co KG and Michaela Walter from opnMe for the provision of BI-3406. We also acknowledge ChatGPT 3.5, which was used to improve clarity, grammar, and syntax of some sentences written for this manuscript.

Conflicts of Interest: The authors declare no conflicts of interest.

References

1. Zucker, I.; Prendergast, B.J.; Beery, A.K. Pervasive Neglect of Sex Differences in Biomedical Research. *Cold Spring Harb. Perspect. Biol.* **2022**, *14*, a039156. [CrossRef] [PubMed]
2. Shansky, R.M.; Murphy, A.Z. Considering sex as a biological variable will require a global shift in science culture. *Nat. Neurosci.* **2021**, *24*, 457–464. [CrossRef] [PubMed]
3. Lee, S.K. Sex as an important biological variable in biomedical research. *BMB Rep.* **2018**, *51*, 167–173. [CrossRef] [PubMed]
4. Drug Safety: Most Drugs Withdrawn in Recent Years Had Greater Health Risks for Women. Available online: https://www.gao.gov/products/gao-01-286r (accessed on 20 December 2023).
5. Bonamici, R.H.R. 34—114th Congress (2015–2016): 21st Century Cures Act. Available online: https://www.congress.gov/bill/114th-congress/house-bill/34 (accessed on 20 December 2023).
6. Arnegard, M.E.; Whitten, L.A.; Hunter, C.; Clayton, J.A. Sex as a Biological Variable: A 5-Year Progress Report and Call to Action. *J. Womens. Health* **2020**, *29*, 858–864. [CrossRef] [PubMed]
7. Woitowich, N.C.; Beery, A.; Woodruff, T. A 10-year follow-up study of sex inclusion in the biological sciences. *eLife* **2020**, *9*, e56344. [CrossRef] [PubMed]
8. Allegra, S.; Chiara, F.; Di Grazia, D.; Gaspari, M.; de Francia, S. Evaluation of Sex Differences in Preclinical Pharmacology Research: How Far Is Left to Go? *Pharmaceuticals* **2023**, *16*, 786. [CrossRef] [PubMed]
9. Zeng, P.-Y.; Tsai, Y.-H.; Lee, C.-L.; Ma, Y.-K.; Kuo, T.-H. Minimal influence of estrous cycle on studies of female mouse be-haviors. *Front. Mol. Neurosci.* **2023**, *16*, 1146109. [CrossRef]
10. Bangasser, D.A.; Cuarenta, A. Sex differences in anxiety and depression: Circuits and mechanisms. *Nat. Rev. Neurosci.* **2021**, *22*, 674–684. [CrossRef] [PubMed]

11. Chowdhury, N.U.; Guntur, V.P.; Newcomb, D.C.; Wechsler, M.E. Sex and gender in asthma. *Eur. Respir. Rev.* **2021**, *30*, 210067. [CrossRef] [PubMed]
12. Radzikowska, U.; Golebski, K. Sex hormones and asthma: The role of estrogen in asthma development and severity. *Allergy* **2023**, *78*, 620–622. [CrossRef] [PubMed]
13. Xu, L.; Huang, G.; Cong, Y.; Yu, Y.; Li, Y. Sex-related Differences in Inflammatory Bowel Diseases: The Potential Role of Sex Hormones. *Inflamm. Bowel Dis.* **2022**, *28*, 1766–1775. [CrossRef] [PubMed]
14. Courchesne, M.; Manrique, G.; Bernier, L.; Moussa, L.; Cresson, J.; Gutzeit, A.; Froehlich, J.M.; Koh, D.-M.; Chartrand-Lefebvre, C.; Matoori, S. Gender Differences in Pharmacokinetics: A Perspective on Contrast Agents. ACS Pharmacol. *Transl. Sci.* **2023**, *7*, 8–17. [CrossRef]
15. Heidari, S.; Babor, T.F.; de Castro, P.; Tort, S.; Curno, M. Sex and Gender Equity in Research: Rationale for the SAGER guidelines and recommended use. *Res. Integr. Peer Rev.* **2016**, *1*, 1–9. [CrossRef] [PubMed]
16. Becher, E.; Oertelt-Prigione, S. The Impact of Sex and Gender in Medicine and Pharmacology. *Sex Gend. Eff. Pharmacol.* **2023**, *282*, 3–23. [CrossRef] [PubMed]
17. Vera, R.; Juan-Vidal, O.; Safont-Aguilera, M.J.; de La Peña, F.A.; Del Alba, A.G. Sex differences in the diagnosis, treatment and prognosis of cancer: The rationale for an individualised approach. *Clin. Transl. Oncol.* **2023**, *25*, 2069–2076. [CrossRef] [PubMed]
18. Ma, J.; Yao, Y.; Tian, Y.; Chen, K.; Liu, B. Advances in sex disparities for cancer immunotherapy: Unveiling the dilemma of Yin and Yang. *Biol. Sex Differ.* **2022**, *13*, 58. [CrossRef] [PubMed]
19. Schafer, J.M.; Xiao, T.; Kwon, H.; Collier, K.; Chang, Y.; Abdel-Hafiz, H.; Bolyard, C.; Chung, D.; Yang, Y.; Sundi, D.; et al. Sex-biased adaptive immune regulation in cancer development and therapy. *iScience* **2022**, *25*, 104717. [CrossRef] [PubMed]
20. Ben-Batalla, I.; Vargas-Delgado, M.E.; von Amsberg, G.; Janning, M.; Loges, S. Influence of Androgens on Immunity to Self and Foreign: Effects on Immunity and Cancer. *Front. Immunol.* **2020**, *11*, 1184. [CrossRef] [PubMed]
21. Klein, S.L.; Flanagan, K.L. Sex differences in immune responses. *Nat. Rev. Immunol.* **2016**, *16*, 626–638. [CrossRef] [PubMed]
22. Hu, W.; Qian, X.; Wang, S.; Gao, L.; Xu, J.; Yan, J. Sex—A potential factor affecting immune checkpoint inhibitor therapy for cancers. *Front. Immunol.* **2022**, *13*, 1024112. [CrossRef] [PubMed]
23. Ye, Y.; Jing, Y.; Li, L.; Mills, G.B.; Diao, L.; Liu, H.; Han, L. Sex-associated molecular differences for cancer immunotherapy. *Nat. Commun.* **2020**, *11*, 1779. [CrossRef] [PubMed]
24. Conforti, F.; Pala, L.; Bagnardi, V.; Viale, G.; de Pas, T.; Pagan, E.; Pennacchioli, E.; Cocorocchio, E.; Ferrucci, P.F.; de Marinis, F.; et al. Sex-Based Heterogeneity in Response to Lung Cancer Immunotherapy: A Systematic Review and Meta-Analysis. *J. Natl. Cancer Inst.* **2019**, *111*, 772–781. [CrossRef] [PubMed]
25. Kim, J.; Ji, E.; Jung, K.; Jung, I.H.; Park, J.; Lee, J.-C.; Kim, J.W.; Hwang, J.-H.; Kim, J. Gender Differences in Patients with Metastatic Pancreatic Cancer Who Received FOLFIRINOX. *J. Pers. Med.* **2021**, *11*, 83. [CrossRef] [PubMed]
26. Grossberg, A.J.; Chu, L.C.; Deig, C.R.; Fishman, E.K.; Hwang, W.L.; Maitra, A.; Marks, D.L.; Mehta, A.; Nabavizadeh, N.; Simeone, D.M.; et al. Multidisciplinary standards of care and recent progress in pancreatic ductal adenocarcinoma. *CA Cancer J. Clin.* **2020**, *70*, 375–403. [CrossRef] [PubMed]
27. Wang, S.; Zheng, Y.; Yang, F.; Zhu, L.; Zhu, X.-Q.; Wang, Z.-F.; Wu, X.-L.; Zhou, C.-H.; Yan, J.-Y.; Hu, B.-Y.; et al. The molecular biology of pancreatic adenocarcinoma: Translational challenges and clinical perspectives. *Signal Transduct. Target. Ther.* **2021**, *6*, 249. [CrossRef] [PubMed]
28. Haigis, K.M. KRAS Alleles: The Devil Is in the Detail. *Trends Cancer* **2017**, *3*, 686–697. [CrossRef] [PubMed]
29. Zhu, C.; Guan, X.; Zhang, X.; Luan, X.; Song, Z.; Cheng, X.; Zhang, W.; Qin, J.-J. Targeting KRAS mutant cancers: From druggable therapy to drug resistance. *Mol. Cancer* **2022**, *21*, 159. [CrossRef] [PubMed]
30. Canon, J.; Rex, K.; Saiki, A.Y.; Mohr, C.; Cooke, K.; Bagal, D.; Gaida, K.; Holt, T.; Knutson, C.G.; Koppada, N.; et al. The clinical KRAS(G12C) inhibitor AMG 510 drives anti-tumour immunity. *Nature* **2019**, *575*, 217–223. [CrossRef]
31. Lee, A. Sotorasib: A Review in KRAS G12C Mutation-Positive Non-small Cell Lung Cancer. *Target. Oncol.* **2022**, *17*, 727–733. [CrossRef] [PubMed]
32. Shoucair, S.; Habib, J.R.; Pu, N.; Kinny-Köster, B.; van Ooston, A.F.; Javed, A.A.; Lafaro, K.J.; He, J.; Wolfgang, C.L.; Yu, J. Comprehensive Analysis of Somatic Mutations in Driver Genes of Resected Pancreatic Ductal Adenocarcinoma Reveals KRAS G12D and Mutant TP53 Combination as an Independent Predictor of Clinical Outcome. Ann. *Surg. Oncol.* **2022**, *29*, 2720–2731. [CrossRef] [PubMed]
33. Hofmann, M.H.; Gerlach, D.; Misale, S.; Petronczki, M.; Kraut, N. Expanding the Reach of Precision Oncology by Drugging All KRAS Mutants. *Cancer Discov.* **2022**, *12*, 924–937. [CrossRef] [PubMed]
34. Kessler, D.; Gerlach, D.; Kraut, N.; McConnell, D.B. Targeting Son of Sevenless 1: The pacemaker of KRAS. *Curr. Opin. Chem. Biol.* **2021**, *62*, 109–118. [CrossRef] [PubMed]
35. Hofmann, M.H.; Gmachl, M.; Ramharter, J.; Savarese, F.; Gerlach, D.; Marszalek, J.R.; Sanderson, M.P.; Kessler, D.; Trapani, F.; Arnhof, H.; et al. BI-3406, a Potent and Selective SOS1-KRAS Interaction Inhibitor, Is Effective in KRAS-Driven Cancers through Combined MEK Inhibition. *Cancer Discov.* **2021**, *11*, 142–157. [CrossRef] [PubMed]
36. Ma, Y.; Schulz, B.; Trakooljul, N.; Al Ammar, M.; Sekora, A.; Sender, S.; Hadlich, F.; Zechner, D.; Weiss, F.U.; Lerch, M.M.; et al. Inhibition of KRAS, MEK and PI3K Demonstrate Synergistic Anti-Tumor Effects in Pancreatic Ductal Adenocarcinoma Cell Lines. *Cancers* **2022**, *14*, 4467. [CrossRef] [PubMed]

37. Hingorani, S.R.; Petricoin, E.F.; Maitra, A.; Rajapakse, V.; King, C.; Jacobetz, M.A.; Ross, S.; Conrads, T.P.; Veenstra, T.D.; Hitt, B.A.; et al. Preinvasive and invasive ductal pancreatic cancer and its early detection in the mouse. *Cancer Cell* **2003**, *4*, 437–450. [CrossRef] [PubMed]
38. Clapcote, S.J.; Roder, J.C. Simplex PCR assay for sex determination in mice. *Biotechniques* **2005**, *38*, 702–706. [CrossRef] [PubMed]
39. Kumstel, S.; Wendt, E.H.U.; Eichberg, J.; Talbot, S.R.; Häger, C.; Zhang, X.; Abdelrahman, A.; Schönrogge, M.; Palme, R.; Bleich, A.; et al. Grading animal distress and side effects of therapies. *Ann. N. Y. Acad. Sci.* **2020**, *1473*, 20–34. [CrossRef]
40. Kumstel, S.; Vasudevan, P.; Palme, R.; Zhang, X.; Wendt, E.H.U.; David, R.; Vollmar, B.; Zechner, D. Benefits of non-invasive methods compared to telemetry for distress analysis in a murine model of pancreatic cancer. *J. Adv. Res.* **2020**, *21*, 35–47. [CrossRef] [PubMed]
41. Kumstel, S.; Schreiber, T.; Goldstein, L.; Stenzel, J.; Lindner, T.; Joksch, M.; Zhang, X.; Wendt, E.H.U.; Schönrogge, M.; Krause, B.; et al. Targeting pancreatic cancer with combinatorial treatment of CPI-613 and inhibitors of lactate metabolism. *PLoS ONE* **2022**, *17*, e0266601. [CrossRef] [PubMed]
42. Deacon, R.M.J. Assessing nest building in mice. *Nat. Protoc.* **2006**, *1*, 1117–1119. [CrossRef] [PubMed]
43. Kumstel, S.; Tang, G.; Zhang, X.; Kerndl, H.; Vollmar, B.; Zechner, D. Grading Distress of Different Animal Models for Gastrointestinal Diseases Based on Plasma Corticosterone Kinetics. *Animals* **2019**, *9*, 145. [CrossRef] [PubMed]
44. Touma, C.; Palme, R.; Sachser, N. Analyzing corticosterone metabolites in fecal samples of mice: A noninvasive technique to monitor stress hormones. *Horm. Behav.* **2004**, *45*, 10–22. [CrossRef] [PubMed]
45. Palme, R. Non-invasive measurement of glucocorticoids: Advances and problems. *Physiol. Behav.* **2019**, *199*, 229–243. [CrossRef] [PubMed]
46. Touma, C.; Sachser, N.; Möstl, E.; Palme, R. Effects of sex and time of day on metabolism and excretion of corticosterone in urine and feces of mice. *Gen. Comp. Endocrinol.* **2003**, *130*, 267–278. [CrossRef] [PubMed]
47. Yushkevich, P.A.; Piven, J.; Hazlett, H.C.; Smith, R.G.; Ho, S.; Gee, J.C.; Gerig, G. User-guided 3D active contour segmentation of anatomical structures: Significantly improved efficiency and reliability. *Neuroimage* **2006**, *31*, 1116–1128. [CrossRef] [PubMed]
48. Nilsson, M.E.; Vandenput, L.; Tivesten, Å.; Norlén, A.-K.; Lagerquist, M.K.; Windahl, S.H.; Börjesson, A.E.; Farman, H.H.; Poutanen, M.; Benrick, A.; et al. Measurement of a Comprehensive Sex Steroid Profile in Rodent Serum by High-Sensitive Gas Chromatography-Tandem Mass Spectrometry. *Endocrinology* **2015**, *156*, 2492–2502. [CrossRef] [PubMed]
49. Borcoman, E.; de La Rochere, P.; Richer, W.; Vacher, S.; Chemlali, W.; Krucker, C.; Sirab, N.; Radvanyi, F.; Allory, Y.; Pignot, G.; et al. Inhibition of PI3K pathway increases immune infiltrate in muscle-invasive bladder cancer. *Oncoimmunology* **2019**, *8*, e1581556. [CrossRef]
50. Billingham, R.E.; Hings, I.M. The H-Y antigen and its role in natural transplantation. *Hum. Genet.* **1981**, *58*, 9–17. [CrossRef] [PubMed]
51. Chai, J.-G.; James, E.; Dewchand, H.; Simpson, E.; Scott, D. Transplantation tolerance induced by intranasal administration of HY peptides. *Blood* **2004**, *103*, 3951–3959. [CrossRef] [PubMed]
52. Hu, X.; Kueppers, S.T.; Kooreman, N.G.; Gravina, A.; Wang, D.; Tediashvili, G.; Schlickeiser, S.; Frentsch, M.; Nikolaou, C.; Thiel, A.; et al. The H-Y Antigen in Embryonic Stem Cells Causes Rejection in Syngeneic Female Recipients. *Stem Cells Dev.* **2020**, *29*, 1179–1189. [CrossRef]
53. Scott, D.M.; Ehrmann, I.E.; Ellis, P.S.; Bishop, C.E.; Agulnik, A.I.; Simpson, E.; Mitchell, M.J. Identification of a mouse male-specific transplantation antigen, H-Y. *Nature* **1995**, *376*, 695–698. [CrossRef] [PubMed]
54. Ray, A.L.; Nofchissey, R.A.; Khan, M.A.; Reidy, M.A.; Lerner, M.R.; Wu, X.; Guo, S.; Hill, S.L.; Weygant, N.; Adams, S.F.; et al. The role of sex in the innate and adaptive immune environment of metastatic colorectal cancer. *Br. J. Cancer* **2020**, *123*, 624–632. [CrossRef] [PubMed]
55. Dakup, P.P.; Porter, K.I.; Little, A.A.; Zhang, H.; Gaddameedhi, S. Sex differences in the association between tumor growth and T cell response in a melanoma mouse model. *Cancer Immunol. Immunother.* **2020**, *69*, 2157–2162. [CrossRef] [PubMed]
56. Kwon, H.; Schafer, J.M.; Song, N.-J.; Kaneko, S.; Li, A.; Xiao, T.; Ma, A.; Allen, C.; Das, K.; Zhou, L.; et al. Androgen conspires with the CD8+ T cell exhaustion program and contributes to sex bias in cancer. *Sci. Immunol.* **2022**, *7*, eabq2630. [CrossRef]
57. Zhang, X.; Cheng, L.; Gao, C.; Chen, J.; Liao, S.; Zheng, Y.; Xu, L.; He, J.; Wang, D.; Fang, Z.; et al. Androgen Signaling Contributes to Sex Differences in Cancer by Inhibiting NF-κB Activation in T Cells and Suppressing Antitumor Immunity. *Cancer Res.* **2023**, *83*, 906–921. [CrossRef] [PubMed]
58. Yang, C.; Jin, J.; Yang, Y.; Sun, H.; Wu, L.; Shen, M.; Hong, X.; Li, W.; Lu, L.; Cao, D.; et al. Androgen receptor-mediated CD8+ T cell stemness programs drive sex differences in antitumor immunity. *Immunity* **2022**, *55*, 1268–1283.e9. [CrossRef] [PubMed]
59. Natale, C.A.; Li, J.; Pitarresi, J.R.; Norgard, R.J.; Dentchev, T.; Capell, B.C.; Seykora, J.T.; Stanger, B.Z.; Ridky, T.W. Pharmacologic Activation of the G Protein–Coupled Estrogen Receptor Inhibits Pancreatic Ductal Adenocarcinoma. *Cell. Mol. Gastroen-terol. Hepatol.* **2020**, *10*, 868. [CrossRef] [PubMed]
60. Blažek, T.; Petráš, M.; Knybel, L.; Cvek, J.; Soumarová, R. Programmed Cell Death Ligand 1 Expression on Immune Cells and Survival in Patients With Nonmetastatic Head and Neck Cancer: A Systematic Review and Meta-analysis. *JAMA Netw. Open* **2023**, *6*, e236324. [CrossRef] [PubMed]
61. Kim, Y.; Wen, X.; Cho, N.Y.; Kang, G.H. Intratumoral immune cells expressing PD-1/PD-L1 and their prognostic implications in cancer: A meta-analysis. *Int. J. Biol. Markers* **2018**, *33*, 467–474. [CrossRef] [PubMed]

62. Mocan, L.P.; Craciun, R.; Grapa, C.; Melincovici, C.S.; Rusu, I.; Al Hajjar, N.; Sparchez, Z.; Leucuta, D.; Ilies, M.; Sparchez, M.; et al. PD-L1 expression on immune cells, but not on tumor cells, is a favorable prognostic factor for patients with intrahepatic cholangiocarcinoma. *Cancer Immunol. Immunother.* **2023**, *72*, 1003–1014. [CrossRef] [PubMed]
63. Zhong, Q.; Shou, J.; Ying, J.; Ling, Y.; Yu, Y.; Shen, Z.; Zhang, Y.; Li, N.; Shi, Y.; Zhou, A. High PD-L1 expression on immune cells, but not on tumor cells, is a favorable prognostic factor in urothelial carcinoma. *Future Oncol.* **2021**, *17*, 2893–2905. [CrossRef] [PubMed]
64. Siegel, R.L.; Miller, K.D.; Wagle, N.S.; Jemal, A. Cancer statistics, 2023. *CA Cancer J. Clin.* **2023**, *73*, 17–48. [CrossRef] [PubMed]
65. Hosein, A.N.; Dougan, S.K.; Aguirre, A.J.; Maitra, A. Translational advances in pancreatic ductal adenocarcinoma therapy. *Nat. Cancer* **2022**, *3*, 272–286. [CrossRef] [PubMed]
66. Mishra, R.; Patel, H.; Alanazi, S.; Kilroy, M.K.; Garrett, J.T. PI3K Inhibitors in Cancer: Clinical Implications and Adverse Effects. *Int. J. Mol. Sci.* **2021**, *22*, 3464. [CrossRef] [PubMed]
67. Hopkins, B.D.; Pauli, C.; Du, X.; Wang, D.G.; Li, X.; Wu, D.; Amadiume, S.C.; Goncalves, M.D.; Hodakoski, C.; Lundquist, M.R.; et al. Suppression of insulin feedback enhances the efficacy of PI3K inhibitors. *Nature* **2018**, *560*, 499–503. [CrossRef] [PubMed]
68. Noch, E.K.; Palma, L.N.; Yim, I.; Bullen, N.; Qiu, Y.; Ravichandran, H.; Kim, J.; Rendeiro, A.; Davis, M.B.; Elemento, O.; et al. Insulin feedback is a targetable resistance mechanism of PI3K inhibition in glioblastoma. *Neuro-Oncology* **2023**, *25*, 2165–2176. [CrossRef]
69. Liao, Y.-N.; Gai, Y.-Z.; Qian, L.-H.; Pan, H.; Zhang, Y.-F.; Li, P.; Guo, Y.; Li, S.-X.; Nie, H.-Z. Progesterone receptor potentiates macropinocytosis through CDC42 in pancreatic ductal adenocarcinoma. *Oncogenesis* **2024**, *13*, 10. [CrossRef] [PubMed]
70. Andrén-Sandberg, Å.; Johansson, J. Influence of sex hormones on pancreatic Cancer. *Int. J. Pancreatol.* **1990**, *7*, 167–176. [CrossRef] [PubMed]
71. Akula, S.M.; Candido, S.; Abrams, S.L.; Steelman, L.S.; Lertpiriyapong, K.; Cocco, L.; Ramazzotti, G.; Ratti, S.; Follo, M.Y.; Martelli, A.M.; et al. Abilities of β-Estradiol to interact with chemotherapeutic drugs, signal transduction inhibitors and nutraceu-ticals and alter the proliferation of pancreatic cancer cells. *Adv. Biol. Regul.* **2020**, *75*, 100672. [CrossRef] [PubMed]
72. Spoletini, I.; Vitale, C.; Malorni, W.; Rosano, G.M.C. Sex Differences in Drug Effects: Interaction with Sex Hormones in Adult Life. *Sex Gend. Differ. Pharmacol.* **2013**, *214*, 91–105. [CrossRef] [PubMed]
73. Davidson, M.; Wagner, A.D.; Kouvelakis, K.; Nanji, H.; Starling, N.; Chau, I.; Watkins, D.; Rao, S.; Peckitt, C.; Cunningham, D. Influence of sex on chemotherapy efficacy and toxicity in oesophagogastric cancer: A pooled analysis of four randomised trials. *Eur. J. Cancer* **2019**, *121*, 40–47. [CrossRef] [PubMed]
74. Wheatley-Price, P.; Le Maître, A.; Ding, K.; Leighl, N.; Hirsh, V.; Seymour, L.; Bezjak, A.; Shepherd, F.A. The influence of sex on efficacy, adverse events, quality of life, and delivery of treatment in National Cancer Institute of Canada Clinical Trials Group non-small cell lung cancer chemotherapy trials. *J. Thorac. Oncol.* **2010**, *5*, 640–648. [CrossRef] [PubMed]
75. Oi Yan Chan, J.; Moullet, M.; Williamson, B.; Arends, R.H.; Pilla Reddy, V. Harnessing Clinical Trial and Real-World Data Towards an Understanding of Sex Effects on Drug Pharmacokinetics, Pharmacodynamics and Efficacy. *Front. Pharmacol.* **2022**, *13*, 874606. [CrossRef] [PubMed]
76. Mitchell, S.C.; Smith, R.L.; Waring, R.H. The menstrual cycle and drug metabolism. *Curr. Drug Metab.* **2009**, *10*, 499–507. [CrossRef] [PubMed]
77. Wald, J.A.; Salazar, D.E.; Chen, H.Y.; Jusko, W.J. Two-compartment basophil cell trafficking model for methylprednisolone pharmacodynamics. *J. Pharmacokinet. Biopharm.* **1991**, *19*, 521–536. [CrossRef] [PubMed]
78. Walle, T.; Walle, U.K.; Cowart, T.D.; Conradi, E.C. Pathway-selective sex differences in the metabolic clearance of propranolol in human subjects. *Clin. Pharmacol. Ther.* **1989**, *46*, 257–263. [CrossRef] [PubMed]
79. Suzuki, T.; Zhao, Y.L.; Nadai, M.; Naruhashi, K.; Shimizu, A.; Takagi, K.; Takagi, K.; Hasegawa, T. Gender-related differences in expression and function of hepatic P-glycoprotein and multidrug resistance-associated protein (Mrp2) in rats. *Life Sci.* **2006**, *79*, 455–461. [CrossRef] [PubMed]
80. Zhang, D.; Hop, C.E.C.A.; Patilea-Vrana, G.; Gampa, G.; Seneviratne, H.K.; Unadkat, J.D.; Kenny, J.R.; Nagapudi, K.; Di, L.; Zhou, L.; et al. Drug Concentration Asymmetry in Tissues and Plasma for Small Molecule-Related Therapeutic Modalities. *Drug Metab. Dispos.* **2019**, *47*, 1122–1135. [CrossRef]
81. Ott, P.A.; Adams, S. Small-molecule protein kinase inhibitors and their effects on the immune system: Implications for cancer treatment. *Immunotherapy* **2011**, *3*, 213–227. [CrossRef] [PubMed]
82. Okkenhaug, K.; Vanhaesebroeck, B. PI3K in lymphocyte development, differentiation and activation. *Nat. Rev. Immunol.* **2003**, *3*, 317–330. [CrossRef] [PubMed]
83. Houde, N.; Beuret, L.; Bonaud, A.; Fortier-Beaulieu, S.-P.; Truchon-Landry, K.; Aoidi, R.; Pic, É.; Alouche, N.; Rondeau, V.; Schlecht-Louf, G.; et al. Fine-tuning of MEK signaling is pivotal for limiting B and T cell activation. *Cell Rep.* **2022**, *38*, 110223. [CrossRef] [PubMed]
84. Yamaguchi, T.; Kakefuda, R.; Tanimoto, A.; Watanabe, Y.; Tajima, N. Suppressive effect of an orally active MEK1/2 inhibitor in two different animal models for rheumatoid arthritis: A comparison with leflunomide. *Inflamm. Res.* **2012**, *61*, 445–454. [CrossRef] [PubMed]
85. Wieder, E.; Kolonias, D.; Benjamin, C.; Shindo, T.; Kim, T.K.; Levy, R.B.; Komanduri, K.V. Trametinib Selectively Inhibits Alloreactivity While Sparing Virus-Specific T Cells. *Biol. Blood Marrow Transplant.* **2014**, *20*, S283. [CrossRef]

86. Vella, L.J.; Pasam, A.; Dimopoulos, N.; Andrews, M.; Knights, A.; Puaux, A.-L.; Louahed, J.; Chen, W.; Woods, K.; Cebon, J.S. MEK inhibition, alone or in combination with BRAF inhibition, affects multiple functions of isolated normal human lymphocytes and dendritic cells. *Cancer Immunol. Res.* **2014**, *2*, 351–360. [CrossRef] [PubMed]
87. Vella, L.J.; Andrews, M.C.; Pasam, A.; Woods, K.; Behren, A.; Cebon, J.S. The kinase inhibitors dabrafenib and trametinib affect isolated immune cell populations. *Oncoimmunology* **2014**, *3*, e946367. [CrossRef] [PubMed]
88. Allegrezza, M.J.; Rutkowski, M.R.; Stephen, T.L.; Svoronos, N.; Tesone, A.J.; Perales-Puchalt, A.; Nguyen, J.M.; Sarmin, F.; Sheen, M.R.; Jeng, E.K.; et al. IL15 Agonists Overcome the Immunosuppressive Effects of MEK Inhibitors. *Cancer Res.* **2016**, *76*, 2561–2572. [CrossRef] [PubMed]
89. Kim, Y.J.; Cribbie, R.A. ANOVA and the variance homogeneity assumption: Exploring a better gatekeeper. *Br. J. Math. Stat. Psychol.* **2018**, *71*, 1–12. [CrossRef] [PubMed]
90. With Two-Way ANOVA, Why Doesn't Prism Offer a Nonparametric Alternative? Test for Normality? Test for Homogeneity of Variances? Test for Outliers?—FAQ 2004—GraphPad. Available online: https://www.graphpad.com/support/faq/with-two-way-anova-why-doesnt-prism-offer-a-nonparametric-alternative-test-for-normality-test-for-homogeneity-of-variances-test-for-outliers/ (accessed on 16 April 2024).
91. Qiu, W.; Su, G.H. Development of Orthotopic Pancreatic Tumor Mouse Models. *Pancreat. Cancer* **2013**, *980*, 215–223. [CrossRef] [PubMed]
92. Erstad, D.J.; Sojoodi, M.; Taylor, M.S.; Ghoshal, S.; Razavi, A.A.; Graham-O'Regan, K.A.; Bardeesy, N.; Ferrone, C.R.; Lanuti, M.; Caravan, P.; et al. Orthotopic and heterotopic murine models of pancreatic cancer and their different responses to FOLFIRINOX chemotherapy. *Dis. Models Mech.* **2018**, *11*, dmm034793. [CrossRef] [PubMed]
93. Torres, M.P.; Rachagani, S.; Souchek, J.J.; Mallya, K.; Johansson, S.L.; Batra, S.K. Novel Pancreatic Cancer Cell Lines Derived from Genetically Engineered Mouse Models of Spontaneous Pancreatic Adenocarcinoma: Applications in Diagnosis and Therapy. *PLoS ONE* **2013**, *8*, e80580. [CrossRef] [PubMed]
94. Li, J.; Byrne, K.T.; Yan, F.; Yamazoe, T.; Chen, Z.; Baslan, T.; Richman, L.P.; Lin, J.H.; Sun, Y.H.; Rech, A.J.; et al. Tumor Cell-Intrinsic Factors Underlie Heterogeneity of Immune Cell Infiltration and Response to Immunotherapy. *Immunity* **2018**, *49*, 178–193.e7. [CrossRef] [PubMed]
95. Reyes, C.M.; Gärtner, P.; Rosenkranz, L.; Grippo, P.J.; Demir, I.E. In vivo Mouse Models of Pancreatic Ductal Adenocarcinoma. *Pancreapedia Exocrine Pancreas Knowl. Base* **2021**. [CrossRef]
96. Saloman, J.L.; Albers, K.M.; Cruz-Monserrate, Z.; Davis, B.M.; Edderkaoui, M.; Eibl, G.; Epouhe, A.Y.; Gedeon, J.Y.; Gorelick, F.S.; Grippo, P.J.; et al. Animal Models: Challenges and Opportunities to Determine Optimal Experimental Models of Pancreatitis and Pancreatic Cancer. *Pancreas* **2019**, *48*, 759. [CrossRef] [PubMed]
97. Garcia, P.L.; Miller, A.L.; Yoon, K.J. Patient-Derived Xenograft Models of Pancreatic Cancer: Overview and Comparison with Other Types of Models. *Cancers* **2020**, *12*, 1327. [CrossRef] [PubMed]
98. Zucker, I.; Prendergast, B.J. Sex differences in pharmacokinetics predict adverse drug reactions in women. *Biol. Sex Differ.* **2020**, *11*, 32. [CrossRef] [PubMed]
99. Wagner, A.D.; Oertelt-Prigione, S.; Adjei, A.; Buclin, T.; Cristina, V.; Csajka, C.; Coukos, G.; Dafni, U.; Dotto, G.-P.; Ducreux, M.; et al. Gender medicine and oncology: Report and consensus of an ESMO workshop. *Ann. Oncol.* **2019**, *30*, 1914–1924. [CrossRef] [PubMed]

Disclaimer/Publisher's Note: The statements, opinions and data contained in all publications are solely those of the individual author(s) and contributor(s) and not of MDPI and/or the editor(s). MDPI and/or the editor(s) disclaim responsibility for any injury to people or property resulting from any ideas, methods, instructions or products referred to in the content.

cancers

MDPI

Supplementary Materials

Sex Matters–Insights from Testing Drug Efficacy in an Animal Model of Pancreatic Cancer

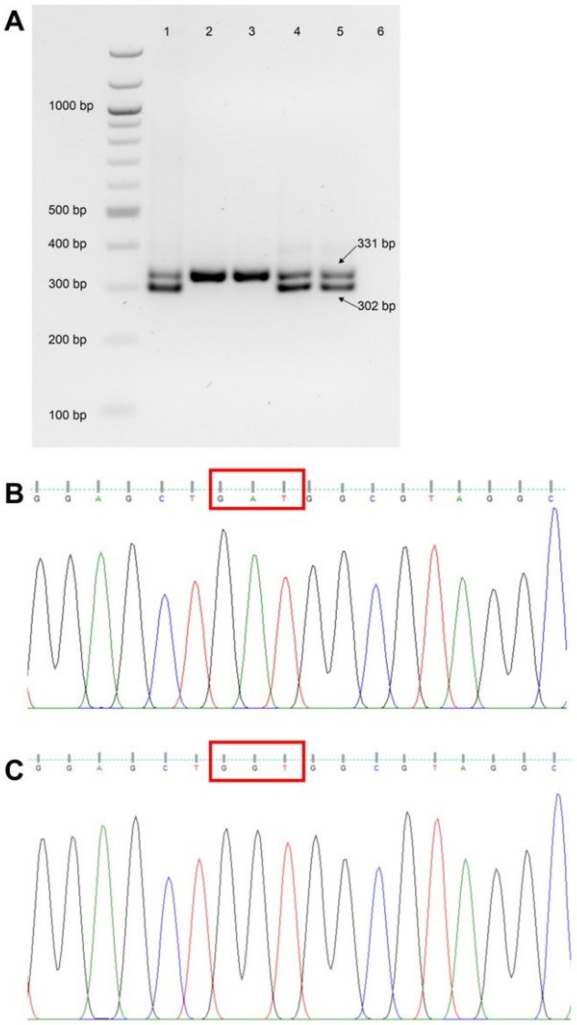

Figure S1. Cell line sex determination and *Kras* G12D mutation verification. A: Jarid 1c/d PCR to verify the sex of the 6606PDA cell line. Lane 1: 6606PDA, lane 2 and 3: female C57BL6/J mice, lane 4 and 5: male C57BL6/J mice, lane 6: negative control. B: Verification of the G12D mutation (G to A

substitution) by Sanger sequencing. C: Sequence of the *Kras* gene in a wildtype C57BL6/J mouse at the same position.

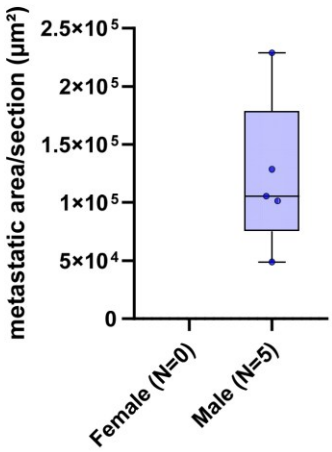

Figure S2. Influence of sex on lung metastasis. Median metastatic area (µm²) in serial histological section of the left lung lobe of female and male mice receiving vehicle solution.

Figure S3. Duodenal invasion of the primary tumor. The red circle shows the invasion into the duodenum and the red arrow shows the primary tumor.

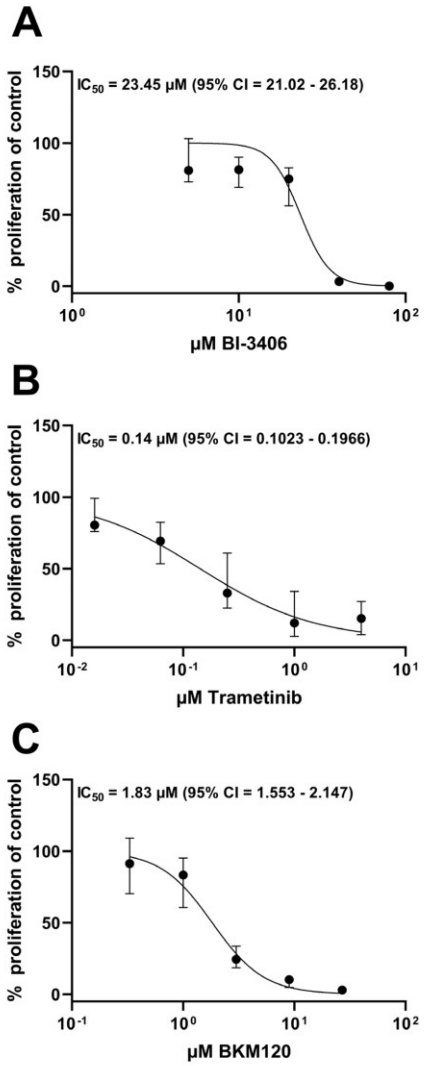

Figure S4. IC_{50} values for inhibition of proliferation (BrdU) for each compound. IC_{50} values for inhibition of proliferation (BrdU) of 6606PDA cells for BI-3406 (A), trametinib (B) and BKM120 (C). Data are shown as median with range. N = 5 for all compounds and concentrations tested.

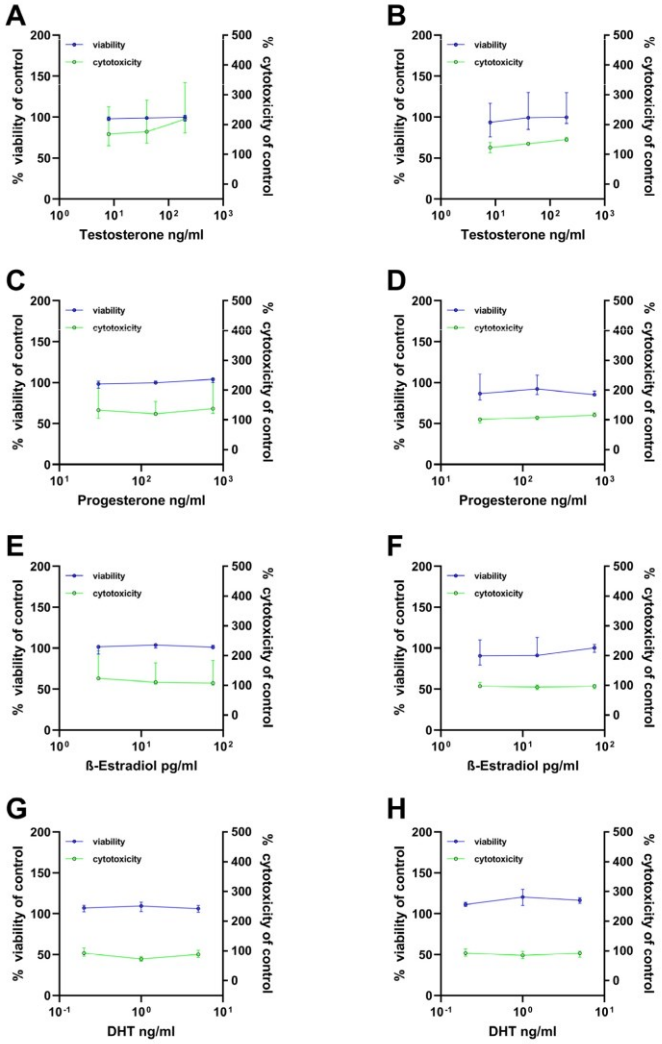

Figure S5. Effects of physiological and supraphysiological sex hormone concentrations on viability and cell death of 6606PDA cells. The effects of physiological and supraphysiological concentrations of testosterone (A, B), progesterone (C, D), 17β–estradiol (E, F), and dihydrotestosterone (G, H) have been tested in cells cultured with either 10% FCS (A, C, E, G) or 2% FCS (B, D, F, H) for 48 h. Data are shown as median with range. N = 3 for all sex hormones and concentrations tested.

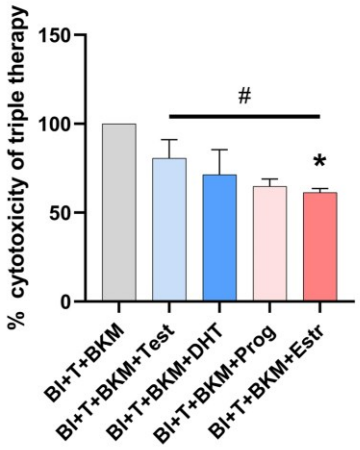

Figure S6. Impact of sex hormones on the efficacy of the combinatorial therapy. The impact of physiological concentrations of either testosterone (8 ng/ml), dihydrotestosterone (0.2 ng/ml), progesterone (30 ng/ml) or 17β-estradiol (3 pg/ml) on the efficacy of the combinatorial therapy have been tested in 6606PDA cells cultured for 48 h with a combination of BI-3406 (BI, 10 μM), trametinib (T, 0.064 μM) and BKM120 (BKM, 1 μM). Data are shown as bar graphs with median and 95% CI. Each combination has been compared to the control (BI+T+BKM, Kruskal-Wallis test with Dunn's post-hoc test, *$p < 0.05$) or each other (Ordinary one-way ANOVA with Tukey post-hoc test, #$p < 0.05$). N = 3 for all each combination. Test: testosterone, DHT: dihydrotestosterone, Prog: progesterone, Estr: 17β–estradiol.

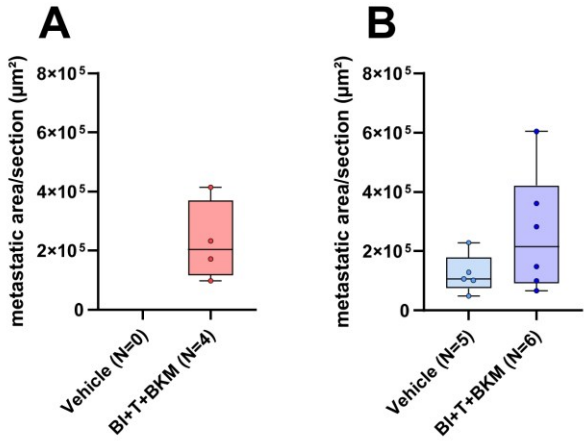

Figure S7. Effect of the combinatorial therapy on the metastatic area in the lung. Median metastatic area (μm²) in serial histological sections of the left lung lobe of female (A) and male (B) mice receiving either vehicle or a combinatorial therapy consisting of BI-3406 (BI), trametinib (T) and BKM120 (BKM).

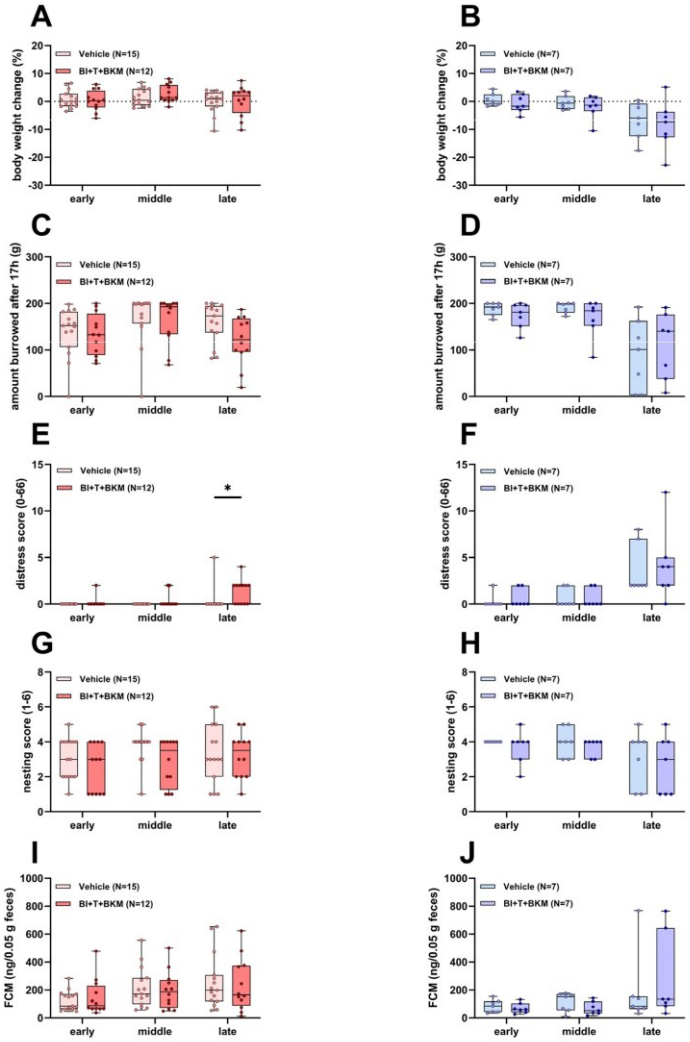

Figure S8. Effect of combinatorial therapy on distress parameters. Body weight (A, B), burrowing activity (C, D), distress score (E, F), nesting activity (G, H), and concentration of fecal corticosterone metabolites (I, J) in surviving female and male mice receiving either vehicle or a combinatorial therapy consisting of BI-3406 (BI), trametinib (T) and BKM120 (BKM) (Two-way repeated measures ANOVA with Sidak's post-hoc test, *$p < 0.05$). Early, middle and late refer to the experimental phases as defined in the methods section.

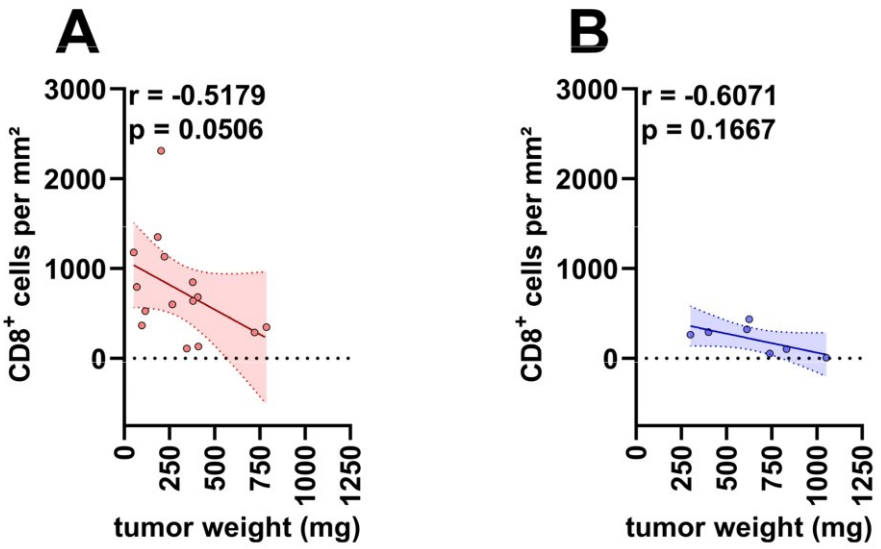

Figure S9. Correlation between the amount of CD8⁺ cells and tumor weight in vehicle-treated animals. Correlation plots (Spearman correlation) with linear regression including confidence intervals (shaded area) of CD8⁺ cells and tumor weight of vehicle-treated female (A, N = 15) and male (B, N = 7) mice.

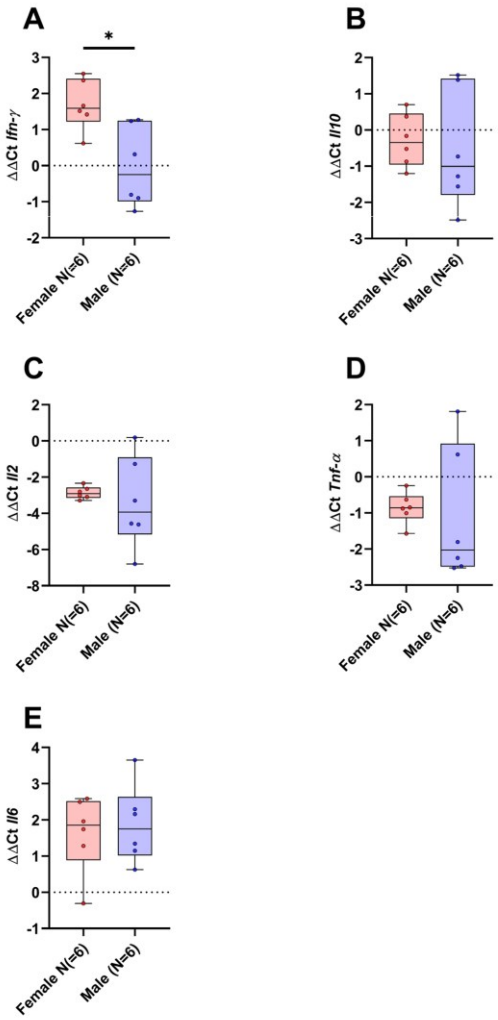

Figure S10. Comparison of relative gene expression of *Ifn-γ*, *Il10*, *Il2*, *Tnf-α* and *Il6* between both sexes. Comparison of relative gene expression of *Ifn-γ* (A, unpaired t-test, *$p < 0.05$), *Il10* (B, unpaired t-test, ns), *Il2* (C, unpaired t-test, ns), *Tnf-α* (D, unpaired t-test, ns). and *Il6* (E, unpaired t-test, ns) between a subset of female and male mice treated with vehicle.

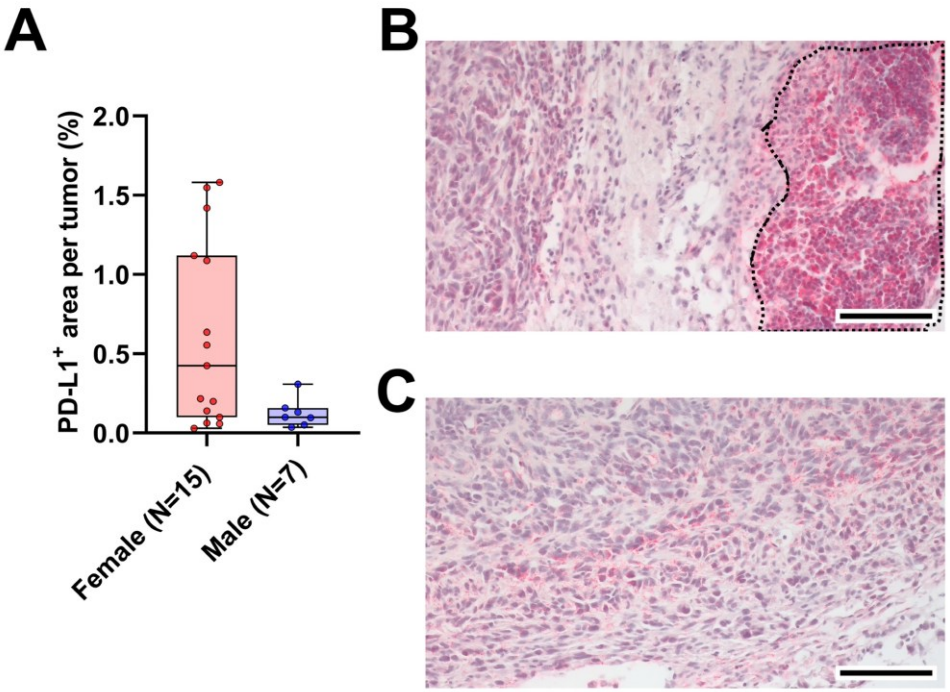

Figure S11. PD-L1 expression in tumors of female and male mice treated with vehicle. A: Comparison of PD-L1-positive area in tumors of vehicle-treated female and male mice (Mann-Whitney test, $p = 0.0556$). B, C: Representative histological sections of anti-PD-L1 stained tumors of surviving female (B) and male (C) vehicle-treated mice (scale bar = 100 µm). The outlined area in B highlights an inflammatory lesion predominantly seen in female mice.

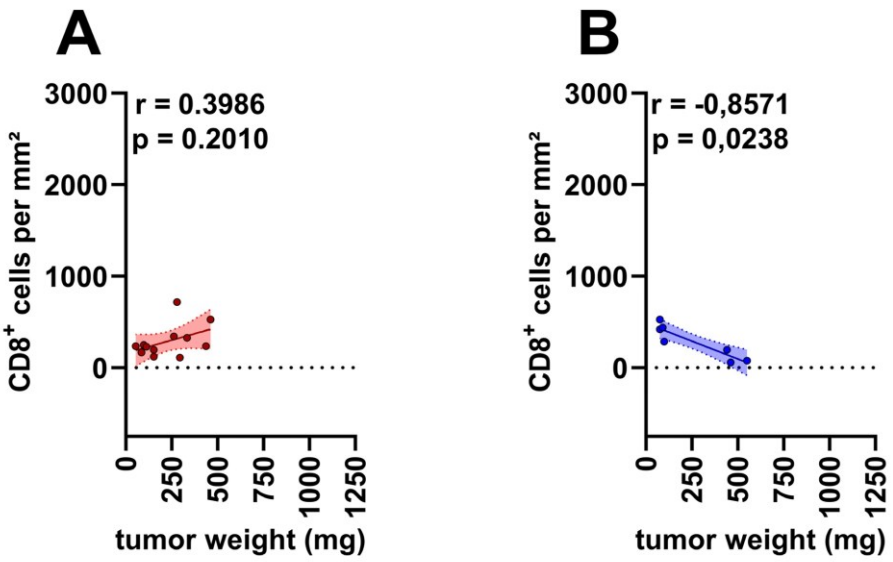

Figure S12. Correlation between the amount of CD8⁺ cells and tumor weight in animals treated with BI-3406, trametinib and BKM120. Correlation plots (Spearman correlation) with linear regression including confidence intervals (shaded area) of CD8⁺ cells and tumor weight of drug-treated female (A, N = 12) and male (B, N = 7) mice.

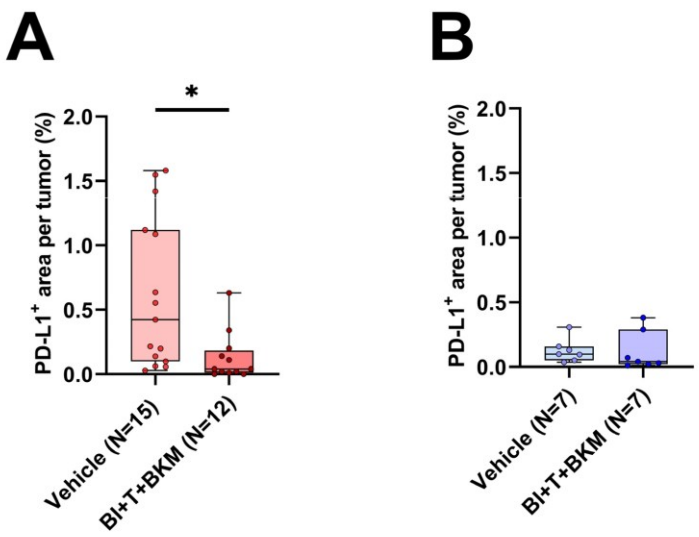

Figure S13. PD-L1 expression in tumors of female and male mice treated with vehicle or BI-3406, trametinib and BKM120. Comparison of PD-L1-positive area in tumors of vehicle and drug-treated female (A) and male (B) mice (Mann-Whitney test,* $p < 0.05$).

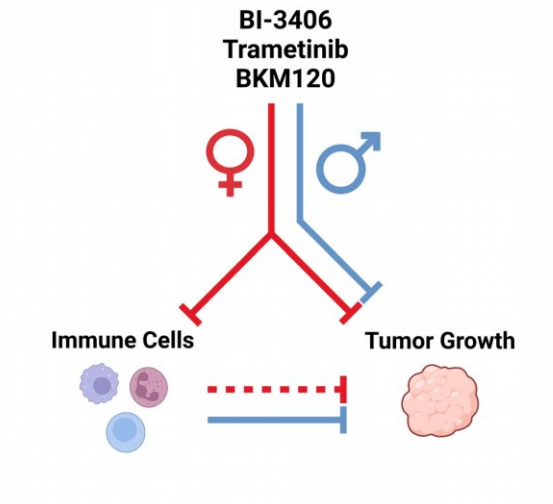

Figure S14. Visualization of hypothesized sex-specific effects. The combination of BI-3406, trametinib and BKM120 reduces tumor growth in both sexes. This reduction is influenced by the inhibition of immune cells predominantly in female animals. Made with biorender.com.

Table S1. Primers used for PCR and sequencing.

Jarid1c/1d forward	**CTGAAGCTTTTGGCTTTGAG**
Jarid 1c/1d reverse	CCACTGCCAAATTCTTTGG
Kras-Exon 1-G12D fw2 259-278	TGGTTCCCTAACACCCAGTT
Kras-Exon 1-G12D rv2 625-649	TTAGAGTTTTACACACAAAGGTGAG
Kras-Exon 1-G12D fw1 400-419 (used for sequencing)	TCTTTTTCAAAGCGGCTGGC

Table S2. PCR conditions (Jarid 1c/d).

Mastermix	**VWR Taq DNA Mastermix (Avantor, Darmstadt, Germany)**
Initial denaturing	94°C for 5 min
Denaturing (40x)	94°C for 20 s
Annealing (40x)	54°C for 1 min
Extension (40x)	72°C for 40 s

Table S3. PCR conditions (KRAS G12D and WT).

Mastermix	**PowerUp™ SYBR™ Green Master Mix (Applied Biosystems, Waltham, USA)**
UDG activation	50°C for 2 min
Activation (Dual-Lock™ DNA polymerase)	95°C for 2 min
Denaturing (40x)	95°C for 15 s
Annealing (40x)	55-60°C for 15 s
Extension (40x)	72°C for 1 min

Table S4. MRI sequences and parameters.

Parameters	**axial**	**sagittal**	**coronal**
TE/TR (ms)	25/3476	35/4553	25/2500
Rare factor	8	8	8
Averages	4	4	4
FoV (mm)	320 x 200	32 x 20	32 x 32
Matrix size	255 x 160	240 x 160	255 x 255
Voxel size (mm)	0.125 x 0.125	0.125 x 0.125	0.125 x 0.125
Slice thickness (mm)	0.8	0.8	0.8
Slices	42	40	22
Acquisition time (min:s)	4:38	6:04	5:47

Table S5. Parameters of the triple quadrupole interface.

Interface ESI parameter	**Value**
Nebulizing gas flow	3 L/min
Heating gas flow	10 L/min
Interface temperature	300 °C
Desolvation temperature	526 °C
DL temperature	250 °C
Heat block temperature	400 °C
Dry gas flow	10 L/min

Table S6. Mass spectrometric parameters of BKM120, BI-3406, trametinib and the internal standard acridine orange.

Substance	Precursor (*m*/*z*)	Product (*m*/*z*)	Dwell time (msec)	Q1 Pre Bias (V)	CE (V)	Q3 Pre Bias (V)	Measuring mode	Measuring time (min)
BKM120	411.3	367.1	515	-10	-35	-26	positive	0-3.5
BKM120	411.3	307.0	515	-11	-40	-22	positive	0-3.5
BKM120	411.3	238.95	515	-11	-46	-26	positive	0-3.5
BI-3406	463.3	205.95	100	-20	-35	-20	positive	4-6.5
BI-3406	463.3	190.9	100	-20	-50	-20	positive	4-6.5
BI-3406	463.3	276.05	100	-19	-28	-21	positive	4-6.5
BI-3406	461.2	375.15	100	13	33	12	negative	4-6.5
BI-3406	461.2	390.2	100	17	24	13	negative	4-6.5
BI-3406	461.2	331.1	100	13	52	14	negative	4-6.5
Acridine Orange	266.3	250.1	100	-14	-35	-28	positive	4-6.5
Acridine Orange	266.3	234.0	100	-14	-52	-26	positive	4-6.5
Acridine Orange	266.3	222.1	100	-14	-34	-24	positive	4-6.5
Trametinib	616.1	490.85	100	-20	-34	-19	positive	6-8
Trametinib	616.1	254.15	100	-20	-40	-19	positive	6-8
Trametinib	616.1	226.05	100	-20	-50	-17	positive	6-8
Trametinib	614.1	531.0	100	24	28	24	negative	6-8
Trametinib	614.1	511.05	100	24	31	24	negative	6-8
Trametinib	614.1	126.9	100	24	50	11	negative	6-8

Table S7. TaqMan qPCR conditions.

Mastermix	TaqMan™ Universal Master Mix II, (Applied Biosystems, Waltham, USA)
UNG incubation	50°C for 2 min
Enzyme activation	95°C for 10 min
Denaturing (40x)	95°C for 15 s
Anneal / Extend (40x)	60°C for 1 min

Table S8. Measured concentrations (LC-MS/MS) of therapeutics in plasma, liver and kidney (median with 5 – 95% confidence interval).

Sex	Sample	BI-3406	Trametinib	BKM120
Male	Plasma (N = 4)	2.1 µM (1.2 – 4.6)[#]	-*	2.6 µM (1.8 – 6.0)
	Liver (N = 3)	3.9 ng/mg (2.5 – 5.4)	0.42 ng/mg (0.089 – 0.69)	3.0 ng/mg (1.3 – 5.1)
	Kidney (N = 3)	2.2 ng/mg (2.0 – 3.0)	0.13 ng/mg (0.084 – 0.17)	0.48 ng/mg (0.33 – 2.5)
Female	Plasma (N = 6)	2.7 µM (0.82 – 4.2)	-*	4.6 µM (2.4 – 6.4)
	Liver (N = 3)	5.1 ng/mg (0.45 – 10)	0.39 ng/mg (0.30 – 0.48)[§]	2.4 ng/mg (0.31 – 8.8)
	Kidney (N = 3)	2.7 ng/mg (0.055 – 9.1)	0.21 ng/mg (0.19 – 0.24)[§]	0.47 ng/mg (0.059 – 7.2)

25% of values below limit of detection (LOD). * 100% of values below limit of detection (LOD). § 33% of values below limit of detection (LOD).

Table S9. p-values for Figure 5.

Tested Difference	p-value (Mann-Whitney test)	p-value (unpaired t-test)
AST (female vehicle vs. therapy)	0.6923	-
ALT (female vehicle vs. therapy)	0.4634	-
creatinine (female vehicle vs. therapy)	-	0.0604

LDH (female vehicle vs. therapy)	0.6483	-
c-peptide (female vehicle vs. therapy)	**0.0026**	-
AST (male vehicle vs. therapy)	-	0.6382
ALT (male vehicle vs. therapy)	-	0.7057
creatinine (male vehicle vs. therapy)	-	0.1680
LDH (male vehicle vs. therapy)	-	0.1686
c-peptide (male vehicle vs. therapy)	**0.0111**	-